Fukushima Daiichi Accident Study (Status as of April 2012)

Randall Gauntt, Donald Kalinich, Jeff Cardoni, Jesse Phillips, Andrew Goldmann, Susan Pickering, Matthew Francis, Kevin Robb, Larry Ott, Dean Wang, Curtis Smith, Shawn St.Germain, David Schwieder, Cherie Phelan

Sandia National Laboratories

Fukushima Daiichi Accident Study
(Status as of April 2012)

Randall Gauntt, Donald Kalinich, Jeff Cardoni,
Jesse Phillips, Andrew Goldmann, Susan Pickering
Sandia National Laboratories
P.O. Box 5800
Albuquerque, New Mexico 87185-MS0748

Matthew Francis, Kevin Robb, Larry Ott, Dean Wang
Oak Ridge National Laboratory

Curtis Smith, Shawn St.Germain, David Schwieder, Cherie Phelan
Idaho National Laboratory

Abstract

In response to the accident at the Fukushima Daiichi nuclear power station in Japan, the U.S. Nuclear Regulatory Commission (NRC) and Department of Energy agreed to jointly sponsor an accident reconstruction study as a means of assessing severe accident modeling capability of the MELCOR code. MELCOR is the state-of-the-art system-level severe accident analysis code used by the NRC to provide information for its decision-making process in this area. The objectives of the project were: (1) collect, verify, and document data on the accidents by developing an information portal system; (2) reconstruct the accident progressions using computer models and accident data; and (3) validate the MELCOR code and the Fukushima models, and suggest potential future data needs. Idaho National Laboratory (INL) developed an information portal for the Fukushima Daiichi accident information. Sandia National Laboratories (SNL) developed MELCOR 2.1 models of the Fukushima Daiichi Units 1, 2, and 3 reactors and the Unit 4 spent fuel pool. Oak Ridge National Laboratory (ORNL) developed a MELCOR 1.8.5 model of the Unit 3 reactor and a TRACE model of the Unit 4 spent fuel pool. The good correlation of the results from the SNL models with the data from the plants and with the ORNL model results provides additional confidence in the MELCOR code. The modeling effort has also provided insights into future data needs for both model development and validation.

CONTENTS

FIGURES

TABLES

ACRONYMS

AC   alternating current
ACRR   annular core research reactor (at SNL)
ADS   automatic depressurization system
ANL   Argonne National Laboratory
ANS   American Nuclear Society
BAF   bottom of active fuel
BWR   boiling water reactor
CRD   control rod drive
CRDHS   control rod drive hydraulic system
CRGT   control rod guide tube
CST   condensate storage tank
CV   control volume
CVH   Control Volume Hydrodynamics (package)
DC   direct current
DOE   Department of Energy
DTRA   Defense Threat Reduction Agency
D/W   drywell
EDG   emergency diesel generator
EPRI   Electric Power Research Institute
FDI   Fuel Dispersal Interactions (package)
FSAR   Final Safety Analysis Report
HPCI   high-pressure coolant injection system
IAEA   International Atomic Energy Agency
IC   isolation condenser
INL   Idaho National Laboratory
INPO   Institute of Nuclear Power Operators
JST   Japanese standard time
LPCS   low-pressure core sprays
MCCI   molten core concrete interaction
MOX   mixed oxide
MSIV   main steam-line isolation valve
MSL   main steam line
NARAC   National Atmospheric Release Advisory Center
NPSH   net positive suction head
NRC   Nuclear Regulatory Commission
ORNL   Oak Ridge National Laboratory
PBF   Prompt Burst Facility (test reactor at INL)
PCV   primary containment vessel (drywell and wetwell)
PCT   peak cladding temperature
PWR   pressurized water reactor
RCIC   reactor core isolation cooling system
RCS   reactor coolant system
RHR   residual heat removal system
RN   RadioNuclide (package)

RPV	reactor pressure vessel
SBO	station blackout
S/C	suppression chamber (i.e., wetwell)
SFP	spent fuel pool
SNL	Sandia National Laboratories
SOARCA	State of the Art Reactor Consequence Analysis
SRV	safety relief valve
SRV1	SRV with the lowest opening pressure set-point (the SRV that opens first)
TAF	top of active fuel
TEPCO	Tokyo Electric Power Company
TMI	Three Mile Island
WW	wetwell

1   INTRODUCTION

1.1   Background

Japan suffered an immense tragedy as a result of the 2011 Tohuku earthquake and resulting tsunami that caused widespread damage to the infrastructure of the country and more than 20,000 deaths, most from the tsunami. The magnitude 9 (M_w)[1] earthquake, centered roughly 20 miles deep and 43 miles east of Japan, took place at 14:46 (JST) on March 11, 2011, and produced catastrophic damage to buildings, roads, communications, and regional electrical power. Damage to the Sendai region was especially large owing to its proximity to the epicenter of the seismic event that produced a tsunami with an estimated height that exceeded 14 meters at the site of the Fukushima reactors. The earthquake at 14:46 JST resulted in a scram and a regional loss of electrical power, requiring the Fukushima Daiichi power plants (Units 1, 2, and 3) to start emergency on-site diesel powered generators to maintain cooling at the plants. Unit 4 was defueled at the time for maintenance, and Units 5 and 6 were in a state of cold shutdown for maintenance.

The first of several tsunamis produced by the earthquake reached the Fukushima Daiichi site at roughly 15:27. At 15:46, a wave exceeding 14 meters flooded buildings resulting in the loss of emergency diesel powered AC generators and producing conditions known as Station Blackout (SBO). DC power was also lost at Units 1 and 2. Units 1, 2, and 3 were effectively isolated from the ultimate heat sink (the ocean), and the emergency cooling systems eventually failed; each of the three units subsequently suffered core damage of varying degrees as a result of loss of water level in the reactor cores. Significant hydrogen generation resulted from the oxidation of the exposed Zircaloy fuel cladding, which occurs at elevated temperatures; this can generate heat greater than the decay heat in the fuel, and therefore may have accelerated the release of fission products from the damaged fuel to the containment vessels. With no way to reject the decay heat from the reactors, the suppression pools quickly became thermally saturated. This produced pressures in the containment vessels that eventually exceeded their design pressures. Containment venting was attempted. However, due to difficulties in accessing and operating vent valves, venting was either unsuccessful or delayed.

Ultimately, the containment systems leaked, failed, or were intentionally vented, resulting in the release of radioactivity to the reactor buildings and the environment. Combustible gasses produced from the core damage and molten core–concrete interaction accumulated in the Unit 1 and Unit 3 reactor buildings, causing explosions and destruction of portions of the buildings. The general sequence of events[2] (with the timelines for the units ordered by postulated time of fuel damage and hydrogen explosions) is shown graphically in Figure 1. Figure 1 illustrates the coincidence of parallel accident progressions, including operation of available emergency systems (isolation condensers (ICs), reactor core isolation cooling (RCIC), and high-pressure cooling injection (HPCI)), emergency reactor depressurization events followed by seawater injection, operator initiated containment venting actions, and subsequent reactor building explosions. Figure 1 serves to reflect the general understanding of the durations of safety systems

---

[1] moment magnitude scale

[2] The events and timings are based on reported events (e.g., earthquake, explosions) and analysis results.

operations, alternative injections, and potential fuel damage. The success of water injection in limiting the duration of fuel damage is uncertain at this time. As investigations into the units are extended, the extent of core damage may become better understood.
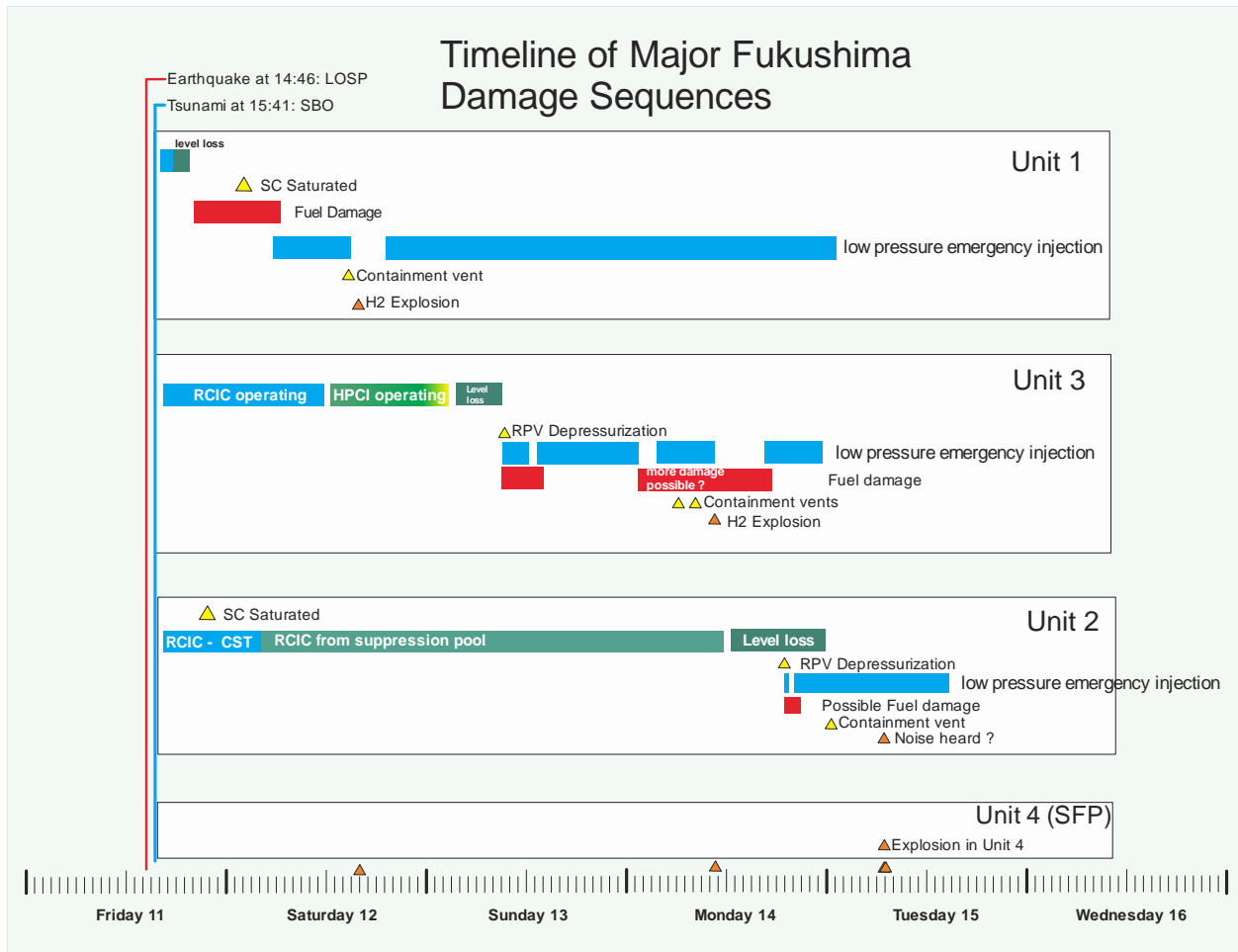
Figure 1. Postulated General Sequence of Events at the Fukushima Daiichi Reactor Site.

The three accidents (i.e., the accidents in Units 1, 2, and 3), while similar in many ways in terms of SBO accident progression, each proceeded to different degrees of core damage, with Unit 1 believed to be the most severely damaged of the three. It is believed that the Unit 1 core damage proceeded to the point of lower vessel head failure that released core materials to the containment cavity where core-concrete interactions likely initiated. Units 2 and 3 are believed to be less damaged. Collectively, the accidents likely reflect varying degrees of core/reactor damage and are therefore an invaluable source of information that can validate/confirm our current understanding of severe reactor accidents and provide new understanding not currently realized in our body of knowledge.

The Fukushima Daiichi event has been rated at the maximum level (Level 7) on the International Atomic Energy Agency (IAEA) nuclear event scale, which means that it released large amounts of radioactive materials accompanied by "widespread health and environmental effects." The accident has caused worldwide public concern that nuclear power may not be safe enough.

Several national governments, including the Government of Japan, have been forced to reconsider their nuclear energy policies. It is imperative that nuclear engineers around the world examine this accident and understand what went wrong.

As of June 2012, fifteen months after the accident, many researchers from different organizations are developing a general consensus on many of the technical questions about what happened inside the reactors and which major safety systems performed well or failed to operate. This report presents the best analysis of the U.S. Government at this time. The analysis is jointly sponsored by the Department of Energy (DOE) and the Nuclear Regulatory Commission (NRC), and it is conducted by several national laboratories. Organizations that are conducting similar analyses include the Electric Power Research Institute (EPRI), the Tokyo Electric Power Company (TEPCO), and others. The researchers do not agree on all aspects of the accident scenario, but they tend to agree on the major sequence of events. Furthermore, they routinely share their results in meetings and email correspondence. As more time passes, it is likely that an even better understanding of the details of the accident will be developed by all the organizations involved.

1.2   Object of the Study

Today, the body of knowledge concerning severe accident progression is reflected largely in the computer codes (such as MELCOR [29] and MAAP [10]) that are used to analyze severe accidents in nuclear power plants for the purpose of predicting damage from accidents such as those at Fukushima Daiichi, predicting radiological consequences of such accidents, and perhaps most importantly, to identify means of mitigating or avoiding such accidents.

The study described herein is focused on using the MELCOR code and known conditions surrounding the accidents in the Fukushima reactors to "reconstruct" the accidents and predict as well as possible plant state parameters (e.g., reactor and containment pressures), the implied core damage and fission product release, and, if possible, the circumstances leading up to the reactor building explosions during the first four days of the accidents; subsequent events are not addressed. The main objectives of these accident reconstructions are to evaluate the ability of MELCOR to accurately predict severe accident progression and to identify areas where the codes such as MELCOR can or should be improved.

The work comprising this study is divided into three major components, executed as a multi-laboratory effort by SNL, INL, and ORNL, where SNL, as the principal developer of the MELCOR code, has the overall lead in the effort in terms of performing MELCOR analyses of the accidents using the latest code version, MELCOR 2.1.

The analyses described in the following sections are based on the best available information at the time of the study. It is recognized that new information will be emerging that may suggest refinement of these analyses may be in order, especially as TEPCO regains access to the plant systems within the containment and the reactors themselves. For example, recently obtained information suggest that actual fire engine water injection flow rates were lower, perhaps significantly lower, than initially indicated, and could materially impact the predicted damage states for Unit 2 and 3. The results obtained in this study are encouraging in terms of capturing

the essential accident signatures and are believed to be useful in identifying areas requiring future characterization in the decommissioning process. New information when available will no doubt lead to improved code analyses and greater confidence in the code predictive capabilities.

1.2.1 Fukushima Data Portal

Since this work and the Fukushima accidents are likely to be widely studied for many years to come, an important objective of this effort is to establish and preserve reliable data and information concerning the accidents in the form of a Data Portal. This aspect of the project is executed by INL, where the aim is to make available for this project and for other researchers, and to preserve into the future reliable and "referenceable" information concerning the accidents. This aspect of the effort gathers into one place, information that is critical to understanding the events at Fukushima Daiichi and provides citations and other information concerning the quality of the data.

1.2.2 Analyses of the Reactor Accidents

Sandia National Laboratories was responsible for developing Fukushima-specific MELCOR models for each of the reactors that was damaged, using the latest MELCOR code version (2.1) and the best modeling practices as developed over many years and demonstrated in the recently published State of the Art Reactor Consequence Analysis (SOARCA) project documentation [41]. The reactor models developed for SOARCA have been refined over the past ten years to reflect best current knowledge of plant systems behavior in severe accident conditions. Sandia used these models to "reconstruct" the accident in Units 1, 2, and 3 using the most likely accident scenarios and to explore alternative "reconstruction" scenarios using other plausible assumptions where significant uncertainty in precise accident progression exists. Oak Ridge National Laboratory performed independent analyses of the Unit 3 reactor accident using an earlier version of MELCOR (version 1.8.5) to evaluate possible code version differences and to support the overall forensics effort in characterizing the accident damage states. These analyses provided an independent evaluation of the HPCI function in the Unit 3 accident.

The MELCOR models (both SNL MELCOR 2.1 and ORNL MELCOR 1.8.5) used in this study were based on the Peach Bottom reactor, a larger but quite similar reactor design to the reactors at Fukushima. The containments are of the General Electric Mk-I design where a torus shaped suppression pool serves to prevent steam over-pressurization of the containment. The models have been modified to accurately represent the Fukushima Units 1, 2, and 3, including important differences in the Fukushima reactors, such as reactor dimensions, number of fuel assemblies and operating power.

1.2.3 Analysis of Potential Accident Development in Spent Fuel Pool of Unit 4

An explosion destroyed the Unit 4 reactor building. Since the Unit 4 reactor was shut down and the fuel stored in the spent fuel pool, clearly the source of flammable gas was not from the Unit 4 reactor. It was initially feared that the cause of the building explosion was from cladding oxidation associated with loss of water level in the spent fuel pool. It was ultimately determined

that the water levels in the spent fuel pool of Unit 4 were never sufficiently low to have permitted initiation of fuel damage, and the source of the flammable gas that destroyed the building is not known with certainty, but suspected to be related to combustible gases transported from the Unit 3 accident via the commonly shared off gas stack. MELCOR and TRACE analyses of potential scenarios for boil-off of the spent fuel pool were examined in this study to determine the margin to initiation of fuel damage that existed in the Unit 4 sequence of events.

Sandia developed a MELCOR 2.1 model of the Unit 4 spent fuel pool and estimated the time required to boil down the pool water and initiate fuel damage for two initial conditions; one where the initial water level was at the top of the pool and another where the water level was initially 0.5 meters above the top of the spent fuel racks. The analyses conclude that the boil-down in either case does not lead to fuel damage that could produce hydrogen within the time frame of the observed building explosion. ORNL performed TRACE analyses of the pool boil down, and predicted boil-down times shorter than the SNL MELCOR 2.1 estimates. The difference in these estimates is due to relative humidity effects on water evaporation within the refueling bay. The MELCOR analyses of the refueling bay show an increase in the relative humidity in the air above the pool surface, thereby reducing evaporation and prolonging the time to fuel uncovering. The results indicate the potential importance of accurately capturing the reactor building behavior (e.g., boundary conditions, buoyancy-driven flow).

1.3   Document Outline

The following sections describe in detail the major elements of the project as previously identified in this section, beginning with a description of the data portal (Section 2). Following this will be descriptions of the MELCOR models for the reactors and specific boundary conditions and assumptions for the Fukushima Daiichi accident analysis (Section 3). The accident analyses themselves are described in Section 4 for each of the Fukushima Daiichi units. Section 5 and 6 continue the reactor accident analysis, presenting the input and the results, respectively, of the ORNL independent assessment of the Unit 3 accident. Section 7 presents the ORNL assessment of potential Unit 4 spent fuel pool boil-down dynamics. Section 8 details the SNL evaluation of potential boil-down scenarios in the Unit 4 spent fuel pool using MELCOR 2.1. Finally, conclusions are presented in Section 9.

2 PORTAL AND TIMELINE DEVELOPMENT

2.1 Overview of the Portal

In order to manage and store the information related to the Fukushima Daiichi event, the analysis team has developed an Internet-based information portal. The intent of this portal is to provide an approach to collecting, storing, retrieving, and validating information and data for use in reconstructing the Fukushima Daiichi accident and to assist the other team members by providing support for the technical basis behind the event reconstruction. This section describes the database design used to establish a centralized information repository to store and manage the Fukushima Daiichi data that has been gathered. The data will be stored in a secured (password protected and encrypted) repository that is searchable and available to researchers at diverse locations. The portal will allow various user roles with varying levels of authority to view only or add and edit data. The portal itself is located at the URL:

https://fukushima.inl.gov

The procedures for registering for and using the portal are located in the user's guide, which can be viewed through the following link.

https://fukushima.inl.gov/Documents/FDASIP%20User%20Manual.pdf

This document is also available under the help tab from the portal home page.

To log in to the portal, a user must Press the "Log In" link located in the upper right-hand corner. Pressing this link takes the user to the Log In screen. If the user has not yet registered for access, he must register by selecting the "Register" link. The Register link will take the user to the registration page and allow him to register for a username and password. Note that all passwords are encrypted. After registering, the request will be considered and then an e-mail will be sent to the user indicating that the appropriate role(s) has been assigned.

Once the user logs in the Home page will be displayed. The Home page shows the user name in the upper right-hand corner with the Log Out link, the menu options based on the user's assigned roles, and the Recent Additions/Changes table. Figure 2 shows the Home page and all of the menu items available to all roles.

Figure 2. Home Page for the Information Portal.

NOTE: A user will see only the menu options to which he has access.

2.2 Types and Examples of Information Stored

In general, four types of data are stored in the database:

- Events (key events identified in the accident sequence timeline)
- Artifacts, including:
  - Plant parameter values (e.g., pressures, temperatures)

- Media files (.pdf, photos, videos, etc.)
- Component states (e.g., component X started at time Y and failed at time Z)

An Event is one of the primary portal objects used to denote points or periods in time when something important to the Fukushima accident took place. The Event object is used to provide a link between the flow of time during the accident (i.e., "the timeline") and supporting (optional) information (such pictures, analysis output, or plant data) called "Artifacts." This concept of linking events to a time line AND assigning supporting information (Artifacts) is shown in Figure 3.
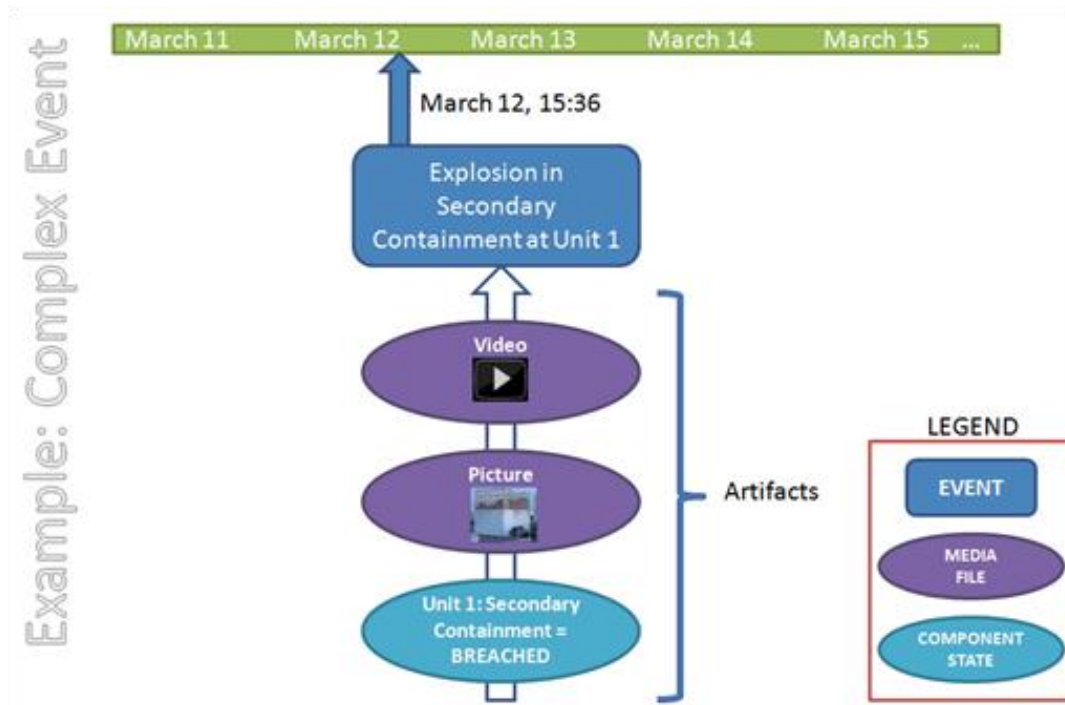
Figure 3. Notional Concept of an "Event" in the Information Portal.

Events are available to the Contributor role for viewing and modification. The Event page shows all events. For each event, all the associated Artifacts (if any) are shown, and any associated Reviews are shown. Additional features of the database structure include:

- A CAUSE defining all of the Primary Causes of concern for the study (i.e. Earthquake, Tsunami, etc.) with Name and Descriptions. A CAUSE may be associated with multiple events.
- An EVENT, which can include multiple review comments from contributors, added as the study progresses.
- A REVIEW, which includes Comments and is identified by the Contributor, Date and Time entered.
- An ARTIFACT that can include multiple review comments from contributors.

- A component state, which is related to an event and includes the state, start date/time, and end date/time. A component state is defined by the combination of Event, Unit, System, and Component.

2.3   Background on Information Sources Used for the Timeline

Each timeline entry is referenced to a source document contained in the Portal as a media file artifact. Various reports and TEPCO press releases were referenced in creating the timeline. Where differences in data existed, priority was given to data released directly by TEPCO over other sources, and more recently released data was given priority over data that was released earlier. The primary source of timeline information was extracted from a TEPCO press release dated 8/10/11 titled "State of Immediate Response after Disaster Struck at Fukushima Daiichi Power Station." This document is broken down by unit with sections related to general timeline information, alternate injection, and containment venting. A recently released Institute of Nuclear Power Operators (INPO) report titled "Special Report on the Nuclear Accident at the Fukushima Daiichi Nuclear Power Station" was also used as a reference to verify timeline data that was created form earlier reports. An early report to the IAEA titled "Report of Japanese Government to the IAEA Ministerial Conference on Nuclear Safety – The Accident at TEPCO's Fukushima Nuclear Power Station" was heavily referenced early on. Several other reports are presented in the Portal for reference and comparison, but may not have been referenced in the timeline creation. A complete list of media file artifacts contained in the Portal is listed in Appendix A.

2.4   Examples of Data Views Available in the Portal

2.4.1 Event Timeline View

Once the data has been entered into the database, the information portal provides a variety of views of this information. For each view, filters are provided to tailor the output to the needs of the user. Clicking the "Generate Timeline" button produces a detailed timeline using the options specified above, as shown in Figure 4.

Timeline for Unit1

Friday, March 11, 2011

12:00:00 PM - ICS/SYS/IC A, Standby

12:00:00 PM - HCI/TDP/HPCI, Standby

12:00:00 PM - SWS/MDP/CCSW, Operating

12:00:00 PM - DCP/BAT/125 V Battery, Operating

12:00:00 PM - PCS/MSV/MSIVs, Normally Open; Not failed

12:00:00 PM - OEP/SYS/Offsite Power Sources, Operating

12:00:00 PM - RPS/ACT/Reactor, Operating

12:00:00 PM - ACP/DGN/EDG 2, Standby

12:00:00 PM - ACP/DGN/EDG 1, Standby

2:46:00 PM - RPS/ACT/Reactor, Reactor Scram

2:46:00 PM - Tohoku Earthquake

2:46:00 PM - Unit 1 Shut Down

2:47:00 PM - OEP/SYS/Offsite Power Sources, No power-loss of power

2:47:00 PM - PCS/MSV/MSIVs, Normally open; fail in closed position

2:47:00 PM - ACP/DGN/EDG 2, Automatically Started

2:47:00 PM - ACP/DGN/EDG 1, Automatically Started

2:47:00 PM - Loss of Offsite Power

2:52:00 PM - ICS/ACT/IC B, Automatically Started

2:52:00 PM - ICS/SYS/IC A, Automatically Started

3:02:00 PM - Unit 1 subcriticality confirmed

3:03:00 PM - ICS/ACT/IC B, Manually Shutdown

3:03:00 PM - ICS/SYS/IC A, Manually Shutdown

3:27:00 PM - 1st Tsunami wave hits unit 1

3:35:00 PM - 2nd Tsunami wave hits unit 1

3:37:00 PM - HCI/TDP/HPCI, Fail to start

3:37:00 PM - SWS/MDP/CCSW, Fail to continue running

3:37:00 PM - DCP/BAT/125 V Battery, Fail to operate

3:37:00 PM - ACP/DGN/EDG 2, Fail to continue running

3:37:00 PM - ACP/DGN/EDG 1, Fail to continue running

3:37:00 PM - Station Blackout, Unit 1

5:30:00 PM - FW1/EDP/Diesel driven fire pump, Manually Started

6:18:00 PM - ICS/SYS/IC A, Manually Started

6:25:00 PM - ICS/SYS/IC A, Manually Shutdown

8:07:00 PM - Reactor pressure checked locally in reactor building, 1015 psia

8:49:00 PM - MCR lit by temporary lighting

9:30:00 PM - ICS/SYS/IC A, Manually Started

11:59:00 PM - Restoration team provides temp power to MCR, D/W pressure 87 psia (600 kPaa)

Details of component state:
IC A (at Unit 1) is in state Standby between
3/11/11 (12:00:00 PM) and 3/11/11 (2:52:00 PM)

Source:
Assumed initial condition

Area: Unit1
System: ICS-Isolation Condenser
Component Type: SYS-System level event
Component: IC A

State:
Standby

Event Time:
3/11/2011 12:00:00 PM spanning to 3/11/2011
2:52:00 PM

Added or last modified by:

Figure 4. Example of the Timeline View.

2.4.2 Component State Chart View

The Component State Chart view allows the portal user to select and view the status of specific Fukushima plant components as to their functionality (e.g., working or not) over time. To use this option, the user must specify which unit to investigate, which components, and over which time. For example, we could show (for Unit 1) the DC Power, the Isolation Condenser, and the Service Water System to be shown for the first 7 days of the event (see Figure 5).

In Figure 5, we see that the DC Power system and Service Water System worked for a short period of time following the earthquake (the green region on the status chart) but then was failed (on March 11, 2011) effectively at the time of the tsunami. The Isolation Condenser A (IC A) was initially in standby, then worked, but eventually failed later on March 11, 2011. This detail can be seen simply by changing the starting/ending date/time options. .
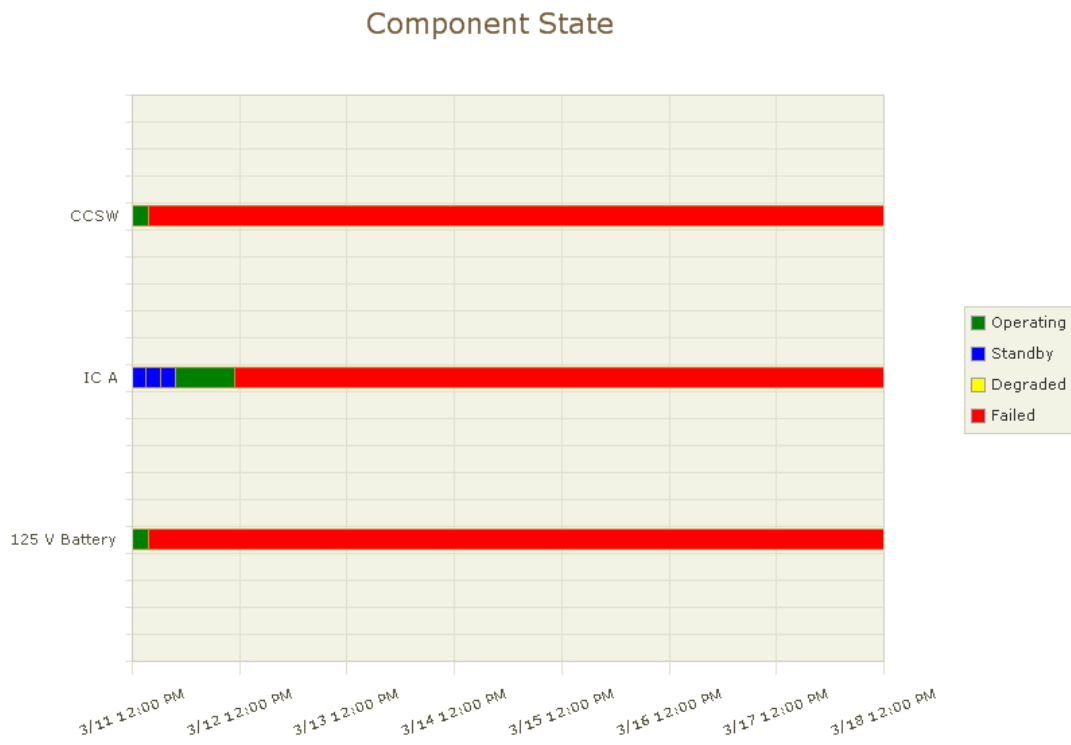
Figure 5. Output from the Component State Chart View.

28

2.4.3 Parameter Data Chart View

The Parameter Data Chart view allows the portal user to select and view the status of specific Fukushima plant physical parameters (e.g., pressures, temperatures, water levels) over time. To use this option, the user must specify which unit to investigate, which plant parameter to investigate (and desired units), and over which time. For example, the Reactor Vessel Level for both the A and B sensors are shown for the first 7 days of the event (see Figure 6).
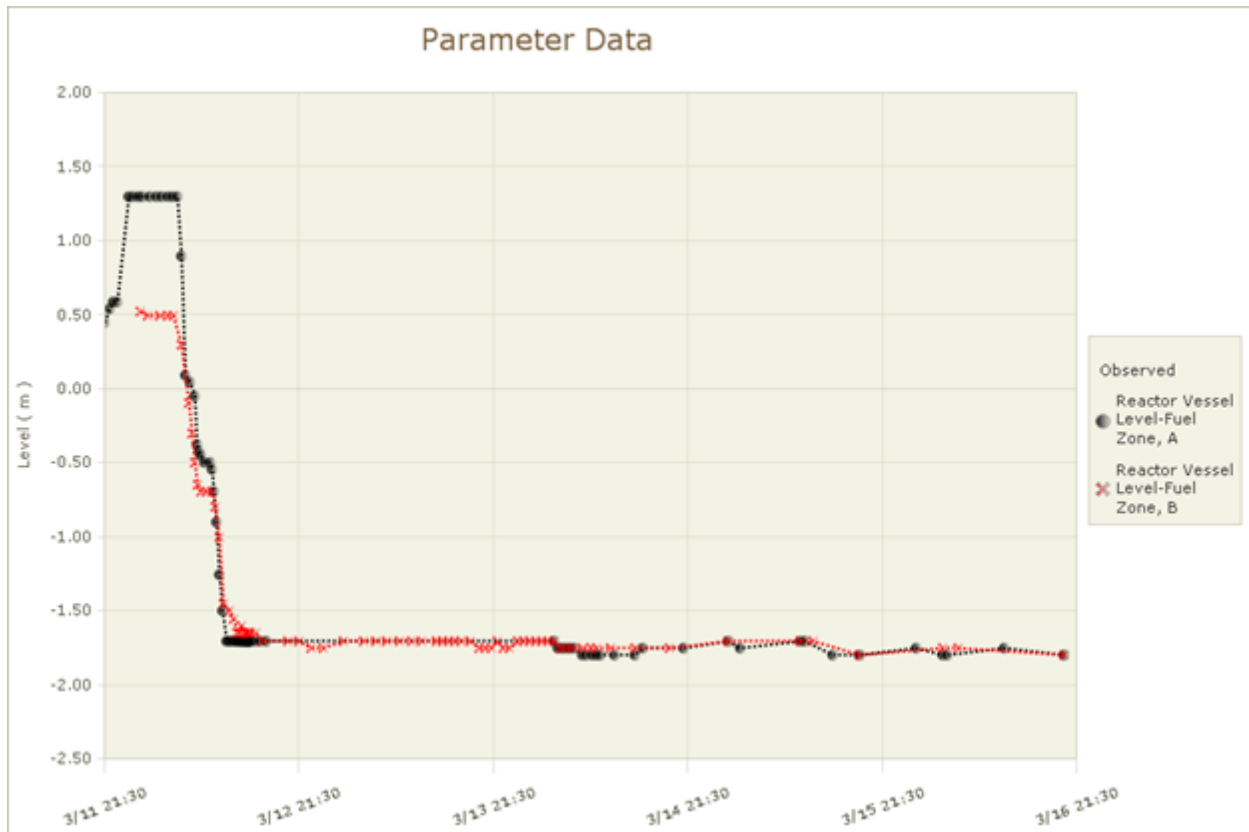
Figure 6. Output from the Parameter Data Chart View.

2.4.4 Radiation Plot View

The radiation plot view allows the portal user to select and view the radiation data that was collected around the Fukushima plant site over time. To use this option, the user must specify which location to investigate over which time. For example, we have selected the West Gate to be shown for the first 11 days of the event (see Figure 7).

29
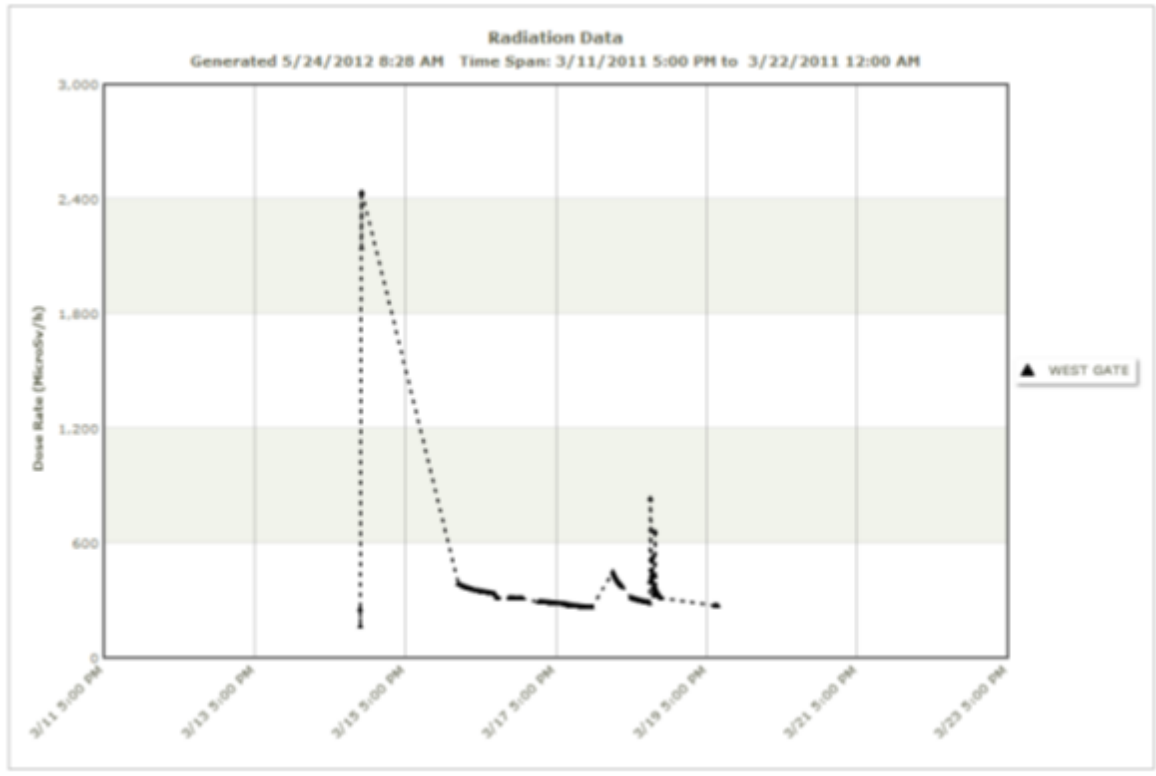
Figure 7. Radiation Data Plot for the West Gate.

2.5   The Event Timelines

One of the primary activities of this effort was to characterize the events of the accident. To do this, we established the accident timeline of events, including equipment actuation and system failures. The accident timeframe for this study begins with the off-shore Tōhoku earthquake on March 11, 2011, at 14:46 (Japan Standard Time), and ends when conditions at the reactors and spent fuel pools became static. The study end date for Reactors 1, 2, and 3 are (based mostly on when stable sea water injection was attained):

- Unit 1 reactor – conduct analysis through March 13, approximately noon.
- Unit 2 reactor – conduct analysis through March 15, approximately 24:00 hrs.
- Unit 3 reactor – conduct analysis through March 14, approximately 24:00 hrs.

Timelines for units 4, 5, and 6 are also included; however, the information is limited as detailed studies were not within the scope of this study.

Key sources for all of the information in the portal include:

- Report of the Japanese Government to the IAEA Ministerial Conference on Nuclear Safety - The Accident at TEPCO's Fukushima Nuclear Power Stations. Government of Japan, June 2011.

- Initial Response of Tohoku-Chihou-Taiheiyo-Oki Earthquake at Fukushima Daiichi and Fukushima Daini Nuclear Power Station, TEPCO, August 10, 2011.

- Additional Report of the Japanese Government to the IAEA - The accident at TEPCO's Fukushima Nuclear Power Stations - (Second Report), Government of Japan, September 2011.

Details of the event timeline are shown in Appendix A.

3 SNL UNIT 1, UNIT 2, AND UNIT 3 MODEL DESCRIPTIONS INPUT, AND ASSUMPTIONS

The Fukushima Daiichi Unit 1, Unit 2, and Unit 3 MELCOR models were developed from the boiling water reactor (BWR) model BWR/4 Mk-I MELCOR, created for the NRC's State of the Art Reactor Consequence Analysis (SOARCA) project. This section contains the summary of that MELCOR model[3] [41], along with information on the changes made to that model to create the Unit 1, Unit 2, and Unit 3 reactor model.

A review of the historical development of the BWR/4 Mk-I MELCOR model is provided in Section 3.1. A brief description of the MELCOR code is provided in Section 3.2. Section 3.3 discusses the implementation of the reactor accident timelines from Appendix A into the MELCOR models, including any modification.

The remaining sections describe the model as divided into the following parts:

- reactor vessel and coolant system
- in-vessel structures and reactor core
- primary containment and reactor building
- mechanisms for induced reactor pressure vessel (RPV) depressurization
- behavior of ex-vessel drywell floor debris
- containment failure model
- radionuclide inventories and decay heat

3.1 SNL BWR/4 Mk-I MELCOR Model History

The MELCOR SOARCA BWR/4 Mk-I model was originally created for code assessment applications with MELCOR 1.8.0 at Brookhaven National Laboratory; it is based on the Peach Bottom Reactor design. The model was subsequently adopted by J. Carbajo at Oak Ridge National Laboratory to study differences between fission product source terms predicted by MELCOR 1.8.1 and those generated for use in NUREG-1150, "Severe Accident Risks: An Assessment for Five U.S. Nuclear Power Plants," issued December 1990, using the Source Term Code Package [3]. In 2001, Sandia National Laboratories refined the BWR/4 core nodalization to support the developmental assessment and release of MELCOR 1.8.5. These refinements concentrated on the spatial nodalization of the reactor core (in terms of fuel and structural material and hydrodynamic volumes) used to calculate in-vessel melt progression. However, the overall scope of the model also expanded to permit a wider spectrum of accident scenarios to be examined, some of which involved operation or delayed failures of plant safety systems.

These developments culminated in a model that was applied in the reassessment of radiological source terms for high burnup and mixed oxide (MOX) core designs, and a comparison of their release characteristics [26] to the regulatory prescription outlined in NUREG-1465, "Accident Source Term for Light-Water Nuclear Power Plants," issued February 1995 [32]. These

---

[3] A comprehensive description of that model is also available in separate documentation [17].

calculations addressed a wide spectrum of postulated accident sequences, which required the following new models to represent diverse plant design features:

- modifications of modeling features needed to achieve steady-state reactor conditions (e.g., recirculation loops, jet pumps, steam separators, steam dryers, feedwater flow, control rod drive hydraulic system (CRDHS), main steam lines, turbine/hotwell, core power profile),
- new models and control logic to represent coolant injection systems (e.g., RCIC, HPCI, residual heat removal system (RHR), and low-pressure core sprays (LPCS)) and supporting water resources (e.g., condensate storage tank (CST) with switchover), and
- new models to simulate reactor vessel pressure management (e.g., safety relief valves (SRVs), safety valves, automatic depressurization system (ADS), and logic for manual actions to affect a controlled depressurization if torus water temperatures exceed the heat capacity temperature limit).

Subsequent work in support of other NRC research programs motivated further refinement and expansion of the model in two broad areas. The first area focused on the spatial representation of primary and secondary containment. The drywell portion of primary containment has been subdivided to distinguish thermodynamic conditions internal to the pedestal from those within the drywell itself. Refinements have also been made to the spatial representation and flow paths within the reactor building (i.e., secondary containment). The second area has focused on bringing the model up to current best practice standards for MELCOR 1.8.6 [13].

The SOARCA BWR/4 Mk-I MELCOR model was chosen as the starting point for the development of the Fukushima reactor models, as it is the current state-of-the-art BWR/4 Mk-I MELCOR model. At Fukushima Daiichi, units 2 and 3 are BWR/4 reactors, while Unit 1 is of a very similar reactor design (BWR/3). Furthermore, Units 1, 2, and 3 all have the Mk-I containment design. The SOARCA BWR/4 Mk-I MELCOR model already contains models of the BWR/4 Mk-I plant design features (as described in the previous bulleted list).

3.2 MELCOR Computer Code Description

MELCOR [29] is a fully integrated, engineering-level computer code that models the progression of severe accidents in light-water reactor nuclear power plants. MELCOR is being developed at Sandia National Laboratories for the U.S. Nuclear Regulatory Commission as a second-generation plant risk assessment tool and the successor to the Source Term Code Package [3]. A broad spectrum of severe accident phenomena in both boiling and pressurized water reactors is treated in MELCOR in a unified framework. These include thermal-hydraulic response in the reactor coolant system (RCS), reactor cavity, containment, and confinement buildings; core heatup, degradation, and relocation; core-concrete attack; hydrogen production, transport, and combustion; fission product release; and transport behavior. Figure 8 illustrates the wide range of processes and phenomena during a severe accident that are modeled in the MELCOR code.

Current uses of MELCOR include estimation of severe accident source terms and their sensitivities and uncertainties in a variety of applications.

Modeling and Analysis of Severe Accidents in Nuclear Power Plants

Severe accident codes are the "Repository" of phenomenological understanding gained through NRC and International research performed since the TMI-2 accident in 1979

Integrated models required for self consistent analysis

Important Severe Accident Phenomena

- Accident initiation
- Reactor coolant thermal hydraulics
- Loss of core coolant
- Core meltdown and fission product release
- Reactor vessel failure
- Transport of fission products in RCS and Containment
- Fission product aerosol dynamics
- Molten core/basemat interactions
- Containment thermal hydraulics
- Fission product removal processes
- Release of fission products to environment
- Engineered safety systems - sprays, fan coolers, etc
- Iodine chemistry, and more

Figure 8. Illustration of the Range of Phenomena and Processes Modeled in the MELCOR Accident Analysis Code.

A distinction should be made at this point between "physics and engineering models" that are inherent in the MELCOR computer code, and the "plant models" that represent a given power plant or experimental facility. The plant models that will be described in subsequent sections are actually input for the MELCOR computer code and are constructed of fundamental modeling objects available in MELCOR. In MELCOR, there are no ready-made pressurized water reactor (PWR) or BWR reactors. Rather the user builds a model of the power plant or experiment (obviously widely different scales) using the MELCOR constructs of control volumes, heat structures, and flow paths. Together these constructs or objects allow the user to define in MELCOR input the flow circuit of the reactor, the coolant system, and the containment.

Within the MELCOR code itself, special models are implemented to represent fuel rods and cladding, working fluid hydrodynamics (flow resistance and pressure drop), heat transfer (conduction, convection and radiation), and working fluid phase changes (boiling and condensation). Models for predicting the oxidation of Zr cladding material with steam, producing heat and hydrogen, account for the availability of steam and the temperature-dependent reaction kinetics. The release of fission products from over-heated fuel pellets account for the wide range

35

of volatility of the fission product species such as noble gas, iodine, and cesium. Fission product aerosols are modeled using a dynamic model that accounts for size distribution effects and aerosol mechanics phenomena, such as gravitational settling. Combustion models treat the burning of flammable gases, such as hydrogen, from cladding oxidation with steam and carbon monoxide, from concrete attack by molten core materials following core melt down and reactor vessel failure. One of the most challenging aspects of modeling severe accidents with core damage is in accounting for loss of rod geometry and the gradual formation of degraded fuel rubble, molten regions, and their spatial movement downward as the core degrades.

The validation of codes such as MELCOR is accomplished by means of comparing code-predicted results against a wide range of separate effects experiments and integral experiments, and correcting modeled physics, where needed, to gain concurrence with data. Separate effects experiments provide data, for example, on Zr oxidation rate as a function of temperature, steam condensation in the presence of non-condensable gas, release rate of Cs from irradiated reactor fuel as a function of temperature, or aerosol particle settling as a function of particle size, just to name a few of the operative phenomena in MELCOR. More challenging, however, is to validate the integrated effects of these separately characterized effects owing to coupling of effects. For example, the decay heat level determines the steam generation rate, and this in turn affects the heat generation rate from cladding-steam oxidation, which in turn affects fuel temperature, which affects fission product release, which in the end affects the decay heat level locally since the fission products determine the decay heat. Similarly, the coolant boiling rate affects cladding oxidation, which influences fuel heatup, which determines fuel melting rate, which affects the transfer of hot debris to the lower water-filled regions of the core, which in turn affects the boiling rate. Larger integral experiments allow the investigation of these coupled phenomenological effects.

MELCOR has been validated against a large number of experimental tests [40], both separate effects test and large integral experiments. As a part the continued development of MELCOR, SNL is updating the validation documentation to include an expanded set of experimental tests and to extend the validation to the latest version of the code (MELCOR 2.1). The assessment of MELCOR against full-scale real-world accidents such as Three Mile Island-2 (TMI-2) and the Fukushima Daiichi accidents, provide the most comprehensive test of MELCOR's models, which is a major aim of this study. This is accomplished by developing user input models for each of the Fukushima Daiichi reactors and representing, as best as is known, the initial and boundary conditions for each accident, and comparing wherever possible known data and details concerning the outcome of the accidents. This process is described in the subsequent sections of this report.

The SNL models for the Unit 1, Unit 2, and Unit 3 reactors, and for the Unit 4 spent fuel pool (SFP), were developed and simulated using MELCOR 2.1 [29]. The ORNL Unit 3 model was developed and simulated using MELCOR 1.8.5, and the ORNL Unit 4 SFP model was modeled using TRACE.

3.3 Event Timelines as Implemented in the Reactor Models

The timelines in this section are the outcome of a meeting held at the EPRI office in Washington, DC in October 2011. The purpose of the meeting was to create timelines for model implementation based on a consensus understanding of the multiple, and sometimes conflicting, sources of timeline information. Participants in the meeting included personnel from the DOE, NRC, INL, SNL, ORNL, EPRI, and the nuclear power industry.

It should be noted that the timelines in Appendix A contain addition information (e.g., observations of the system) that is not necessary to define MELCOR model input for the units; that information is omitted from the timelines in this section for clarity.

In some instances, timeline accident sequence events were modified during the model development process to account for the slow, but constant, shift in the understanding of the accident progression and system response, both internal, given the improved understanding of the events through iterative model development, and through the incorporation of the externally released reports and findings. These modifications are shown in ***bold italics*** in the timelines presented in this section (see Table 1, Table 2, and Table 3). Moreover, pointers are provided at the end of each timeline table to the sections that contain explanations of the modifications.

The last two operations of the ICs were not implemented in the Unit 1 MELCOR model (see Section 3.4.1.1). An explanation of why the drywell (D/W) venting was not implemented and the modification made to the wetwell (WW) venting are provided in Section 3.6.1.2.

An explanation for the assumed RCIC stop time is provided in Section 3.4.1.3. The timing of seawater injection is discussed in Section 3.4.1.4. The WW and D/W venting operations, which were omitted, are discussed in Section 3.6.1.3.

The containment spray activation at 41 hours was not implemented into the model since there is no clear pressure decrease in the containment near 41 hours (in fact, containment pressure is rapidly increasing after 40 hours (see Figure 56)). (Note: this spray activation is unrelated to the S/C sprays that are now believed to have been used near 22 hours via fire engine pumps.) Explanations for determining the exact time of the RPV depressurization and the S/C vent open/close times are provided in Section 3.7.4.3 and Section 3.6.1.4, respectively. It should also be noted that the explosion in the reactor building of Unit 4 occurred 87 hours after Unit 3 shutdown, and about 19 hours after the explosion at Unit 3.

Table 1. Unit 1 Timeline

Date and time	Time after scram [hr]	Event
3/11 14:46	0.00	Earthquake; Reactor scrammed
3/11 14:47	0.02	MSIVs* close due to loss of instrument power, loss of normal heat sink
3/11 14:52	0.10	Isolation Condensers automatically starts (Train A and B)
3/11 15:03	0.28	Isolation Condensers (Train A and B) manually stopped to control cool down rate
3/11 15:07	0.35	Containment A and B spray systems activated
3/11 15:17	0.52	Isolation condenser train A manually started
3/11 15:19	0.55	Isolation condenser train A manually stopped
3/11 15:24	0.63	Isolation condenser train A manually started
3/11 15:26	0.67	Isolation condenser train A manually stopped
3/11 15:27	0.68	First tsunami wave hits
3/11 15:32	0.77	Isolation condenser train A manually started
3/11 15:34	0.80	Isolation condenser train A manually stopped
3/11 15:35	0.82	Second tsunami wave hits
3/11 15:41	0.92	Station Blackout; containment sprays stopped
3/11 18:18	*3.53*	*Isolation condenser train A manually started (not implemented in the model)*
3/11 18:25	*3.65*	*Isolation condenser train A manually stopped (not implemented in the model)*
3/11 21:30	*6.73*	*Isolation Condenser train A manually started (not implemented in the model)*
3/12 5:46	15.00	Fresh water injection from fire water pump starts, 80,000 liters injected by 14:53
3/12 9:05	*18.32*	*Drywell venting attempted (model assumes no venting)*
3/12 11:00	*20.23*	*Isolation condenser train A manually stopped (not implemented in the model)*
3/12 14:30	*23.73*	*Wetwell vented using portable generator and air compressor (model assumed vent value re-closure consistent with TEPCO wetwell pressure data)*
3/12 14:53	24.12	Fresh water injection stopped due to running out of fresh water. 80 ton total injection
3/12 15:36	24.83	Hydrogen explosion in the reactor building
3/12 19:04	28.30	Seawater injection from the firewater system starts
3/14 0:00	57.20	Seawater injection from the firewater system ends
3/15 0:00	81.20	Seawater injection from the firewater system starts
3/15 14:36	96.00	End of simulation

* MSIVs are main steam-line isolation valves

Table 2. Unit 2 Timeline

Date and time	Time after scram [hr]	Event
3/11 14:46	-0.05	Earthquake
3/11 14:47	0.00	Scram
3/11 14:50	0.05	RCIC starts
3/11 14:51	0.06	RCIC stops
3/11 15:00	0.22	RHR starts wetwell cooling
3/11 15:02	0.25	RCIC starts
3/11 15:27	0.67	Tsunami wave
3/11 15:28	0.68	RCIC stops
3/11 15:27	0.80	Tsunami wave
3/11 15:36	0.82	RHR stops
3/11 15:39	0.87	RCIC starts
3/11 15:41	0.90	Station blackout
3/12 4:20	13.55	RCIC suction - wetwell
3/14 13:25	*66.80*	*RCIC stops (assumed)*
3/14 16:34	*73.78*	*Seawater injection ready (ignored)*
3/14 18:06	75.32	RPV depressurizes via SRV 1
3/14 19:20	*76.55*	*Seawater injection stops (ignored)*
3/14 19:54	*77.12*	*Seawater injection starts (TEPCO start time)*
3/14 21:00	*78.22*	*WW vent operation (model assumes no venting)*
3/14 21:20	78.55	SRV 2 opens
3/14 23:00	80.22	SRV 2 closes
3/15 00:02	*81.25*	*D/W vent operation (model assumes no venting)*
3/15 14:00	95.22	SRV 2 opens
3/15 14:47	96.00	End of simulation

Table 3. Unit 3 Timeline

Date and time	Time after scram (hr)	Event
3/11 14:46	-0.05	Earthquake
3/11 14:47	0.00	Reactor scram
3/11 15:05	0.30	RCIC starts
3/11 15:25	0.63	RCIC stops
3/11 15:27	0.67	1st tsunami wave
3/11 15:35	0.80	2nd tsunami wave
3/11 15:38	0.85	Loss of AC power
3/11 16:03	1.27	RCIC starts
3/12 11:36	20.8	RCIC stops
3/12 12:35	21.8	HPCI starts
3/12 21:30	30.7 – 35.9	DC battery depletion
3/13 02:42	35.9	HPCI stops
3/13 07:39	*41.0*	*Containment sprays started (neglected)*
3/13 8:55	*42.1 – 42.35*	*RPV depressurizes via SRV (indeterminate)*
3/13 9:17	*41.8 – 42.5*	*S/C**vent open (indeterminate) (1)*
3/13 9:23	42.6	Freshwater injection starts
3/13 11:17	44.5	S/C vent close (1)
3/13 12:23	45.6	Freshwater injection ends
3/13 12:41	45.9	S/C vent open (2)
3/13 13:11	46.4	Seawater injection begins (1)
3/13 14:11	47.4	S/C vent close (2)
3/13 20:59	54.2	S/C vent open (3)
3/13 22:17	55.5	Seawater injection ends (1)
3/14 0:59	58.2	S/C vent close (3)
3/14 3:23	60.6	Seawater injection begin (2)
3/14 10:23	67.6	S/C vent open (4)
3/14/ 11:01	68.2	Reaction building explosion / seawater injection ends (2)
3/14 11:45	69.0	S/C vent close (4)
3/14 16:29	73.7	Seawater injection begins (3)
3/14 16:39	73.9	S/C vent open (5)
3/14 22:15	79.5	S/C vent close (5)
3/15 14:47	96.0	End of simulation

** S/C refers to suppression chamber (i.e., wetwell).

3.4   Reactor Vessel and Coolant System

Excluding the core region, the RPV is represented by seven hydrodynamic control volumes, nine flow paths, and 24 heat structures. Nodalization for the core region between the core top guide and the bottom of active fuel are described in detail in Section 3.5.1. Figure 9 illustrates the reactor vessel nodalization by comparing the actual vessel design (on the left) to the MELCOR control volume representation (on the right). In Figure 10, control volumes are indicated by "CV" followed by the three-digit control volume number, and flow paths are indicated by "FL" followed by the three-digit flow path number.

Appended to the MELCOR control volumes representation of the RPV shown in Figure 9 are several additional control volumes and flow paths representing a variety of reactor support systems, such as:
- reactor recirculation piping,
- main feedwater and steam lines,[4] and
- connections to emergency coolant injection and heat removal systems.

The MELCOR representation of the entire reactor coolant system is illustrated in Figure 10. Collectively, these ancillary systems permit the model to properly calculate steady state, as well as a wide variety of transient conditions.

3.4.1 Implementation of Fukushima Information

The dimensions of the RPV were taken from a limited set of proprietary TEPCO drawings and from proprietary RPV information provided by TEPCO. Where information was lacking, SOARCA MELCOR BWR/4 Mk-I model data (i.e., information from a reactor of similar design) were used either directly or in the process of developing scaled surrogate values.

Additional changes were made to the BWR/4 Mk-I reactor model to include Fukushima-specific systems and/or modify systems to incorporate Fukushima-specific information. This includes extensive modifications that model the unique accident sequences for each unit, such as important events and operator actions.

---

[4] Note that each steam line is individually represented in the Fukushima reactor models.
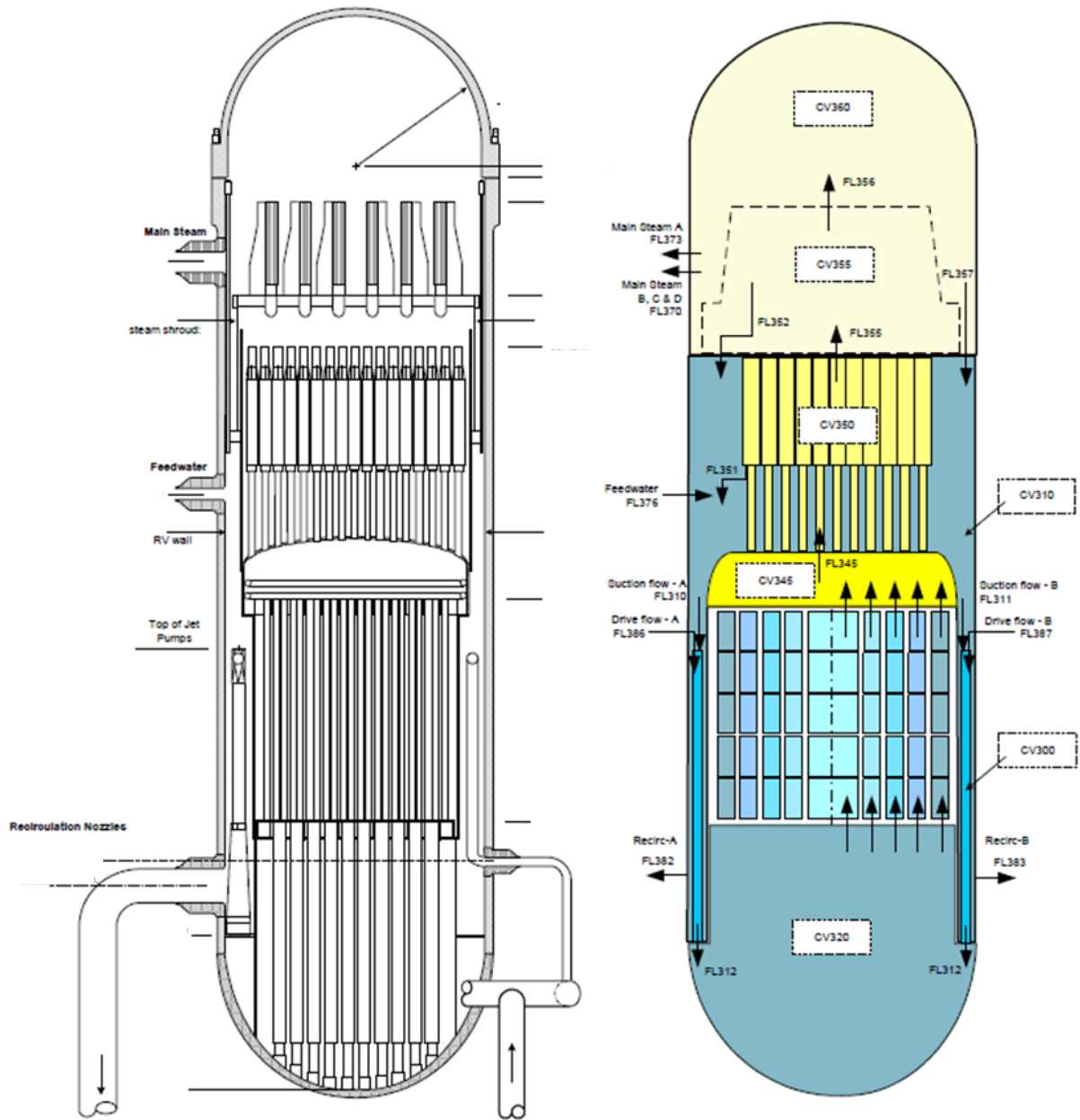
Figure 9. Reactor Vessel Cross-Section Detail and MELCOR Hydrodynamic Nodalization.
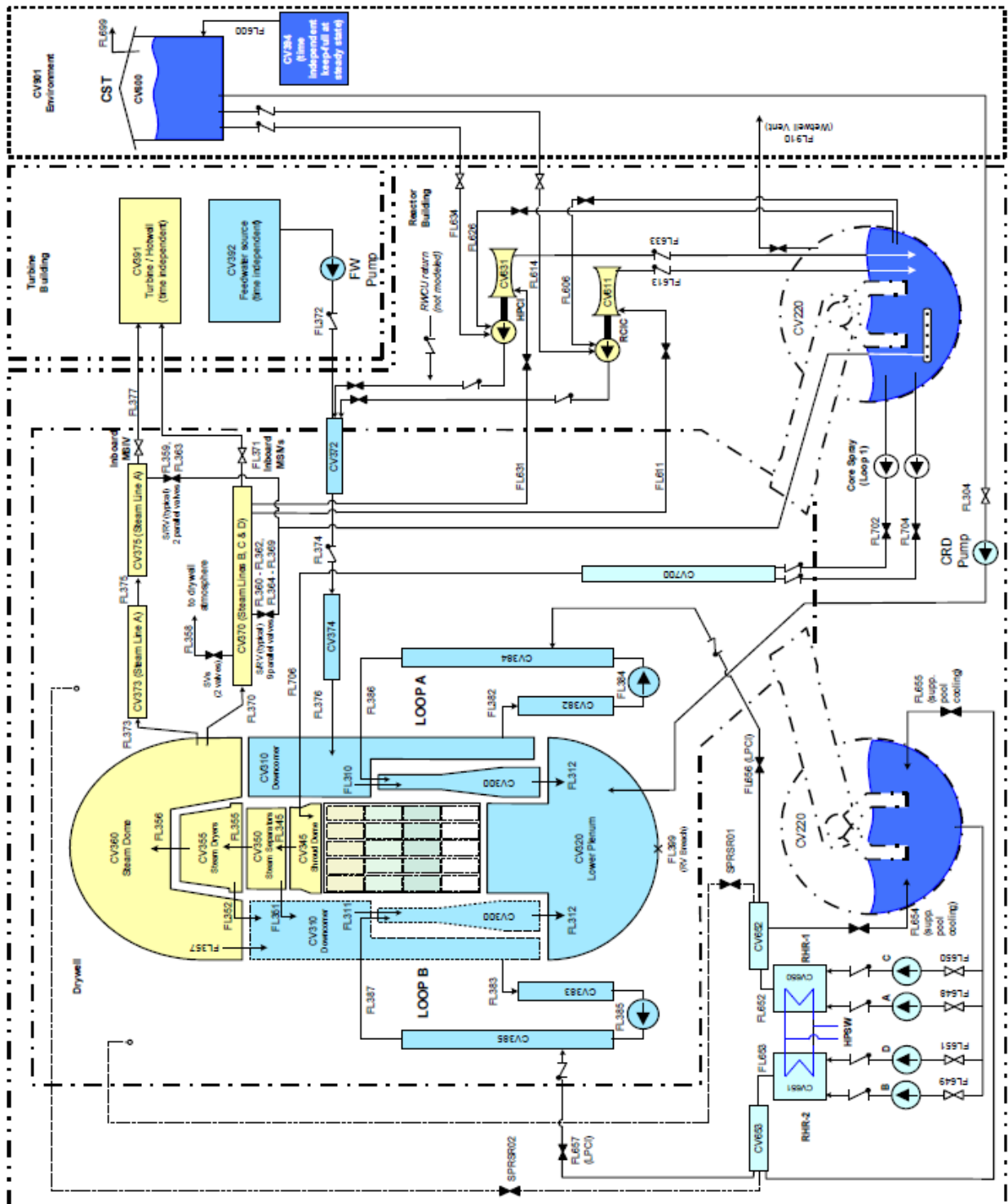
Figure 10. Spatial Nodalization of Reactor Pressure Vessel and Coolant System.

3.4.1.1 Isolation Condensers (Unit 1)

The Unit 1 reactor is equipped with isolation condensers. Each IC has a rated capacity of 42.2 MW [44]. The capacity is calculated by multiplying the rated capacity by a pressure-based utility factor [45] (see Table 4) to account for the decrease in IC efficiency at lower pressures. In the model, a simple negative energy source function (equal to the 84.4 MW times the utility factor) is used to simulate the operation of the ICs.

Table 4. IC Utility Factor

Pressure [Pa][5]	Utility Factor [-]
3.26E+06	0.12
4.13E+06	0.33
5.07E+06	0.55
6.15E+06	0.80
7.24E+06	1.00

The IC operation as specified by the Unit 1 timeline was modified. For the last two operating periods (3.53 – 3.65 hr; 6.73 – 20.23 hr), IC operations were not included in the Unit 1 analysis due to the brevity of the first operation period and the model prediction of RPV depressurization prior to the last operation of the IC. Furthermore, the presence of non-condensable gases and aerosols (as predicted by the MELCOR model) is assumed to largely disable the ICs' functionality.

3.4.1.2 High-pressure Coolant Injection System (Unit 3)

The HPCI is a high-pressure steam-driven pump system. The HPCI turbine continually draws steam from the steam lines and discharges it to the S/C pool. The mass flow rate of the steam through the turbine depends on the pressure in the RPV, the density of steam in the steam lines, and the pressure difference between the RPV and wetwell. The turbine operates continuously in this manner throughout the HPCI operation.

The HPCI injection maintains the downcomer water level within an upper and lower range relative to an "instrument zero" water level. Once the downcomer water level falls below the low level, the HPCI injects water at full capacity from the CST into the feedwater lines. If the CST depletes, the HPCI uses the wetwell pool to inject water into the feedwater lines. Since the HPCI injection is at full capacity, it rapidly fills the downcomer water level to the upper bound cut-off for HPCI injection, where the full HPCI flow is then diverted to the wetwell via a minimum bypass flow line in the SNL model. In this fashion, the HPCI can simultaneously maintain RPV water level and lower containment pressure (if CST is available). However, new information released after the completion of the SNL analyses suggests that HPCI injection for Unit 3 was throttled using the test line instead of the minimum flow line. Also, containment sprays are said to have depressurized the containment from 22 to 30 hours instead of wetwell cooling by the HPCI minimum flow line. This new information is not incorporated in the SNL Unit 3 model in Section 4.3.

---

[5] A utility factor of 0.12 is used for pressures less than 3.26E+06 Pa

3.4.1.3   Reactor Core Isolation Cooling System (Unit 2 and Unit 3)

The RCIC operates by extracting steam from a main steam line to drive a turbine mechanically linked to the injection pump. The exhaust steam from the turbine is transferred to the suppression pool. Pump suction is initially aligned to the CST and may be redirected to the suppression pool as was the case in Unit 2. RCIC injection can be adjusted by the operators by repositioning the governor valve located on the turbine and/or the test-line valve position. Neither operational state is specifically addressed in the available documentation; therefore, a RCIC pump injection controller was imposed to reproduce the available reactor water level data. This allows the reactor water inventory to be relatively correct prior to subsequent events occurring, assuming high veracity of the available data, such as safety system actuation or core degradation.

In Unit 2, the RPV pressure and level data suggests RCIC deterioration or failure beginning at 66.8 hr, due to the observed increase in pressure and decrease in level from available data. The RCIC failure time was reduced from the timeline-indicated value to the earliest indication of deterioration. RCIC failure is modeled by halting steam draw and water injection. Depending on the failure mechanism, RCIC may have continued to allow steam to flow from the RCS.

3.4.1.4   Fresh Water and Seawater Injection (Unit 1, Unit 2, and Unit 3)

Water (fresh water and/or seawater) injection rates were taken from TEPCO data. The injection rates are presented in Figure 11, Figure 12, and Figure 13 for Unit 1, Unit 2, and Unit 3, respectively. Their timings are also reflected in the timelines for the units (see Table 1, Table 2, and Table 3).

The nominal injection rates shown in Figure 11 are used in Unit 1.

For Unit 2 there was an initial period of seawater injection. However there is uncertainty regarding when the injection started, when it stopped (due to the pump being out of fuel), and when it was restarted (see Table 2). Therefore, the TEPCO-provided injection rate timing was used in place of the injection rate timings defined in the timeline (see Figure 12).

Nominal injection rates shown in Figure 13 are used for the Unit 3 fresh water injection. The seawater injection for Unit 3 is modeled using a surrogate pump curve (specifically, W.S. DARLEY & Co. Pump Model 2BE10BS). The pump curve allows RPV pressure feedback to influence the injection rate. A similar injection model was looked at for the Unit 1 and Unit 2 models but was not implemented in time for this report.
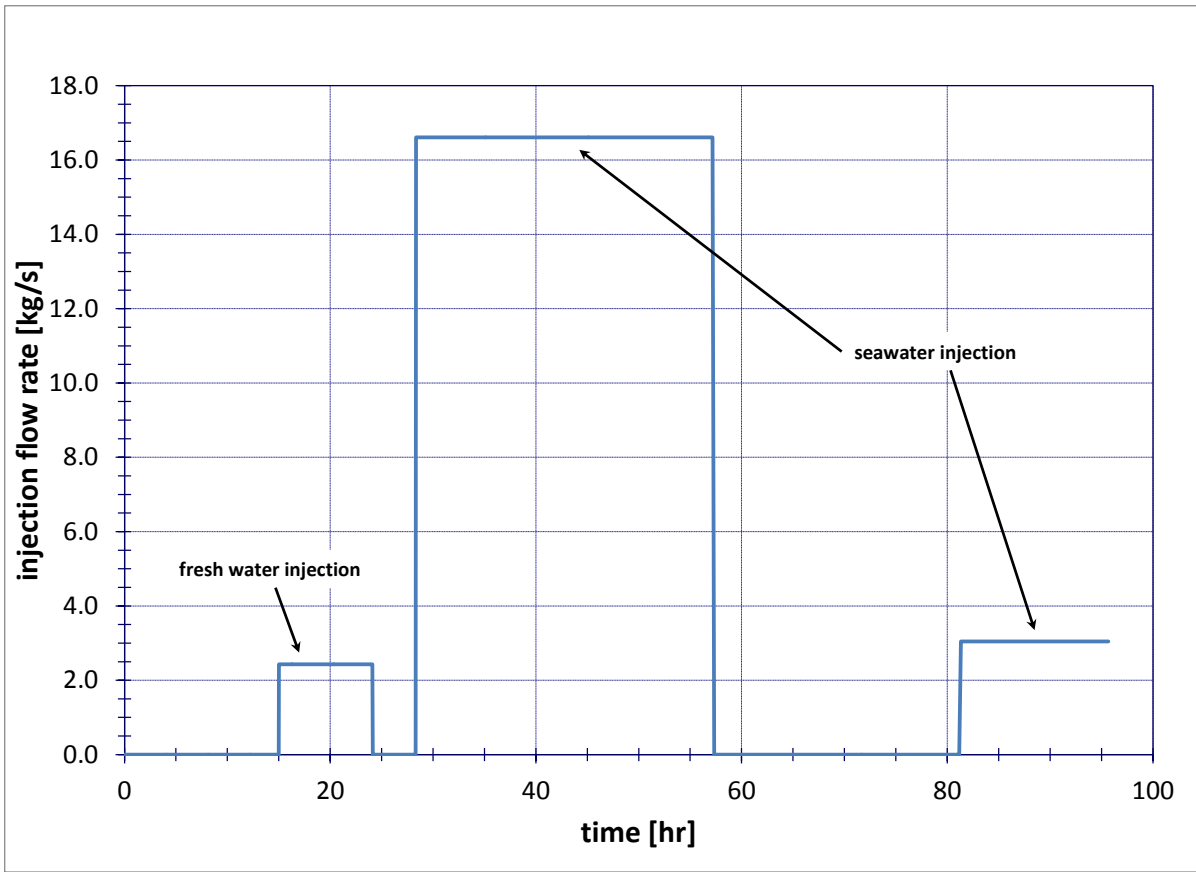
Figure 11. **Nominal TEPCO Fresh Water and Seawater Injection Rates Used in the Unit 1 MELCOR Model.**
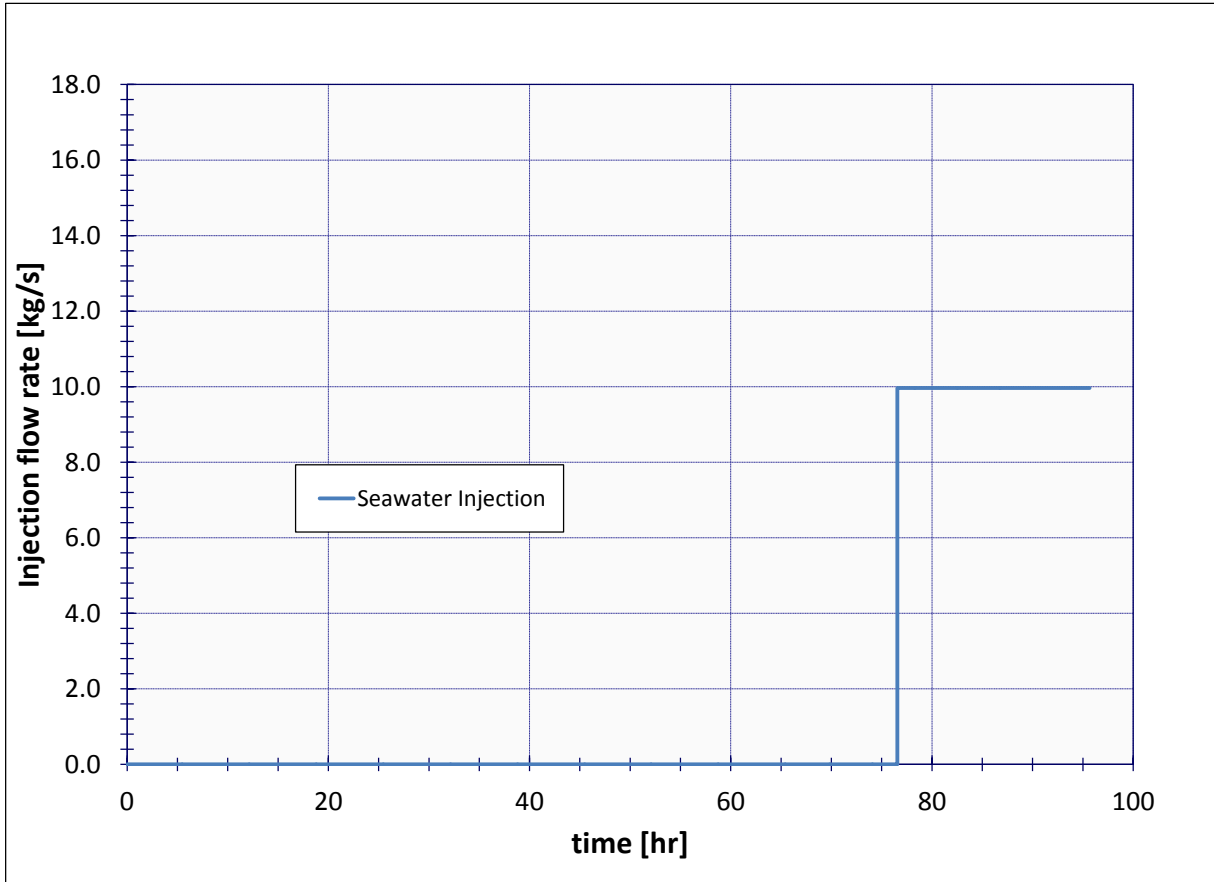
Figure 12. Nominal TEPCO Seawater Injection Rates Used in the MELCOR Unit 2 Model.
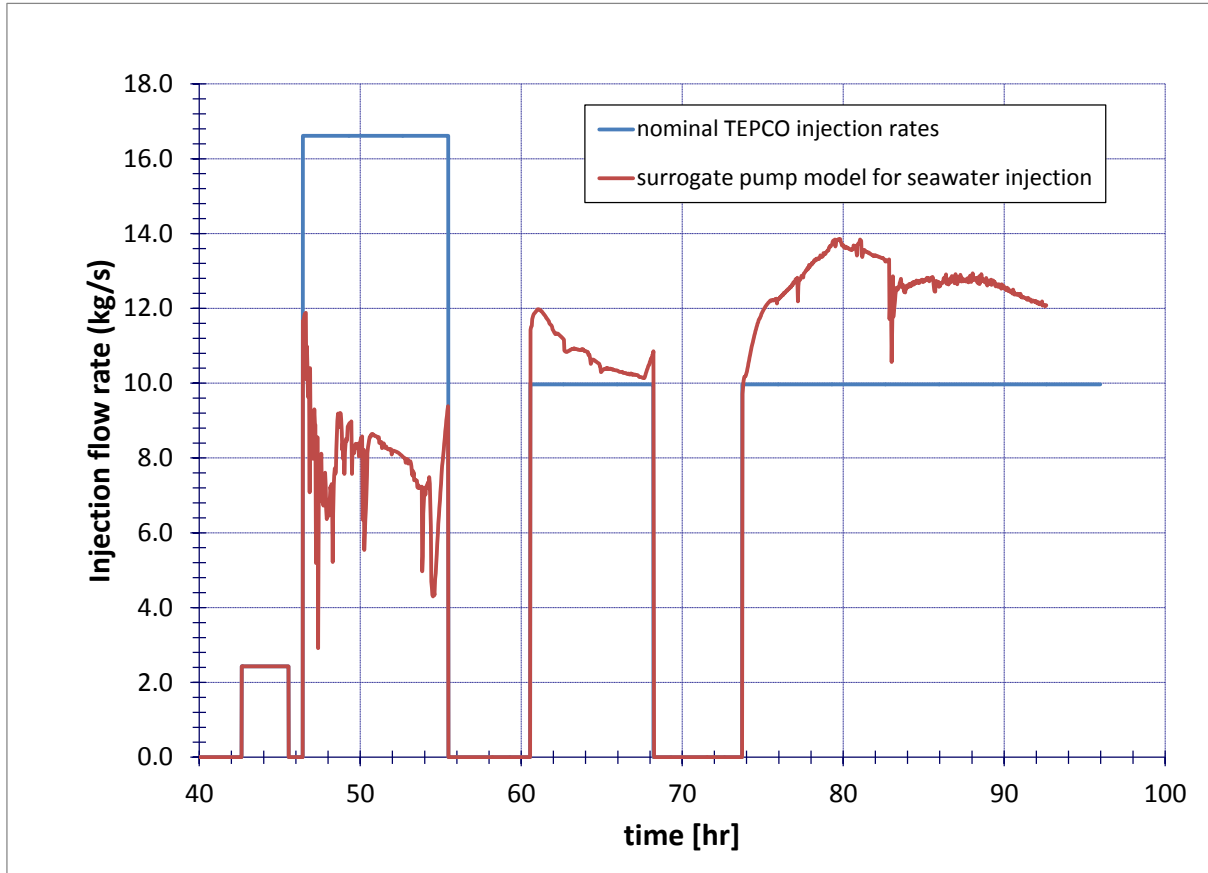
Figure 13. Unit 3 Nominal TEPCO Injection Rates and Injection Rates Using a Surrogate Pump Model.

3.5   In-Vessel Structures and Reactor Core

Structures within the RPV are described in the next three sections. First, Section 3.5.1 describes the general configuration of the spatial nodalization of the core and structures below the core. Certain aspects of this nodalization, and some characteristics of the MELCOR model of material degradation, are tailored to the unique design features of BWRs. These are briefly summarized in Section 3.5.2. Finally, Section 0 mentions the manner in which in-vessel structures above the core are treated in the MELCOR model.

3.5.1   General Configuration of MELCOR In-Vessel Nodalization

In MELCOR, the core region includes a cylindrical space extending vertically downward along the inner surface of the core shroud from the core top guide to the reactor vessel lower head. It also extends radially outward from the core shroud to the hemispherical lower head in the region of the lower plenum below the base of the downcomer, preserving the curvature of the lower head from this point back to the vessel centerline.

The core and lower plenum regions are divided into concentric radial rings and axial levels. Each core cell may contain one or more core components, including fuel pellets, cladding, canister walls, supporting structures (e.g., the lower core plate and control rod guide tubes), non-supporting structures (e.g., control blades, the upper tie plate, and core top guide) and once fuel damage begins, particulate and molten debris.

The spatial nodalization of the core is shown in Figure 14. The entire core and lower plenum regions are divided into six radial rings. The radial distance between each of the five rings is not uniform. Radial ring 6 represents the region in the lower plenum outside of the core shroud and below the downcomer. Ring 6 exists only at the lowest axial levels in the core model.

The core and lower plenum are divided into 17 axially stacked levels. The height of a given level varies but generally corresponds to the vertical distance between major changes in the flow area, structural materials, or other physical features of the core (and below core) structures. Axial levels 1 through 5 represent the open space and structures within the lower plenum. Initially, this region has no fuel and no internal heat source but contains a considerable mass of steel associated with the control rod guide and in-core instrument tubes. During the core degradation process, the fuel, cladding, and other core components displace the free volume within the lower plenum as they relocate downward in the form of particulate or molten debris.
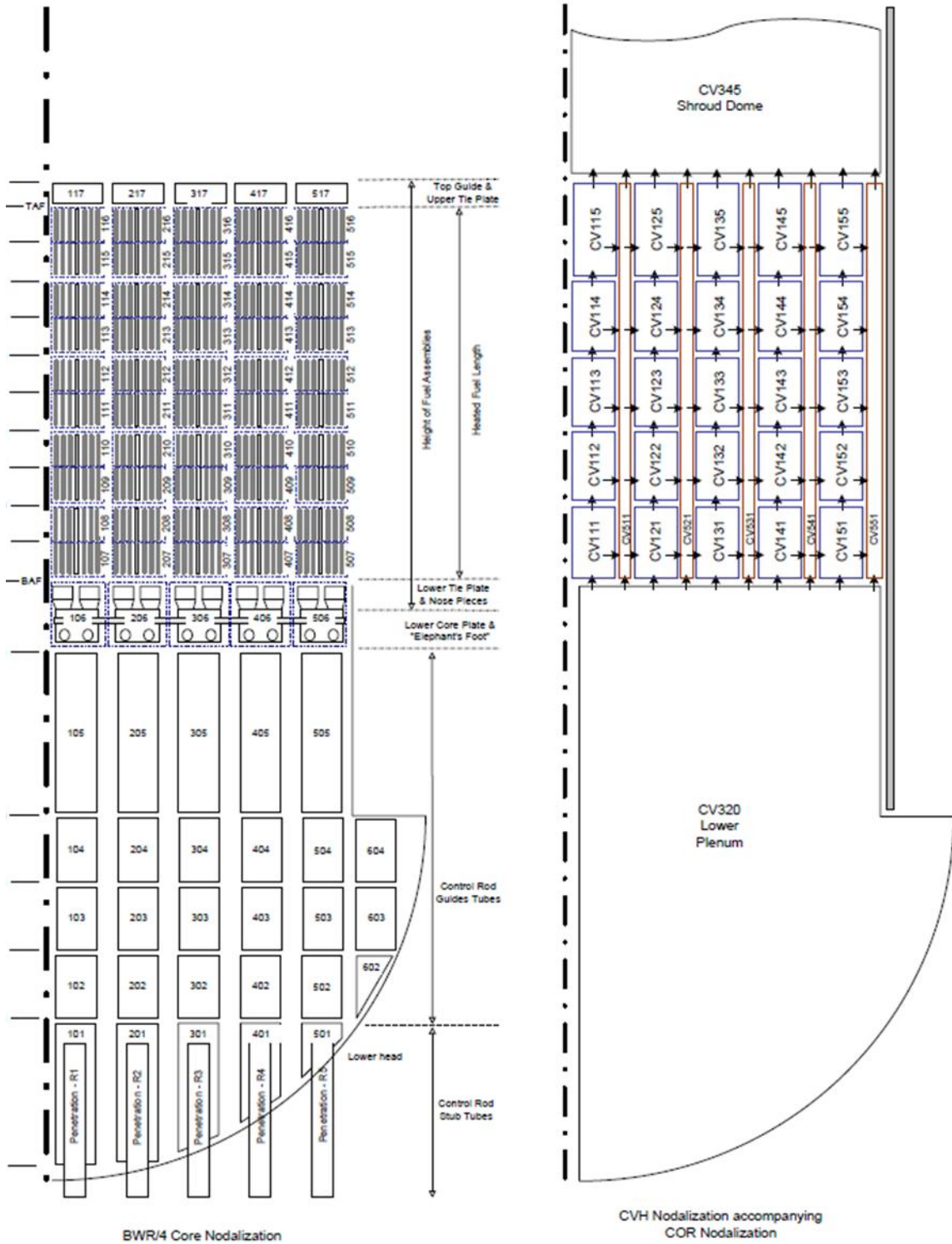
Figure 14. Spatial Nodalization of the Core and Lower Plenum.

Axial level 6 represents the steel associated with fuel assembly lower tie plates, fuel nose pieces, and the lower core plate and its associated support structures. Particulate and molten debris formed by failed fuel, canister, and control blades above the lower core plate will be supported at this level until the lower core plate yields. Axial levels 7 through 16 represent the active fuel region. All fuel is initially in this region and generates the fission and decay power. Axial level 17 represents the nonfuel region above the core, including the top of the canisters, the upper tie plate, and the core top guide.

3.5.2 Treatment of Unique Design Features of a BWR Core

Several design features of the BWR core, and associated structures located below the core, merit special attention in modeling severe accidents. These are not discussed exhaustively here, but a few are mentioned to illustrate the way in which the modeling approach to this type of reactor differs from the approach used to model a Pressurized Water Reactor (PWR), or other designs.

3.5.2.1 Fuel Channels and Control Blades

Each BWR fuel assembly in the core is shrouded by a solid rectangular channel box, which confines coolant flow to that single assembly. Therefore, cross-flow between adjacent assemblies is not possible in a BWR unless a pair of adjacent channel boxes fails. Figure 15 illustrates this configuration for a module of four fuel assemblies, which surrounds a single control blade. Unlike control rod clusters in a typical PWR, which are inserted directly into certain fuel assemblies, the control blade in a BWR is inserted into the interstitial space between (and outside) adjacent fuel channels.

The MELCOR hydrodynamic model for this configuration recognizes the vertical constraint placed on flow through the core unless or until structural damage to fuel channels occurs. The in-core heat transfer model also accounts for lateral (or radial) differences in the materials adjacent to "bladed" sides of a channel (i.e., sides neighboring a control blade) versus "unbladed" sides, which communicate only with a neighboring fuel channel. As fuel temperatures rise in the core during an accident simulation, axial and radial heat transfer calculations account for oxidation of Zircaloy fuel cladding and the Zircaloy channels. Separate failure criteria are used to ascertain when highly oxidized fuel rods and highly oxidized channels can no longer maintain their normal upright configuration and collapse into particulate debris.

An additional model has been added to characterize the structural integrity of the fuel rods under highly degraded conditions. The new model acknowledges a thermal-mechanical weakening of the oxide shell as a function of time and temperature. As the local cladding oxide temperature increased from the Zircaloy melting temperature (represented as 2098 K in MELCOR) towards 2500 K, a thermal lifetime function accrues increasing damage from 10 hours to 1 hour until a local thermo-mechanical failure. Similar time-at-temperature failure criteria are applied to oxidized channel boxes, but at any point in time, channel temperatures and degree of material oxidation differ from those associated with adjacent fuel assemblies. Therefore, the collapse of channel boxes into particulate debris typically occurs at a different time from the collapse of fuel assemblies in the same radial ring of the core.

Radial cross-flow from one ring of the core nodalization to a neighboring ring is possible if the channels in both rings melt or collapse to open a flow path in the radial direction. As indicated in the nodalization diagram on the right-hand side of Figure 14, radial flow out of the interior region of the channels within a particular ring must first flow into the neighboring core bypass area (i.e., the space between channels normally occupied by control blades.) If the stainless steel clad control blades and Zircaloy channel boxes in the neighboring fuel channel also melt or collapse, fluid could continue to flow radially out of the bypass region into the neighboring channel, and so on. Circular natural circulation flow patterns within the core region can, therefore, only occur after a sufficient number of channel boxes (properly distributed) melt, or otherwise relocate downward, creating open space in the radial direction.

The axial nodalization of the core is designed, in part, to account for changes in material composition and mass along the axial length of a typical fuel assembly. For example, Figure 15 does not explicitly show the fact that some BWR fuel assembly designs (modern 10×10 assemblies, for example) incorporate fuel rods of different lengths within a single assembly. As a result, the amount of UO_2, and other constituents can differ at the top of an assembly from the bottom. Discrete locations of fuel rod spacers along the axial height of an assembly also affect local Zircaloy mass. The distribution of material mass within the axial nodalization of the core takes these variations into account.

3.5.2.2   Lower Plenum Structures

The COR Package in MELCOR, which models the oxidation, melting, and downward relocation of overheated core materials, extends downward below the lower core plate into the RPV lower plenum. Molten core debris that flows, or particulate debris that falls, under gravity into the lower plenum collects as a mixed debris bed on the inner surface of the lower head. In a BWR, this region is filled with a forest of vertical cylinders that house the drive mechanisms for core control blades as well as in-core instrumentation. Figure 16 depicts a typical configuration of a control rod guide tube (CRGT) in this region of the RPV.

The MELCOR model accounts for the structural mass and surface area of the CRGTs, which participate in heat transfer within the debris bed that accumulates around them. The physical space occupied by intact CRGTs displaces volume available for debris to occupy in the lower plenum.[6] Therefore, debris accumulates to an elevation higher than the value that would be calculated by neglecting the volume of the CRGTs. Debris heat transfer and continued oxidation of metallic components within the lower head account for the heat capacity and stainless steel composition of the CRGTs. The CRGTs are modeled as vertical columns, which fail (buckle) when load carried by the CRGTs exceeds their residual strength, which decreases as heat is transferred from core debris. The calculation of CRGT integrity is performed on a radial ring-by-ring basis, with five rings in the model as indicated in the diagram on the left-hand side of Figure 14.

---

[6] Debris relocating to the lower plenum is assumed to accumulate in the volume between intact CRGTs, and not within them, based on observations from melt relocation experiments for BWR geometries (e.g., see NUREG/CR-6527).

Notable BWR Core Design Features

1. Core top guide

3. Fuel assembly upper tie plate

6. Channel box
7. Cruciform control blade
8. Fuel rod
9. Spacer
10. Core plate

Figure 15. Module of Four BWR Fuel Assemblies and Associated Channel Boxes.
(Illustration courtesy of General Electric)
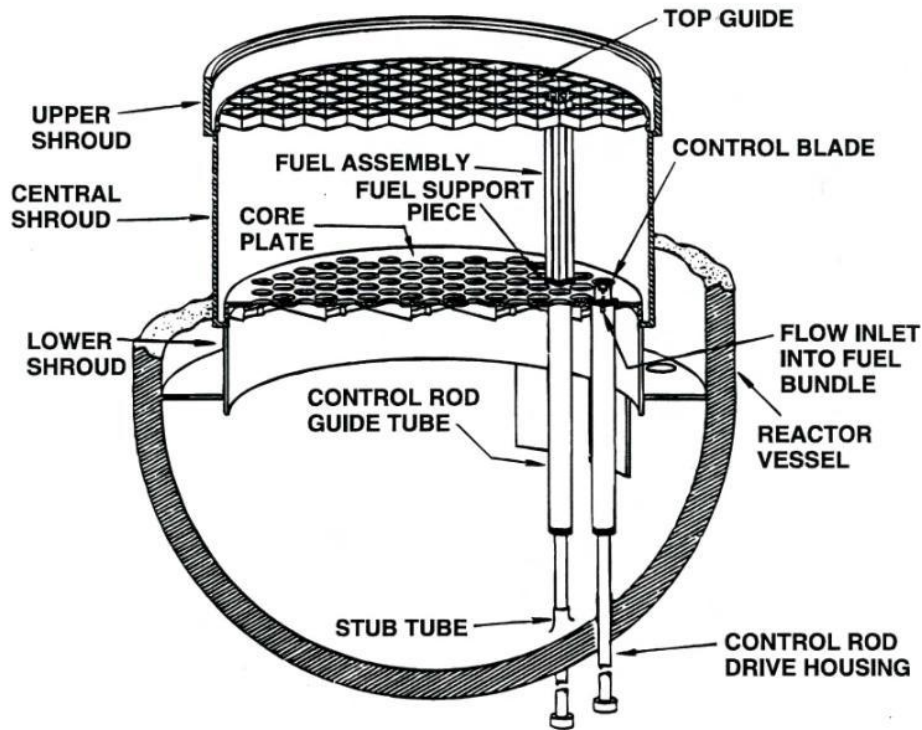
Figure 16. BWR Lower Plenum Structures.

Collapse of the CRGTs has two important effects on the composition and mass of debris in the lower plenum prior to lower head failure. The first, and most important, is that all core rested on or positioned above the lower core plate within that ring collapses as particulate debris into the lower plenum. This fragmented core debris is not uniformly mixed with the debris bed already in the lower plenum, but is added to the top of the debris bed according to the spatial nodalization shown in Figure 14. Therefore, the material composition and porosity of debris within the debris bed can vary considerably within the two-dimensional spatial nodalization of the lower plenum. Second, the material composition of the CRGTs themselves is added to the debris bed at the location where the intact components were originally positioned. This has the tendency to increase the surface area of metallic components in the lower plenum because the surface area of particulate debris is generally higher than the surface area of the intact CRGT columns.

Thermal interactions between molten core debris and penetrations through the lower head are not explicitly modeled in the calculations. A simple, lumped parameter model for bulk heat transfer to a penetration assembly is available in MELCOR; but the model is not sufficiently refined to calculate multi-dimensional heat transfer and phase change that would occur in the neighborhood of a CRGT or instrument penetration, or to calculate molten material drainage into an open penetration, as could occur in a BWR RPV drain line. This limitation in MELCOR, combined with observations from several large-scale experimental programs that examined failure mechanisms of lower heads with penetrations [4], led to a modeling approach that focuses on creep rupture of the hemispherical lower head as the dominant mechanism for lower head failure. This approach is supported by the observation that none of the MELCOR calculations predicts elevated RPV pressure at the time debris temperatures are sufficiently high to challenge lower

head integrity (each reactor vessel at Fukushima depressurized before core relocation is predicted by MELCOR). That is, detailed analysis of lower head penetration failure [27] suggests internal pressures greater than those obtained in the calculations are necessary to eject a penetration assembly from the lower head.

3.5.3   In-Vessel Structures above the Core

The COR Package in MELCOR does not explicitly model the mechanical response (i.e., potential material melting or collapse) or oxidation of structures above the core top guide. This is an inherent limitation in the architecture of MELCOR. As indicated in Figure 9, several large steel structures. which can absorb a substantial amount of energy carried away from the core during the early periods of core damage. are positioned above the core. They also represent a significant surface area for deposition of fission product aerosols released from the core. These structures most notably include the upper shroud dome, steam dryers, and separators.

The thermal response and fission product deposition properties of these structures are modeled using one-dimensional heat structures. This modeling approach, combined with the nodalization and connectivity of control volumes above the core, provides sufficient spatial resolution to calculate the time-dependent temperature response of each structure. A limitation of this modeling approach is that the mechanical response of these structures, material melting, oxidation, or collapse, and the potential for incorporation of steel into core debris, is not modeled. Changes in the flow area through this region of the RPV that might be caused by changes in structure geometry are also not modeled.[7]

3.5.4   Implementation of Fukushima Information

There was insufficient information available regarding in-vessel and core structures (e.g., fuel assembly type, assembly layout, control blades, guide and instrument tubes, upper and lower core plates, shroud dome, steam separators, steam dryers, etc.) to develop MELCOR input. As a surrogate for Fukushima-specific fuel assembly data, GE 8×8 assembly data (obtained and developed into a form sufficient for MELCOR input as part of previous Peach Bottom analyses) were used. Surrogate information for the in-vessel structures was developed based in information from the SOARCA MELCOR BWR/4 Mk-I model.

Near the end of the project, proprietary assembly layout information was received from TEPCO. The ring nodalization in the models was modified based on this information.

3.5.4.1   Modification to Bypass Control Volumes

During model development, it was found that the initial bypass volume nodalization (five bypass control volumes (CVs) in each radial ring) was causing a significant decrease in the model time-step size, resulting in very long run times (on the order of two to five weeks to complete a 96-hr simulation). In order to decrease model run-time, the bypass control volumes were merged (one bypass CV in each radial ring).

---

[7] In the Fukushima accident progressions, melting or collapse of these structures would occur only after core damage and relocation, hence would not affect these processes.

3.6 Primary Containment and Reactor Building

The primary containment of the Mk-I design consists of two separate regions: a drywell and a wetwell. As shown in Figure 17, each region is explicitly represented in the MELCOR model with distinct hydrodynamic control volumes, flow paths, and heat structures to preserve the geometric configuration and major functional features of the Mk-I design (e.g., steam pressure suppression, fission product scrubbing, and surface deposition). The drywell is further divided into four connected volumes to account for non-uniformities in the temperature and composition of the atmosphere during late phases of a severe accident.

The internal volume, airflow flow pathways, and structures of the reactor building are modeled in considerable detail as illustrated in Figure 18 and Figure 19. The reactor building fully encloses the primary containment and participates in the release pathway of fission products from the containment to the environment by offering a large volume within which an airborne radionuclide concentration can be diluted by expansion into and mixing with the building atmosphere.
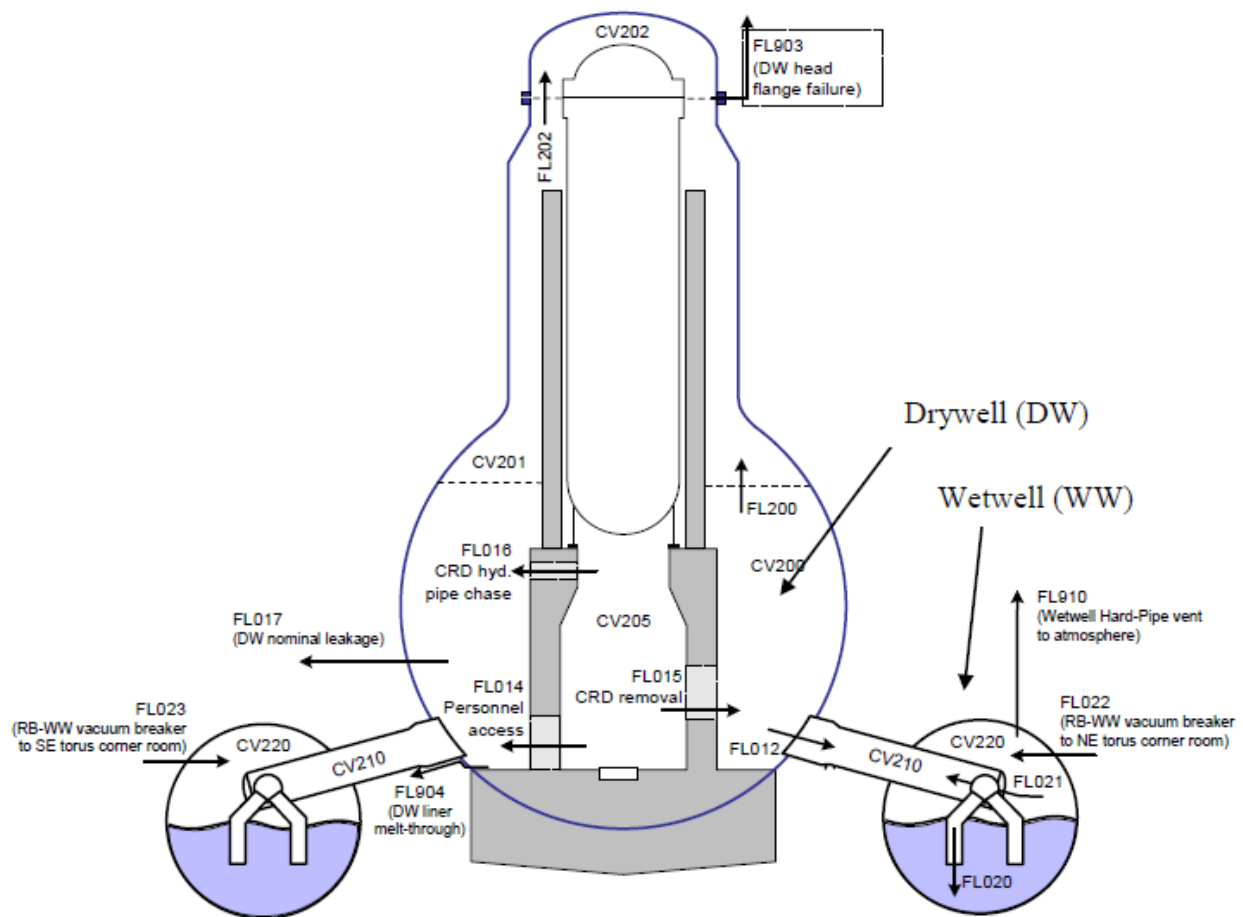
Figure 17. Hydrodynamic Nodalization of the Primary Containment.
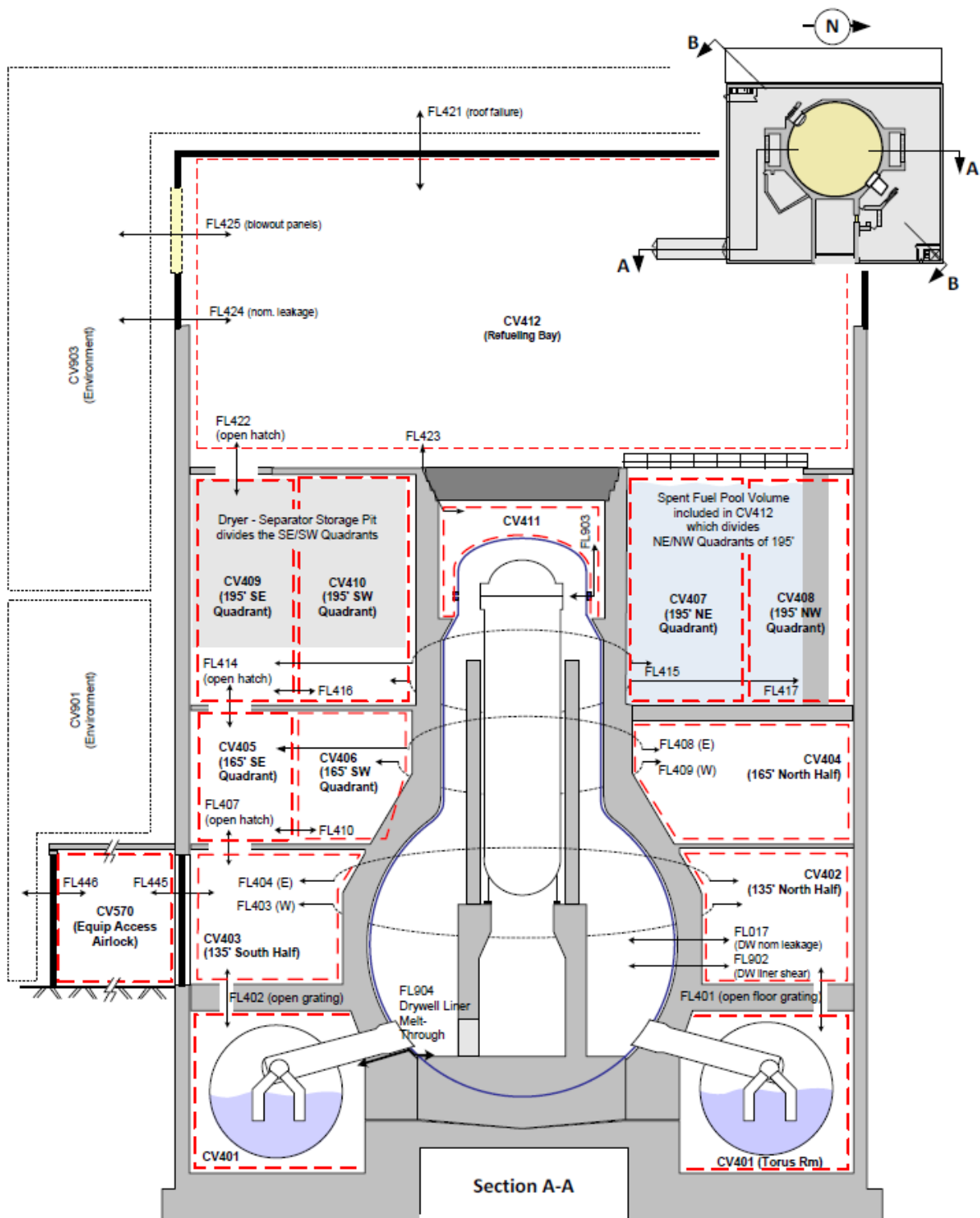
Figure 18. Hydrodynamic Nodalization of the Reactor Building (A).
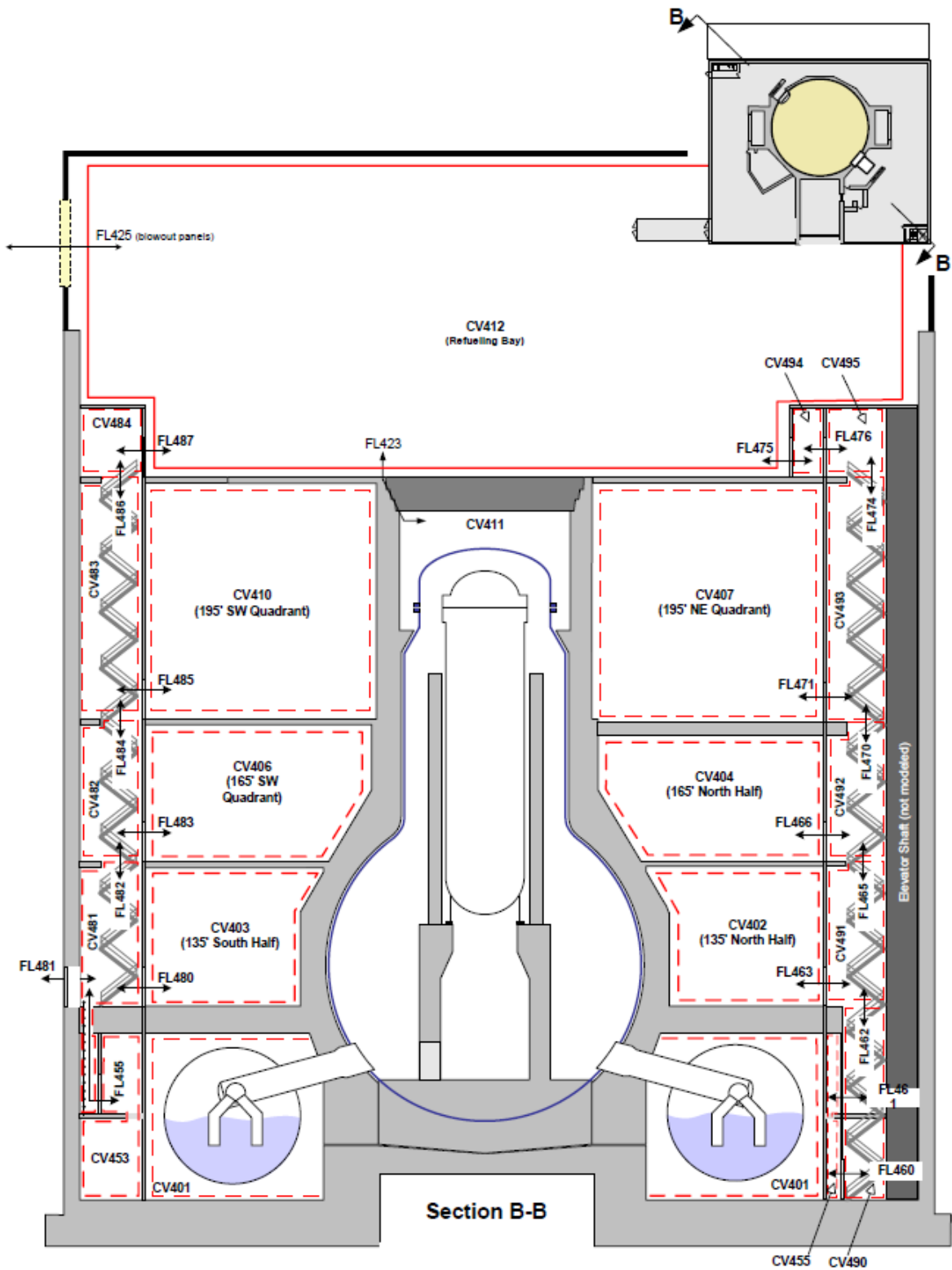
Figure 19. Hydrodynamic Nodalization of the Reactor Building (B).

The airborne concentration of fission product aerosols within the reactor building is attenuated by gravitational settling and other natural deposition mechanisms. The building is also equipped with a ventilation system with aerosol and charcoal filters, which would greatly aid in reducing an airborne radioactive release. However, these systems would not be available during the particular accident scenarios examined in this work because of a loss of electrical power or other equipment failures. Therefore, the reactor building is occasionally referred to as a secondary containment, although it has a negligible capacity for internal pressure.

3.6.1 Implementation of Fukushima Information

The dimensions of the Unit 1, Unit 2, and Unit 3 containments were taken from a very limited set of proprietary TEPCO drawings.

Information at the level of detail needed to create the Fukushima reactor buildings in the Unit 1, Unit 2, and Unit 3 MELCOR models was not available. Instead, the reactor building as modeled in the SOARCA MELCOR BWR/4 Mk-I model was used. Minor modifications were made to the reactor building elevations consistent with the Fukushima reactor containments.

3.6.1.1 Drywell Head Lifting Pressure (Unit 1)

During the initial Unit 1 model development, it was noted that the MELCOR containment pressure results after RPV depressurization were consistently lower than the TEPCO containment pressure data. This was due to the drywell head beginning to lift, and hence venting the containment into the reactor building at a pressure of 82 psig (the value from the SOARCA BWR/4 Mk-I model). As no information is currently available regarding the functional relationship between the pressure difference across the drywell head and drywell head flange leakage area for Unit 1, the TEPCO containment pressure data between 12 and 24 hr (the period during which the containment pressure is constant and at a magnitude indicative of drywell head flange leakage) was used to calibrate the Peach Bottom drywell head flange leakage model to be consistent with the drywell head flange leakage conditions reflected in the TEPCO containment pressure data. It was determined that for Unit 1 the pressures in the pressure vs. flange open area relationship were 4 psig greater than in Peach Bottom characterization.

3.6.1.2 Drywell and Wetwell Venting (Unit 1)

In the Unit 1 timeline drywell venting is reported to have been attempted at 18.32 hr after reactor scram. However, examination of the TEPCO pressure data shows no drop in drywell pressure at this time (see Figure 30 in Section 4.1), and subsequently TEPCO has stated that venting did not occur. It appears that that while actions were taken to vent the drywell, they were unsuccessful. Therefore, this event is not implemented in the MELCOR model.

Wetwell venting (at 23.73 hr after reactor scram) is also reported in the Unit 1 timeline. The TEPCO pressure data do show a drop in wetwell pressure at this time. However, when this was implemented into the MELCOR model, the resultant pressure drop was much larger (down to 1 atm) than shown in the TEPCO pressure data. It is postulated that while wetwell venting did occur as reported in the timeline, it terminated before the containment completely depressurized.

To capture this, the wetwell venting was terminated in the model when the wetwell pressure was reduced to the value consistent with the TEPCO wetwell pressure data.

3.6.1.3   Drywell and Wetwell Venting (Unit 2)

Several attempts to perform venting were performed on-site for Unit 2, but given that no visible corresponding depressurizations of containment were observed in the TEPCO containment pressure data, vent operations were not included in the Unit 2 analysis.   While the venting attempts may have resulted in some limited release, the lack of impact of the venting on the containment pressure suggested limited flow and/or duration.

3.6.1.4   Wetwell Venting (Unit 3)

The MELCOR model initiates the first wetwell vent at 42.5 hours. The timing of the first wetwell vent must be precise in order to capture the timing and magnitude of the peak containment pressure. Venting before the RPV depressurizes results in MELCOR calculating pressures that do not agree with the TEPCO pressure data for the RPV and containment. The exact opening/closing timing for further venting actions is determined by closely examining the TEPCO data for the containment pressure in Unit 3 (i.e., the open and close times were chosen in an attempt to capture the peaks and valleys of the TEPCO data).

The wetwell vent for Unit 3 is modeled as an 8″ diameter flow path from the torus airspace to lower volume in the reactor building (the torus room). Gases released by wetwell venting were assumed to flow into to the torus room (see Figure 18) in the Unit 3 model because extensive damage was observed in the lower regions of the Unit 3 reactor building. The extent of damage near the base of the building may have resulted from combustible gases igniting in the lower compartments of the reactor building. Other potential ingresses to the reactor building exist, given the propensity for penetration failures as well as the general leakage between the containment and the reactor building. The nature of slow leaks that allow hydrogen to dissipate may have been preventative in producing combustible limits, which may support rapid hydrogen ingress. The common belief that Unit 4 received combustibles from the Unit 3 may suggest the ingress to the Unit 3 reactor building occurred through the reactor building's ventilation ducting as well. The ingress path remains unknown at the time of this report.

3.6.1.5   Containment Leakage (Unit 2)

Poor agreement was observed when comparing the TEPCO containment pressure data and the initial analyses of Unit 2, which utilized typical containment design leakage. A similar comparison can readily be made between Unit 2 and Unit 3 containment data, given each employed RCIC for the first 13 hr in relatively similar configurations, which demonstrate a significantly slower pressurization rate for Unit 2. To reconcile the difference between Unit 2 and Unit 3, as well as the initial Unit 2 analyses, a leak was postulated in the Unit 2 model to explain the suppressed pressure response within containment. After performing several analyses varying the potential leak sizes and characteristics, a 2-in-diameter-equivalent leak path, which provided reasonable results, was incorporated into the model. The 2-in-diameter-equivalent leak path connects the vapor spaces of the suppression chamber to the torus room.

The containment leakage pathway assumption was made as a modeling assumption to explain the observed pressure trend. While there is no data available that indicates the onset of this leakpath/heat loss, effects corresponding to an assumed containment leakage pathway are clearly indicated by ~8 hr. Such a leak could have developed any time up to 8 hours after the event.

It is now recognized that water in the torus room is a possible alternative cause of the depressurization trend seen in the TEPCO containment data. SNL MELCOR model developers were not made aware that there may have been water in the torus room until after the Unit 2 analysis was completed.

It is acknowledged that examination of the integrity of the pressure retaining boundaries, such as containment and the safety system injection system components external to containment, may find sites for system leakage that could be identified as contributors to the observed pressure trends. Moreover, as RCIC largely controlled the progression of the accident sequence during the first 70 hours, any future examination of the system could uncover information that would better characterize the RCIC system operation and better explain the observed discrepancies.

3.6.1.6   Changes to Refueling Bay (Unit 1, Unit 2, and Unit 3)

The following changes were made to the refueling bay:

- The temperature for the environment control volume associated with the reactor building refueling bay was changed to 278 K (5 °C), which is more consistent with the weather conditions at the Fukushima reactors at the time of the accident than the original value of 286 K (13 °C)
- The heat transfer coefficient for the external surface of the refueling bay was changed to 29.4 W/m^2-K to be more consistent with the wind conditions at the Fukushima reactors at the time of the accident than the original value of 5.0 W/m^2-K
- The thickness of the refueling bay roof was changed to 1/10 in, which is more typical of metal roofing materials than the original 1 in value.

3.7   Mechanisms for Induced RPV Depressurization

Mechanisms for induced depressurization of the RPV in BWR severe accident sequences were first introduced to the U.S. NRC MELCOR models in the calculations performed for the reactor security assessment in 2002-2003. The principal motivation at the time was to correct previous calculations of high-pressure accident sequences (e.g., SBO), which allowed SRVs to continue cycling for several hours after the onset of core damage, when gas discharge temperatures exceeded values at which material damage to moving valve components would challenge normal valve behavior. Specific values at which this could occur are discussed later. Data was not available to support a deterministic valve degradation model. As a result, an intuitive approach was used to capture the basic idea that moving valve components would eventually break or seize when sufficient heat was transferred from the flow gas stream to the valve body. Mechanisms for RPV depressurization in the Fukushima MELCOR models are discussed in this section.

There are three RPV depressurization mechanisms considered in the SOARCA MELCOR BWR/4 Mk-I model:

- SRV stochastic failure
- SRV seizure at high temperatures
- Main steam line failure

RPV depressurization can also be modeled by a manual opening of an SRV.

A description of each mechanism is provided in this section, along with discussions of how the RPV depressurization models were implemented (as needed) in each of the Fukushima reactor models.

3.7.1 SRV Stochastic Failure

The possibility that a cycling SRV would randomly fail to open, or to reclose after opening, was not represented in the MELCOR calculations previous to the SOARCA analyses. However, several hundred cycles have been calculated for some accident sequences, such as station blackout, which raised concerns that random failures should not be ignored.

Control logic was added to the SOARCA BWR/4 Mk-I MELCOR model to calculate the cumulative probability of random failure of a cycling SRV to reclose based on a user-specified failure rate. Failure was assumed to occur when the cumulative probability (i.e., confidence of failure) reached 90%.

3.7.2 SRV Seizure at High Temperatures

An initial criterion for high-temperature valve failure was based on manufacturers' information describing the strength of stainless steel, published by the Stainless Steel Information Center. Softening or loss of strength of stainless steel (300 series) was described as "about 1000 ºF" (811 K). The same reference also suggested the maximum service temperature for intermittent exposure of stainless steel components is 1600 ºF (1100 K). It was assumed that "service temperature" referred to the temperature of the thermal environment within which steel components operate. In the case of a valve, this was assumed to be the internal gas temperature. Therefore, in earlier analyses, a cycling valve was judged to cease functioning properly when the internal gas temperature exceeded a value between the two referenced values (i.e., somewhere between 811 K and 1100 K). In particular, valve seizure (failure to reclose) was assumed to occur if the valve was exposed to discharge gas temperatures greater than ~1000 K for several cycles.

In the current SOARCA MELCOR BWR/4 Mk-I MELCOR model, valve seizure was assumed to occur if the valve was exposed to discharge gas temperatures greater than 900 K.

3.7.3 Main Steam Line Failure

The Larson-Miller creep rupture model[8] that is available in MELCOR [29] is applied to a heat structure representing the RPV nozzle to main steam line A and (separately) to the heat structure representing the horizontal section of the main steam line piping immediately adjacent to the RPV nozzle (approx. 3.5 m in length). The nozzle is assumed to have twice the thickness of the main steam line pipe. The main steam line (MSL) is assumed to be made of 318 stainless steel.[9]

3.7.4 Implementation of Fukushima Information

3.7.4.1   RPV Depressurization (Unit 1)

SRV seizure at high temperatures and MSL failure were both evaluated in during Unit 1 model development. It was found that SRV seizure at high temperatures would occur before MSL failure, as the seizure temperature (900 K) is reached before the temperatures at which the MSL will fail (~1150 K). However, if the open area fraction is small, then the RPV will not depressurize rapidly enough to prevent the RPV gas temperature from continuing to rise to the point at which MSL failure occurs. Conversely, if the open area fraction is large, then RPV depressurization will be rapid enough to prevent the RPV gas temperature from rising into the range where MSL failure would occur.

Development cases were run with SRV seizure at high temperatures (with both small [0.03] and large [1.0] open area fractions) and MSL failure enabled, as well as with SRV seizure at high temperatures only and MSL failure only. It was found that MSL failure, either by itself or in conjunction with SRV seizure at high temperatures with a small open fraction, produced containment pressures that best matched the TEPCO containment pressure data, and that both configurations produced similar results. The MSL failure only configuration was carried forward for the analyses in Section 4.1.

The SRV stochastic failure model was disabled in in the Unit 1 model.

3.7.4.2   RPV Depressurization via SRV Operator Action and Failure (Unit 2)

During RCIC operation, the RPV pressure data deviates from the SRV set point 5 hours after scram. To account for the difference, a SRV reseat failure was postulated and implemented at 5.33 hours. A constant open area fraction of 0.03 was selected to represent the reseat failure.

The Unit 2 RPV depressurization was implemented by opening an SRV at 75.32 hours, as indicated in the Unit 2 timeline. A pressure excursion occurred shortly after 77 hours. Operators opened a second SRV, as indicated in the Unit 2 timeline at 78.55 hours, to restore low RPV pressure. Closure of the second SRV, as indicated in the timeline, occurred at 80.22 hours; the second SRV was reopened at 95.24 hours. The preceding SRV states have been included in the model.

---

[8] At temperatures that result in the creep rupture model predicting rapid failure (on the order of seconds), the failure mechanism is actually due to the decrease in yield strength.
[9] TEPCO has subsequently informed the SNL MELCOR model developers that the main steam line is actually made of carbon steel. A sensitivity case was run with a carbon steel main steam line; its results were not substantially different from the case with a 318 stainless steel main steam line.

The SRV stochastic failure model was disabled in in the Unit 2 model.

3.7.4.3   RPV Depressurization via Manual SRV Opening (Unit 3)

In the Unit 3 timeline exact timing of the SRV opening that depressurized the reactor is not clear because operators had to scavenge batteries in order to energize the solenoid to open the SRV. Close examination of the pressure data for the RPV and containment suggests the SRV opened at 42.13 hours. Opening the SRV at this time allows the MELCOR model to capture both the RPV pressure data and the timing of the peak containment pressure that follows the RPV depressurization.

The SRV stochastic failure model was disabled in the Unit 3 model.

3.8   Behavior of Ex-Vessel Drywell Floor Debris

The MELCOR Cavity (CAV) package models the attack on the basemat concrete by hot (often molten) core materials. The effects of heat transfer, concrete ablation, cavity shape change, and gas generation are included, using models taken from the CORCON-Mod3 code. The coding of the models is identical to that in CORCON-Mod3, but interfaces have been modified for integration into the MELCOR framework. This integration couples the Cavity package models to thermal-hydraulic boundary conditions in the Control Volume Hydrodynamics (CVH) package, to sources of core debris from the Core (COR) and/or Fuel Dispersal Interactions (FDI) package, and to the standard MELCOR input, output, plotting, and restart capabilities. The fission-product release models in CORCON-Mod3—originally developed as the separate VANESA code—are included in MELCOR as part of the RadioNuclide (RN) package.

The drywell floor is subdivided into three regions (i.e., cavities) for the purposes of modeling molten-core/concrete interactions[10] (see Figure 20). The first region, which receives core debris exiting the reactor vessel, corresponds to the reactor pedestal floor and sump areas (CAV 0). Debris that accumulates in CAV 0 can flow out through a doorway in the pedestal wall to a second region representing a 90 degree sector of the drywell floor (CAV 1). If debris accumulates in this region to a sufficient depth, it can spread further around the annular drywell floor into the third region (CAV 2). This discrete representation of debris spreading is illustrated in Figure 20.

---

[10] The cavity model described in this section is taken from the SOARCA BWR/4 Mk-I model.
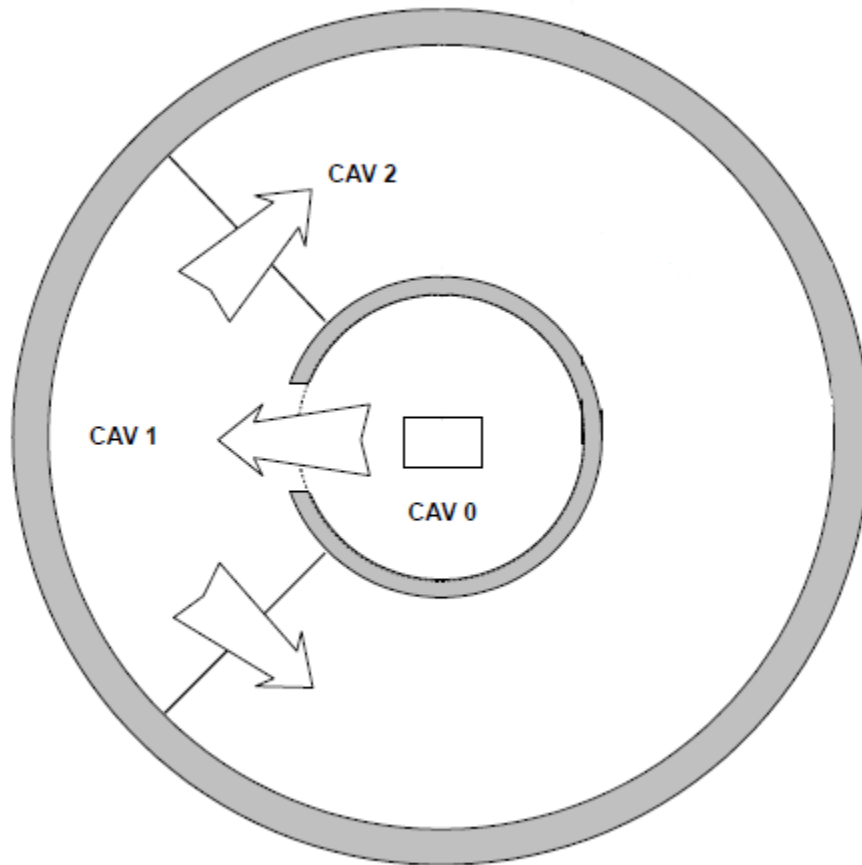
Figure 20. Drywell Floor Regions for Modeling Molten-Core/Concrete Interactions.

Two features of debris relocation within the three regions are modeled. The first represents bulk debris spill over or movement from one region to another. A control system monitors the debris elevation and temperature within each region, both of which must satisfy user-defined threshold values for debris to move from one region to its neighbor. More specifically, when debris in a cavity is at or above the liquidus temperature of concrete, all material that exceeds a predefined elevation above the floor/debris surface in the adjoining cavity is relocated (i.e., 6 inches for CAV 0 to CAV 1 and 4 inches for CAV 1 to CAV 2). When debris in a cavity is at or below the solidus temperature of concrete, no flow is permitted. Between these two debris temperatures, restricted debris flow is permitted by increasing the required elevation difference in debris between the two cavities (i.e., more debris head required to flow).

The second control system manages the debris spreading radius across the drywell floor within CAV 1 and CAV 2 to approximate liner attack; note this is not implemented for molten core/concrete interaction rates. Debris entering CAV 1 and CAV 2 is not immediately permitted to cover the entire surface area of the cavity floor. The maximum allowable debris spreading

radius is defined as a function of time. If the debris temperature is at or above the concrete's liquidus temperature, then the maximum transit velocity of the debris front to the cavity wall is calculated (i.e., results in 10 minutes to transverse CAV 1 and 30 minutes to transverse CAV 2). When the debris temperature is at or below the concrete solidus, the debris front is assumed to be frozen, and lateral movement is precluded (i.e., debris velocity is 0 meters per second). A linear interpolation is performed to determine the debris front velocity at temperatures between these two values.

Full mixing of all debris into a single mixed layer is assumed in each of these debris regions. The specific properties for concrete composition, ablation temperature, density, solidus temperature, and liquidus temperature are specified.

It must be noted that lateral debris mobility is strongly affected by geometric details of the drywell floor design, and these design features vary among BWRs with a Mk-I containment. The volume of debris that can be sequestered in the sump (and, therefore, not available for lateral movement toward the drywell liner) spans a wide range. Further, the steel liner at the periphery of the drywell floor may be protected or elevated above the surface of the floor by a concrete curb in some plants.

The MELCOR model setting "CORCON BASALT" [29] is used to specify the drywell floor concrete composition. Solidus and liquidus temperatures in the cavity debris spreading model were changed to be consistent with "CORCON BASALT". Otherwise, due to a lack of Fukushima specific information, the cavity from the SOARCA BWR/4 Mk-I model was implemented.

3.9   Containment Failure Model

The SOARCA MELCOR BWR/4 Mk-I containment incorporates criteria for opening leak pathways through the containment pressure boundary by two distinct mechanisms. The first mechanism, which occurs in all the calculations involving sufficient core damage and breach of the RPV lower head, is drywell liner melt-through. The second mechanism is leakage through the drywell head flange when high internal temperatures and pressure develop within the containment. These mechanisms are valid for incorporation into the Fukushima reactor models since that they, like the SOARCA MELCOR BWR/4, have Mk-I containments.

3.9.1.1   Drywell Liner Melt-through

If debris flows out of the reactor pedestal and spreads across the drywell floor, as described in Section 3.8, and contacts the outer wall of the drywell, the steel liner will fail, opening a release pathway to the lower reactor building. Heat transfer between the steel liner and molten core debris is not explicitly calculated in the MELCOR model, due to limitations of the CAV Package, which addresses ex-vessel model debris behavior. The model assumes an opening in the drywell liner occurs 15 minutes after debris first contacts the drywell wall. This time delay represents an average of estimates for failure time discussed in NUREG/CR-5423 [33] for situations in which the drywell floor is not covered with water.

3.9.1.2 Containment Over-pressure

The SOARCA Mk-I model has a containment that consists of a drywell and a toroidal-shaped wetwell, which is half-full of water (i.e., the pressure suppression pool). The drywell has the shape of an inverted light bulb. The drywell head is removed during refueling to gain access to the reactor vessel.

Figure 21 shows an example of a drywell head flange. Note that the drywell head flanges for the Fukushima reactors may be different.[11] The drywell head flange is connected to the drywell shell with bolts. The flanged connection also has gaskets.

The drywell head flange bolts are pre-tensioned during reassembly of the head. This pre-tension also compresses the gaskets in the head flange. During accident conditions, the containment vessel may be pressurized internally. The internal pressure would then begin to counteract the pre-stress in the bolts. When the internal pressure produces counter-stress equivalent to the bolt pre-stress, elastic strain of the head bolts will occur, allowing a small gap to open up between the mating surfaces of the flange. Further increase in the internal pressure would result in leakage at the flanged connection. Because the bolt stress is in the elastic range of the stress-strain curve, when the containment pressure decreases, the gap reduces as the bolt contracts and the leakage area is thereby reduced. In reality, some permanent strain may take place in the flange region and seal degradation may also take place such that the leakage area may not reduce to zero as the containment pressure decreases. MELCOR's model for bolt strain is ideal in this sense.
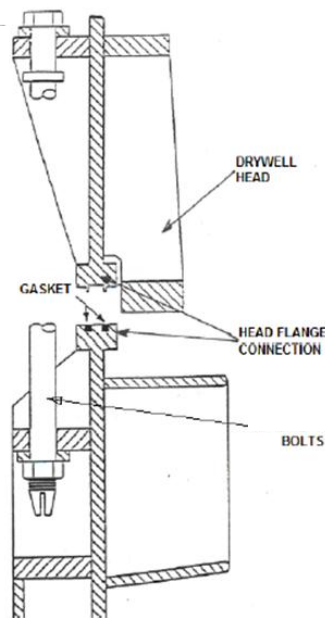
Figure 21. Example of Drywell Head Flange Connection Details.

---

[11] At the time this report was prepared no Fukushima specific information regarding the drywell head flange configuration was available.

At high temperatures (greater than 755 K (900 °F)), upward and radial thermal growth of the drywell would lead to binding of small and large penetrations against the biological shield wall and failure. In addition, radial growth of the containment may also cause the seismic stabilizers to punch through the upper portion of the drywell at high temperatures [25]. This observation is consistent with the results of previous studies that show that the drywell is likely to fail at the low-pressure range of 0-65 psig (0-0.448 MPa) [25]. Therefore, it can be concluded that the drywell is likely to fail under any appreciable pressure load at structure temperatures of 900 °F or greater.

3.9.2 Implementation of Fukushima Information

3.9.2.1 Drywell Head Lifting Pressure (Unit 1)

During the initial Unit 1 model development it was noted that the MELCOR containment pressure results after RPV depressurization were consistently lower than the TEPCO containment pressure data. This was due to the drywell head beginning to lift (in the MELCOR analysis), and hence venting the containment into the reactor building, at a pressure of 82 psig (0.565 MPa) (the value from the SOARCA BWR/4 Mk-I model). In order to better match the TEPCO containment pressure data during the period of sustained and nearly constant high pressure, based on the presumption that the leveling off of the observed pressure was likely due to leaking at the drywell head flange, the MELCOR curve for DW pressure versus leak area was adjusted upwards by 4 psig (0.026 MPa) (see Figure 22). Without this adjustment, the MELCOR model would predict the sustained maximum containment pressure at a lower value (82 psig [0.565 MPa]).
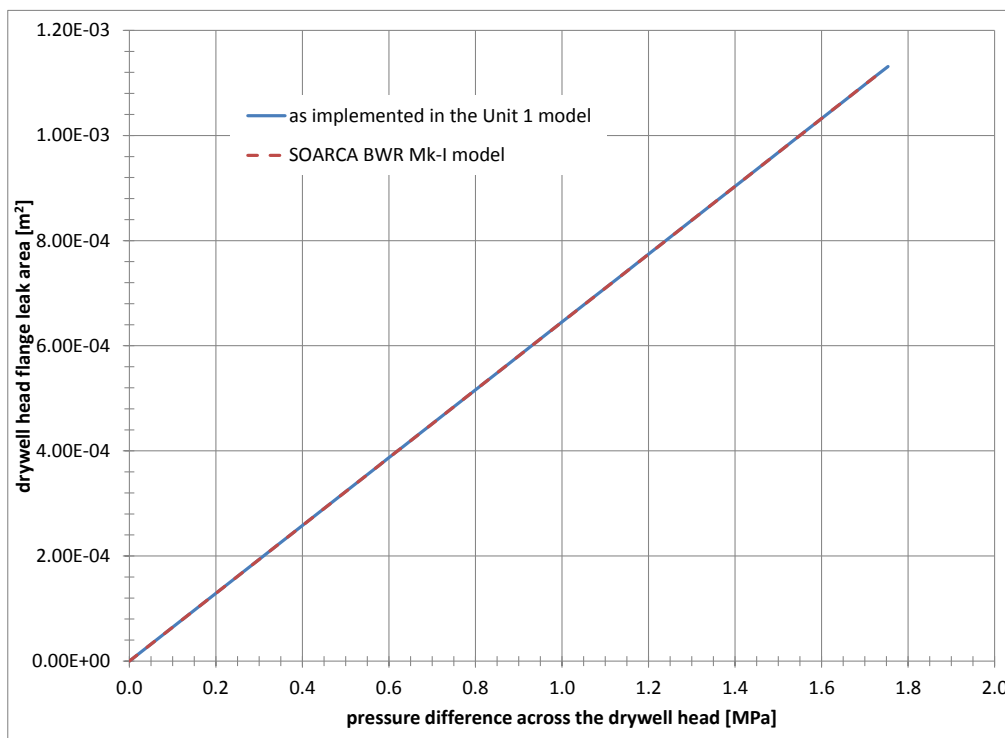
Figure 22. Drywell Head Flange Leakage versus Containment Pressure.

3.10 Radionuclide Inventories and Decay Heat

An important input to MELCOR is the initial mass of radionuclide groups in the fuel and their associated decay heat. These values are important to the timing of initial core damage and the location and concentration of the initial radioactive source. The radionuclide groups in a nuclear reactor come from three primary sources:

- fission products
- actinides
- other radioisotopes which are formed from the radioactive decay of fission products and actinides.

Radionuclide inventories for the Fukushima reactors were not available at the time the MELCOR models were developed. Instead, radionuclide inventories for the Fukushima reactors were approximated by scaling the Peach Bottom inventory by the ratio of the operating power of the Fukushima reactor of interest to the operating power of Peach Bottom (see Table 5).

Table 5. Reactor Operating Power and Inventory Scaling Factor

Reactor	Operating Power[12] [MW]	Inventory Scaling Factor [-]
Unit 1	1380	0.393
Unit 2	2381	0.678
Unit 3	2381	0.678

The inventories in Peach Bottom SOARCA were derived from several mid-cycle TRITON[13] calculations. The Fukushima reactors at the time of the accidents were at approximately mid-way through their cycles. Since radionuclide production is proportional to burn-up for many nuclides (although, of course, isotopes/isomers with substantial neutron cross-sections saturate), a simple power rate ratio was used to estimate the Fukushima inventories. Although the analyses did not concentrate on RN releases, the power-scaling method was used in order to model the lower RN inventories in the Fukushima reactors. Down-scaling the Peach Bottom inventories by other ratios, such as initial fuel load or number of fuel assemblies, results in roughly the same reduced inventories. This same scaling method was initially used to approximate the decay heat information used in the models.

Near the end of the model development and analysis process, decay heat information (e.g., decay power vs. shutdown time and axial/radial power distributions) and radionuclide inventories were provided by TEPCO. The decay heat information was incorporated into Unit 1, Unit 2, and Unit 3 reactor models. TEPCO identified that the decay heat information and the radionuclide inventory information were from separate calculations and were not completely consistent. (Integrated neutronics analysis tools, such as the TRITON sequence in ORNL's SCALE package, can be used to generate consistent decay heat and radionuclide inventory data for use in

---

[12] Peach Bottom has an operating power of 3514 MW.
[13] TRITON is an element of the SCALE based code system developed at Oak Ridge National Laboratory.

MELCOR model input [41, 22].) There was not sufficient time to develop a method to resolve this consistency issue; hence, the TEPCO radionuclide inventories were not implemented in the models. In the MELCOR input for each unit, inventories (from scaled Peach Bottom data) were allocated throughout the cores in a manner consistent with the axial and radial decay power distributions provided by TEPCO (i.e., regions with higher decay power have greater radionuclide masses).

4   SNL UNIT 1, UNIT 2, AND UNIT 3 ANALYSES AND RESULTS

MELCOR-predicted results will be presented in this section, and where available plant data are provided for comparison. Essentially the only recorded plant data is in the form of pressure data for the reactor pressure vessel, the drywell, and the wetwell, and water level data. The water level data is particularly problematic in that single instances of large vessel depressurization render all subsequent level measurements suspect because of water flashing effects on the manometer type measurement instruments.

4.1   Unit 1 Results

In the Unit 1 accident, as with all of the affected reactors, following the earthquake reactor shutdown was accomplished and for the first hour before the arrival of the Tsunami, safety systems functioned properly. In particular for Unit 1, the isolation condensers were activated on isolation of the reactor pressure vessel from the turbines by closure of the main steam isolation valves. The high effectiveness of the isolation condensers initially led to a cooldown rate in excess of 100 °F (55 K) per hour,[14] which exceeded the maximum recommended cooldown rate of the reactor. The operators did not know at the time that a tsunami was to arrive shortly, and were following procedures to protect the reactor (i.e., thermal stresses from large temperature changes that affect the fatigue of the vessel and the plant) and shut down the IC operation. The predicted cooldown from IC operation is shown in Figure 23. There were four operations of the isolation condensers during the first hour, one lasting about 10 minutes and three more with durations of approximately one minute. They are shown as short periods of decreasing reactor temperature and pressure where the cycling SRV effects are briefly suppressed as seen in Figure 23 and Figure 24. Both ICs were operating during the first cooldown, thereafter only one IC unit was employed.

---

[14] Personal communication with TEPCO staff.
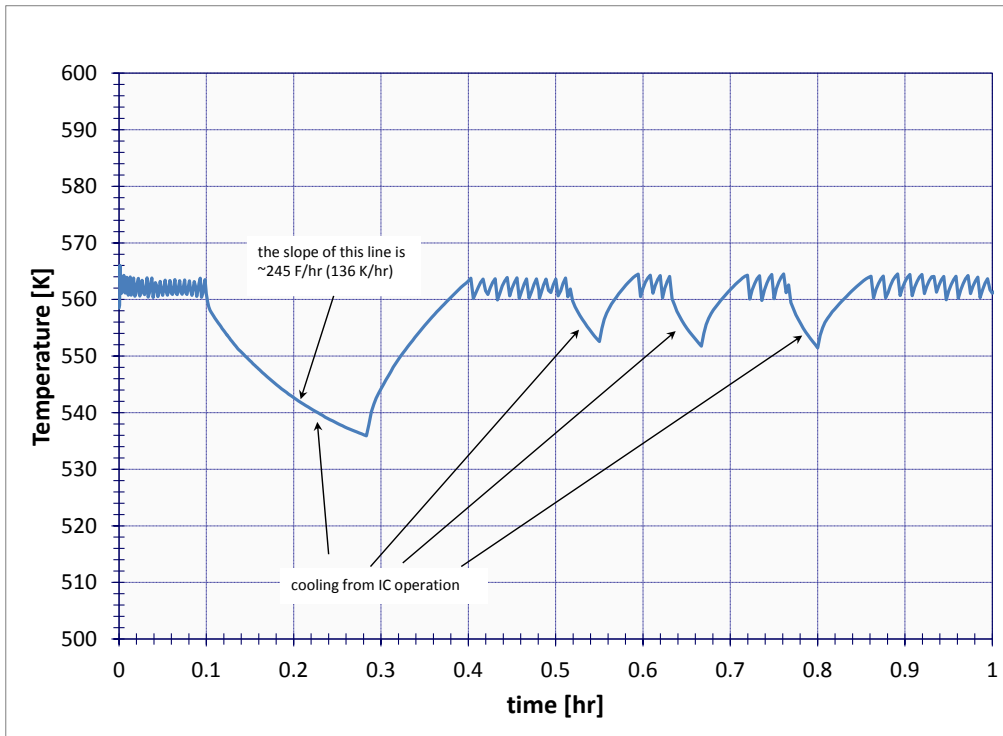
Figure 23. MELCOR Predicted RPV Temperature While IC Operation Was in Effect (Unit 1).
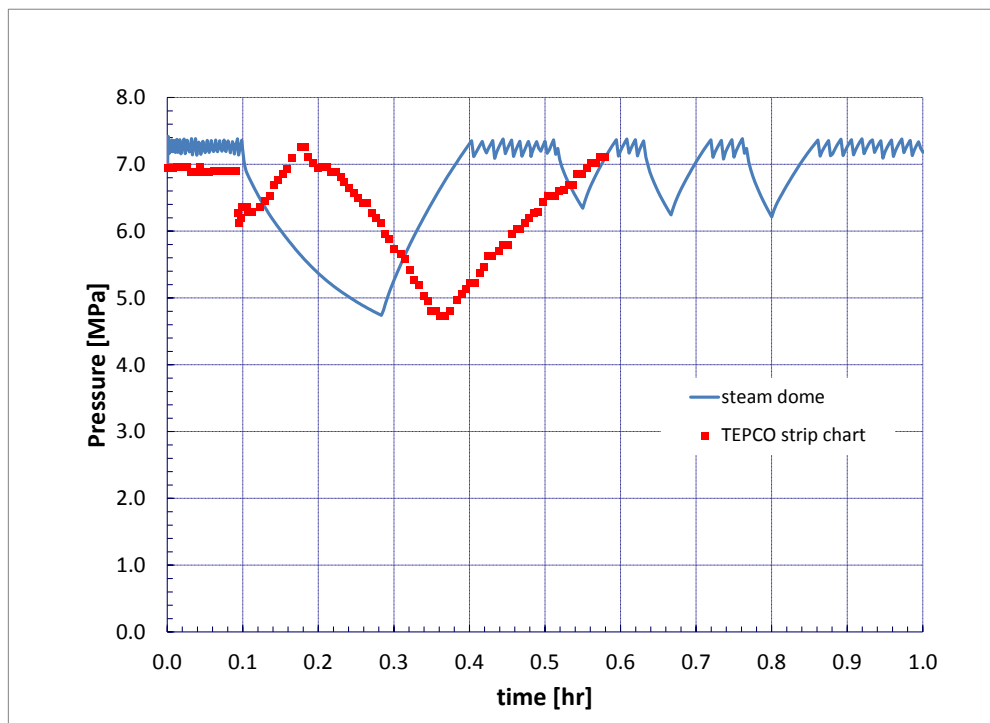
Figure 24. MELCOR Predicted RPV Pressure Response during Operation of the Isolation Condensers, Compared with TEPCO Strip Chart Data (Unit 1).

72

Following the arrival of the tsunami, all AC and DC power was lost at Unit 1. The IC system was not aligned for operation at the time, and the IC valves could not be re-opened, and would not be opened again until significant core damage had already taken place.

With loss of heat rejection, the RPV pressure thereafter remained at the SRV setpoint as shown in Figure 24, with steam from the vessel venting through the SRV to the suppression pool as water was lost from the primary system. The loss of water through the cycling SRVs led to core uncovering in a short period of time as shown in Figure 25.
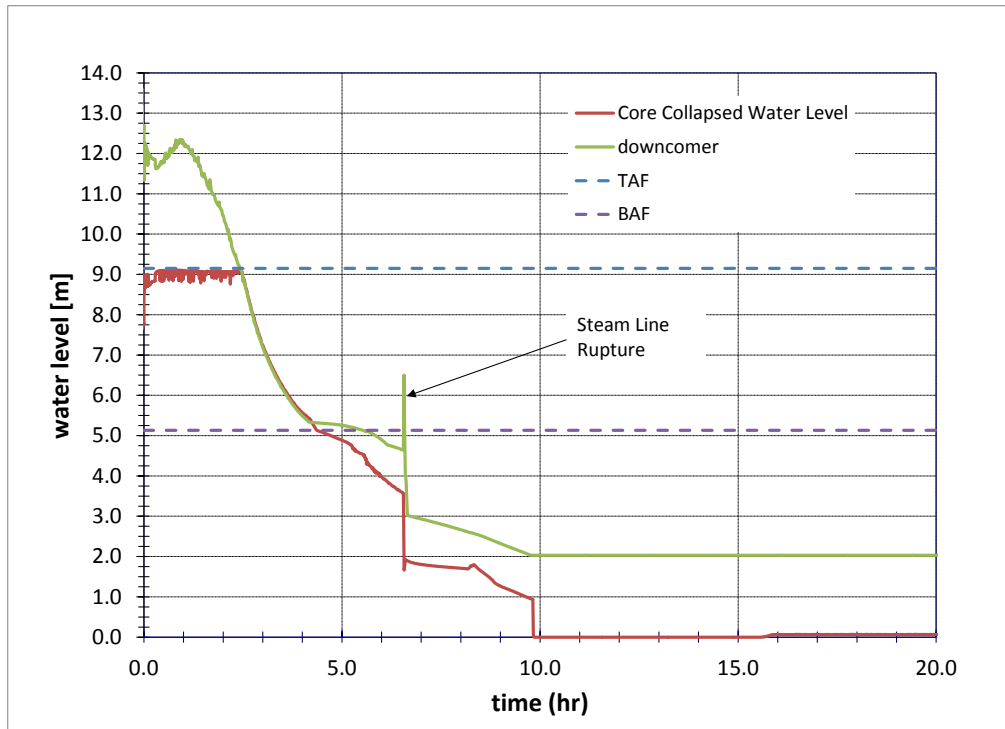
Figure 25. MELCOR Predicted Water Level in the Reactor Core and Downcomer Regions (Unit 1).

As the core water level decreased, initially the steam generation cooled the exposed fuel rods; but as the water level dropped to near the bottom of the active fuel, the steaming rate had diminished to a sufficiently low level that the rods were no longer convectively cooled and heatup commenced. After fuel cladding temperatures exceed 1300 to 1400 K, steam-oxidation of the Zircaloy cladding becomes significant, producing an increased fuel heat-up rate from the exothermic oxidation reaction, as well as producing hydrogen from the reaction with steam. Fuel heatup is shown in Figure 26.[15] Note that by four hours, core damage and hydrogen generation had initiated (see Figure 26, Figure 27 and Figure 28). The generation of hydrogen gas at 4 hr would later render the isolation condensers ineffective when they were subsequently activated

---

[15] Each trace in Figure 26 represents the fuel temperature in a single COR cell. The purpose this plot is to show the over trends in fuel temperature; it is not meant allow detailed examination or comparison between individual COR cell fuel temperatures.

(manually) at ~6.5 hr due to the accumulation of the non-condensable gas in the heat exchanger tubes (see Section 3.4.1.1).
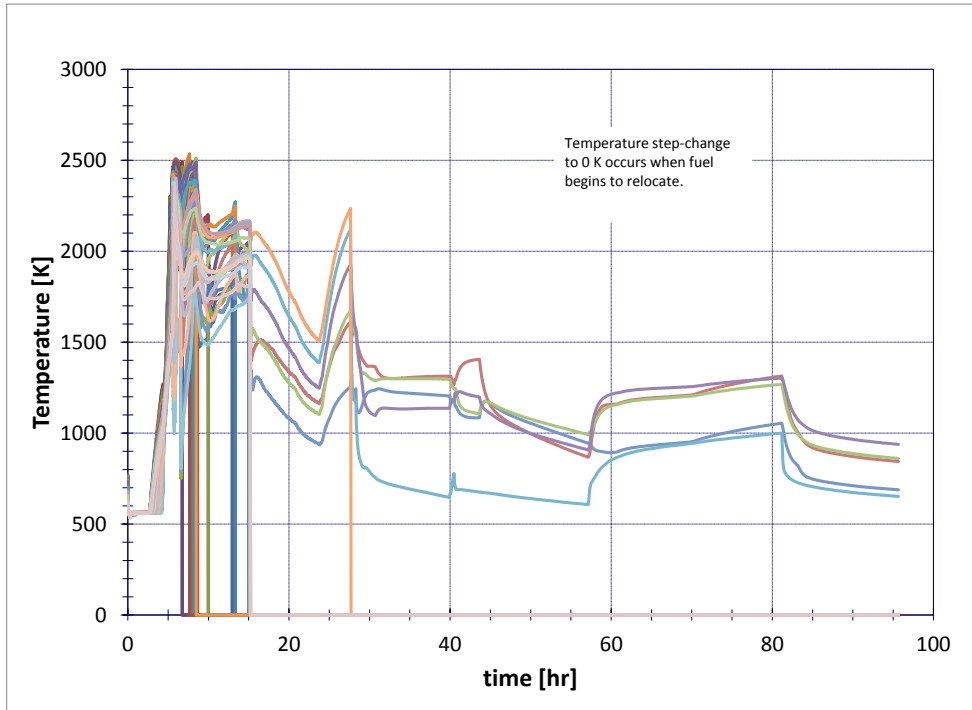
Figure 26. MELCOR Predicted Fuel Temperatures in the Reactor Core (Unit 1).
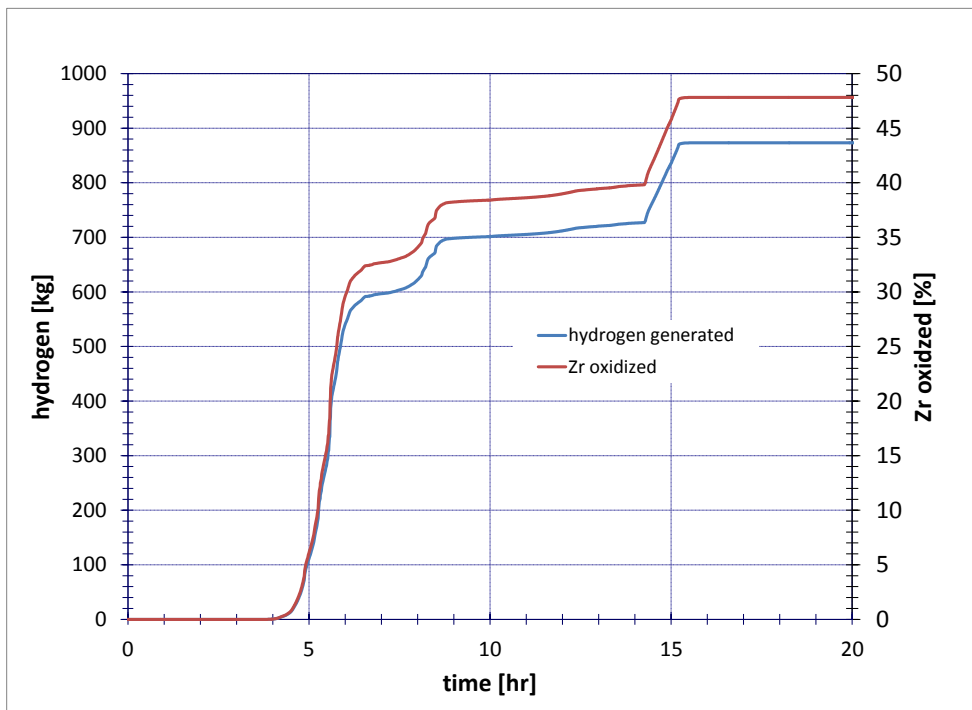
Figure 27. MELCOR Predicted Hydrogen Generation from Fuel Cladding Oxidation (Unit 1).
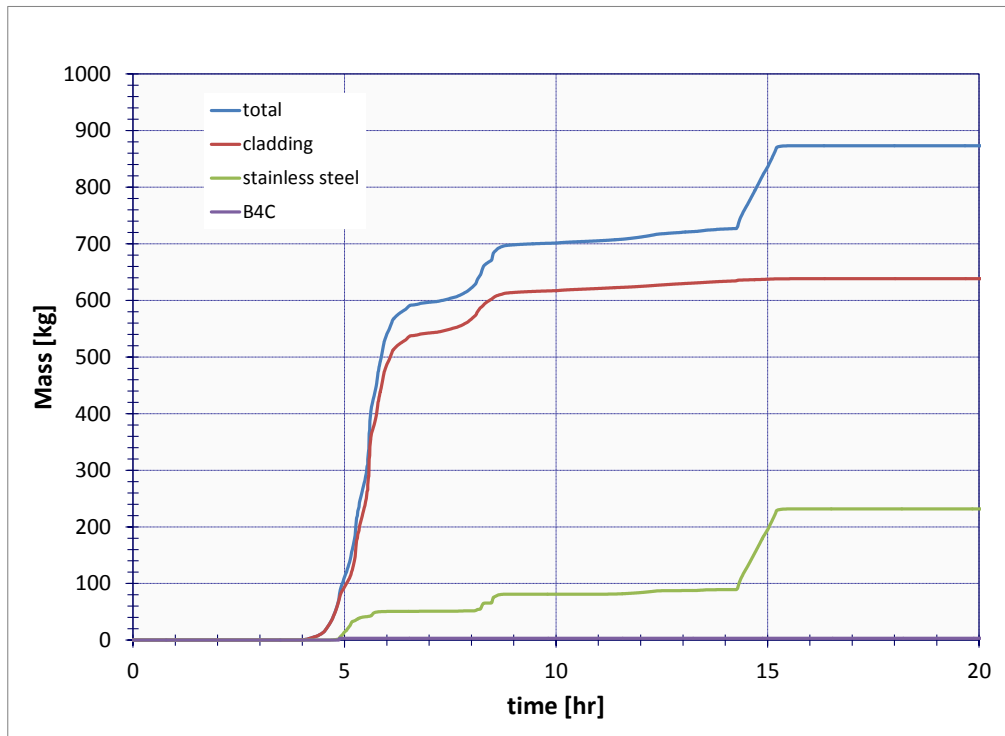
Figure 28. MELCOR Predicted Hydrogen Generation from Fuel Cladding, Stainless Steel, and B4C Oxidation (Unit 1).

After 5 hr the model shows that core exit gas temperatures began to significantly increase, with superheated steam and hydrogen gas flowing into the main steam line associated with the cycling SRV. Steam line temperatures are shown in Figure 29. This hot gas heated the steam line significantly, and because the reactor pressure was high (at the lowest SRV set point), thermal creep in the hottest steam line eventually led to failure of the main steam line[16] and a depressurization of the RPV at about 6.6 hours as seen in Figure 30. This integrity of the pressure boundary for over five hours and the loss of pressure boundary sometime thereafter predicted in the model is consistent with the available data (see Figure 30) which shows the RPV held pressure for more than 5 hours but underwent a significant decrease by 12 hours.

---

[16] The MSL failure model result reported herein is not the same as a design basis accident direct failure of the MSL (i.e., main steam line break) by the earthquake.
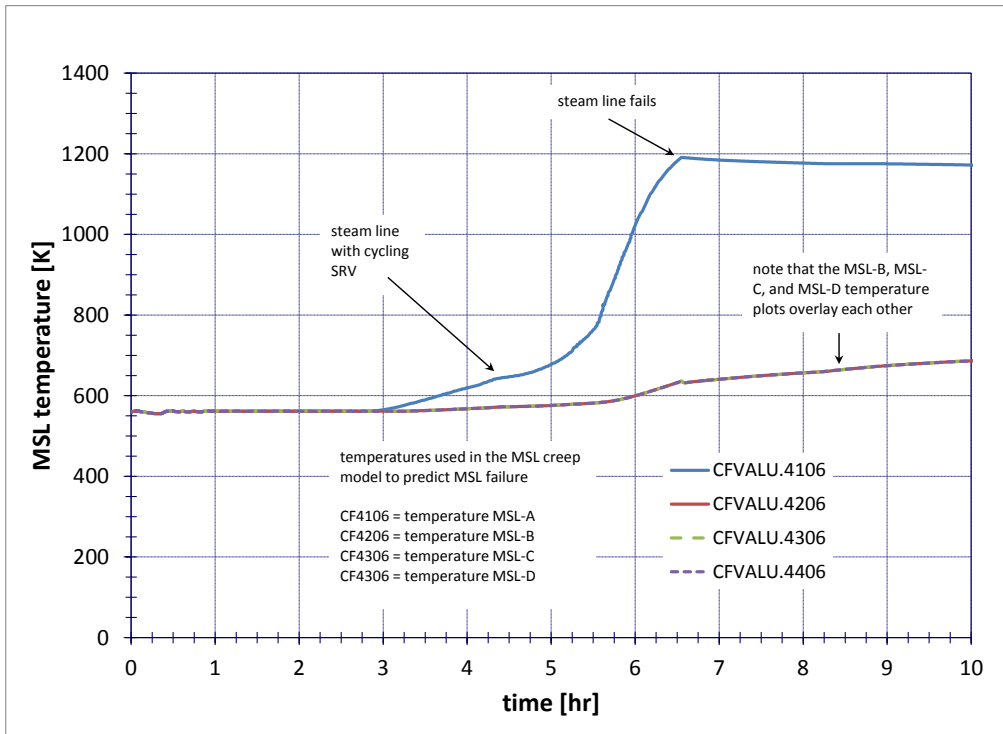
Figure 29. MELCOR Predicted Steam Line Temperatures (Unit 1).
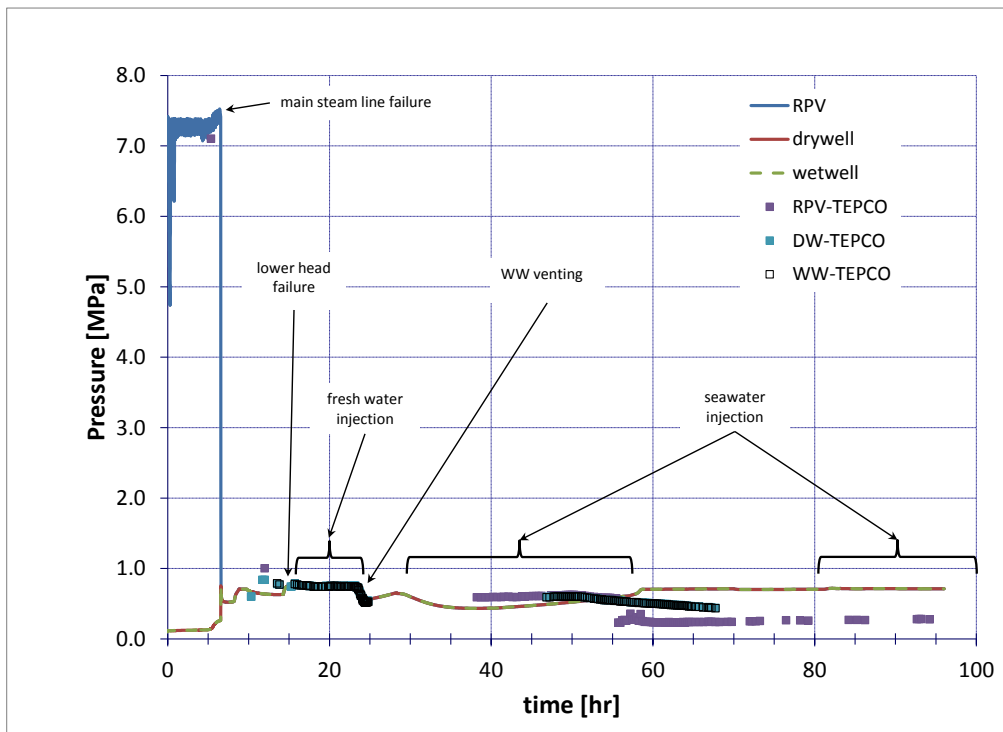
Figure 30. MELCOR RPV and Containment Pressure Prediction Compared to TEPCO Data (Unit 1).

Note that the limited TEPCO pressure data for the RPV, drywell, and wetwell compare reasonably well with the MELCOR prediction. While main steam line failure was predicted by MELCOR, an alternative scenario is also deemed possible where the cycling SRV seizes open due to excessive cycling and high temperature gases degrading the valve. While not documented in this report, predicted drywell pressure for the alternative "stuck-open" SRV case does not compare as favorably with the measured values, producing a lower post-blowdown DW pressure. This is due to more RPV thermal energy being deposited in the still subcooled suppression pool.

After 5.5 hr, core materials begin to accumulate in the lower vessel head region (see Figure 31), drying out the lower plenum water and heating the vessel head, and by 14 hours, lower head failure is predicted to occur by melting of the head wall, as seen in Figure 32. Some 139,000 kg of core materials (UO_2, Zr, Stainless Steel, and oxides) and lower vessel head steel is predicted to have accumulated on the lower reactor cavity concrete following head failure (see Figure 33). The relocated material is mostly solid (i.e., particulate debris). Due to its low temperature (see Figure 37) the relocated core debris does not move from the pedestal cavity region (CAV 0) to the cavity regions adjacent to the drywell liner (CAV 1 and 2) (see Figure 20).

Note that by the time that fresh water injection is commenced at 15 hours, the core is predicted to have already melted through the lower head and begun to thermally attack the concrete floor of the reactor cavity. The core condition near the time of vessel head failure is shown in Figure 34. The figure contains two 2-D (cylindrical geometry) representations of the reactor core and lower-vessel at different points in time. The pink material is intact fuel and cladding, grey represents void or steam, blue material is liquid water (not present in Figure 34), yellow material is steel, green material is particulate debris, and any red material is molten debris (barely visible). Black dots overlaid on a core cell represent high porosity for the debris in that cell. At the end of the simulation, a substantial amount of fuel and cladding remains in the outer and lower regions of the core, and this material does not relocate to the containment cavity after vessel breach.
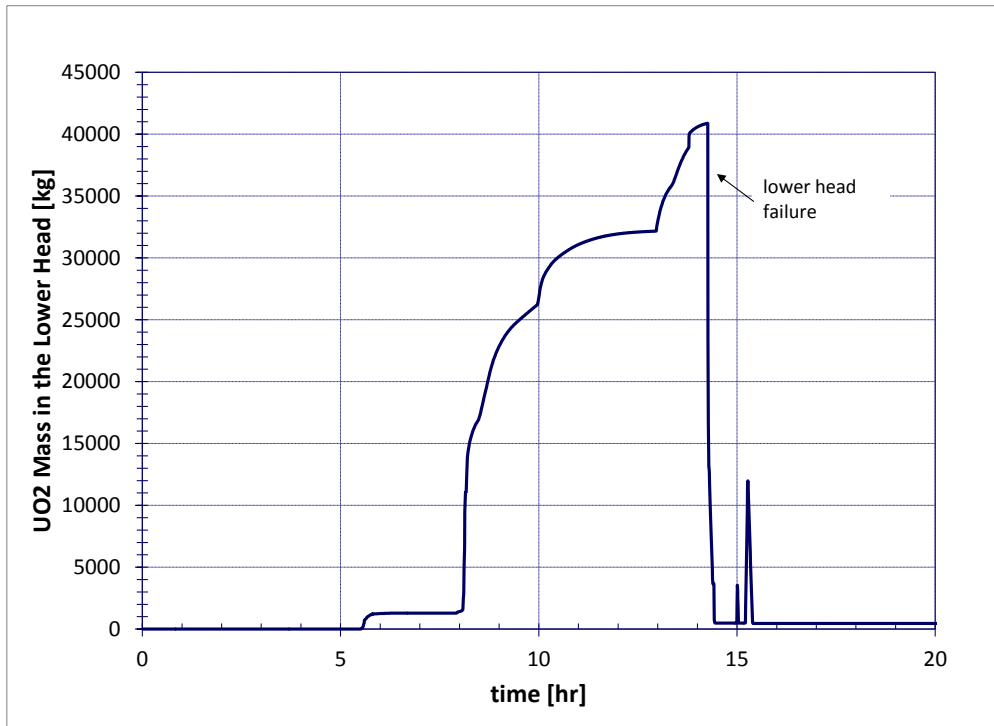
Figure 31. MELCOR Predicted Accumulation of Fuel Materials in the Lower Plenum Region of the Reactor (Unit 1).
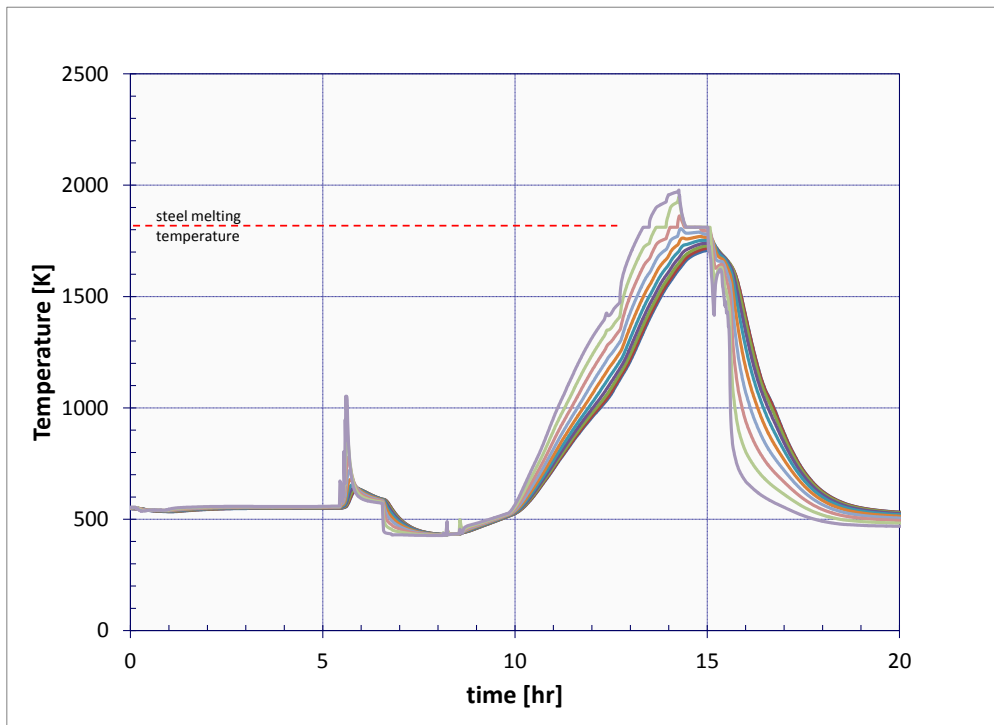
Figure 32. MELCOR Predicted Lower Head Wall Node Temperatures (Unit 1).
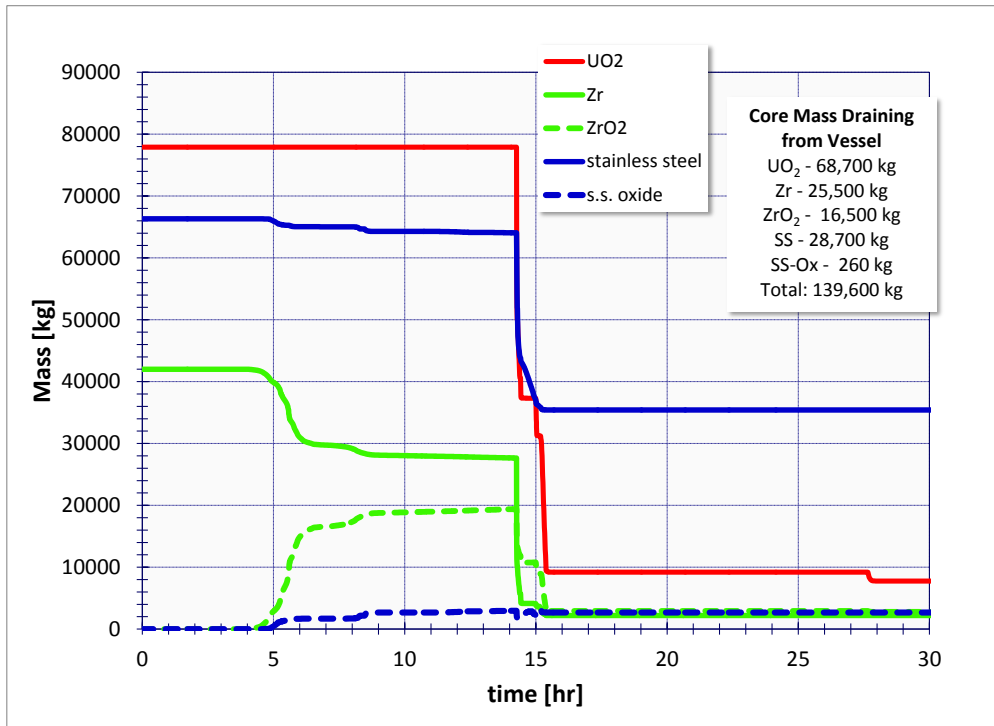
Figure 33. MELCOR Predicted Mass Remaining in the Vessel on Failure of Lower Head (Unit 1).
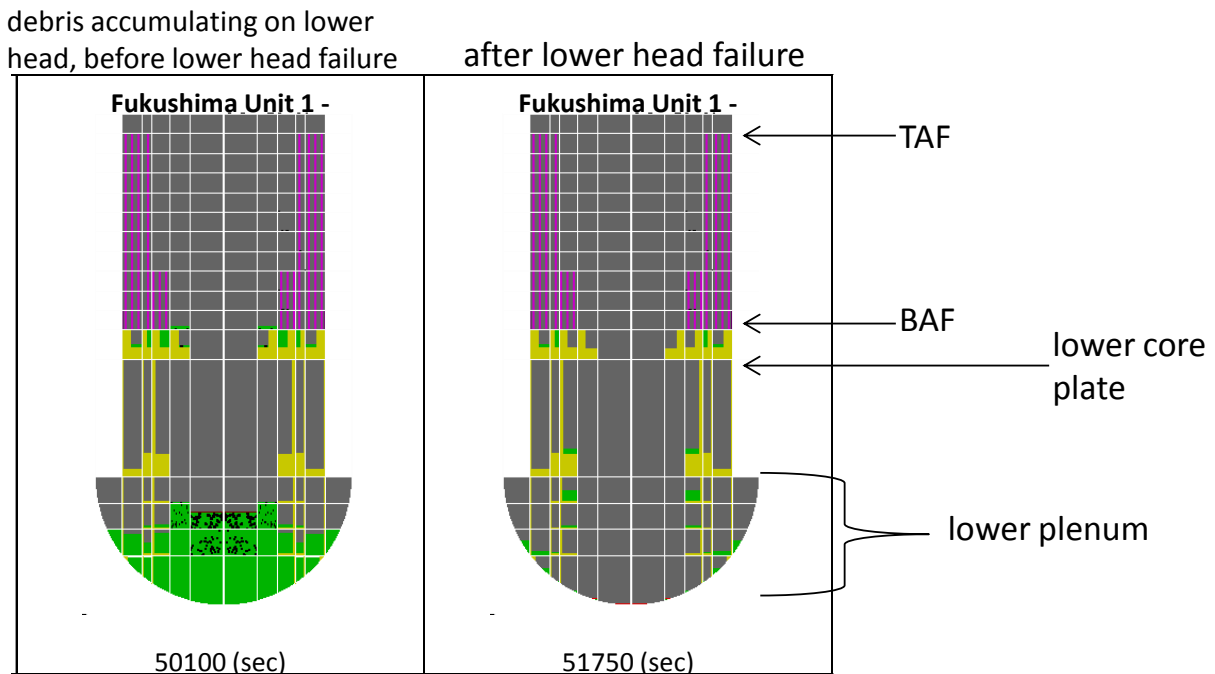
Figure 34. MELCOR Predicted Core Damage State near Time of Lower Head Failure (Unit 1). NOTE: Some intact fuel assemblies remain in the core region.

Figure 35 shows the predicted redistribution of decay heat, accounting for fission product release and transport in the RPV and relocation of decay heat bearing materials to the lower cavity region.

The heat generated from the exothermic chemical heating and the fuel decay heat in the reactor cavity region is shown in Figure 36, along with the heat transfer to the seawater that was being dumped onto the cavity floor through the vessel breach.
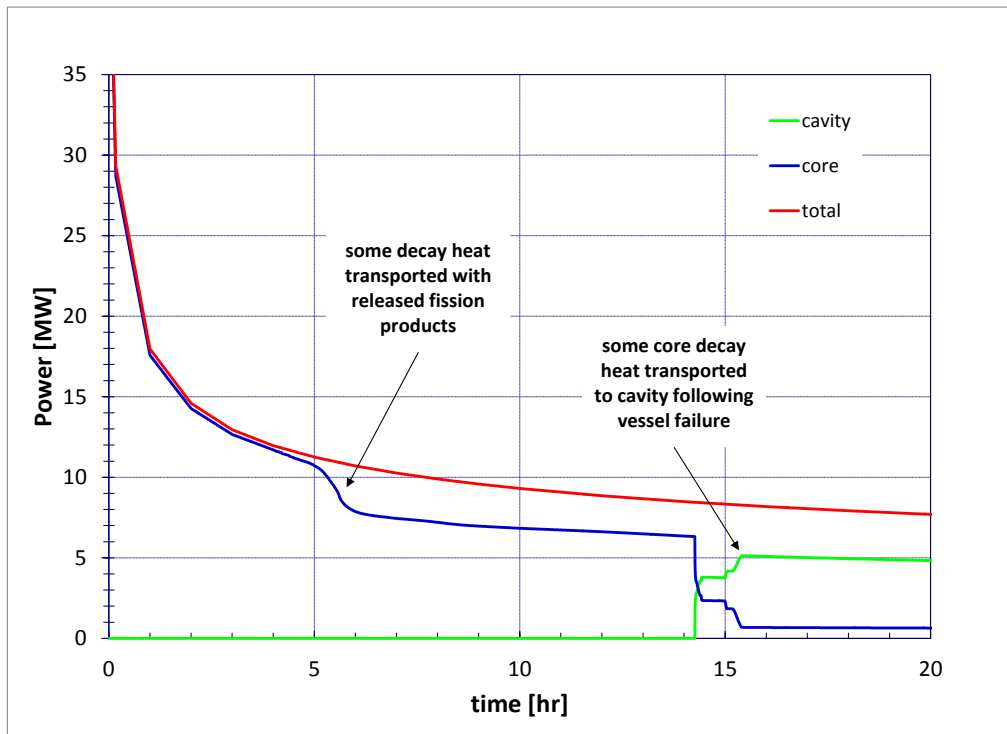
Figure 35. MELCOR Predicted Distribution of Decay Heat During Core Damage: Fuel Releases Diminish In-Core Decay Heating and Vessel Failure Transfers Decay Heat from Vessel to Cavity (Unit 1).
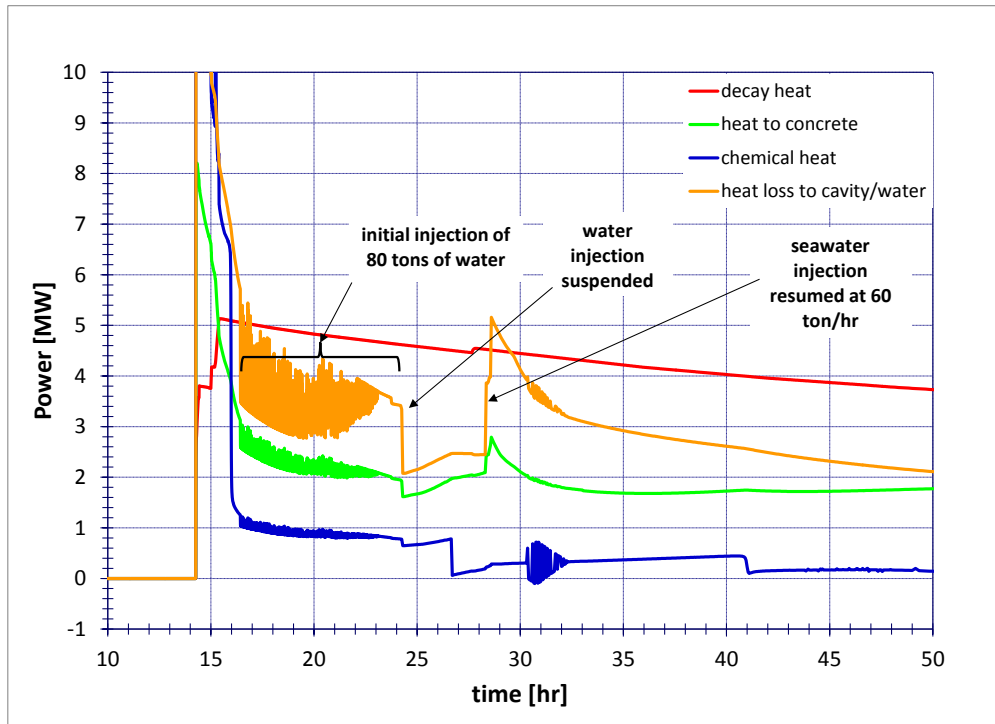
Figure 36. MELCOR Predicted Decay Heat and MCCI Chemical Heat in the Reactor Cavity (Unit 1)

NOTE: The enhanced cooling of the MCCI at ~15 hours is due to seawater entering the cavity through the vessel rupture.

The temperature of the core-concrete interaction hovers just above the ablation temperature, indicating a relatively low intensity molten core-concrete interaction (MCCI), as shown in Figure 37. The MCCI both melts and erodes the concrete, and produces non-condensable gases from concrete decomposition (CO, CO_2) and H_2 from the oxidation of metals in the core melt, principally Zr and stainless steel, and steam. The MELCOR-predicted erosion depth from the cavity MCCI is about 1.5 meters by 30 hours.[17]

The MCCI reaction products are shown in Figure 38. Nearly 600 kg of CO and 400 kg of H_2 are produced by 24 hours, roughly the time at which manual containment venting was achieved. These non-condensable gases, which are released to the reactor drywell containment volume, occupy considerable volume when compared to the free volume of the reactor drywell. These gases cause the pressure in the drywell to rise to the point that the drywell head bolts are elastically strained, opening a vent path to the refueling bay at the upper drywell head flange region. The vent path opens just enough to relieve the gas generation and hovers at a value of about 0.7 MPa (110 psi) as seen in Figure 39 where calculated and measured drywell pressures are shown. Notice that when the manual containment venting operation is accomplished just before 24 hours, the drywell pressure is decreased to below the value required to maintain the head bolt strain for leakage and the head flange leak is predicted to stop thereafter. The strain in

---

[17] It is likely that debris quenching is being under-predicted in the model, and that more realistic quenching would result in a lesser erosion depth with the debris ultimately being quenched (i.e., MCCI being terminated).

the head bolts is the elastic range since the stress level is predicted to be well below the yield stress.
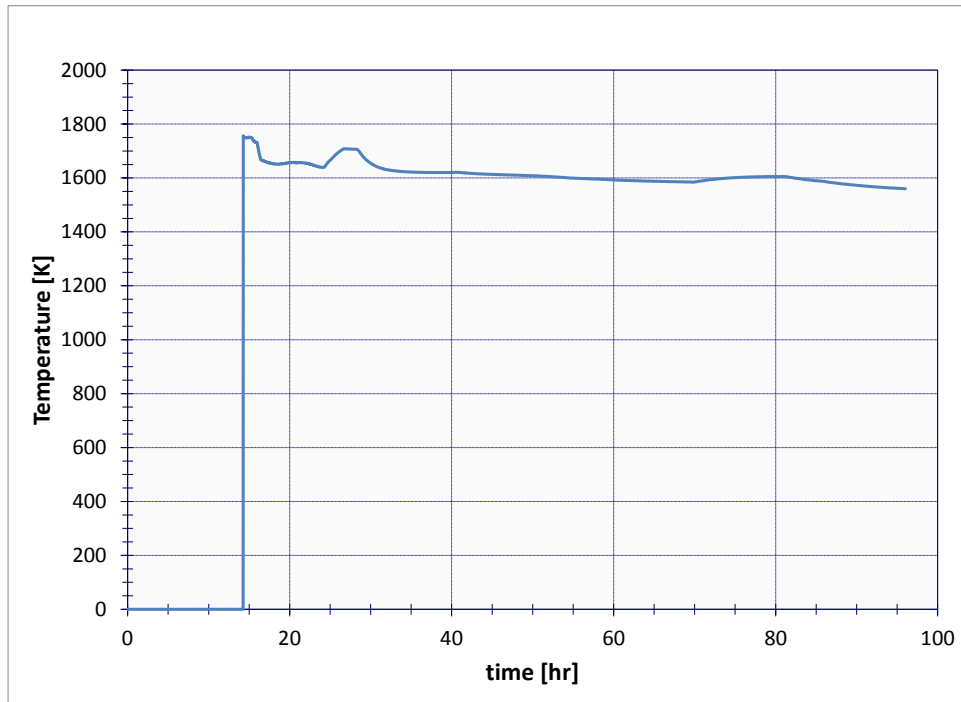
Figure 37. MELCOR Predicted Temperature of Core-Concrete Interaction Materials (Unit 1).
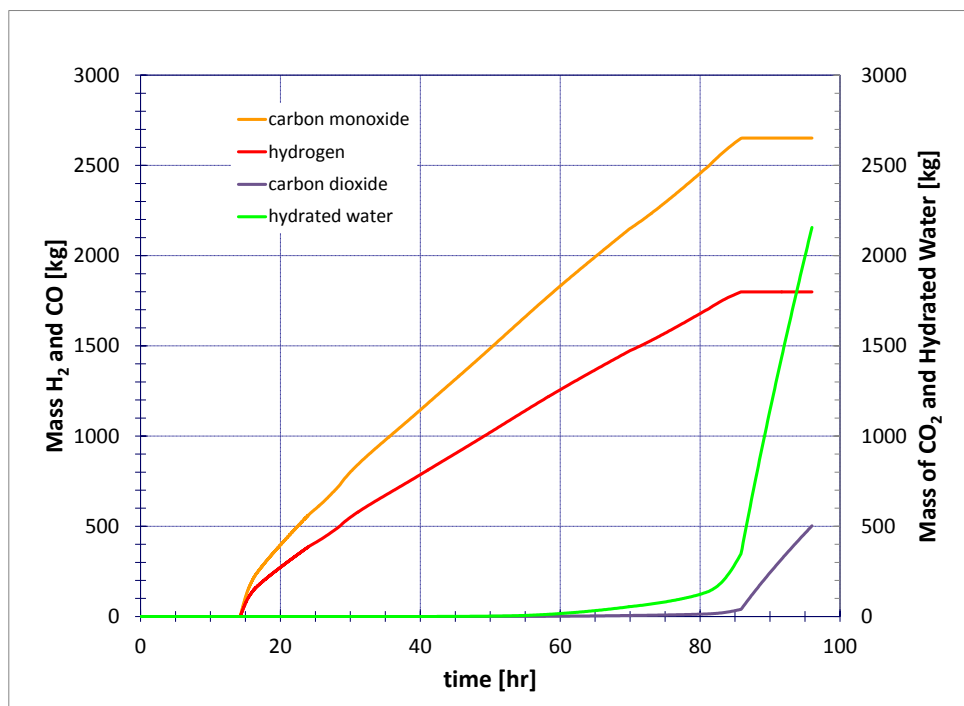
Figure 38. MELCOR Predicted Reaction Products from Core-Concrete Interaction (Unit 1).
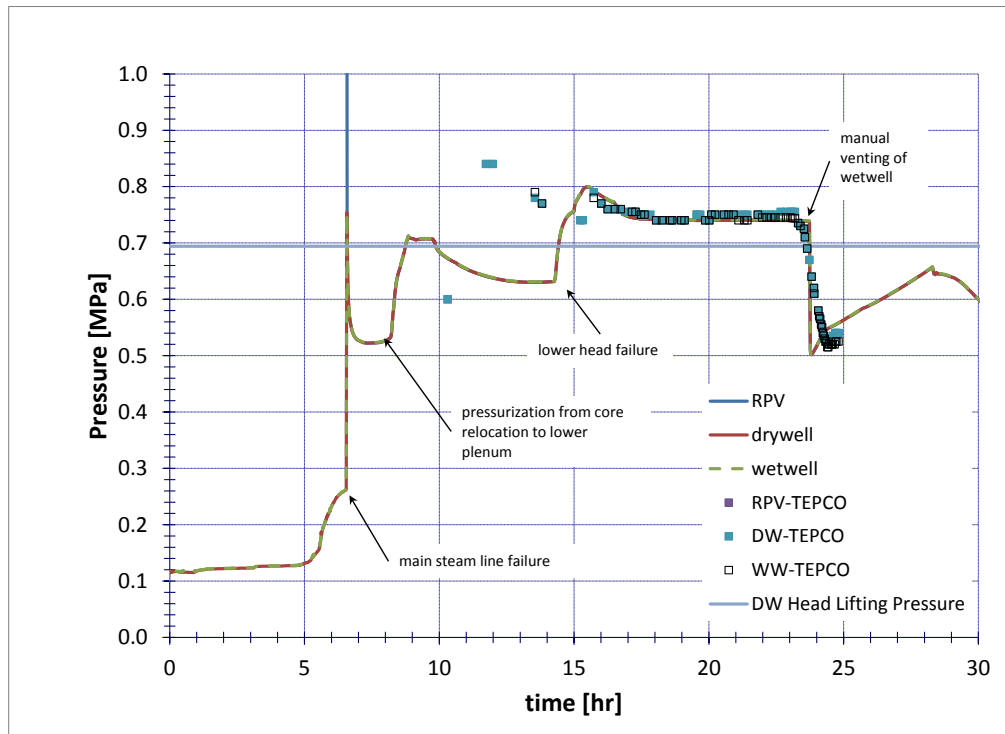
Figure 39. MELCOR Predicted Containment Pressure During the MCCI Gas Generation Phase Up To the Point of Manual Containment Venting (Unit 1).

The leakage through the head flange region is shown in Figure 40. Notice that there is a momentary leak caused by the transient pressurization when the steam line failed; however, the principal leak initiated at ~14 hours when the core materials exited the failed vessel head and began to interact with the concrete. Note also that a large constituent of the leaking gases is actually steam, initially from the boildown of water residing in the cavity from the earlier steam line rupture, and later from the addition of water to the RPV (which goes to the cavity) at ~15 hours.

The CO, H_2, and steam that escapes through the head flange leak enters the refueling bay and begins to displace the air in the building. Both CO and H_2 are, of course, flammable; however, the steam escaping with those gases inerts the mixture, preventing immediate combustion, and additionally, oxygen is simultaneously being purged from the building. There is considerable sensitivity to the precise gas composition within the refueling bay to the steam condensation rate in this room.

Figure 41 shows the total hydrogen produced in-vessel and through MCCI, as well as the total mass of hydrogen leaked into the refueling building, and the instantaneous mass of hydrogen resident in the refueling bay.
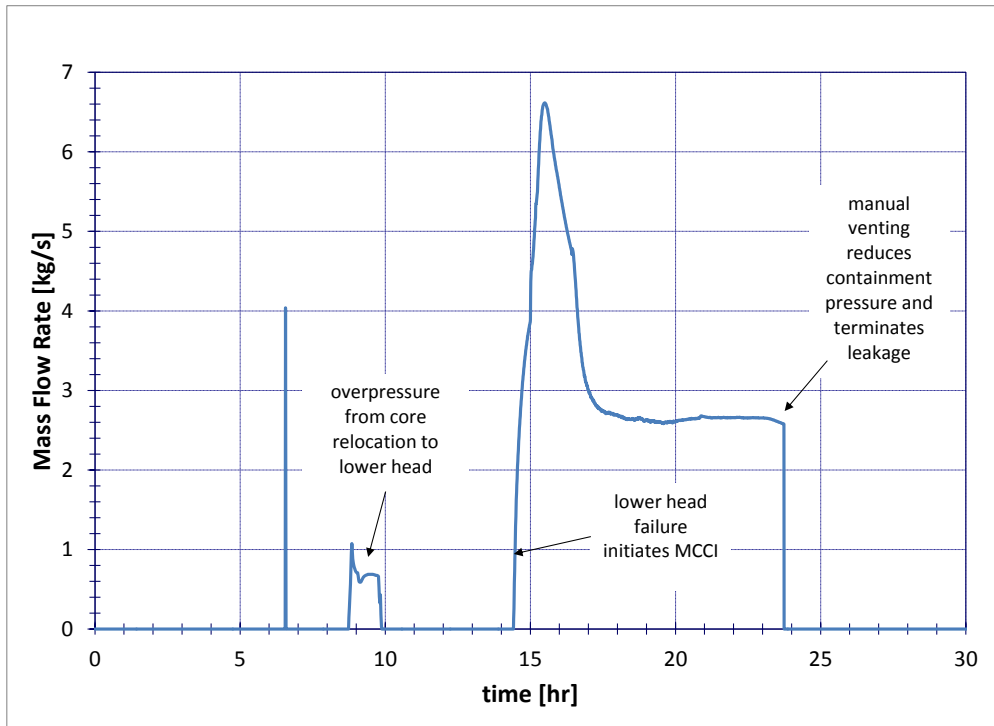
Figure 40. MELCOR Predicted Mass Flow of Gases and Steam through Drywell Head Flange Leak (Unit 1).
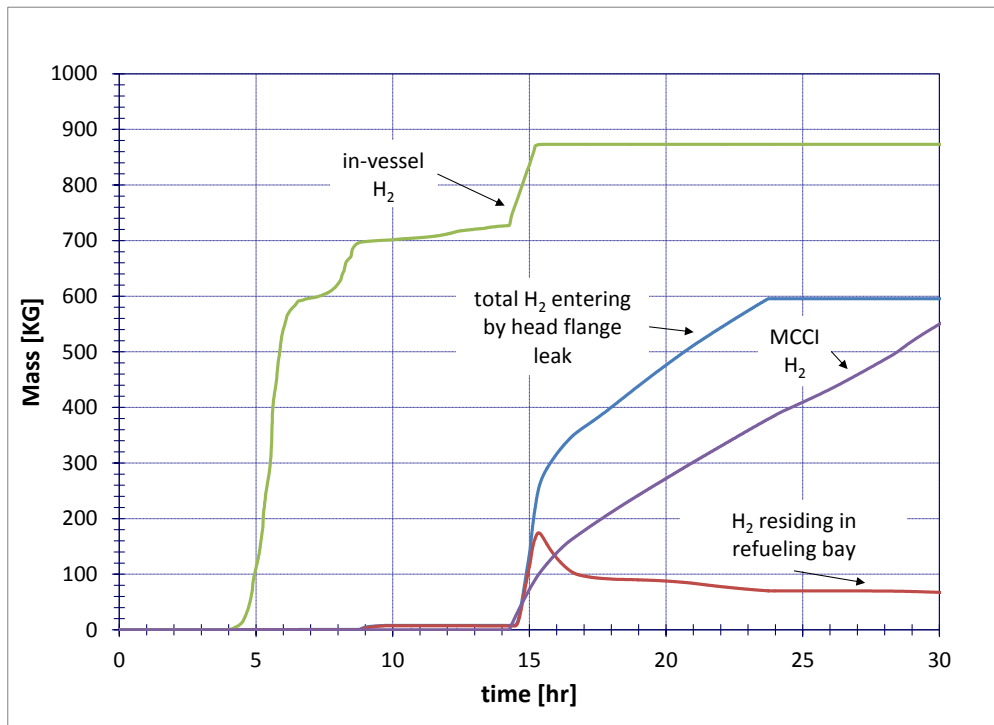
Figure 41. MELCOR Predicted Hydrogen Generation, Total Transport through Head Flange Leak, and Amount Resident in Refueling Bay (Unit 1).

The mass of hydrogen present in the refueling bay at any point in time is determined by the balance of inflow (head flange leak) versus outflow (building leakage), and this in turn is strongly affected by the relative pressure difference between the refueling bay and the outside environment. The present analysis includes some increased heat transfer through the refueling bay to account for cool conditions and sea breezes, and may be over-estimating steam condensation, since relative vacuum conditions are calculated for the duration of time that steam escapes the drywell head flange. This condition draws outside air into the building, reducing the mole fraction of the CO and H_2 for the given amount of mass resident in the building. The composition of the atmosphere in the refueling bay is shown in Figure 42 (mole fraction) and in (mass) in Figure 43.

As can be seen in Figure 42, for the most part, up until the venting operation, the steam molar concentration in the refueling bay is greater than 50%, effectively inerting the environment in spite of accumulation of ~100 kg of hydrogen and ~100 kg of CO.

Additionally, the mole fraction of the combustible CO and H_2 are generally below 10%, also discouraging spontaneous ignition. The manual venting operation just prior to 24 hours, however, led to profound changes in the refueling bay atmosphere, resulting in conditions supporting deflagration of the CO and H_2 gas,[18] as will be described as follows.
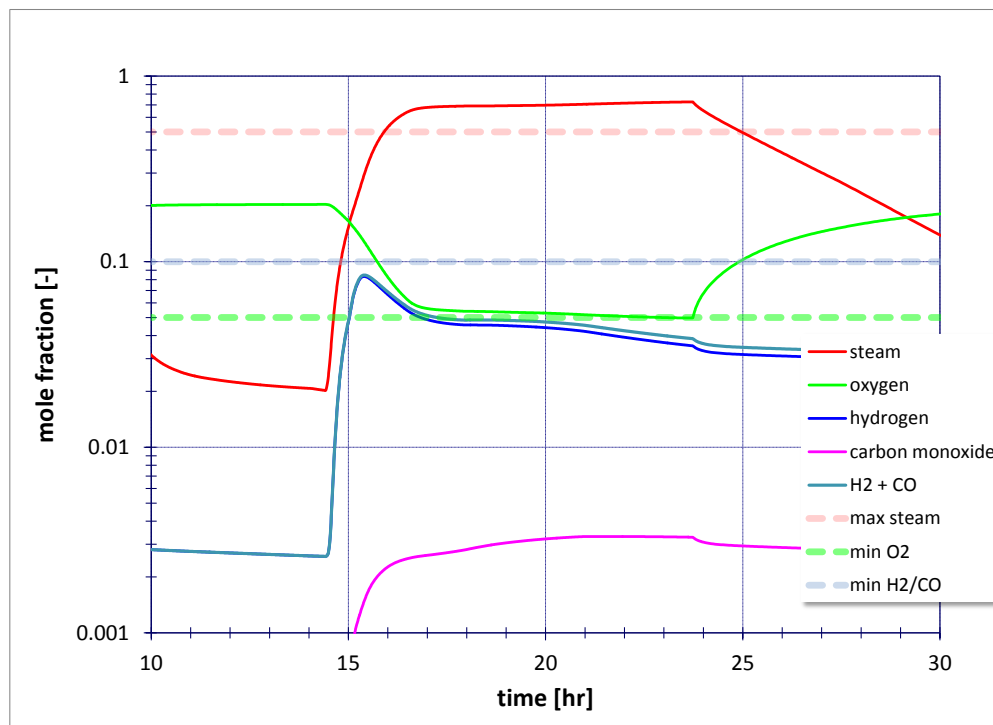
Figure 42. MELCOR Predicted Molar Composition of Atmosphere in the Refueling Bay during the Predicted Head Flange Leak Period. Shown Are Gas Mole Fractions and Min/Max Conditions for Hydrogen Deflagration (Unit 1).

---

[18] Note that CO gas production is from MCCI, as predicted by the Unit 1 MELCOR model. Production of H_2 is from both oxidation of core materials (e.g., cladding, stainless steel, B4C) and from MCCI.
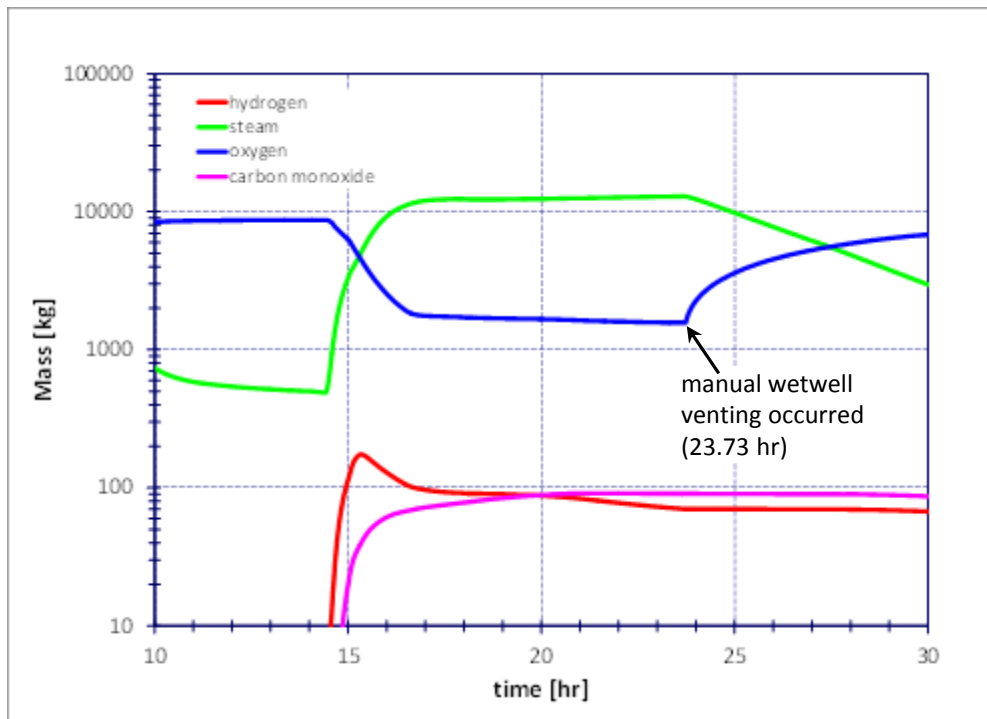
Figure 43. MELCOR Predicted Mass Composition of Atmosphere in the Refueling Bay during the Predicted Head Flange Leak Period (Unit 1).

The manual venting operation just prior to 24 hours reduced the containment pressure as intended; however, this reduction in internal drywell pressure also allowed the drywell head flange bolts to contract and close off the leak path to the refueling bay, thereby terminating the leakage of steam in the building. Up to this point, the continuous steam leakage produced largely from the boiloff of the water injected to the RPV had kept conditions in the refueling bay inert both from high steam mole fraction and by purging oxygen from the building. After the venting operation terminated the leak of steam to the refueling bay, the steam residing within the refueling bay atmosphere began to condense as the building temperatures dropped due to heat losses from the building. The condensation of steam produced a relative vacuum in the refueling bay, which in turn began to draw in air from the outside of the building through the natural leakage paths in the building. This effect both decreased the steam mole fraction and increased the oxygen content, as seen in Figure 43.

Within about an hour after the manual venting operation, conditions supporting burning of the gases are essentially attained—the explosion that destroyed the reactor building was observed at ~25 hours. While the drywell head flange leakage predicted by MELCOR provides an ample source of hydrogen to the refueling bay to explain a hydrogen explosion, an alternative scenario has also been identified that is directly associated with the manual venting operation. It has been proposed that due to the total loss of power, dampers that isolate the drywell vent path from the reactor building may have failed in an open position and that flammable gas intended to be sent to the release stack via the standby gas treatment system may have instead vented directly into the reactor building. In this case, an additional source of flammable gas may have also been a contributor to the observed explosion at roughly 25 hours.

86

Predicted fission product releases are shown in Figure 44 for cesium iodine (CsI). Environmental releases are predicted to be on the order of 1 to 2 percent of the core inventory.
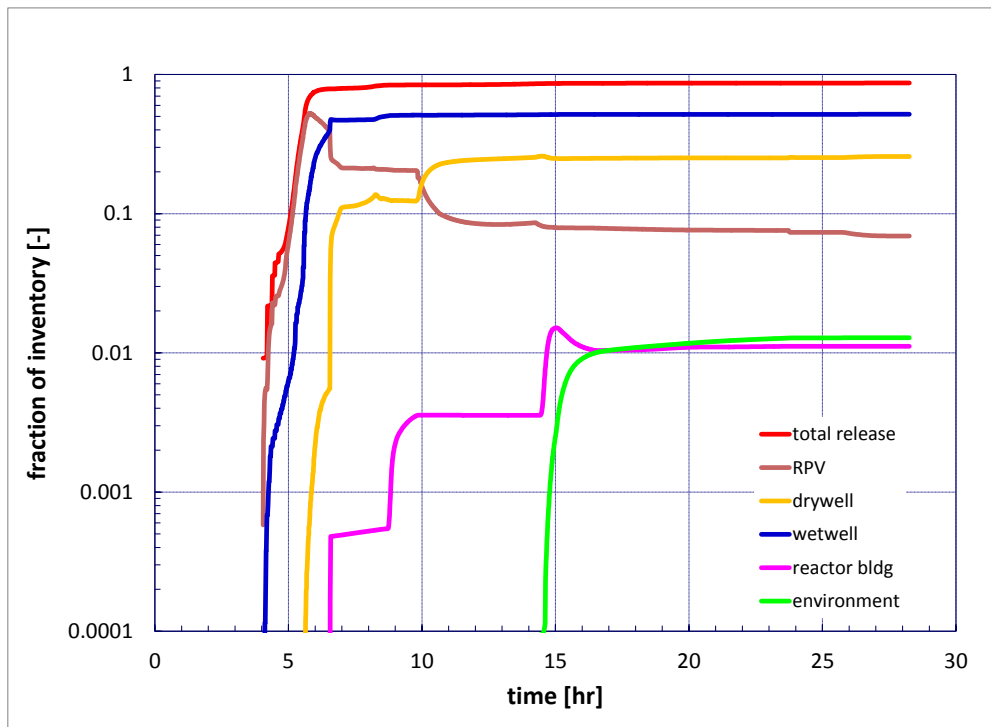
Figure 44. MELCOR Predicted CsI Distribution (Unit 1).
Note that release to environment from the reactor building explosion is not reflected in this distribution.

The results presented in this report for the Unit 1 accident are likely the most accurate of the three reactor accident scenarios described in this report, mainly because the boundary conditions are the simplest and most well characterized. That said, we also recognize that alternative sequence progressions may be identified in the future for the Unit 1 scenario that could equally well reproduce the available data, and as potentially new data or information becomes available concerning plant damage state, such as observation of a steam line rupture or some alternative RPV failure, these analyses may be revised and improved. Nevertheless, the analyses reported here are believed to provide valuable insights in the key events of the plant damage progression and can be useful in both guiding decommissioning activities and identifying areas for further study in the reactor disassembly process.

4.2   Unit 2 Results

The earthquake that occurred on March 11, 2011, initiated a loss of off-site power accident. Due to the seismic event, the reactor was shut down by an automatic scram. Automatic isolation of the reactor coolant system (RCS), contiguous to scramming the reactor, was accomplished through closing the main steam-line isolation valves (MSIVs); the diesel generators were also started. Due to isolating the RCS, the pressure of the primary vessel began to rise as liquid water was converted to steam by the heat generated from radionuclides. As the pressure increased, the safety relief valves (SRVs) self-actuated to relieve pressure, allowing steam generated in the RCS to pass into the suppression pool. The loss of liquid water inventory via the SRVs was managed by the operators manually starting the reactor core isolation cooling system (RCIC) at 180 s.

RCIC is aligned to inject liquid water, initially, from the CST to the reactor. The RCIC pump shaft is mechanically linked to a turbine. Power is provide by a steam extraction line, drawn from a main steam line, to the turbine, which exhausts the waste steam to the suppression pool within the primary containment vessel. The injected water replenishes the lost inventory. Automatic shutdown of RCIC is achieved when the water level in the reactor reaches the high level.

Before the loss of generator-produced AC/DC power (due to the tsunami) operators were required to manually restart RCIC three times due to the high-level signal shutdown. SRV cycling and RCIC operation may have maintained vessel level and reactor pressure as seen in Figure 45 and Figure 46, respectively, until RCIC failed.

Similar to the events at Unit 1, the tsunami that inundated the site disrupted the remaining power supplies; diesel generators and battery power were lost. RCIC was operating at the time of the station blackout and continued to do so for nearly 70 hours. A determination of the RCIC failure state due to a loss of DC power was not available; therefore, RCIC water injection was modeled to track the available water level data, assuming the data are acceptable, until RCIC was observed to deteriorate and/or fail. In this respect, RCIC injection is treated as a boundary condition to minimize the uncertainty associated with its operational state. The maintenance of RPV water level based on the available level data is presented in Figure 45.

The water level data were recorded from the reference leg, an uncompensated leg of water with the piping exposed to the drywell atmosphere. The water in the leg is fed via condensation from a condensate bulb (or pot) connected through piping to the RPV vapor space. During normal operation, the reference leg is full and all newly condensed water flows back into the reactor. The water in the reference leg, though stratified, is subcooled. A large depressurization of the primary coolant would be necessary to flash the reference leg inventory. Once flashed, the reference leg would erroneously report a higher water level than the actual water level in the reactor. Given that the deviation in pressure never approached the saturation pressure for the ambient temperature of containment, to which the reference water temperature is thermally coupled, flashing of the reference leg was unlikely during RCIC operations. Alternatively, should the RPV become flooded above the reference leg penetration site, an incorrect core level

reading would occur. Missing data during the first hours of the transient precludes determining the status of the water level instrumentation.

Steam released from the RPV, given expectations of the nominal accident progression, is either due to the SRV cycling or steam utilized for RCIC turbine operation. The RPV pressure trend, Figure 46, depicts a deviation from the SRV cycling set-point when the RPV begins to depressurize and remains below the SRV cycling set-point until RCIC fails. Prior analyses [19, 47] of the RCIC operating at capacity do not predict a depressurization of the RPV throughout the period when RCIC was operational; therefore, a leak from the RPV has been assumed. In addition, it was assumed the cycling SRV failed to completely reseat when the RPV began to depressurize, around 5.33 hrs.
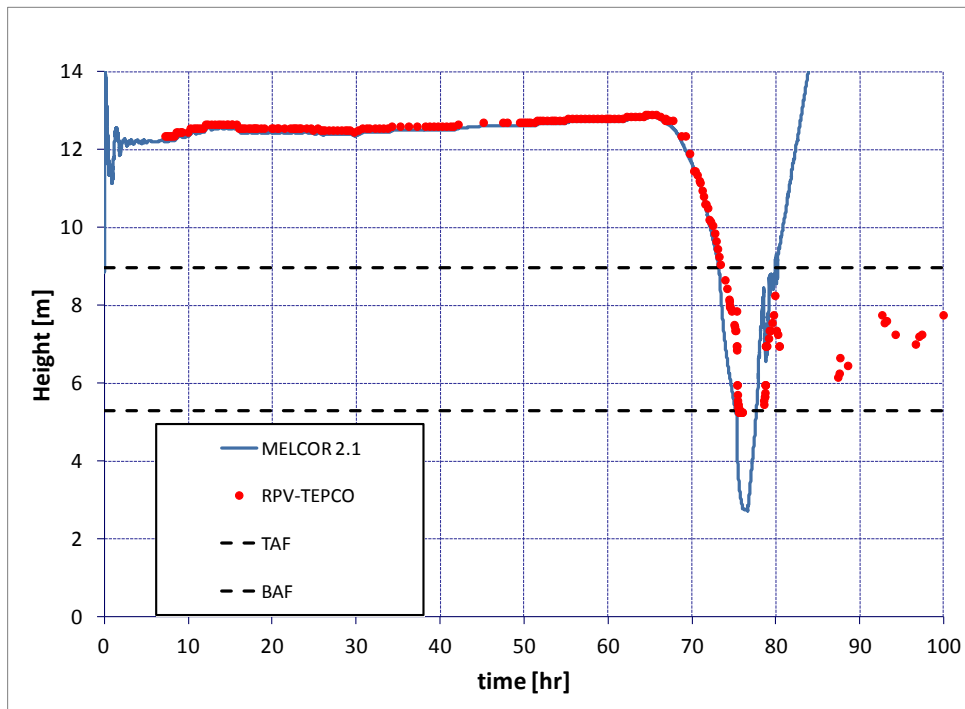
Figure 45. MELCOR Predicted RPV Water Level Compared with TEPCO Data (Unit 2).
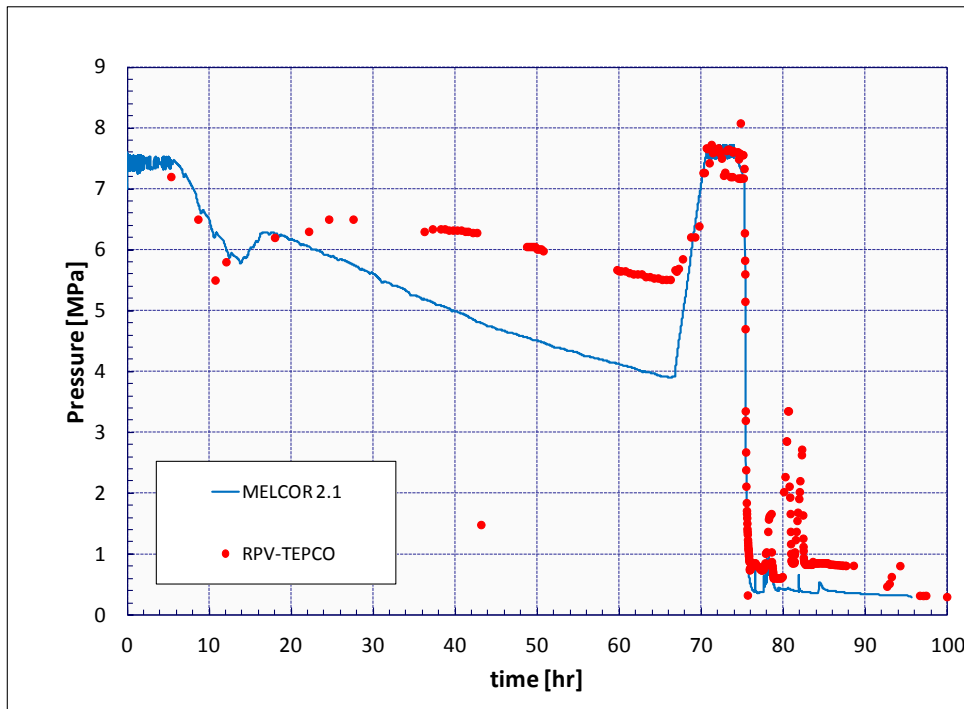
Figure 46. MELCOR Predicted RPV Pressure Compared with TEPCO Data (Unit 2).

The water injected by RCIC from the CST increases the total water inventory within the reactor system. Given the nearly constant RPV water level, the injected water is ultimately transported to the suppression pool inventory via the SRVs and RCIC turbine exhaust. The result is an increase in the suppression pool water inventory. At 13 hrs, operators were concerned about the water level height in the suppression chamber as well as the eventual depletion of the CST inventory; therefore, the RCIC pump suction was switched from the CST to the suppression pool [15]. Though unclear as to the means with which operators performed this action, RCIC pump injection changeover was implemented into the model. The changeover from CST to suppression pool water reduces the heat capacity of the injected water. The CST water temperature is approximately in thermal equilibrium with the environment, whereas the suppression pool has been heated by continual operation of RCIC and the SRVs. The analysis depicts a slight pressurization event corresponding with the changeover due to the difference in injected water heat capacity.

Although the suppression pool acts as a potential injection source for the RPV, another primary function of the suppression pool is to act as an energy sink to limit pressure excursions experienced within the containment. In the case of severe accidents where radioactive products may potentially escape the RCS, containment provides an additional barrier preventing environmental releases. To preserve the containment barrier, steam rejected to the suppression pool via the SRVs and RCIC turbine is condensed in the suppression pool. While the suppression pool remains subcooled, the pressurization of the drywell from steam rejection is due to mass and energy transfer from the pool surface due to vaporization. As the pool

90

temperature increases, the pool subcooling is diminished and the suppression pool begins to approach saturation condition, as seen in Figure 47. Once saturated, the suppression pool heat capacity is essentially depleted, and thereafter, steam released in the suppression pool fails to condense within the pool and instead passes to the suppression chamber vapor space. Pressurization of the suppression chamber vapor space forces the vacuum breakers connecting the suppression chamber and drywell to open. This releases steam into the drywell pressurizing the drywell as well. The MELCOR analysis predicts saturation of the suppression pool at 9 hours. Once saturated, the pressurization of containment is expedited.
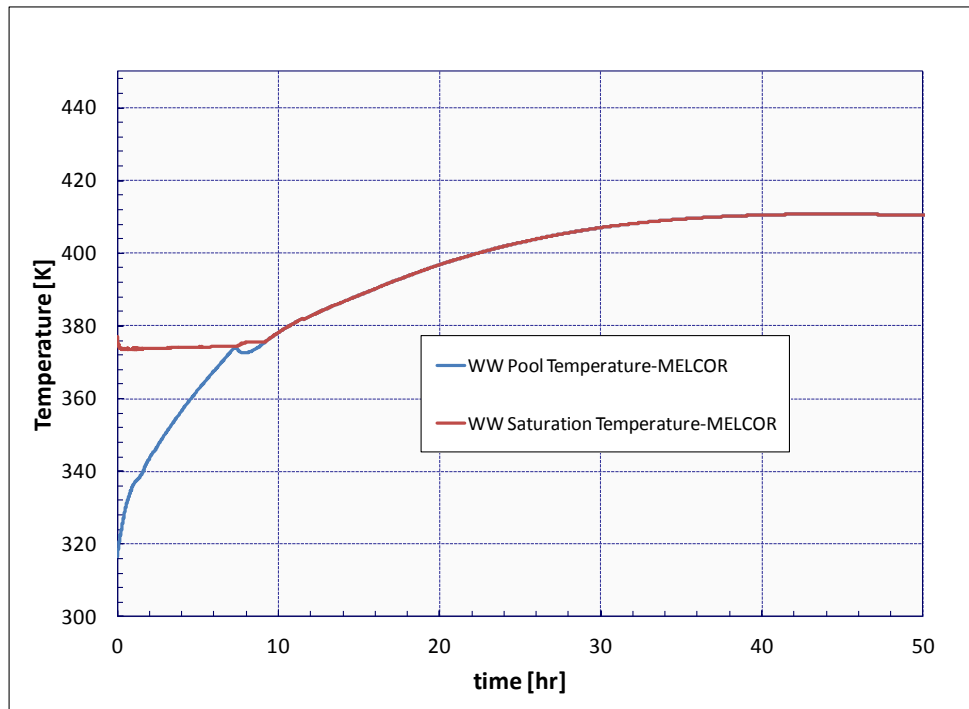
Figure 47. MELCOR Predicted Suppression Pool Water Temperature and Saturation Temperature (Unit 2).

Prior analyses [19, 47] have demonstrated containment pressurization far exceeding the observed Unit 2 containment pressure data. A possible explanation for the observed deviation from the data trend is that a leak has formed somewhere in the containment boundary, reducing the observed pressurization rate. Analyses performed for Unit 2 have assumed an unspecified leak forming in the containment boundary equivalent to a 2-in. diameter hole (see Section 3.6.1.5). Sensitivity to the timing with which the containment breached formed is negligible prior to the suppression pool becoming saturated. Figure 48 depicts the containment pressurization calculated by the analysis.
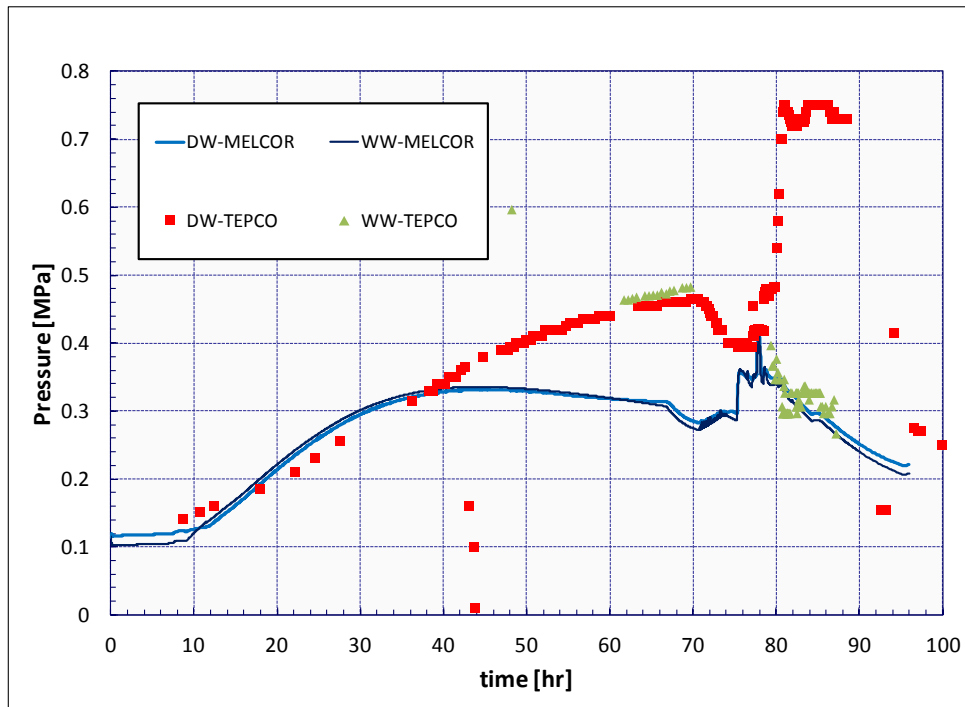
Figure 48. MELCOR Predicted Containment Pressure Compared to TEPCO Data (Unit 2).

After the failure of the RCIC system at around 67-70 hr, water injection to the RPV was lost and the RPV re-pressurized to the SRV cycling set-point. Steam flow to the suppression chamber stopped momentarily, or decreased, while the RPV re-pressurized to the SRV cycling set-point and the containment pressure began to decrease. Once the lowest set-point SRV began cycling again, containment pressure continued to decrease which seems inconsistent with the results of the analysis as well as general expectations.

To reinstitute water injection, onsite fire engine pumps were aligned to inject seawater.[19] The reported shutoff head of the fire engine pumps was 100 psig (0.69 MPa) [15], which required the RPV to be depressurized to allow seawater injection to commence. Shortly after 75 hr, operators actuated an SRV from the control room to depressurize the RPV. The RPV pressure quickly decreased to roughly the required pressure to permit seawater injection. As expected from the MELCOR calculation, the depressurization event resulted in a pressure rise in the calculated containment trend. Unexpectedly, the data do not produce corresponding containment pressurization in response to the RPV depressurization. Given the narrow range to initiate injection and the rapid rise in containment pressure observed around 80 hr by the control room operators, attempts were made to vent the drywell to the environment to allow the RPV pressure to be further reduced. INPO reported [15] that the rupture disk, with an actuation set-point of 76.7 psia (0.53 MPa), located in the containment vent line, was never actuated by the drywell pressure. This suggests that the containment pressure was at least below the rupture disk set-point, assuming vent alignment was successful completed.

---

[19] Due to a lack of Fukushima plant specific information, it was assumed that the seawater injection was through the core sprays. During comment resolution, it was pointed out by TEPCO that injection actually occurred via the LPCI.

In addition to the inconsistencies of the drywell pressure data observed, the suppression chamber and drywell pressure data diverged prior to 80 hr and remained so for a prolonged period. While direct releases to the drywell can result in pressure deviation between the suppression chamber and drywell, prolonged deviations cannot be maintained due to the limited RPV inventory and the vacuum breakers and drywell vents, which allow vapor to flow between the suppression chamber and drywell. The drywell vents and vacuum breakers require a differential pressure on the order of a few psi to begin equilibrating containment pressure. This suggests one of the available data sets for the containment pressure may well be erroneous shortly after RCIC failed.

Seawater injection was reported to have initiated at 77 hr. Two fire engine pumps were started within three minutes of each other. In the analysis, the seawater injection is modeled as a constant injection as reported by TEPCO [46], nearly 10 kg/s throughout the remainder of the analysis; the actual seawater injection rates are specifically dependent on the characteristics of fire engine pump and discharge pressure. Shortly after seawater injection was believed to have started, the RPV began to re-pressurize, exceeding the shut-off head of the fire engine pumps. Operators opened a second SRV to restore low RPV pressure to accommodate continual seawater injection. The second SRV was reported to have closed at 80.2 hr [15] resulting in a second observed pressurization spike.

The MELCOR analysis of the RPV response after the system re-pressurized in response to the RCIC failing is presented in Figure 49. During the SRV cycling, the MELCOR trend separates from the SRV actuation set-point earlier than the data. This suggests that in the model water level is no longer in sufficient contact with the active fuel to maintain the steam production rate, resulting in a slow depressurization prior to the operators actuating relief mode operation of an SRV to depressurize the RPV. Given this lower water level, in comparison to the RPV water level data, the amount of core degradation may be overestimated at this point in the analysis.

Following depressurization, sea water injection began. In the analysis, the injection of cold water quickly produces a pressurization response similar to the pressure increase seen at 78 hr. After the second SRV was opened to relieve the pressure, the second pressure excursion, resulting from closing the second SRV, is not apparent in the MELCOR analysis. This would result if the seawater water injection was overestimated. Application of the constant seawater injection rate quickly floods the vessel (see Figure 50). Given the magnitude and rate of the re-pressurization, the available heat capacity of the RPV water inventory is most likely inconsistent. The final pressure excursion seen in Figure 49 is also not present in the MELCOR analysis.

At this time, it is believed that the actual seawater injection is less than assumed in the MELCOR analysis, most likely due to RPV pressure exceeding the effective shutoff head of the injection pumps or some other yet unrecognized leak. The observed RPV pressure spikes after 80 hours suggest quenching of hot fuel by water is taking place, possibly as core materials degrade and fall into the lower plenum of the vessel. This would imply significantly greater core damage than currently captured in this MELCOR analysis. Future analyses should focus on refining the effective seawater injection, giving consideration to the observed RPV pressure.
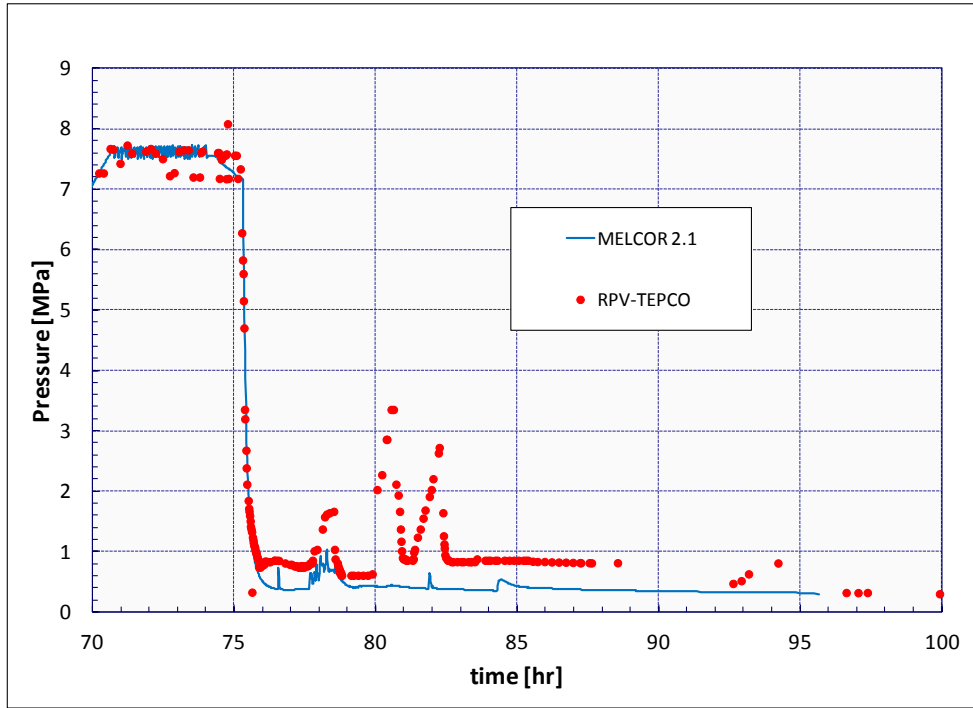
Figure 49. MELCOR Predicted Late-Time RPV Depressurization Compared to TEPCO Data (Unit 2).
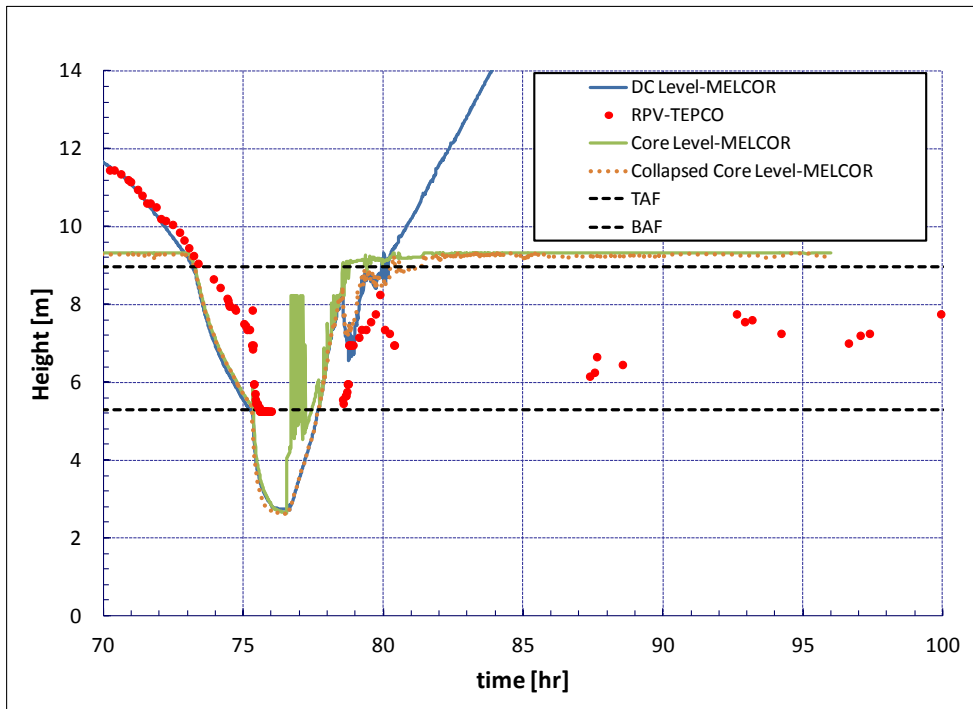
Figure 50. MELCOR Predicted Late-Time RPV Level Compared to TEPCO Data (Unit 2).

The onset of hydrogen production due to zirconium oxidation, signifying core damage, can be observed from the cumulative hydrogen produced in Figure 51, which occur shortly after the RPV water level falls below active fuel (see Figure 52). Figure 52 depicts the reactor core and vessel at two different points in time (in 2-D cylindrical geometry). The pink material is intact fuel and cladding, blue material is liquid water, yellow material is steel, and green material is particulate debris. The figure demonstrates that MELCOR predicts very little fuel and cladding damage for Unit 2. At 96 hours, only the majority of the top axial node (the top guide level that contains no active fuel) has relocated to the lower core plate as particulate debris. The initiation of the seawater injection near 77 hours rapidly restores water level above the top of active fuel (TAF).
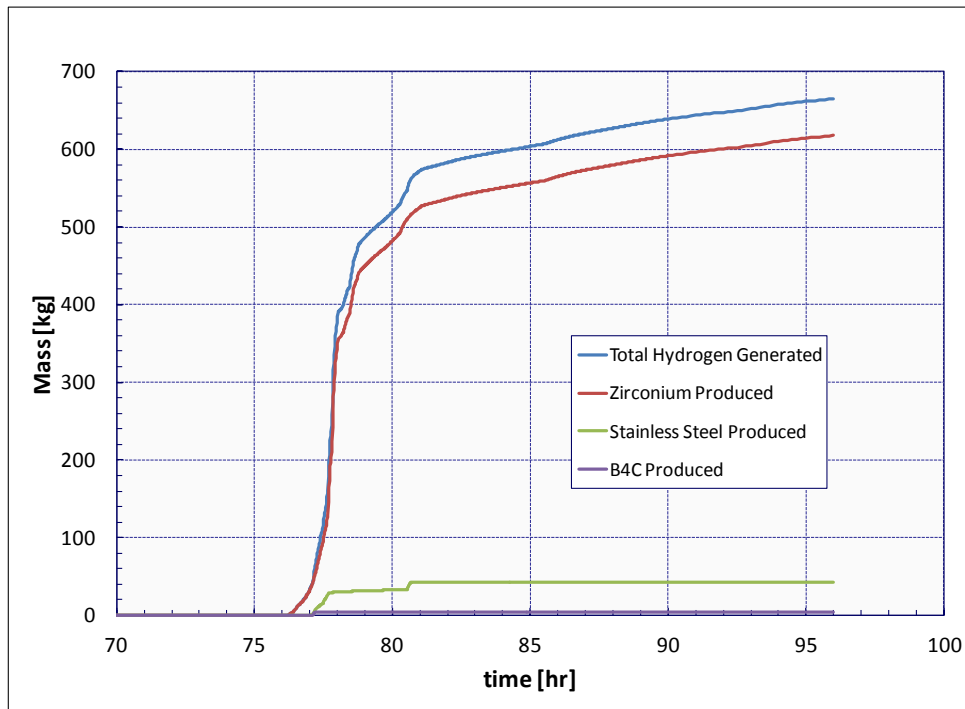
Figure 51. MELCOR Predicted Hydrogen Generation (Unit 2).
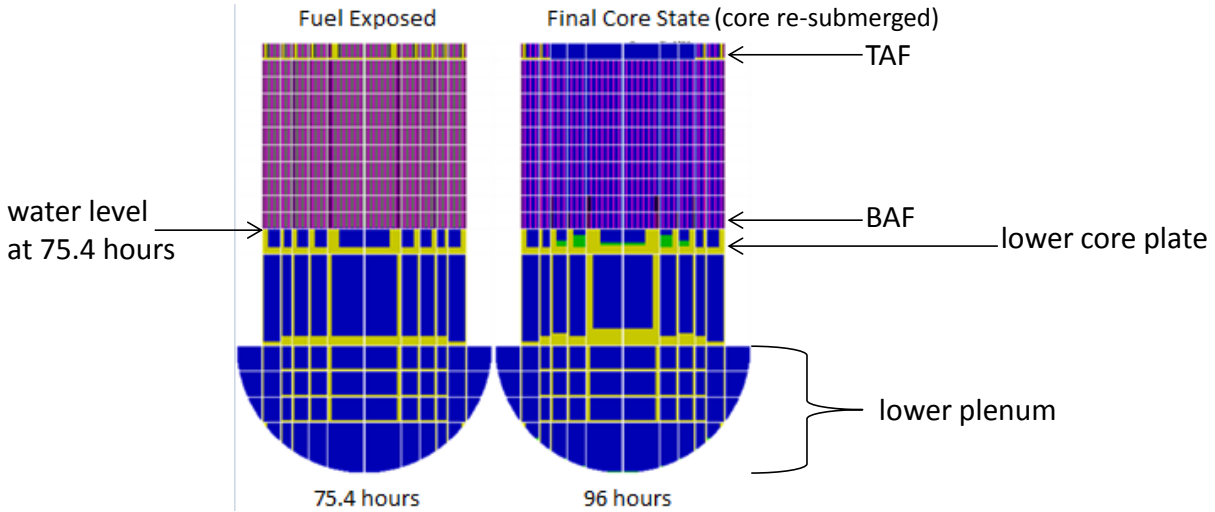
Figure 52. MELCOR Predicted Core Damage States (Unit 2).

The loss of core coverage resulted in core damage and radionuclides were released from the fuel. The steam released from the RPV transported fission products outside of the RCS barrier to the wetwell pool through the open SRVs. From the wetwell, the fission products not retained in the suppression pool were available for transportation outside of containment to the reactor building and ultimately the environment due to the nominal containment leakage as well as the assumed containment failure. Figure 53 presents the corrected[20] release fraction distribution of CsI within the RPV, containment, reactor building, and environment.

---

[20] Scrubbing of aerosolized fission products released from the SRVs to the wetwell was found to be in error due to inaccurate bubble diameter specification. The SOARCA Peach Bottom long-term station blackout decontamination factor (~100) was imposed through post processing to adjust the CsI capture in the wetwell. The original Unit 2 analysis decontamination factor for the reactor building was assumed to be unchanged.
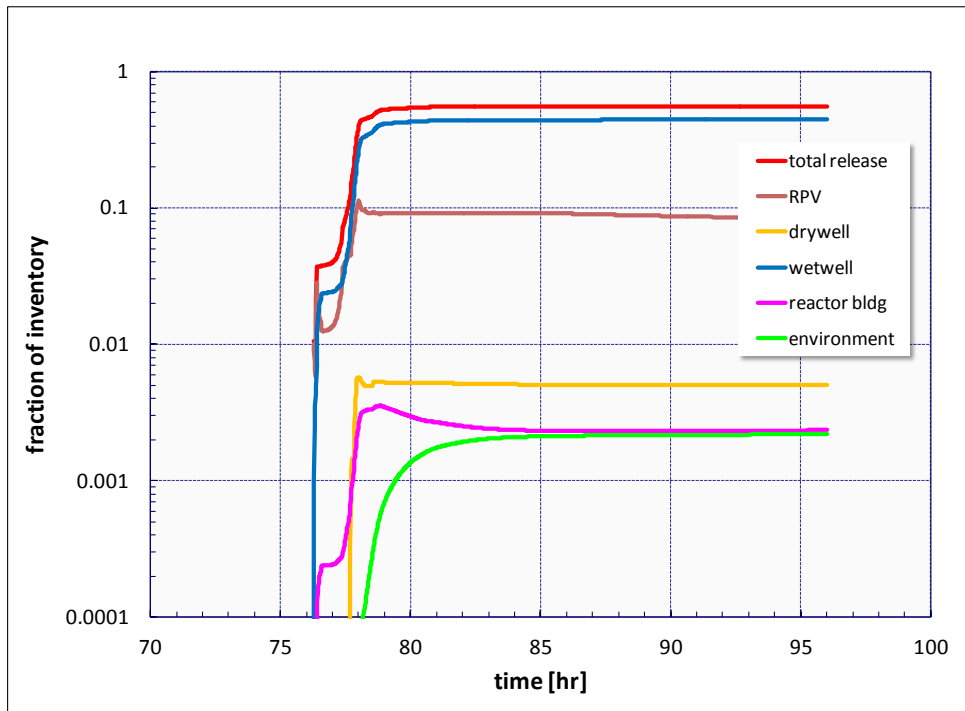
Figure 53. MELCOR Corrected CsI Distribution (Unit 2).

This analysis of the Unit 2 accident progression made use of the full stated water injection flows reported by TEPCO. Recently obtained information suggests that full injection flow was not actually attained owing to high pressure in the containment acting against the low pressure pumping capacity of the fire engines. This would suggest lower injection flows may be appropriate which would imply greater damage than predicted in these analyses. It is also postulated that torus room flooding may be have delayed suppression pool saturation and may be an alternative explanation for the slower-than-expected containment pressurization rate which in this analysis is attained by hypothesizing a small leak in the containment pressure boundary. Future analyses will take this emerging information into consideration. The current analyses nevertheless provide valuable insights into the overall damage progression of the Unit 2 sequence.

4.3 Unit 3 Results

From approximately the time of reactor shutdown to 36 hours, the RCIC and HPCI systems inject water into the RPV, remove decay heat, and maintain the RPV water level near nominal levels. Figure 54 shows the predicted and measured RPV pressure response for unit 3. Figure 55 shows the core and RPV water levels. From 0 to 20.8 hours, the RCIC is modeled as operating essentially continuously in order to maintain a target RPV water level; simultaneously, SRV1 cycles during this time period in the analysis. The SRV operation and the RCIC turbine exhaust both eject steam to the saturated wetwell, which pressurizes the containment (see Figure 56). The operation of the HPCI, having 9.9 times the capacity of the RCIC system in the SNL model (965 t/hr vs. 97 t/hr), results in a rapid depressurization of the RPV at 21.8 hours as a result of the large steam draw from the RPV. The HPCI turbine also discharges exhaust steam to the wetwell pool. At 42.13 hours, the RPV depressurizes via manual SRV opening. Small spikes in the RPV pressure are calculated to occur from 45 to 50 hours due to hot core materials falling from dry upper regions of the core into the water that is still present in the lower regions of the core. The measured data also show some transient spikes in this time period.
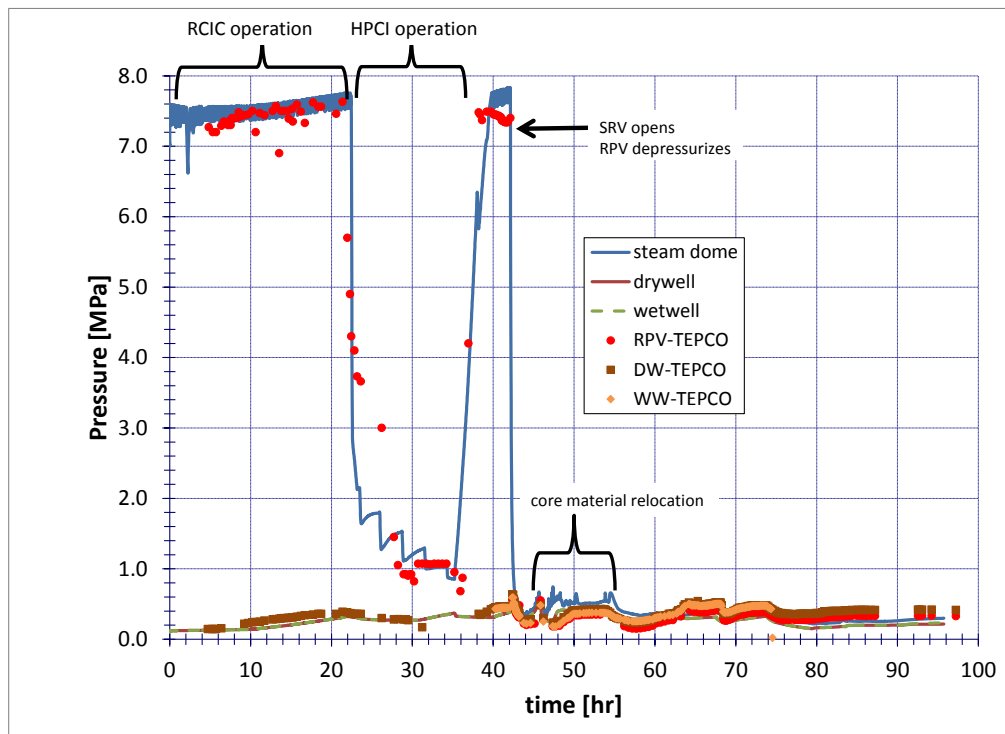
Figure 54. MELCOR Predicted RPV and Containment Pressures Compared to TEPCO Data (Unit 3).

As shown in Figure 55, the water level is maintained by the RCIC and HPCI until 36 hours. (Note: the "core swollen water level" is the two-phase mixture level in the core region of the MELCOR model. Its maximum level is just slightly above TAF, around 9.5 meters, which is the highest axial extent of the COR package in the model.) The operation of the HPCI leaves the RPV in a cool and low-pressure state, with the water level 4-5 meters above TAF. At 36 hours, the HPCI injection ceases and the HPCI turbine stops drawing steam from the reactor. Since the

98

decay heat is no longer being removed by flowing coolant, the water in the core region heats up and the RPV begins to re-pressurize. Increased voiding and thermal expansion of the water in the RPV causes a temporary rise in RPV water level, despite the fact that all water injection into the RPV has stopped. Once pressure reaches the SRV set-points, water level in the RPV begins to drop at a rate of ~1 m/hour due to continued boiling and water inventory loss through the cycling SRVs. After the RPV is manually depressurized at 42.13 hours, the water level drops rapidly below the TAF. The fuel is exposed beginning at 42.33 hours; hence, after depressurizing, it only takes 12 minutes to uncover the active fuel in the core.

Using the surrogate seawater pump model, MELCOR predicts that the core was nearly uncovered again near 60 hours, but a subsequent seawater injection quickly refilled the RPV. Further refinements to the likely overly optimistic pump model for the seawater injection (see Figure 13) may allow MELCOR to predict another core uncovering and the accompanying Zircaloy oxidization; it appears the flow rate of the second seawater injection (from 60.55 hours to 68.2 hours) needs to be reduced. With the current containment and vent model, this would be necessary in order for MELCOR to calculate flammable gas mixtures in the reactor building near 68 hours, the time of the explosion in the Unit 3 reactor building. Alternatively, reductions in injection rates may cause MELCOR to predict vessel failure, and ex-vessel MCCI starting near 60 hours could increase containment pressure and generate H_2 and CO for the explosion at 68 hours.
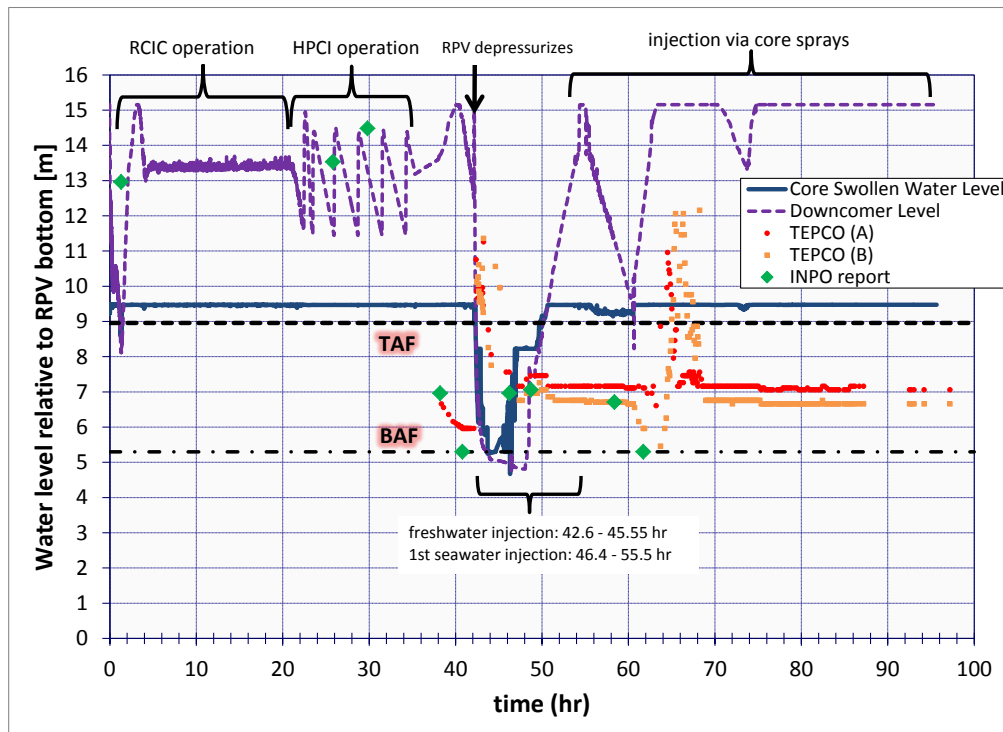
Figure 55. MELCOR Predicted Core and Downcomer Water Levels Compared to TEPCO Data (Unit 3).

Figure 56 shows the drywell and wetwell pressure response. The wetwell and drywell pressures are nearly identical; thus, they are indistinguishable in Figure 56. The RCIC steam exhaust and the steam discharged from the cycling SRV #1 cause the containment pressure to increase until the HPCI starts at 21.8 hours. (Note: the wetwell pool saturates near 10 hours.) Since RPV water level is maintained by RCIC operation, the HPCI initially transports some cold water from the CST to the wetwell (via the minimum flow line), causing a temporary depressurization of the containment. At this point the wetwell is sub-cooled again. Near 30 hours, the CST inventory is calculated to become depleted and cold water stops flowing to the wetwell. HPCI steam exhaust quickly re-saturates the wetwell and containment pressure is calculated to increase. At 36 hours the HPCI stops, at which point the HPCI turbine ceases operation and steam exhaust no longer flows to the wetwell. Near 40 hours, the RPV pressure reaches the SRV set-points, and steam from the RPV pressurizes the containment. At 42.13 hours, the RPV is fully depressurized via SRV opening, producing the largest peak in the containment pressure (caused by the sudden and large flow of hot steam from the RPV to the wetwell, via the open SRV). The maximum containment pressure calculated by MELCOR is 80.1 psia (0.55 MPa). The TEPCO data lists a maximum drywell pressure of 92.4 psia (0.64 MPa) and a maximum wetwell pressure of 85.6 psia (0.59 MPa).
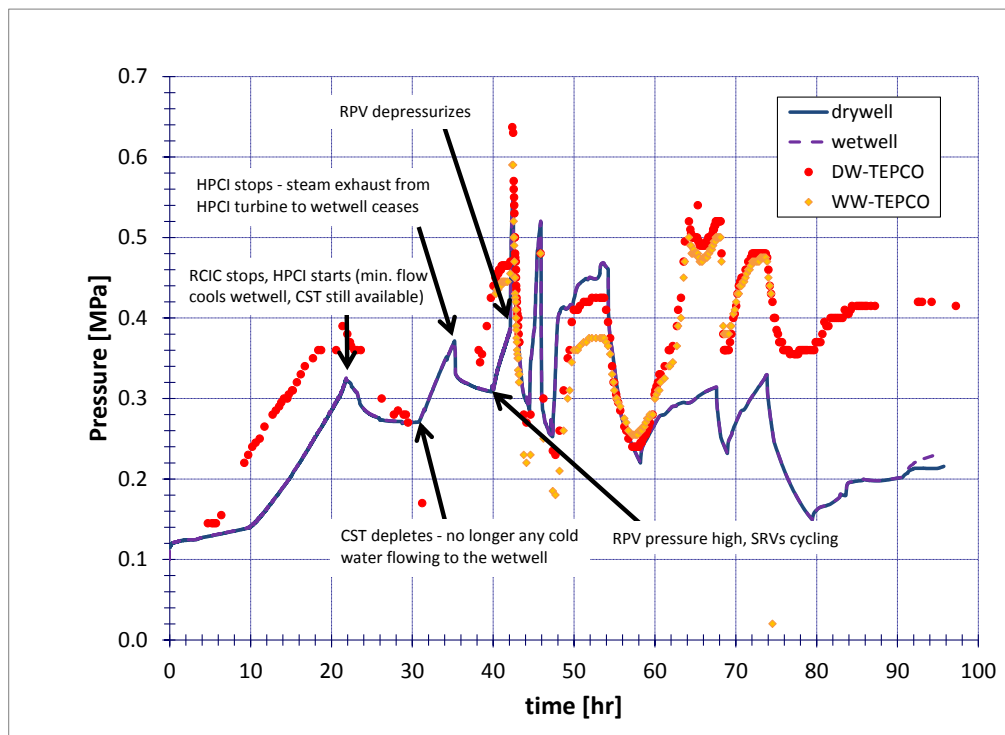
Figure 56. MELCOR Predicted Drywell and Wetwell Pressures Compared to TEPCO Data (Unit 3).

Figure 57 again shows containment pressure, but it highlights the comparison between the MELCOR calculation and the TEPCO Unit 3 data after 40 hours. Noted on the figure are the vent opening and closing times, which were chosen in an attempt to capture the peaks and valleys of the TEPCO containment pressure data. Also shown on Figure 57 are the injection flow rates using the surrogate pump model (green dotted curve). It demonstrates that excessive

seawater injection, particularly after 60 hours, may be suppressing pressure in the RPV and containment. Additional core uncovery and hydrogen generation near 60 hours may be the cause of the high containment pressure around this time. This would also correlate well with the reactor building explosion at 68 hours. As previously mentioned, ex-vessel H_2 and CO generation could also be the cause of the high containment pressure and reactor building explosion.
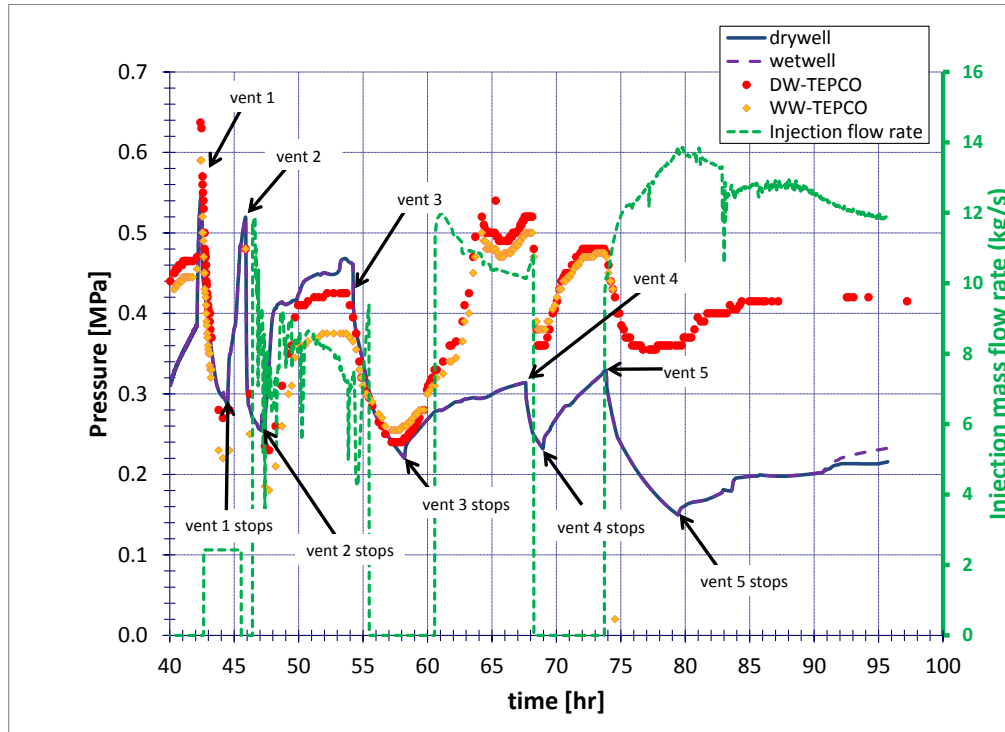
Figure 57. MELCOR Predicted Unit 3 Containment Pressure and Water Injection Flow Rates (40 - 96 hr).

Figure 58 shows the hydrogen mass generated (left axis) and the peak cladding temperature (right axis) after 40 hours. Zircaloy, steel, and boron-carbide (not shown on Figure 58) oxidation begin at a low level after 43 hours when peak cladding temperatures have exceeded 1100 K. By 90 hours, 1327 kg of total hydrogen is generated due to steam-metal oxidation reactions. At this point, approximately 70% of the original zirconium metal in the core is oxidized. Significant flow blockages caused by debris relocation and re-freezing reduce the cooling capability of the freshwater and seawater injection, thereby causing high maximum core temperatures after 44 hours.
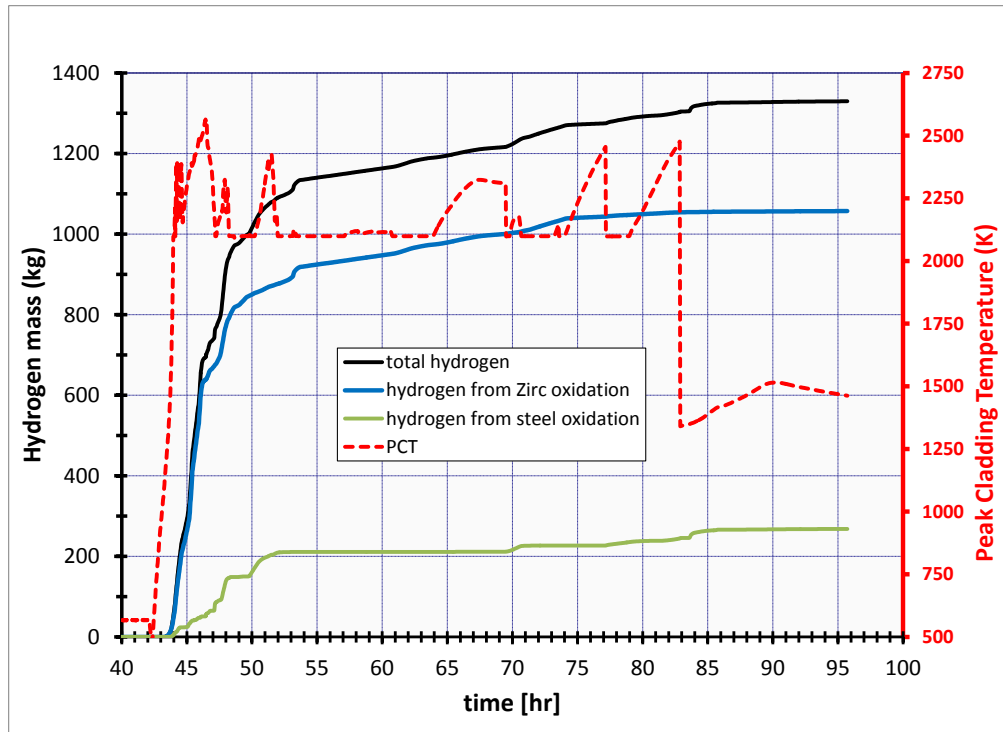
Figure 58. MELCOR Predicted Hydrogen Generation and Peak Cladding Temperature (PCT) for Unit 3.

In order to attain conditions favoring a detonation or deflagration in the reactor building, a MELCOR control volume must contain an appropriate mixture of air, hydrogen, steam, carbon-monoxide, and carbon-dioxide. Core material is predicted to be retained in-vessel throughout the simulation (96 hours), so there are no core-concrete reactions to generate hydrogen and carbon-monoxide by this process. Thus, a potentially explosive mixture would result from a volume containing the appropriate concentrations of air, steam, and hydrogen, where the hydrogen concentration is greater than 10% by volume as calculated by MELCOR. With the current seawater injection model and the current wetwell vent model (a flow path from the wetwell to a lower reactor building volume), MELCOR does not predict explosive mixtures near 68.2 hours, but much sooner near 45-55 hours, as shown in Figure 59. Near 68.2 hours, the gas volume concentrations of the reactor building volumes are approximately 70-75% steam, 20-25% air, and less than 4% hydrogen. Most of the hydrogen that was present in the reactor building from 45 to 55 hours has leaked out by 68 hours. However, there is a slight increase in hydrogen concentration at 68.2 hours due to a wetwell vent occurring at 67.6 hours.

With the current containment and vent model, there would need to be another period of core uncovering and Zircaloy oxidation after vent #3 (at 58.2 hours) in order to generate sufficient hydrogen for an explosion to occur at 68.2 hours. As discussed earlier, the current seawater injection model does not allow for this. The core nearly uncovers at 60 hours, but the uncovering is prevented by seawater injection. Hydrogen generated after 60 hours would be stored in the wetwell until the #4 vent at 67.6 hours, where it would then move to the lower reactor building.
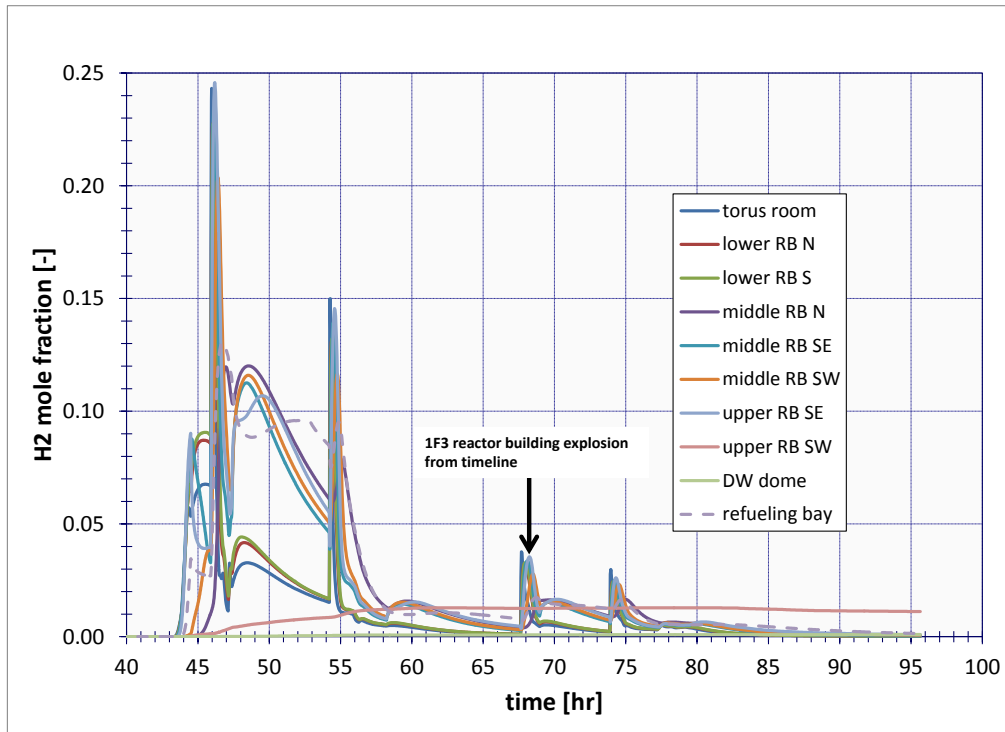
Figure 59. MELCOR Predicted Hydrogen Distribution in the Reactor Building (Unit 3).

The progression of the core damage is illustrated by Figure 60. The figure contains three 2-D representations of the reactor core and lower-vessel at different points in time. The pink material is intact fuel and cladding, the blue material is water, the yellow material is steel, the green material is particulate debris, and the red material is molten debris. Core material relocation begins at 44.2 hours when steel and Zircaloy melts in the top code node, which is the upper tie plate where there is no fuel. The first major fuel relocation starts at 46.5 hours when the fuel and cladding melt in ring 1, axial levels 13-16. By 96 hours, the majority of rings 1-4 have been damaged (converted to particulate debris), and the top core node has completely relocated. The fuel and cladding in ring 5 are not melted. Significant steel, Zircaloy, and UO_2 debris rests on the lower core plate and in the fuel region at 96 hours.

By 96 hours, approximately 52% of the initial UO_2 inventory has been converted to debris, and approximately 54% of the initial B_4C inventory has been converted to debris. The "final core state" depicted in Figure 60 does not take into account further core damage that may result from loss of emergency injection after 96 hours.
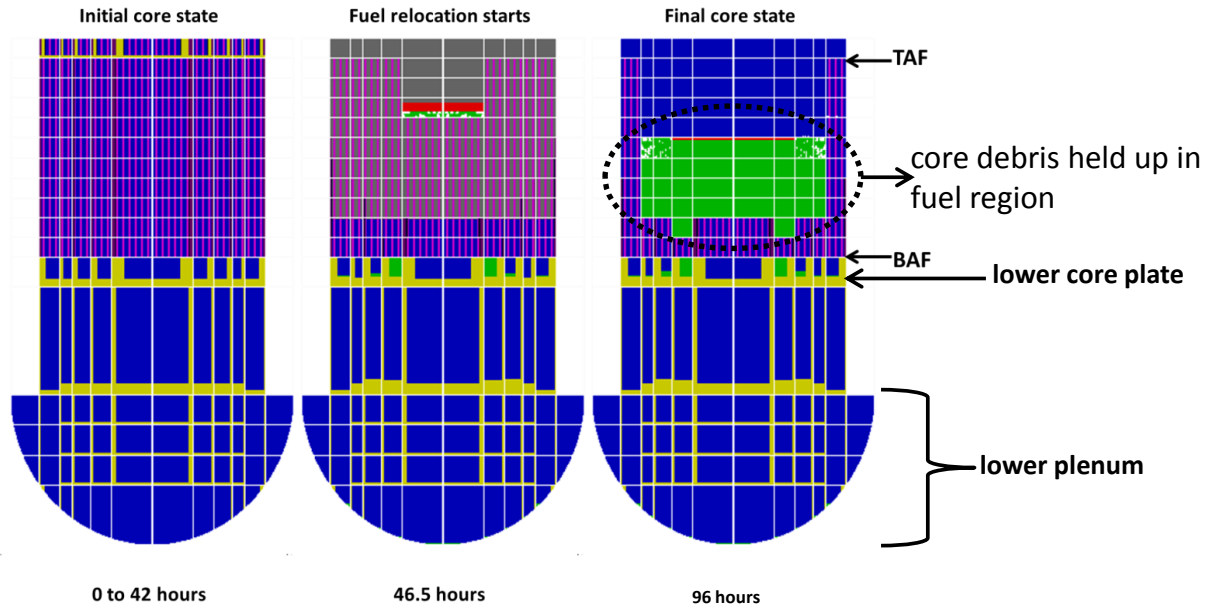
Figure 60. MELCOR Predicted Core Damage Progression (Unit 3).

Figure 61 depicts the MELCOR radionuclide class releases to the environment for Unit 3. Approximately 86% of the noble gas group is released to the environment. The initial inventory of the noble gas group is 360 kg, which includes the radioactive elements xenon, krypton, and radon. Less than 1.0% of the other radionuclide classes are released to the environment. Also note that Figure 61 does not show the effects of the reactor building explosion at 68 hours, which would probably increase the radionuclide release to the environment.
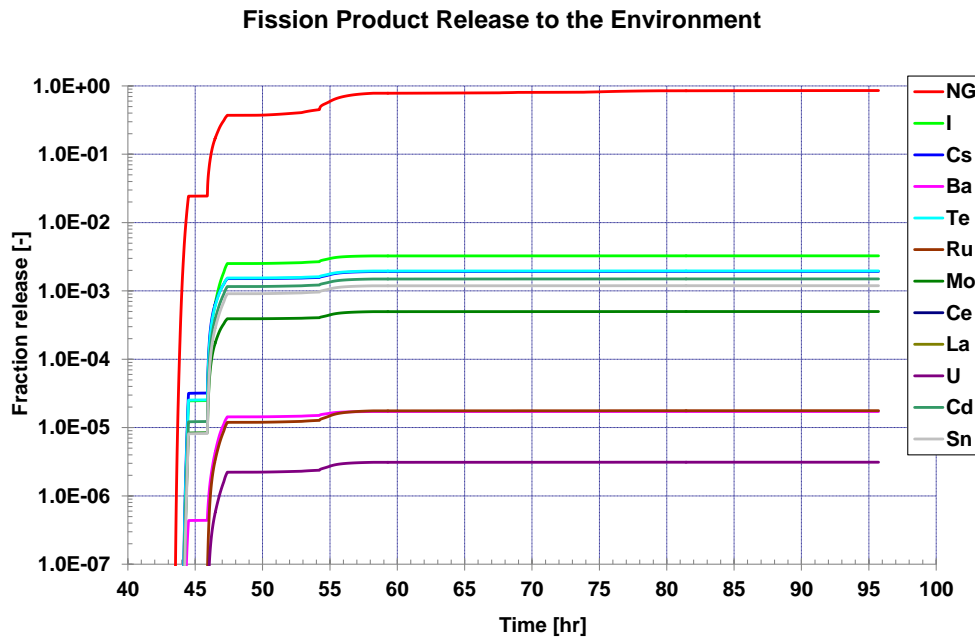
Figure 61. MELCOR Predicted Radionuclide Release to Environment (Unit 3).

As with the Unit 2 analyses, recently obtained information suggests that actual emergency water injection flow following RPV depressurization may be been significantly less than the initially reported values by TEPCO. The unit 3 analysis made a first attempt at accounting for the effect of high containment pressure on the effectiveness of the low pressure pumping equipment by considering a rudimentary pump-head curve. It is likely that the actual water injections were still less than the values suggested from the provisional pump-head curve model, implying that actual core damage may be more extensive than predicted in this analysis. Future refinements of these analyses will focus on sensitivity to the injection water flow. Nevertheless, the Unit 3 analysis shown in this study replicates many of the important accident progression signatures and is encouraging in terms of improving our understanding of these accidents and the capabilities of the severe accident codes.

4.4 Comparison of Radiation Detector Readings to Accident Progression Events

Figure 62 depicts the dose rate near the main gate of the Fukushima Daiichi plant from March 11 to March 16 [39]. The TEPCO dose rate data provides qualitative evidence for some events during the accidents. Some of the peaks on Figure 62 occur simultaneously with operator actions and known events, such as containment venting and reactor building explosions. However, several other peaks do not line up with any events from the timelines or the MELCOR simulations. There are also times when one would expect to see a peak in dose rate according to an event or simulation result, yet the data does not show a spike in dose rate at the exact same time.
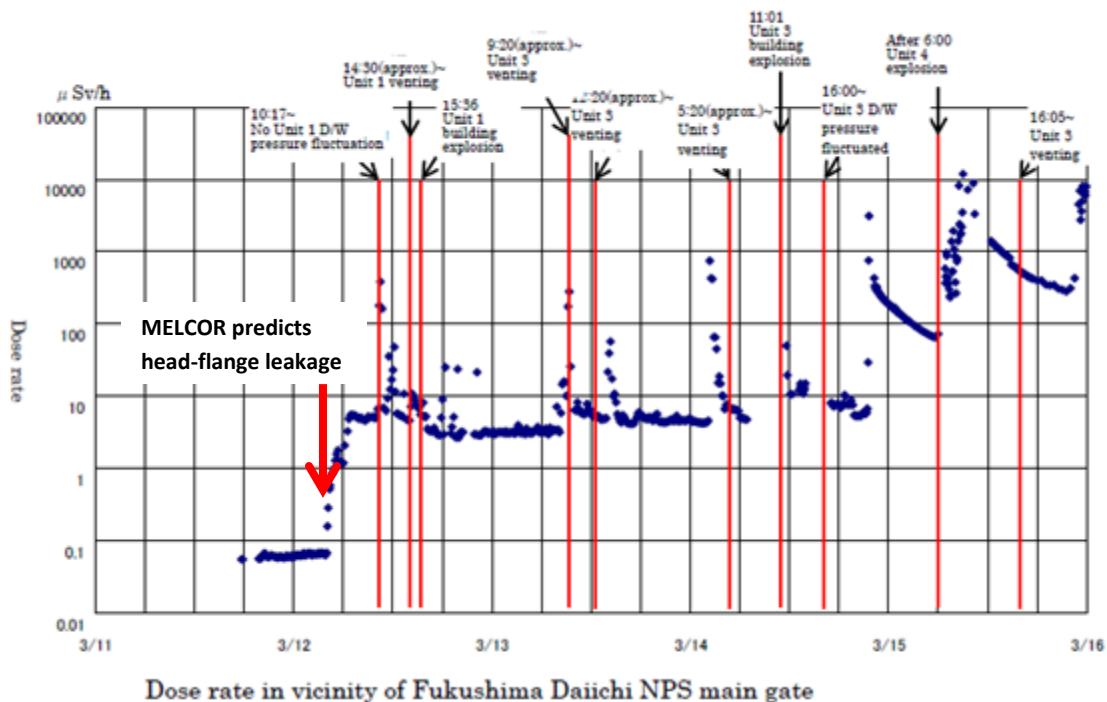
Figure 62. Comparison of Radiation Detector Readings to Accident Progression Events.

105

The dose rate data provides corroborative evidence for some of the events from the timelines, which were implemented into the MELCOR models as boundary conditions. For example, prior to containment venting at Unit 1 (which occurred at ~24 hr), MELCOR predicts substantial core damage and radionuclide release from the fuel, as well as some of the radionuclides being released to the containment. Hence, upon venting, an increase in dose rate would be expected for a detector located at the main gate; such an increase is seen in Figure 62. Furthermore, MELCOR predicts containment leakage for Unit 1 at the drywell head flange at ~15 hours after scram (5:50 AM on March 12). The initial increase in dose rate shown in Figure 62 corresponds with the MELCOR model prediction of radionuclide release through containment leakage at the drywell head flange.

The behavior of a radiation detector across a site boundary during three severe nuclear accidents is a complicated problem that depends on many variables, such as the specifics of the detector design, the 3-D arrangement of the plant, shielding (such as metal and concrete obstructions) between the radiation source and the detector, and the time-varying wind velocity. And while gamma rays, which are what the detector actually measures, are not affected by wind velocity, the gamma-emitting radionuclides definitely are affected. The position of radionuclides relative to the detector will affect the detector response, as will their position behind any shielding material. A mechanistic analysis of this data would require a coupled radionuclide and radiation transport simulation (e.g., MACCS for radionuclide dispersion and MCNP for gamma particle transport to the detector).

5   ORNL UNIT 3 MODEL DESCRIPTION, INPUT, AND ASSUMPTIONS

5.1   ORNL BWR Mk-I MELCOR Model History

The MELCOR Peach Bottom model utilized by Oak Ridge National Laboratory (ORNL) to study the Unit 3 accident for Fukushima Daiichi deviates in its history from the SNL model described in Section 3.1 starting in 2003. At this time, the Peach Bottom input deck was provided back to ORNL by Mark Leonard of dycoda, LLC, who had taken the original deck created by Juan Carbajo of ORNL and added a large array of control functions that mimic not only the operation of the safety systems but also the manual operation of the safety relief valves for proper temperature control in the wet well [28]. The input deck provided to Robert Sanders at ORNL for review was written for MELCOR 1.8.5.

Sponsored by the Defense Threat Reduction Agency (DTRA), Matthew Francis made modifications to the control functions within the input deck [11] to model the operators' procedures to follow the BWR Owners' Group Emergency Procedure and Severe Accident Guidelines if AC power was restored after a long-term station blackout [2]. Francis also made modifications to the input deck that modeled the connection of the emergency cooling system to a "large source of water [river water] for post-accident flooding of the primary containment" in accordance with Peach Bottom's Final Safety Analysis Report (FSAR) [23]. It is this model that was revitalized for the emergency response following the Fukushima Daiichi accident.

In July 2005, the MELCOR computer code was modified to version 1.8.6. One of the most notable changes from 1.8.5 to 1.8.6 was the elimination of the Bottom Head (BH) package. While many of the BH features were added to the COR package, some features pertaining to guide-tube failure modeling and the specific modeling of the conglomeration of the hot material in the lower plenum were significantly modified. Due to access and to investigate differences between code versions, ORNL utilized version 1.8.5 of MELCOR.

5.2   Fukushima Specific Modeling and Development

The following sections provide an overview and describe specific changes made to the Peach Bottom model to reflect the plant-specific characteristics and accident scenario. Features modified include (among others) the core power, reactor pressure vessel volume and diameter, radionuclide inventory, RCIC and HPCI flow rates, and SRV set-points.

More specifically, the RPV volumes and masses, D/W volume, S/C and CST volume and initial water mass, the core decay power and fuel loading, SRV set points, and the flow rate capacity for the HPCI and RCIC were modified to reflect Fukushima Daiichi Unit 3. The timeline events, including reactor scram timing, loss of AC and DC power timing, RCIC and HPCI availability, S/C venting availability, operator action to depressurize the RPV, and the timing and flow rate of the fire injection line were prescribed to the model. The logic controlling the RCIC and HPCI flows through the minimum flow and system test line were added and modified. Likewise, a flow path and timing for water injection from the fire engines were added. The S/C nodalization was refined.

The modifications exclude alteration of the elevations/heights of the vessels, piping, and building. A limited comparison between information for some components of Unit 3 and the model showed the relative elevations were comparable. The decay power was scaled; however, the relative distribution of decay power (power profile) was unmodified.

The following sections briefly describe the methods, modeling, scaling, and assumptions used for the "best estimate" results presented in Section 6.2. Insight from preliminary simulations are discussed in Section 6.3. The preliminary simulations used different sets of modeling assumptions, primarily for the RCIC, HPCI, and PCV sprays, which are noted in their respective sections.

5.2.1 Components and Nodalization

The model contains the major components, including the reactor core, RPV, steam and recirculation lines, PCV (drywell, wetwell, and sprays), RCIC, HPCI, reactor building with various rooms and stairwells, an outside environment, CST, and injection line for the fire engines. The overall layout of the reactor vessel and cooling systems are similar to SNL's model as illustrated in Figure 10. However, the "shroud dome" and "steam separators" control volumes are combined into one control volume in the ORNL model. In addition, a flow line into the feed water line was added for the water injection via the fire engines.

The reactor core is modeled similar to SNL's as illustrated in Figure 14. The ORNL model divides the core into five concentric rings with nine axial core segments (1-top of assemblies, 6-active fuel, 1-lower assembly, 1-lower plate). There are five axial segments capturing the control rod drive (CRD) tubes in the lower plenum as similar to SNL's model. The volumes, masses, and flow area were scaled in the radial direction based on either the ratio of assemblies or CRD tubes.

The S/C nodalization was modified to include eight divisions in the circumferential direction in contrast to a single control volume for the entire torus as modeled by SNL (see Figure 63 and Figure 64). This includes modeling eight D/W to S/C vents. Two different S/C nodalizations were investigated (see Section 6.3.3). In Figure 63 and Figure 64, the items in red are included in the eight S/C nodalization; whereas, items in green are also included in the 16 S/C nodalization. The RCIC and HPCI venting occurs in CV120 (see Figure 63) which also contains the SRV with the lowest set point. This was done to provide a conservative estimate of the local heat up rate of the S/C. The actual vent locations are likely different from that modeled. The nodalization refinement was performed to capture spatial variations of temperature in the suppression pool. The impact of S/C nodalization is discussed in Section 6.3.3.

The D/W is modeled similar to SNL's model as shown in Figure 17 except one control volume was used for the non-pedestal D/W region instead of three. The cavity for molten corium concrete interactions are modeled the same as in SNL's model as illustrated in Figure 20. The modeled volumes of the D/W and S/C are summarized in Table 7 as compared to similar U.S. plants. While there are variations in the volumes between plants, the modeled volumes for Unit 3 are comparable.

The reactor building nodalization is very similar to that illustrated in Figure 18 and Figure 19. However, the ORNL modeling results were not extended to include an analysis of the building response.
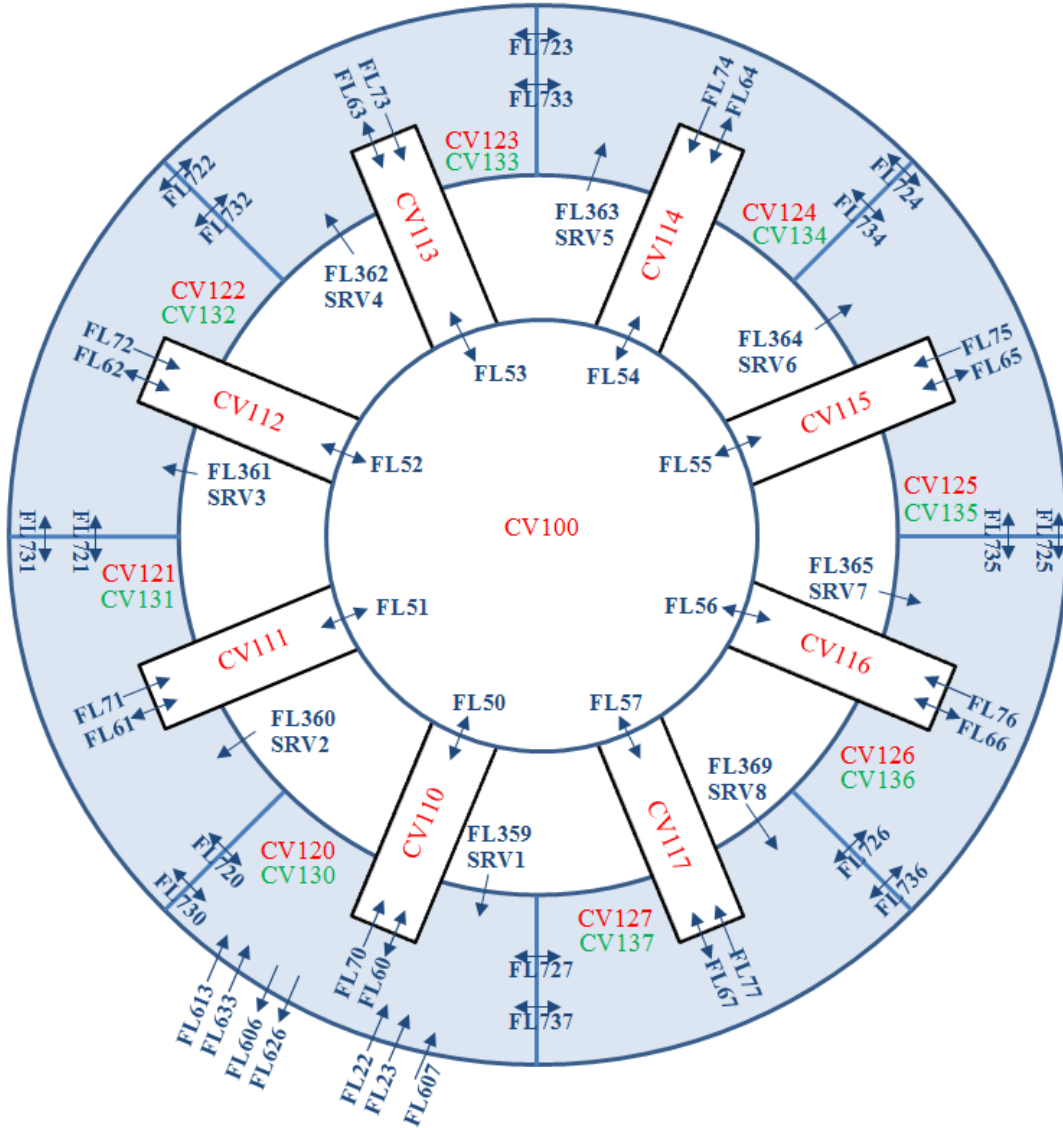
Figure 63. S/C Nodalization Top View.

Table 6. S/C Nodalization Top View Key

FL series	Description	FL series	Description
73x	S/C-S/C section upper flow	613	RCIC steam outlet
72x	S/C-S/C section lower flow	633	HPCI steam outlet
07x	Vent vacuum breaker	606	RCIC S/C suction
06x	Vent/downcomer outlet	626	HPCI S/C suction
05x	D/W-Vent flow	607	RCIC minimum flow line
359-369	SRV steam flow	22, 23	Pool to room vacuum breaker
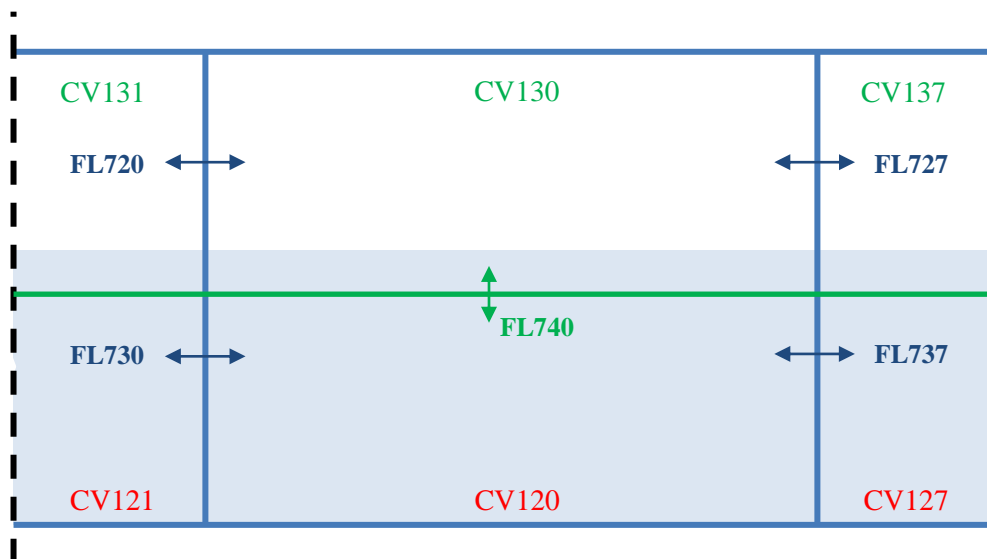
Figure 64. S/C Nodalization Side View

Table 7. PCV Volumes

Volumes [m³]	Fukushima Unit 3 [as modeled]	Dresden Unit 2&3 [6.2-18]	Hatch Unit 1 [8]	Hatch Unit 2 [8]	Browns Ferry
D/W gas	4240	4481	4135	4142	4502
S/C gas	3160	3194 (min) 3293 (max)	3197 (min) 3282 (max)	3109 (min) 3194 (max)	3370
S/C water	2980	3293 3392	2564 (max)	2564 (max)	3823
PCV Total	**10380**	**11067**	**9896**	**9815**	**11695**

5.2.2 Applied Timeline

For comparison and frame of reference, within Section 5, times listed in '{ }' are the elapsed time since reactor shutdown (14:47 March 11, 2011).

Table 8 summarizes the key timeline of events based on the IAEA reports [20, 21] up until 24:00 on March 14, 2011 {81:13}. These events have been applied as boundary conditions to the model. However, the PCV is allowed to vent only after the S/C reaches the rupture disk failure pressure (528 kPa abs) after the vent lineup is completed.

Table 8. ORNL Unit 3 Prescribed Timeline

Time	Event
{00:00}	Reactor SCRAM
{00:18}	RCIC startup
{00:38}	RCIC shutdown – due to high water level
{00:51}	SBO (batteries available)
{01:16}	RCIC startup
{20:49}	RCIC shutdown
{21:48}	HPCI startup
{35:55}	HPCI shutdown
{38:36}	Venting prep. – AO[*] large valve was opened
{41:48}	Venting prep. – MO[**] valve manually opened 15%
{41:54}	Venting prep. – WW vent lineup complete, awaiting rupture disk failure
{42:21}	RPV depressurization – operator activation of SRV
{42:38}	Start – Water addition from fire engines (fresh)
{44:30}	Venting – AO large valve confirmed closed (no venting)
{45:33}	Stop – Water addition from fire engines (fresh)
{46:25}	Start – Water addition from fire engines (salt)
{53:23}	Venting – AO large valve judged to be open (venting)
{58:23}	Stop – Water addition from fire engines (salt)
{60:33}	Start – Water addition from fire engines (salt)
{60:53}	Venting – AO small valve energized
{62:33}	Venting – WW venting carried out using AO small valve (venting)
{63:23}	Venting – AO small valve confirmed open (venting)
{68:14}	Unit 3 explosion in reactor building
{68:14}	Stop – Water addition from fire engines (salt)
{73:43}	Start – Water addition from fire engines (salt)
{87:13}	Unit 4 explosion in reactor building

 * AO = Automatically Opened

 ** MO = Manually Opened

5.2.3   Decay Heat and Radionuclide Inventory

The decay heat has been modeled in MELCOR using the American Nuclear Society's National Standard for light water reactors (ANSI/ANS-5.1-1979). The decay heat curve is scaled based on full power operation of 2381 MWth. The 32 MOX assemblies were treated as standard UO_2 fuel assemblies as a simplification. The impact of the MOX assemblies on the decay heat and radionuclide dispersion should be further investigated. The American Nuclear Society (ANS) standard decay heat curve likely provides a conservative (high) level of decay heat compared to actual Unit 3 decay heat. The axial and radial profiles are the same as those used in the Peach Bottom model. More than likely, minor discrepancies exist between the actual and assumed decay heat power profiles.

5.2.4   Steam Condensation

The condensation of submerged/rising steam bubbles in a pool is modeled in MELCOR using the product of two empirical efficiencies. The first efficiency accounts for the bubble rise distance. The second efficiency accounts for the water sub-cooling. The product of the two efficiencies determines the fraction of steam condensed in the pool versus passed through the pool to the atmosphere. For the "best estimate" simulations, the pool sub-cooling efficiency was modified using sensitivity coefficient 4405. The water sub-cooling efficiency was set to 100% for pool sub-cooling of 6 K instead of the default 5 K. This was performed to decrease the steam condensation rate in the S/C. Past tests performed at the Monticello nuclear power plant and modeling results [5] suggest it is possible for the S/C to thermally stratify, decreasing condensation of the steam vented through the SRVs. As the S/C modeling used in this study does not allow for thermal stratification, the empirical pool sub-cooling efficiency was decreased to empirically capture this effect. This is the only sensitivity coefficient that was modified from the original ORNL Peach Bottom model. More detailed description of the steam condensation modeling can be found in the MELCOR manual in the control volume hydrodynamics section [29].

5.2.5   Safety Relief Valve Set Points

The SRV open points are based on the set point data provided in Table IV-2-1 of Reference 20. The valve actuation was set to depend on the main steam line pressure and not the differential pressure between the main steam line and S/C. This modeling approach is consistent with assuming the SRV's are of the two-stage target rock design. The valves were modeled using T-O-F trip logic in MELCOR. This logic was used in the legacy Peach Bottom model. Within each of the groups of valves, the valve set points were staggered by 0.001 MPa (see Table 9). This was done to aid numerical stability. In reality, the valve set point uncertainty is likely greater than 0.02%. The valves were modeled to close after decreasing to 97% of the valve open set point. The SRV numbers indicated in the table correspond to S/C pool locations indicated in Figure 63.

Table 9: SRV Set Points

SRV Number	Plant Info. [20] (kg/cm^2 gage)	Plant Info. (MPa abs.)	As Modeled (MPa abs.)	
			Opens	Closes
1	75.9	7.545	7.545	7.319
2			7.613	7.385
3	76.6	7.613	7.614	7.386
4			7.615	7.387
5			7.682	7.452
6	77.3	7.682	7.683	7.453
7			7.684	7.454
8			7.685	7.455

5.2.6   RCIC Operation

The RCIC was used to maintain the reactor water level for an extended time. The RCIC was manually started at {00:18} and tripped at {00:38} due to high water level [20, 21]. The RCIC was then manually re-started at {01:16} and ran until it unexpectedly shutoff at {20:49} [20, 21].

The RCIC can take suction from either the S/C or the CST. Taking suction from the S/C would accelerate the RCIC (and later the HPCI) reaching the net positive suction head (NPSH) limit. The operators likely aligned the RCIC suction to the CST to extend the RCIC and HPCI operation time.

If the RCIC is assumed to run at 100% capacity, the simulation would predict periodic startup-shutdown of the RCIC. Allowing the RCIC to continually start and stop decreases the reliability of the RCIC. The control room operators have the ability to adjust the speed of the RCIC as well as divert RCIC pumped flow into to the S/C by actuating the minimum flow bypass line or to the CST by actuating the system test line. The operators likely manually operated the RCIC and bypass lines to prevent continuous start/stopping.

The operator log book [36] states "RCIC mini - flow valve "Open"" at 16:03 on March 11 {1:16} This indicates the minimum flow line was open during startup of the RCIC; however, this line is typically open until the pump is up to speed. A TEPCO representative at the January 25, 2012, indicated that, based on the December 22, 2011 TEPCO report, the system test line may have been used (sending water to the CST) and not the minimum bypass line. The operator log book [36] also states "RCIC: 19L/s" at 16:45 {1:58} (the pump capacity is listed as 97 t/h (27 L/s) in [20.,IV-15]). This suggests the operators manually decreased the speed of the RCIC. Currently, the speed at which the RCIC was operated as a function of time and the timing of RCIC water injections into the RPV are unknown. In addition, detailed performance characteristics of the RCIC system (liquid flow rate vs. steam demand) are currently unclear.

The current simulation assumes the RCIC system is similar to the systems in the Peach Bottom and Hatch [8] nuclear power plants (see Table 10). The RCIC operation model used for the "best estimate" simulation (Section 6.2) assumes the RCIC is set to operate at 100% steam flow and 75% liquid flow. The resultant performance curve (taking the 75% liquid flow into account) is given in Figure 65. The RCIC is aligned to take suction from the CST. The pumped water flow is

directed to the feed water line of the RPV when the water level reaches RCIC startup point. When the water level reaches RCIC trip point, the injected water flow is diverted back to the CST through the system test line.
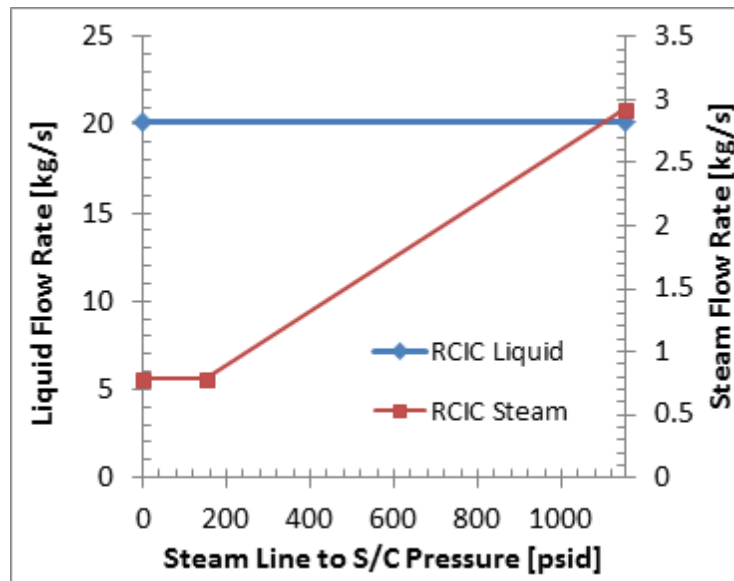
Figure 65. RCIC Performance Curve.

Table 10. RCIC & HPCI Flow at 100% Capacity

Flow [ton/hr]	ORNL Peach Bottom MELCOR model	Hatch Unit 2 [8]
HPCI Pump	1134	963.3
HPCI Turbine	85.3 @ 1115 psid 42.8 @ 115 psid	85.2 @ 1120 psid 49.7 @ 115 psid
RCIC Pump	136	90.7
RCIC Turbine	14.76 @ 1115 psid 3.96 @ 150 psid	10.0 @ 1152 psid 3.02 @ 147 psid

5.2.7   HPCI Operation

The HPCI system operates in a similar fashion as the RCIC system. However, the pumping capacity of the HPCI is 965 tons/hr [20], which is approximately 10× greater than that of the RCIC. As with the RCIC, the HPCI operates automatically by default. Under automatic mode, the HPCI turns on and off (water injection from the HPCI pump and steam flow through the HPCI turbine). Similar to the RCIC, the speed of the HPCI can be manually set by an operator in the control room and bypass lines (system test line and minimum flow line) can be opened and closed.

The steam requirements for the pump to operate at 100% (965 tons/hr) are assumed to be similar to the Peach Bottom and Hatch nuclear power plants. However, the operation of the HPCI turbine at high D/W pressures (75 psia) and low RPV pressures (119-155 psia) is not well known.

Due to large uncertainty, a feasibility analysis for HPCI operation was performed. The reactor decay heat produces approximately 665 GJ (roughly 256 tons of steam at either 7MPa or 0.101 MPa including water heat up) over the period of HPCI operation. The steam demand to run the HPCI is 85.3-42.8 tons/hr. If the HPCI was run for the full duration of availability and at 100% capacity, 1204-604 tons of steam would be required and 13,622 tons of water would be pumped. Less steam is generated than the HPCI turbine demands, and the core requires much less water to maintain the RPV liquid level than the HPCI provides. To maintain the reactor water level over this interval, a time averaged 2% of the HPCI pump capacity is needed.

It is unlikely the HPCI can be throttled down to 2% capacity. It is not recommended to be run the HPCI below 2000 rpm (~1/2 speed) [6]. Information has not yet been obtained to understand the performance of the HPCI under off-nominal operation. If the HPCI operated at ½ speed over the full duration of availability, the steam demand would likely still be higher than the steam produced by the decay heat, and the pumped liquid flow would still be much greater than that needed to maintain the RPV liquid level. (Note: Additional steam is generated from the depressurization of the RPV and also from cooling the RPV/core structures from the saturation temperature at 7 MPa to the saturation temperature at 1 MPa.)

The volume of water available in the CST provides an additional constraint on water injection. The total CST capacity was assumed to be 2500 m^3 [20, 21] and the CST appears to have been 66.1% full at the onset of the accident [36]. This yields 1650 m^3 or 1647 tons of water available for injection using the RCIC or HPCI. Assuming the RCIC injected 552 tons of water (about the amount needed to maintain the water level during Interval 1, then 1095 tons of water would be available for the HPCI. This is more than sufficient to offset the decay heat over this period. If the HPCI was operated at 100% capacity, and no water was diverted back to the CST, the CST would be depleted in 1.13 hrs. If 1095 tons of water were suctioned from the CST over the duration of HCPI operation (and no flow was diverted back to the CST), then the HPCI pump would have operated at a time averaged capacity of 8%.

Because of the HPCI performance uncertainties at off-nominal conditions, the "best estimate" results presented in Section 6.2 use two different assumed HPCI performance curves and trip conditions. In both cases, the "system test line" was periodically opened to divert HPCI pumped water flow back to the CST, instead of to the RPV, to maintain the liquid height in the RPV and continuous HPCI operation. The impact of different assumed HPCI performance curves are investigated in Section 6.3.1.

The first method (A) used the HPCI performance curve in Figure 66. The steam is throttled to 50% of full operation and the pump is throttled to 25% full operation (already accounted for in figure). When the main steam line pressure dropped below 100 psig, the HPCI was assumed to trip due to low steam pressure. It is assumed this trip is manually reset whenever it occurs until the HPCI shuts down at {35:55}.

The second method (D) used the HPCI performance curve in Figure 67. The steam is throttled to 87.5% of full operation and the pump is throttled to 75% full operation (already accounted for in Figure 67). This method assumed the system does not trip for low steam line pressures.

Information concerning the manual manipulation of the HPCI is currently unavailable. The performance of the HPCI under the throttled conditions at low RPV-to-S/C differential pressures is also based on crude estimates. Pump/turbine performance curves and more detailed operator action details would be useful in justifying the currently modeled or a modified model of HPCI operation. Although likely similar to BWR plants in the U.S., additional information on the HPCI trip set points/conditions used in the Fukushima Plant would also be useful. The assumed HPCI operation should be checked against actual operator action and actual HPCI performance at off-nominal conditions.
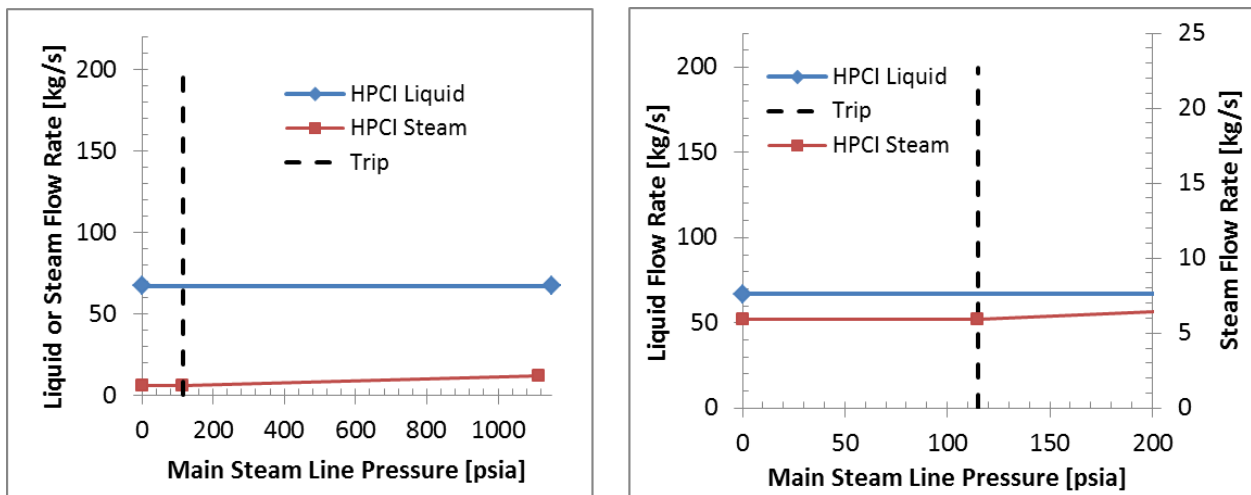
Figure 66. HPCI Performance Curve A.
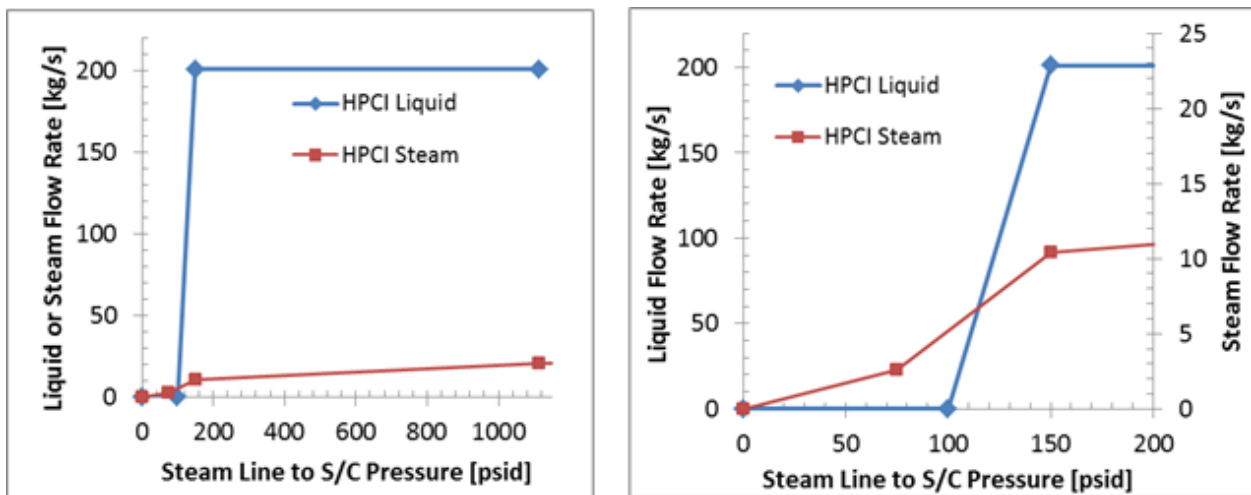
Figure 67. HPCI Performance Curve D.

5.2.8 PCV sprays

Important details concerning the use of the diesel driven fire pump and PCV sprays are provided in the English translation of the operator log book [36]. These entries are summarized in Table 11.

Table 11. Diesel Driven Fire Pump Activity from Operator Log Book [36]

{13:40}	D/D FP Pump "Activation Confirmation" (Activation Failed Cause Unknown)
{20:26}	D/D FP Pump "Manually Activated at Site"(Confirmed) / "Stop" (Automatically Activated after Being Stopped at Main Control Room)
{20:49}	D/D FP Pump "Emergency Stop" (Activated for Confirmation but Did Not Stop. Stopped by Emergency Stop PB)
{21:19}	D/D FP Pump "Manually Activated"
{21:53}	FP No.2 - 3 Tie Valve (301, 22) "Close" (AM Panel Flow Rate Hunching Observed)
{23:13}	D/D FP Pump Fuel Supply (Reception Valve Open Supply only for the line) 172↑195LInhaling Pressure: 0.02MPa D/D FP Pump Inlet Pressure: 0.02MPa Discharge Pressure: 0.35MPa
{26:48-}	No.2 Light - Oil Tank D/D FP Pump Transfer Line Structure (Integrator Pump Bypass)
{29:13}	D/D FP Pump Fuel Tank 130L
{33:58}	D/D FP Pump Light Oil Supply 70↑110L Inlet Pressure: 0MPa Discharge Pressure: 0.42MPa
{36:18}	D/D FP Pump Injection into Reactor MO - 10 - 27B 15% Open Probable Flowing Sound at 7% Inlet Pressure: 0↑0.14MPa Discharge: 0.4↑0.61MPa
{38:21}	S/C Spray Start MO - 10 - 25B Close
{40:12}	D/W Spray Instruction (Emergency Measures Head Office)
{40:52}	D/W Spray Start (from RHR B System)
{40:56}	Torus Spray Stop MO - 10 - 38B Closed
{40:56}	LPCI Injection Line Structure Start RHR B System
{47:43}	Units 2 - 3 FP Tie Valve "Closed" (Unit 2 side v - 201)
{55:28}	D/D FP Pump Stop (No Fuel)

Through plotting the fuel level (Figure 68) it appears the DD-FP was operating continuously from {21:19} to {55:28}. Also, the discharge pressure of the DD-FP is above the D/W pressure but below the RPV pressure during the period of HPCI operation (Figure 69). Furthermore, as discussed later and seen in Figure 69, there is a decrease in the D/W pressure after the DD-FP started at {21:19}.

It has been assumed the DD-FP was operating from {21:19} to {55:28} and was used to inject water through the PCV sprays. This assumption is supported by feedback from the January 25, 2012 meeting, where a TEPCO representative indicated that the December 22, 2011 TEPCO interim report, currently in Japanese, contains information that the sprays were used. However, the two IAEA reports [20, 21] and the INPO report [15] do not mention PCV sprays being used during the {21:19}-{36:00} timeframe. The assumed location, timing, and duration are given in Table 12. A constant flow rate of 400 GPM was assumed based on simulations performed during development (Section 6.3.4) and not based any knowledge of actual pump capacity or usage. The validity of these assumptions needs to be investigated.
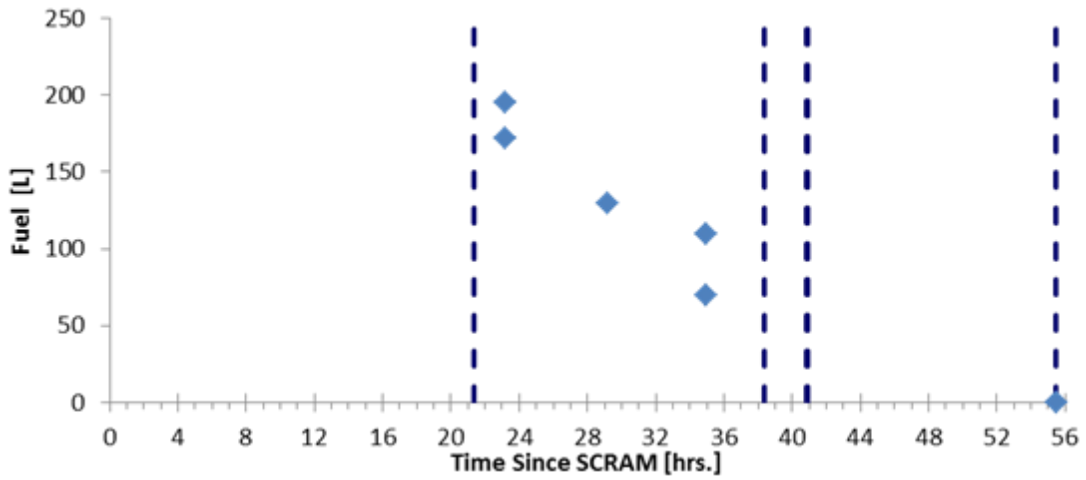
Figure 68. Diesel Driven Fire Pump Fuel Level.
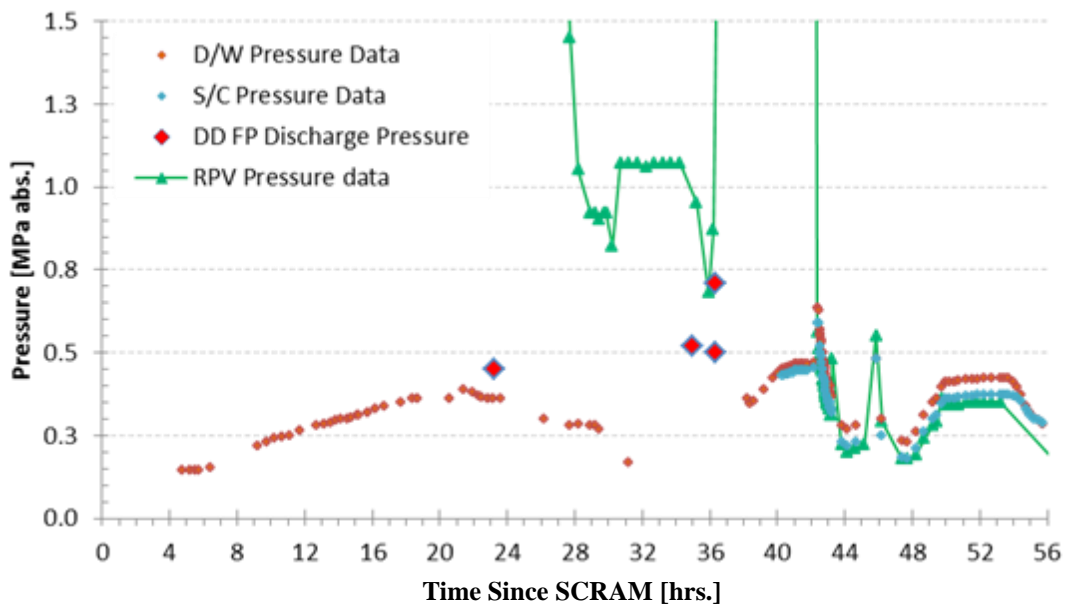
Figure 69. Diesel Driven Fire Pump Discharge Pressure.

Table 12. Modeled PCV Spray Timing and Location

Timing	Location
{21:19}-{36:18}	S/C
{38:21}-{40:56}	S/C
{40:52}-{54:28}	D/W

119

Although the capacity of the system is currently unknown, an estimate can be made through a simple analysis. From the fuel levels reported [36], the diesel driven fire pump appears to be using approximately 8 L/hr. of fuel. The engine power, assuming 100% efficiency and a fuel energy density of 34 MJ/L, is calculated to be 75.6 kW. Pumping water from 1 atmosphere to 401.325 kPa abs. (approximately the indicated discharge pressure) takes 0.3 kJ/kg at 100% efficiency. Assuming 100% efficiency, the system has a pumping capacity of 15 m^3/min or 3960 GPM. Even assuming 25% system efficiency, the system has a capacity (990 GPM)—over twice the assumed flow rate of 400 GPM. While this is a rough analysis, it suggests the 400 GPM spray flow is possible. However, the capacity of the water source, system efficiency, manner in which it was operated, and many other details are unknown.

5.2.9 Fire Engine Water Injection

TEPCO has provided data for the total volume of water injected per day by the fire engines [37]. Using this data and the duration per day the water was being injected (derived from [20], [21]) an estimate of the time averaged water injection rate can be made. The calculation results are summarized in Table 13. For the simulations, it is assumed all injected water makes its way into the reactor pressure vessel. While data for the total volume injected is provided, the data cannot be used to determine the instantaneous injection rate. In addition, the uncertainty of the injected volume data is currently unknown. Finally, it is uncertain how much of the injected water actually made it into the reactor core region.

Table 13. Modeled Fire Engine Water Injection

Day	Injected Water Vol. [37]	Injected Water Mass	Fire Engine Injection Duration [20, 21]	Avg. Injection Rate during Fire Engine Injection Period
	(kL)	(tons)	(s)	(tons/hr)
3/13	390	389.2	49380	28.4
3/14	319	318.4	58860	19.5
3/15	774	772.5	86400	32.2

The timing, duration, and flow rate of water from the fire engines that are applied to the model are summarized in. This table was developed based on the timing of injections from [20, 21] and the results from Table 13. The data in Table 14 is plotted in Figure 70 for comparison to the water injection rates assumed by SNL, Figure 13. The impact of the volume and rate of water injection is discussed in Section 6.3.7.

Table 14. Fire Engine Water Injection Timing and Rate

Day	Fire Engine Injection Timing	Duration	Injection Rate	
	{hr : min}-{hr : min}	[hr : min]	[tons/hr.]	[kg/s]
3/13	42:38-45:33	2:55	28.38	7.88
	45:33-46:25	0:52	0	0
	46:25-57:13	10:48	28.38	7.88
3/14	57:13-58:23	1:10	19.47	5.41
	58:23-60:33	2:10	0	0
	60:33-68:14	7:41	19.47	5.41
	68:14-73:43	5:29	0	0
	73:43-81:13	7:30	19.47	5.41
3/15	81:13-	-	32.19	8.94
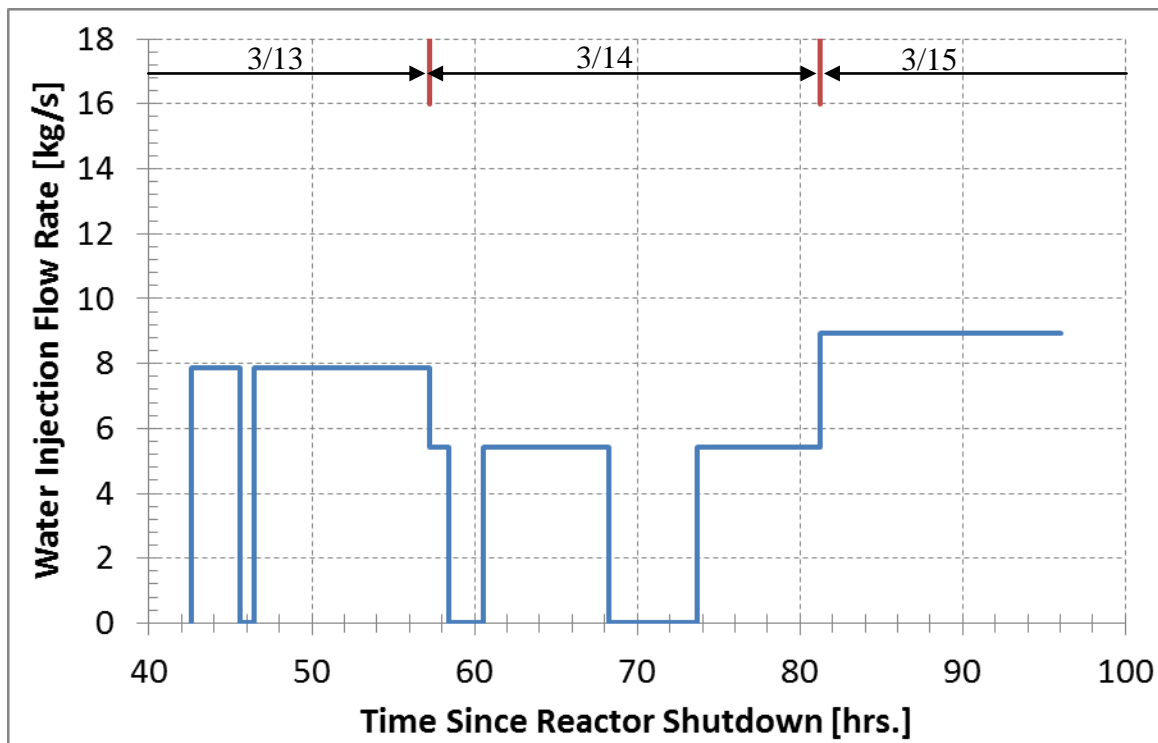
Figure 70. Modeled Unit 3 Water Injection Rates and Timing Based on TEPCO Data.

5.3 Data used for Comparison

The publically available data provided by TEPCO for the RPV, D/W and S/C pressure and the RPV water level [34] was used for comparison. This data is contained within the Data Portal developed by INL (see Section 2.5). Note that there are timeframes where data is unavailable.

This is especially true for the RPV temperatures data [35], which begin at 6:30 on March 19, 2011. There are also questions concerning the validity and uncertainty of the measurements

There are two other data sources that are not included in the comparison. First, data in the form of strip chart recordings for the RPV pressure, in addition to other parameters, has been released by TEPCO. Much data is limited to the first 1.5 hours; however, some data, such as the RPV pressure, is provided up to 40 hours after the accident initiation. The translation, digitization, and vetting of the strip chart data is not publically available. Second, on December 22, 2011, TEPCO released an interim report on the Fukushima Daiichi accident.[21] There may be additional valuable information in this report regarding data, operator actions, timeline of events, etc.

---

[21] The interim report was not available in English until late May/early June 2012; well beyond the model development and analysis timeframe for this work.

6   ORNL UNIT 3 ANALYSES AND RESULTS

6.1   Overview

This section summarizes the results of the Unit 3 modeling effort performed by Oak Ridge National Laboratory for Fukushima Daiichi Unit 3 with the MELCOR v1.8.5 code. This effort paralleled development of MELCOR v2.1 models for Fukushima Daiichi Units 1-3 by SNL. The purpose of the ORNL effort was to:

- Provide independent complimentary simulation results for comparison against the results of SNL
- Understand the accident sequence and predict the state of the reactor core
- Identify additional data needs and knowledge gaps
- Assess the ability of MELCOR to model severe BWR accidents
- If applicable, investigate modeling features available in MELCOR v1.8.5 that are not supported by MELCOR v2.1

In Section 6.2, the results from two "best estimate" simulations are discussed in detail. The only modeling difference between the two simulations is the manner in which the HPCI was modeled. The results are first illustrated in figures with comparison to plant data where available. This is followed by extended discussion of certain events and phenomena as they occurred during the accident progression. In Section 6.3, insight gained from preliminary simulations is discussed. While these simulations were performed under different sets of modeling conditions, they provide insight into the impact of various modeling and accident sequence assumptions. These simulations also helped inform development of the "best estimate" model.

Within Section 6, times listed in '{ }' are the elapsed time since reactor shutdown (14:47 March 11, 2011).

6.2   Results: Current Best Estimate

The section presents two "best estimate" predictions for the ORNL modeling effort performed using MELCOR 1.8.5. The two simulations assume two different HPCI operation models (see Section 5.2.7). The simulation results are discussed in sequence, with respect to intervals of time, and compared to the available data. Figure 71 through Figure 79 display the predicted reactor and D/W pressure, core water level, core configuration, H_2 generation, water temperatures and cladding temperature. The analysis focuses on the first 48 hours after reactor shutdown.
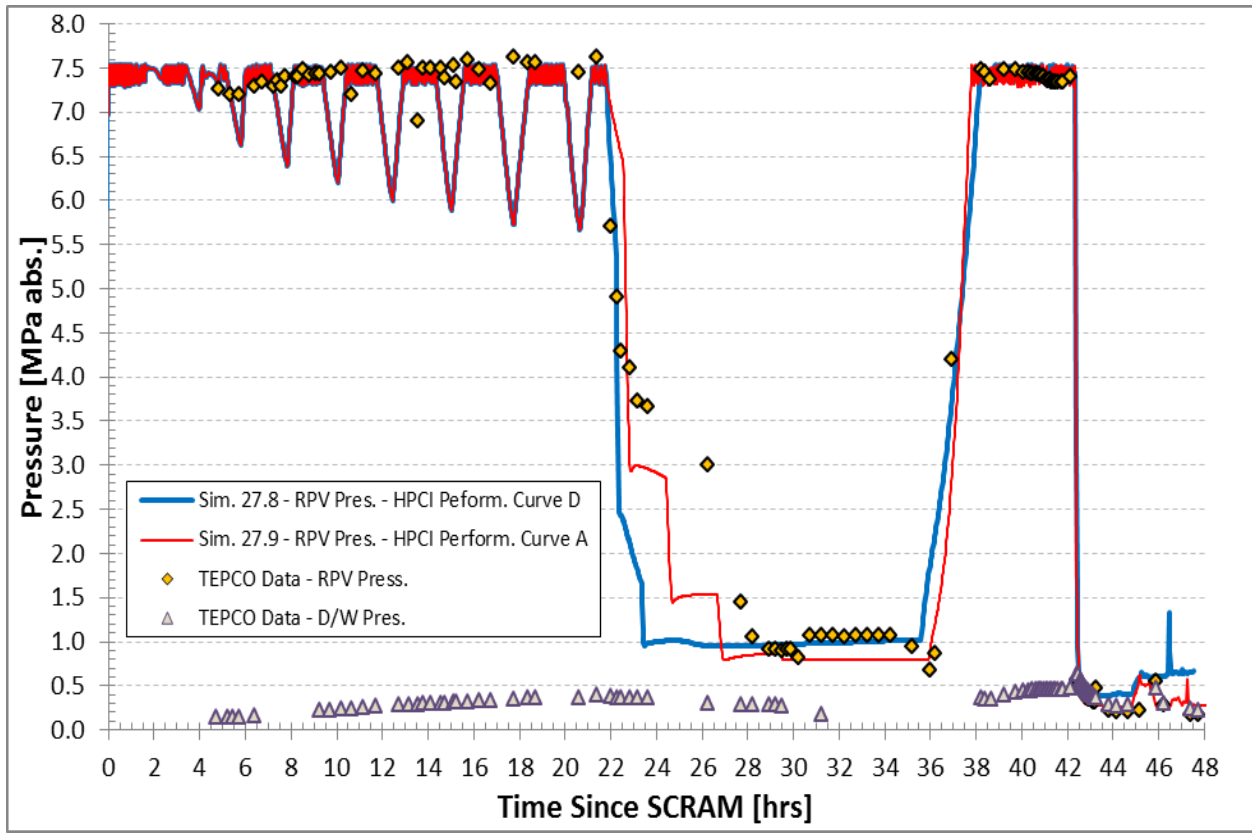
Figure 71. MELCOR Predicted RPV Pressure Compared to TEPCO Data.
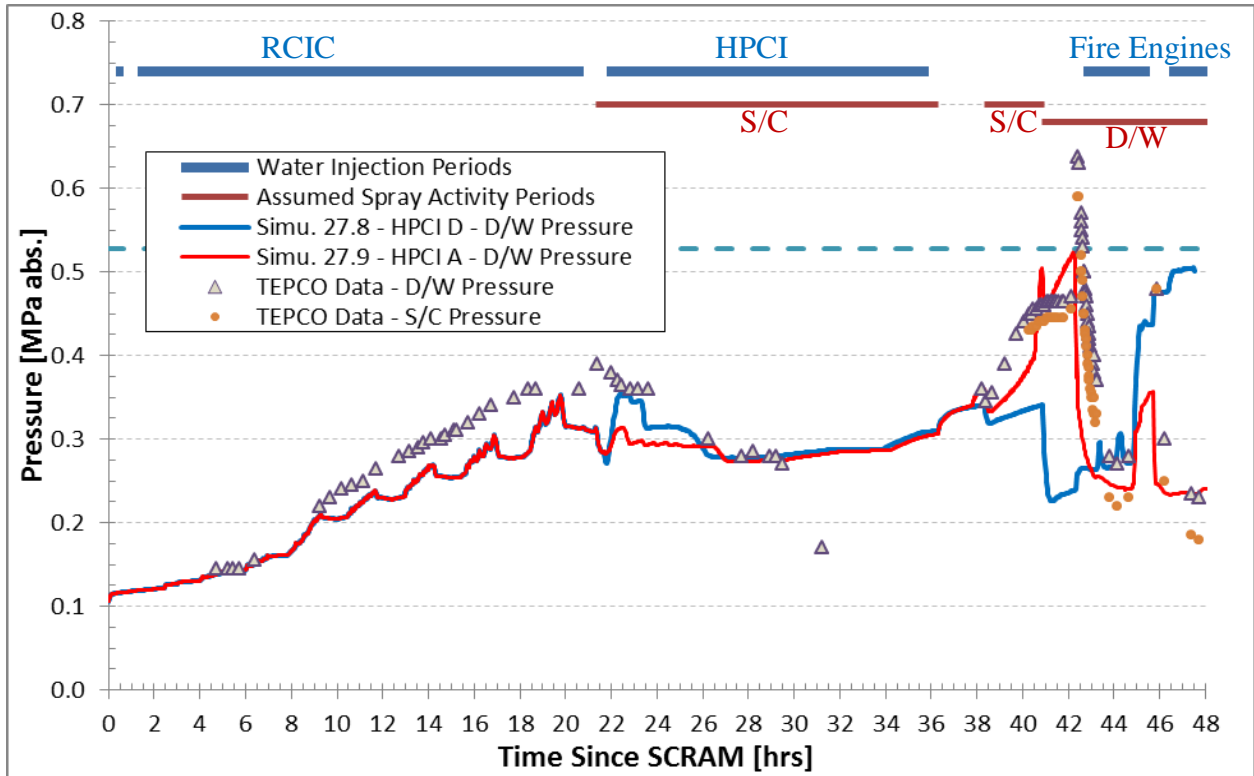
Figure 72. MELCOR Predicted D/W Pressure Compared to TEPCO Data.
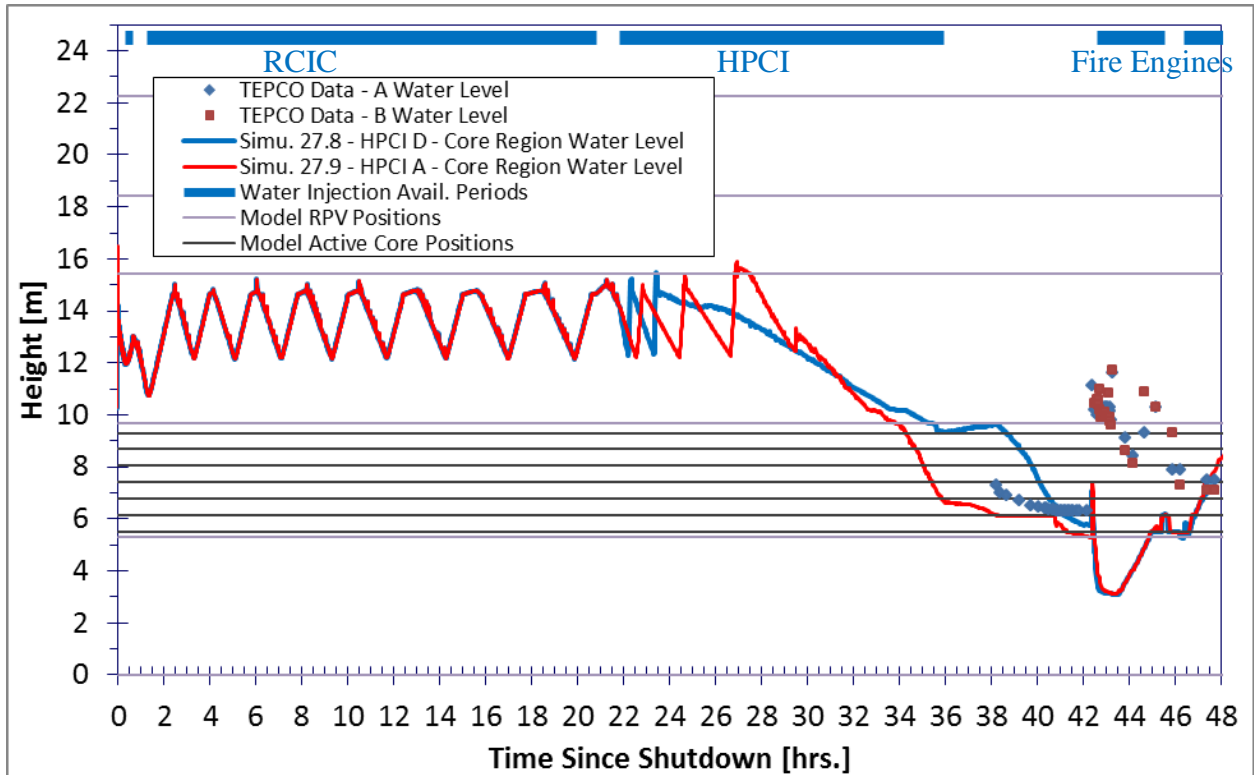
Figure 73. MELCOR Predicted Water Level Compared to TEPCO Data.
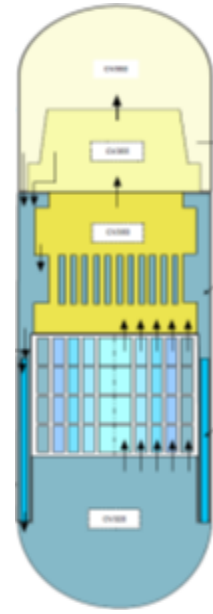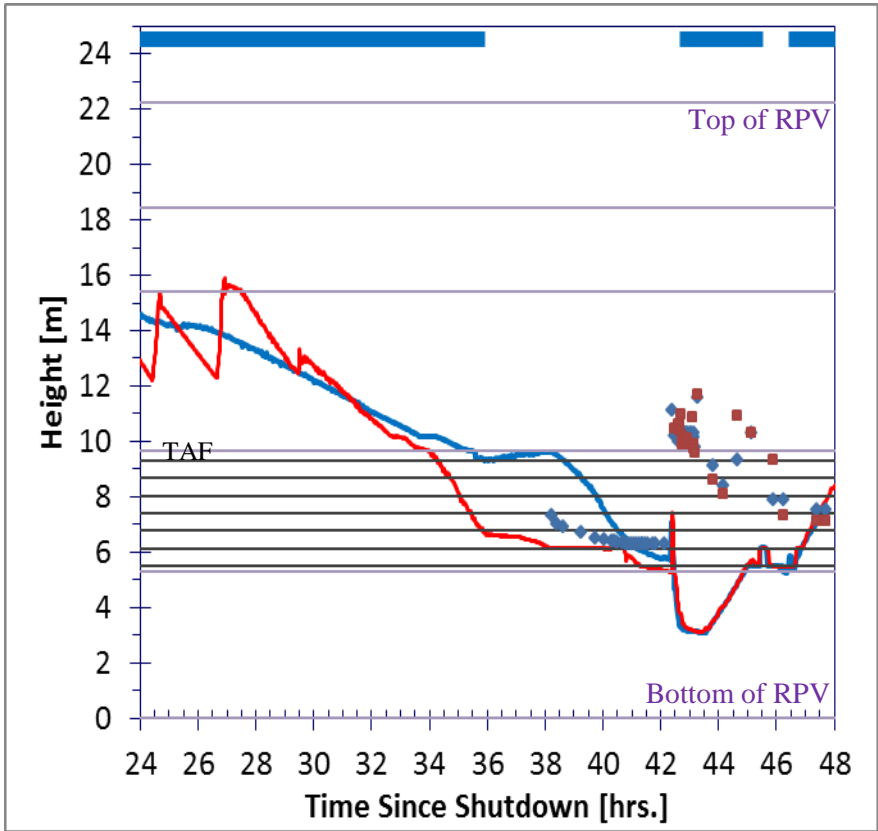
Figure 74. RPV Level Reference Illustration.

{42:00}

		4009	4009	2565
		4009	4009	2565
930	928	4152	4152	2565
11022	10931	4152	4152	2565
8708	9209	4152	4152	2565
5133	5351	4152	4152	2565

{48:00}

				2565
				2565
				2565
9539	9423	8084	8623	2565
9263	9473	7614	8585	2565
6802	8598	7258	6681	2565
330	330	42	267	
85	103	109	125	
4	7	40	51	

Core map:

114	214	314	414	514
113	213	313	413	513
112	212	312	412	512
111	211	311	411	511
110	210	310	410	510
109	209	309	409	509
108	208	308	408	508
107	207	307	407	507
106	206	306	406	506
105	205	305	405	505
104	204	304	404	504
103	203	303	403	503
102	202	302	402	502
101	201	301	401	501

Figure 75. Fuel Mass Location and Water Level at 42 and 48 hrs. for Sim. 27.9 (HPCI A).
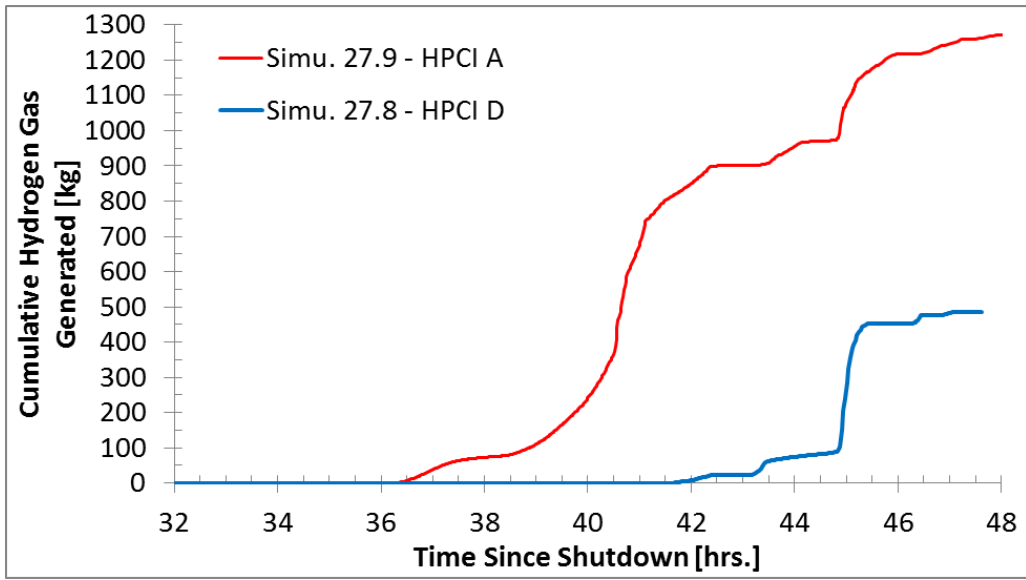
Figure 76. MELCOR Predicted Integral H$_2$ Generation.
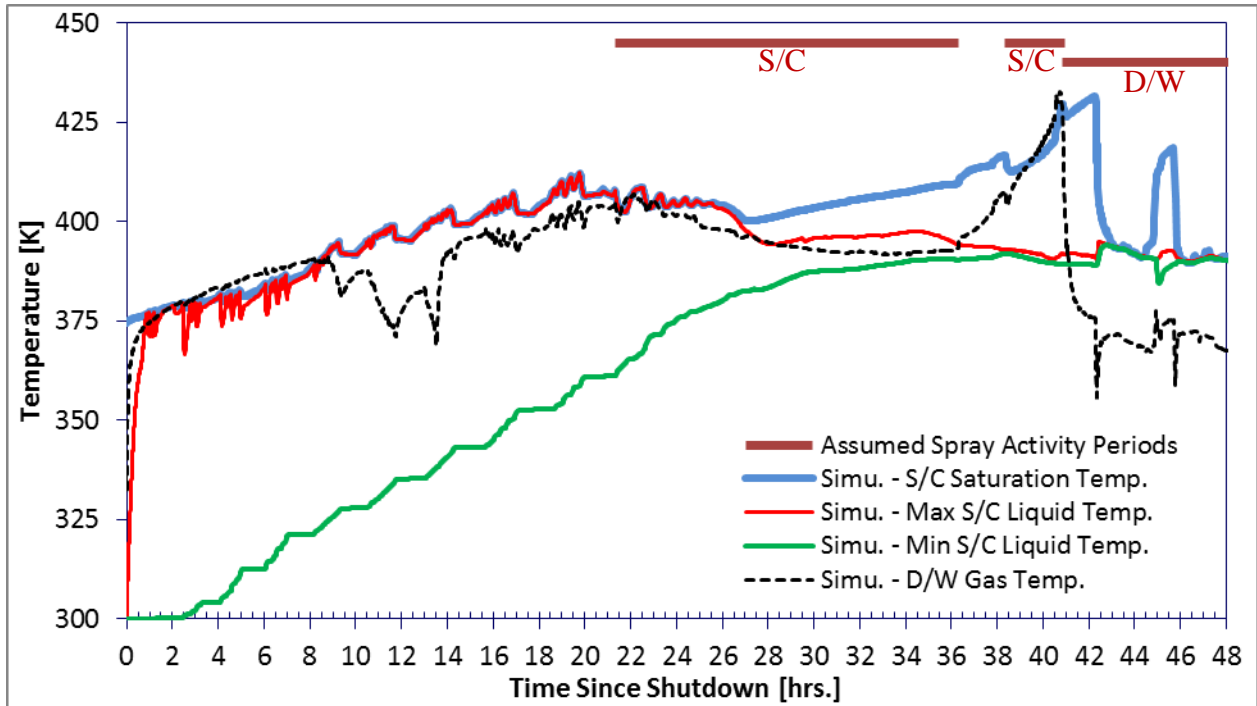
Figure 77. MELCOR Predicted S/C and D/W Temperatures - Sim. 27.9 (HPCI A).

129
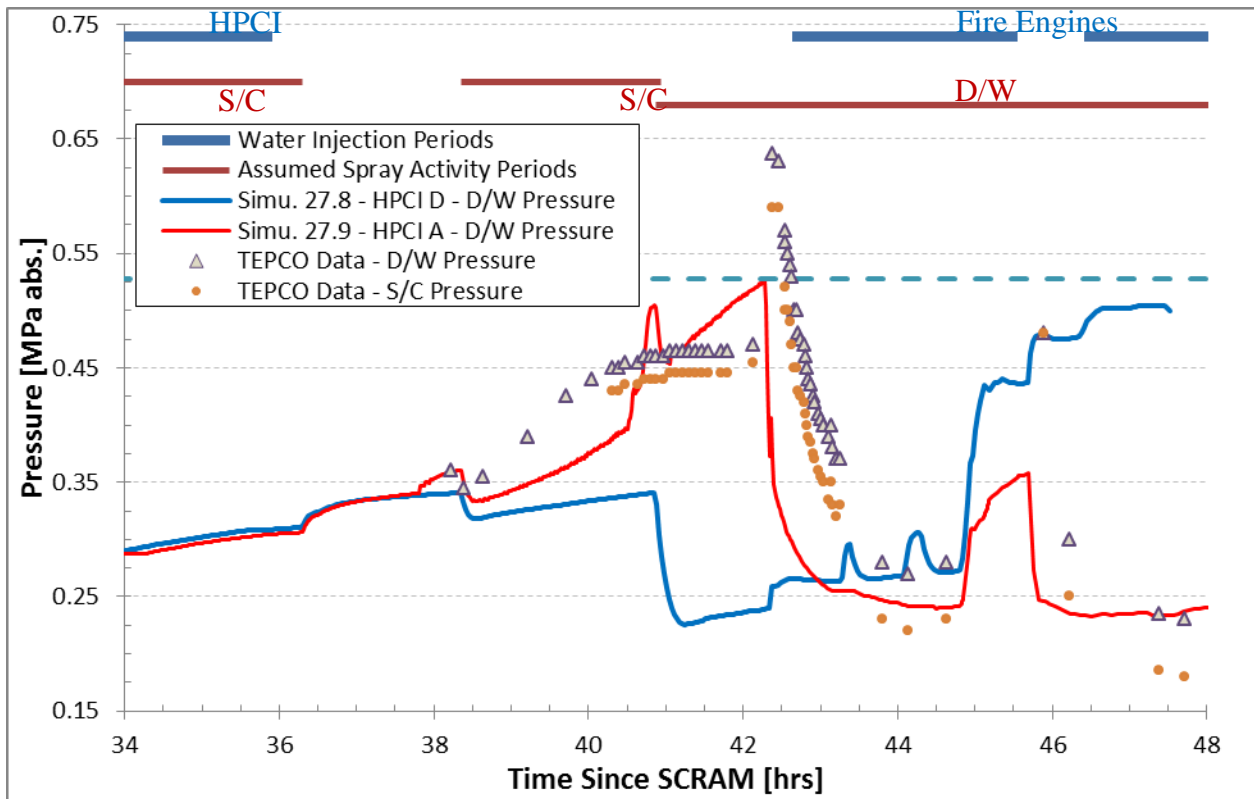
Figure 78. MELCOR Predicted D/W Pressure Compared to TEPCO Data.
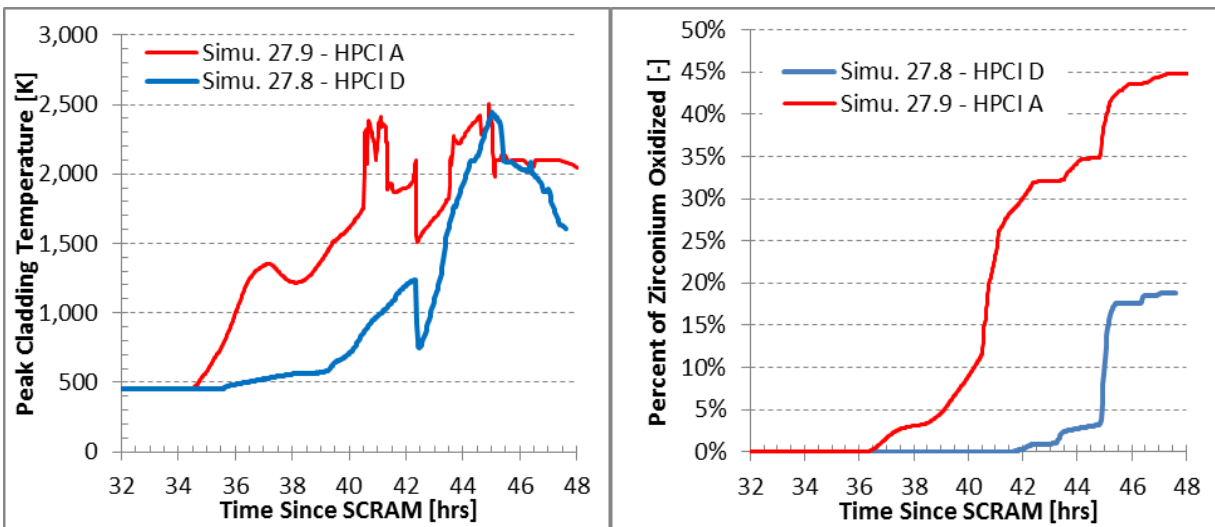
Figure 79. MELCOR Predicted Peak Cladding Temperature and Fraction Oxidized.

6.2.1 Interval 1: SCRAM, RCIC Operation, PCV Pressurization

The simulation begins 180 seconds before the earthquake arrives at the plant. This allows the model to reach pre-shutdown steady-state operation conditions. The simulation SCRAMSs the reactor at {00:00}, modeling the reactor shutdown due to the earthquake at 14:47, March 11, 2011. Shut down of the reactor and closure of the MSIVs were reported to have been completed as normal [20, 21, 15].

The RCIC system maintains core cooling by occasionally injecting water into the reactor. The drops in RPV pressure, Figure 71, occur when the RCIC flow is diverted from the CST to the reactor. The steam generated in the core is vented into the S/C through the RCIC turbine and the SRV with the lowest set point. The steam causes one section of the S/C to become saturated within 50 minutes. The entire pool reaches saturation only after the S/C is vented {42:21}.

6.2.1.1 D/W Pressurization

The steam venting to the S/C causes an increase in pressure of the S/C and interconnected D/W. The S/C acts to condense the steam, lowering the pressure increase.

The Unit 3 D/W pressure data indicates the pressure increased at a relatively high rate (~4 Pa/s) during Interval 1 (Figure 72). Preliminary simulations under predicted the D/W pressurization rate. A few factors were identified and analyzed which could affect the D/W pressurization:

Decay heat
The amount of steam produced and vented to the S/C directly influences the PCV pressurization rate. The decay heat used in the simulation, which is driving the steam generation, is based on the ANS standard curve. Additional description can be found in the MELCOR user manual [29]. Based on information provided by TEPCO, the ANS decay heat curve may over predict the decay heat by 9-10%. Decreasing the decay heat in the simulation would decrease the D/W pressurization rate (increasing the discrepancy).

PCV volume
The volumes used for the Unit 3 PCV was compared against other Mk-I PCVs (See Table 7). The PCV volumes are similar, with only ~13% deviation from the modeled Unit 3 PCV volume. The impact on PCV pressurization would be proportional to changes in the PCV volume. While the Unit 3 PCV may be slightly larger or smaller than the values used in the simulation, the impact on pressurization would be similarly small.

PCV leak rate
The PCV may leak through small pathways that are intrinsically present in the PCV or ones that open as the PCV heats up and pressurizes. The current simulation includes leakage from the PCV in the form of a 6.4 mm diameter pathway from the PCV into the reactor building. The simulation predicts a leak rate of 34.1 kg/hr at PCV pressure of 528 kPa abs. During this period, steam is being generated in the RPV and vented into the PCV at a rate a several hundred times higher than the leak rate. This small leak rate is not responsible for the under prediction in pressurization.

Steam condensation rate – efficiency

As steam is vented into the S/C (through the SRVs and RCIC & HPCI steam turbine flow), it is condensed by the water pool. However, if the steam is vented at only one location, or is rapidly vented, the S/C may not efficiently condense the steam. If the steam venting rate overcomes the condensation rate, steam will be introduced into the S/C and D/W atmosphere. In this case, a non-equilibrium amount of steam can build up in the S/C causing the PCV to pressurize.

Accident management guidelines in the United States recommend the SRVs be manually actuated in an order such that the steam is vented as evenly as possible into the S/C. However, if the operators lose the ability to manually actuate the SRVs or an SRV becomes stuck open, the steam may be vented through only one SRV into the S/C. In the simulations, the steam is primarily vented through a single SRV (the one with the lowest set point).

If the SRV-vented steam was directly vented into the D/W, or into the S/C gas space, the steam would cause the PCV to quickly pressurize. The impact of an SRV venting directly into the D/W was investigated (see Section 6.3.4). From that analysis, it is unlikely the steam was directly vented into the D/W (i.e., through a broken SRV pipe) as the predicted pressurization response is not consistent with the observed D/W pressure data.

Two MELCOR modeling aspects have been identified that may affect the condensation of the vented steam.

A) The nodalization of the S/C affects the models ability to capture phenomena such as localized saturation and stratification of the S/C as well as the formation of complex convection cells. The impact of the S/C nodalization is discussed in Section 6.3.3. The "best estimate" model uses eight control volumes to model the S/C. It is believed further refinement of the S/C nodalization should be investigated to resolve the pressurization discrepancy.

B) Basic empirical models are used to determine steam bubble condensation within a liquid pool (see Section 5.2.4 and Reference [29]). Minor variations to these models, through sensitivity coefficient 4405, may have a large impact on steam condensation.

Recirculation pump seal leakage

The possibility for recirculation pump seal leakage has been suggested by subject matter experts. As discussed in Section 6.3.2, there exists a possibility for substantial leakage (>100 GPM). If this leakage occurred, the flashing of leaked coolant would increase the D/W pressure. This possibility has not been included in the "best estimate" model. The impact of pump seal leakage is investigated in Section 6.3.2. The impact of seal leakage should be investigated further.

6.2.2 Interval 2: HPCI Operation, PCV Sprays & Pressure, Core Response

In Interval 2 {20:49-42:21}, the RCIC is unavailable {20:49} and the HCPI becomes available {21:48-35:55}. As noted in Section 5.2.8, it was assumed that S/C sprays were used during this period.

6.2.2.1 RPV Depressurization

The Unit 3 data indicates the RPV depressurized during the HPCI operation period. The HPCI startup {21:48} occurs between the two data points which indicate the onset of D/W depressurization {21:23-21:58}.

The RPV depressurization is not likely attributed to a rupture in the primary system, as the RPV later re-pressurizes. If a leak occurred around the HPCI, outside the PCV, then the HPCI room would have heated up and caused a HPCI system trip. Employees were reported to have passed through the HPCI room in order to access the RCIC room at a later time [21]. This suggests the HPCI room was not filled with steam.

In the simulation, initially the steam draw of the HPCI turbine is much higher than the steaming rate due to the decay heat. This causes the RPV to depressurize. Around an RPV pressure of 1 MPa abs., the steam demand of the HPCI comes into equilibrium with the rate of steam generated by the decay heat. The point at which the steam production/demand comes into equilibrium is sensitive to the performance curve of the HPCI (see Section 6.3.1).

The simulation does not well predict the pressurization data available during the depressurization stage; however, the general trend is reproduced. Additional information into how the HPCI was operated and its performance characteristics is needed to resolve the depressurization discrepancy.

6.2.2.2 D/W Depressurization

The D/W pressure data indicates a decrease beginning between the data points at {21:23} and {21:58}. This coincides with the onset of HPCI operation {21:48} and around the time the diesel driven fire pump (DD-FP) was started {21:19} [36]. The Unit 3 data indicates the pressure continues to decrease with a single data point at {31:13}, indicating a pressure of 170 kPa abs. This depressurization rate (approximately -4 Pa/s) is approximately the same magnitude as pressurization rate in Interval 1.

Except for the single data point at {31:13}, the "best estimate" simulations reproduce the Unit 3 D/W pressure data in Interval 2 fairly well. The activation of the S/C sprays (at 400 GPM) is responsible for the decrease and trend in the D/W pressure. Other factors that may impact the D/W pressure during this period have been identified:

S/C or D/W venting
Venting operations would cause a decrease in PCV pressure. However, there is no mention of venting operations during this period [20, 21].

S/C pool cooling using HPCI minimum flow line
While the HPCI operates, steam is released into the S/C. This would tend to increase the D/W pressure. If water was diverted from the CST to the S/C through the minimum flow line (instead of being passed back to the CST through the system test line, as currently modeled), the

subcooled water could absorb some energy resulting in steam condensation and a decrease in D/W pressure. However, the magnitude and rate of this effect depends on the water injection rate, steam venting rate into the S/C from the HPCI, and the initial conditions of the S/C and D/W. In some scoping simulations, it appears diverting flow from the HPCI into the S/C causes a minor decrease (~50 kPa reduction) in D/W pressure. The magnitude of the effect may be influenced by model nodalization and/or the condensation process modeling. Also, note the volume of the CST and S/C provides limits on this cooling mechanism.

S/C or D/W leakage

At the onset of HPCI operation, the simulation predicts the D/W pressure and temperature are approximately 345 kPa abs. and 403 K. The data suggests the D/W pressure was 390 kPa abs. (56.6 psi). A large amount of steam is vented to the D/W soon after HPCI startup, as evident in the RPV depressurization. Elevated PCV temperatures and pressures could cause a leakage pathway to open (a seal failure in a PCV head, access hatch, or other penetration).

Preliminary simulations (see Section 6.2) suggested a fairly high leakage rate (>75 kg/s) would be needed to reproduce the D/W data trend. One possible scenario is that a leak path opened at a pressure around 390 kPa abs. remained open until sealing around 170 kPa abs., and then remained sealed during the re-pressurization from 170 kPa abs. to 390 kPa abs. (and possibly beyond). The merits of a large hysteresis (220 kPa, 32 psi) between the leak path opening and closing points should be questioned. The data indicates the D/W later pressurizes to greater than 400 kPa abs after the HPCI operation stopped. This suggests it is unlikely a moderately sized PCV rupture occurred that is responsible for the pressure decrease in Interval 2.

Currently, the decrease in D/W pressure during the period in Interval 2, as indicated by the data, is believed to be caused by the use of PCV sprays. The precise timing, duration, and flow rate of the PCV sprays is currently unknown.

6.2.2.3   Water Level

The simulation predicts a gradual decrease in the water level during Interval 2. Due to the assumed HPCI steam demand characteristics (see previous discussion), the RPV pressure equilibrates around 1 MPa abs. Note that the water level is sensitive to the assumed HPCI pump performance curve (see Section 6.2.1).

For HPCI performance D simulation, the HPCI tripped 21 minutes before {35:55} when the HPCI was to finally shut off. The cause for the early predicted failure is currently unclear. This was the only simulation where this occurred and the cause will be further investigated.

Based on the HPCI performance A, the HPCI trips when the main steam line pressure reaches 114.7 psia. Due to the frequent tripping and the time needed (30 seconds) for the pump to get to speed, only limited water is injected from {29:30} to {35:55}. Based on the HPCI performance D, at this RPV-S/C pressure differential, the HPCI injects slightly less water than that needed to maintain the core water height.

Ultimately, HPCI performance D injects more water than that of HPCI performance A (Figure 80). The water level at {35:55} is very near TAF (9.32 m from RPV bottom) for HPCI performance D, while the water level is 2.63 m below TAF (6.67 m from RPV bottom) for HPCI performance A.

6.2.2.4   RPV Re-pressurization

As the steam draw of the HPCI stops, the RPV re-pressurizes back to the minimum SRV set point pressure. The simulation predicts the re-pressurization rate quite well.

Note that if the water level is high at on onset of RPV re-pressurization, the pressurization rate is much slower. Figure 81 shows the RPV re-pressurization behavior for simulations 27.8, 27.9 & 28.0. Simulation 28.0 uses a different HPCI performance curve such that the water level remains high (see Section 6.3.1). The water level at {35:55} for simulation 28.0 is 3.1 m above TAF. (12.4 m above the RPV bottom). The actual re-pressurization rate is bounded by simulations 27.8 and 27.9, where the starting water level is TAF and 2.63 m below TAF, respectively. This suggests the water level was at or below TAF when the RPV began re-pressurizing around {35:57}.
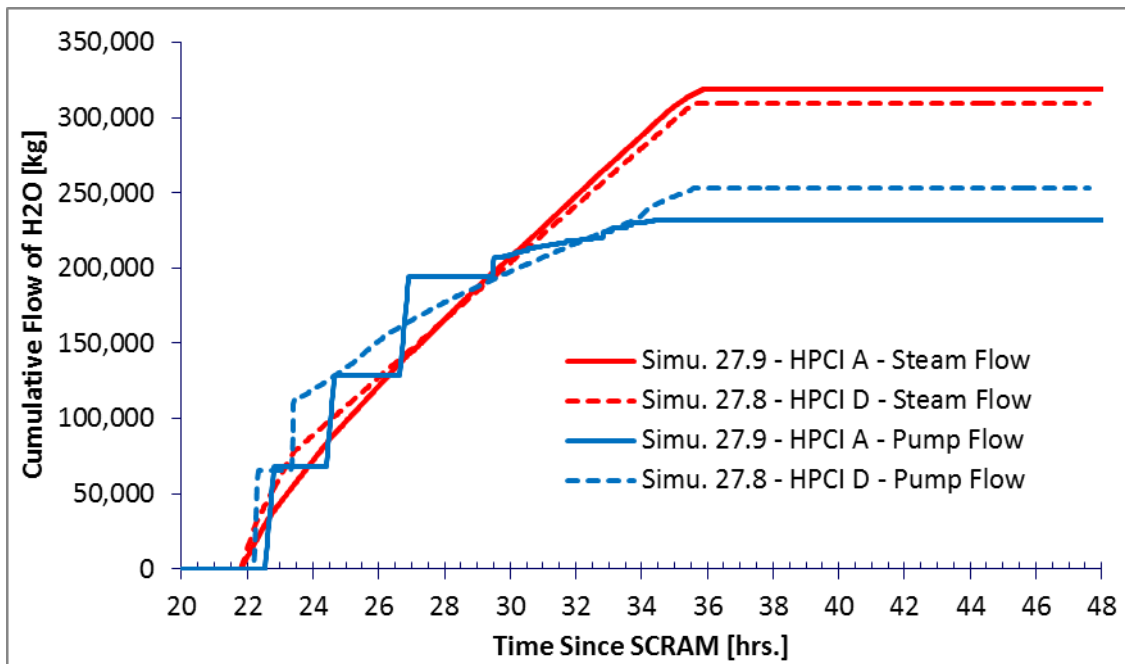
Figure 80. Cumulative HPCI Steam and Liquid Flow.
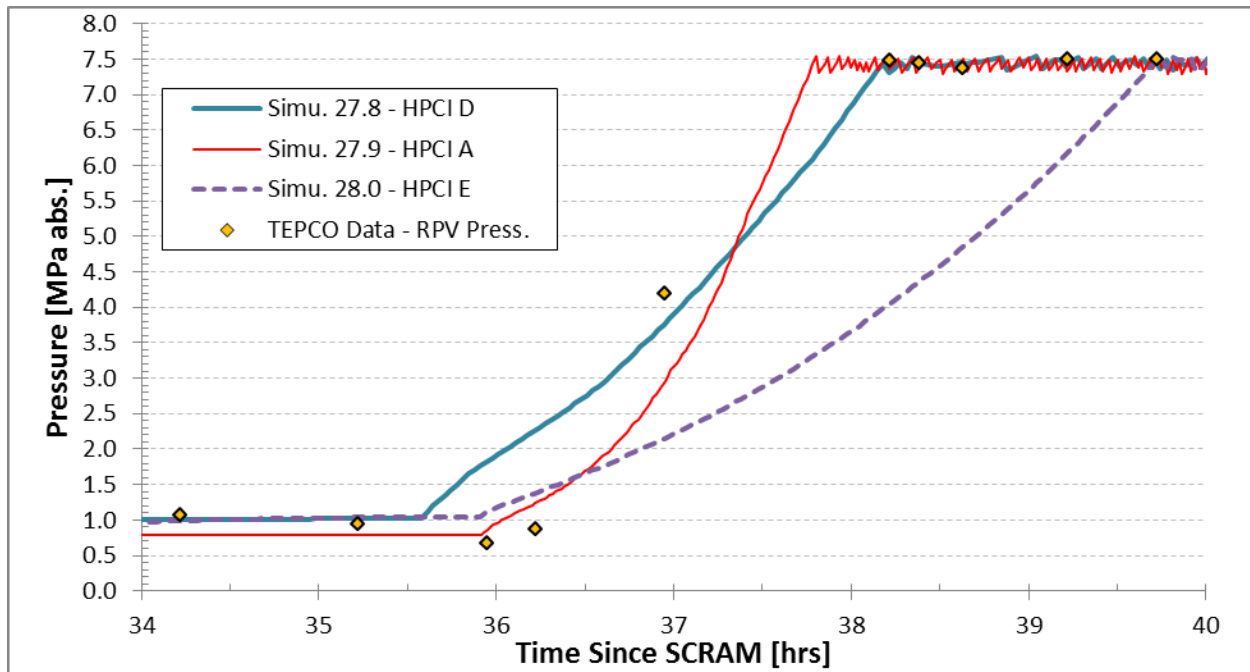
Figure 81. MELCOR Predicted RPV Re-pressurization.

6.2.2.5 D/W Re-pressurization

The TEPCO data indicates the D/W was re-pressurized starting around the data point at {38:13}. The pressurization rate of approximately 19 Pa/s during the period of {38:30-40:00} is much greater than that observed during the first 20 hours (4 Pa/s). Three phenomena impacting this re-pressurization have been identified:

PCV sprays
Using the PCV sprays would either cause a decrease in the D/W pressure or a decrease in the rate of re-pressurization.

During this period, the S/C and later the D/W sprays are assumed to be active. There is a slight drop in D/W pressure between the TEPCO data points at {38:13} and {38:23}. The English translation of the operator log book [36] indicates the S/C sprays were activated at {38:21} (see Section 5.2.8). Both simulations capture the pressure decrease caused by the startup of S/C spray activity. This evidence adds confirmation of spray activity initiation at this point.

Core failure
The D/W pressure in the simulation using "HPCI A" modeling methodology increased despite the use of containment sprays. This is due to the additional energy and non-condensable gas released from core cladding oxidation and failure. In the simulation, the first gap release occurs at {36:20} with subsequent hydrogen gas generation.

In the simulation using "HPCI D" modeling methodology, the gap releases and cladding oxidation were delayed until around {41:52}. As shown, without the additional energy release

136

and non-condensable gases, the D/W pressure is predicted to increase only slightly between {38:00} and {41:00}.

Seal leakage

The TEPCO data indicates the RPV was again at high pressure starting with the point at {38:13}. Flashing of water from a leaking recirculation pump seal could cause the D/W to re-pressurize. Both "best estimate" simulations did not include seal leakage.

Given the above discussion, the PCV sprays were active starting at {38:21}. The D/W pressurization during this period was caused by core failure, recirculation pump seal leakage, or a combination of both. To have core failure at this time, the HPCI water injection earlier had to be insufficient to cool the core. Based on the RPV re-pressurization rate, the water level was likely at TAF or lower supporting the possibility for core failure around this time.

6.2.3 Interval 3: RPV De-pressurization, Fire Engine Water Addition

In Interval 3, the RPV is noted to have been depressurized by remote activation of an SRV around {42:21} [20, 21]. The S/C vent lineup was complete at {41:54} with only the rupture disk preventing venting [20, 21]. As the TEPCO D/W and S/C pressure data seem to have plateaued prior to venting, the depressurization of the RPV likely caused the PCV pressure to rise enough to fail the rupture disk.

In the simulation using "HPCI D" modeling methodology, the S/C pressure never reaches the rupture set point and thus the PCV is never vented (up to simulation end). This is inconsistent with the data (outside dose measurements and PCV pressure) and the sequence of events as we currently know them. Thus, this simulation is not discussed further.

In the simulation using "HPCI A" modeling methodology, the S/C pressure reaches the rupture set-point at {42:18} and the S/C vents. This occurs before the RPV-modeled venting at {42:21}. Despite this, the PCV TEPCO pressure data and predicted PCV pressures follow similar trends. The RPV depressurization causes the water level to drop below the core plate. At the assumed water injection rate and periods of the fire engines, it takes approximately 6.5 hrs to refill the core to TAF. At 48 hours in the "HCPI A" simulation, a significant portion of the core has failed (Figure 75) and approximately 45% of the zirconium has oxidized (Figure 79). However, the water injected by the fire engines is refilling the core (Figure 73) and the peak core cladding temperature has stabilized (Figure 79).

It should be stressed that after reactor de-pressurization, the core failure/stabilization is highly dependent upon the rate, timing, and duration of water injection from the fire engines.

6.3   Results – Insight from Preliminary Investigations

Several simulations were run during model development in order to understand the system response to changes in assumed boundary conditions (i.e., PCV sprays, D/W leakage, fire engine water addition, recirculation pump seal leakage) and modeling methodologies (i.e., HPCI Performance and S/C nodalization). As the model was under development, the following simulations (Section 6.3.1 – Section 6.3.8) were run with varying sets of boundary conditions. The general modeling setup/assumptions are indicated before each section. While the simulations should not be directly compared, the results do provide insight into the trends and impacts of various modeling changes.

6.3.1   HPCI Operation and Performance

These simulations were performed under the modeling conditions described in Section 5.2.

The performance of the HPCI, under off-nominal conditions, was found to largely impact core failure before initiation of the fire engine water injection. To investigate the impact, the HPCI operation and performance were modeled in five different ways.

The first method (A) used the HPCI pump and turbine curve in Figure 66. When the main steam line pressure dropped below 100 psig, the HPCI was assumed to trip due to low steam pressure. It is assumed this trip is manually reset whenever it occurs until the HPCI shuts down at {35:55}.

Methods B, C, E used the HPCI pump and turbine curves shown in Figure 82 through Figure 84, and method D used the curves shown in Figure 67. The low steam pressure trip at 100 psig was removed. As shown Figure 85 and Figure 86, the HPCI performance has a large impact on the water level and reactor pressure. Table 15 summarizes the time until first fuel gap release and cladding failure.
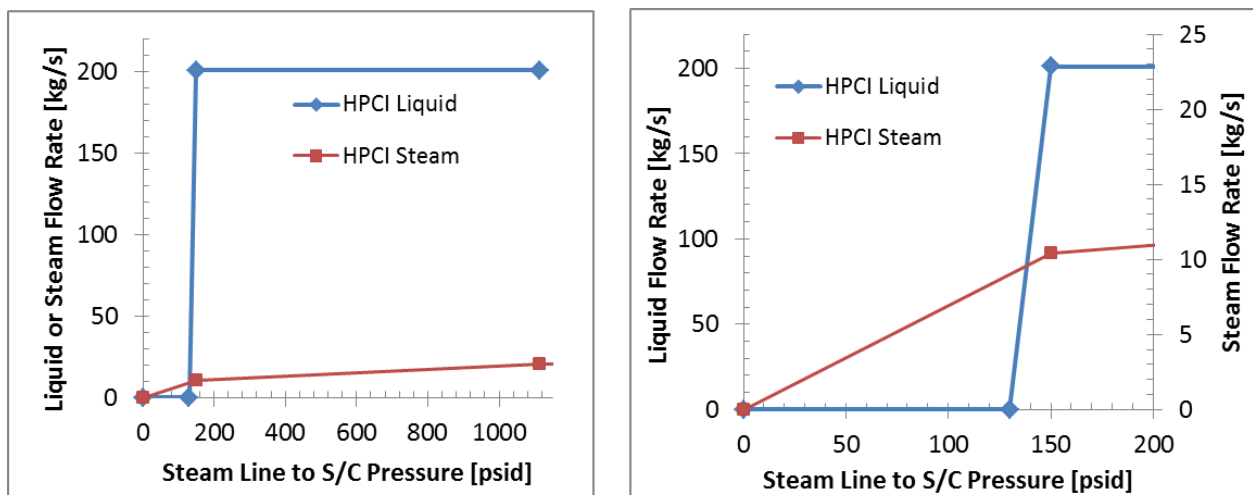
Figure 82. HPCI Performance Curve B.
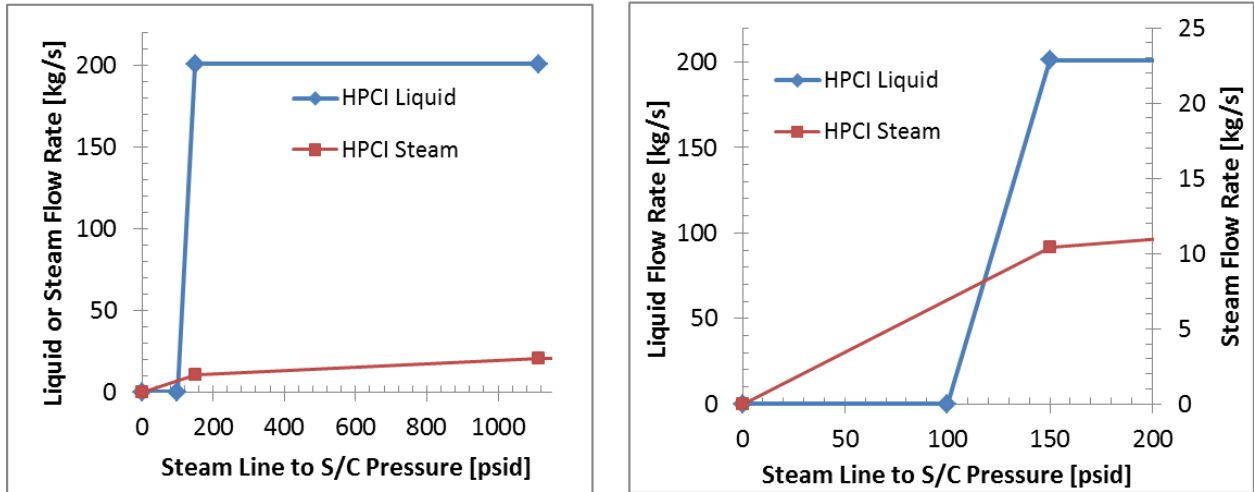
Figure 83. HPCI Performance Curve C.
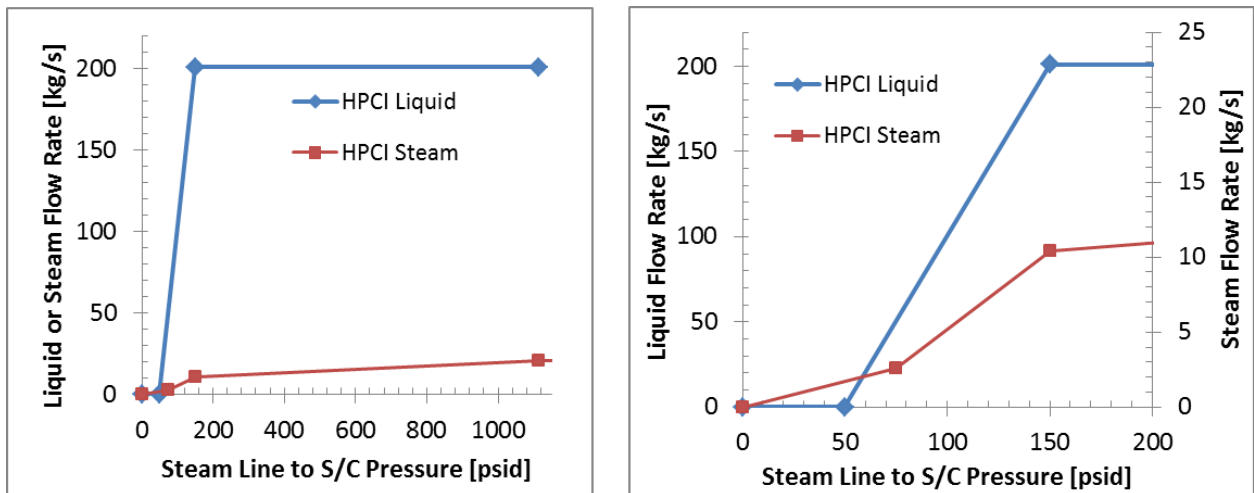
Figure 84. HPCI Performance Curve E.

Table 15. HPCI Performance on Core Failure Timing

HPCI Performance	First Clad Gap Release	First Clad Failure
A	{36:20}	{40:55}
B	{29:02}	{29:55}
C	{29:40}	{30:33}
D	{41:52}	{45:04}
E	{43:16}	{44:17}
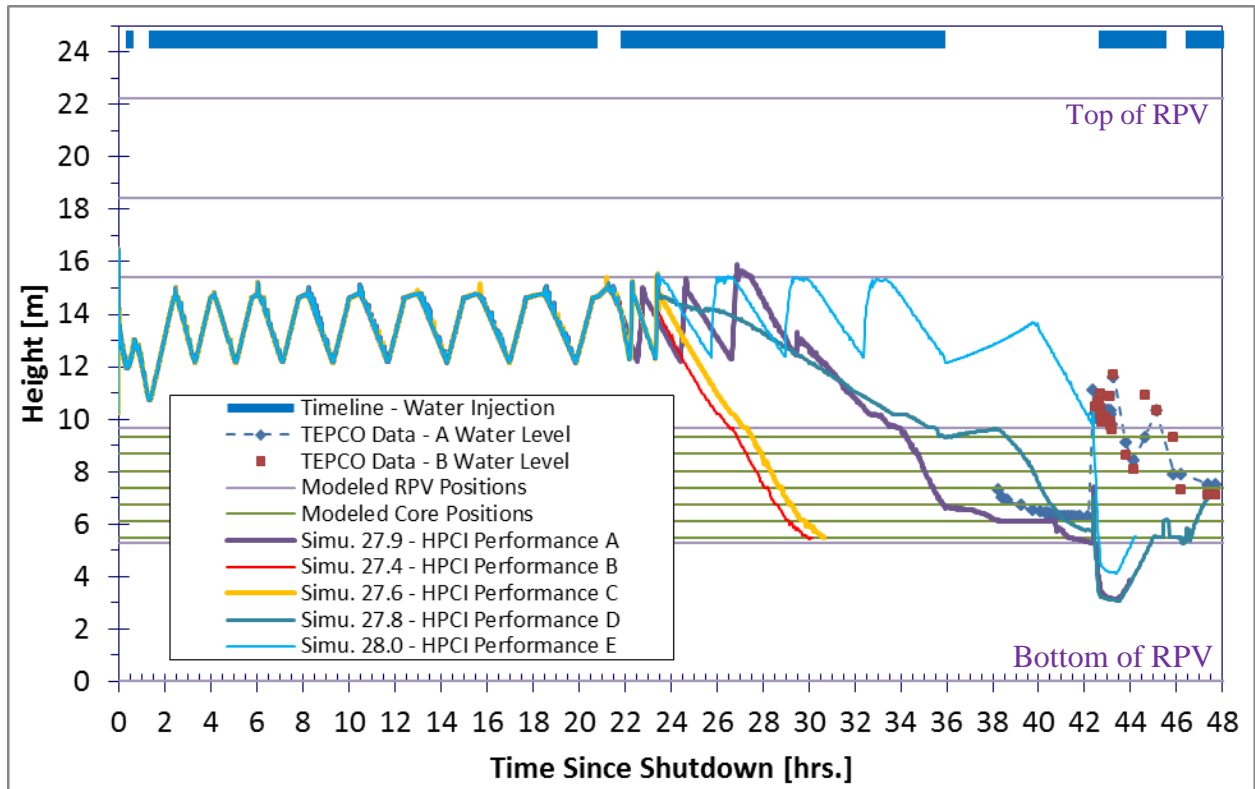
Figure 85. HPCI Performance on Water Level.
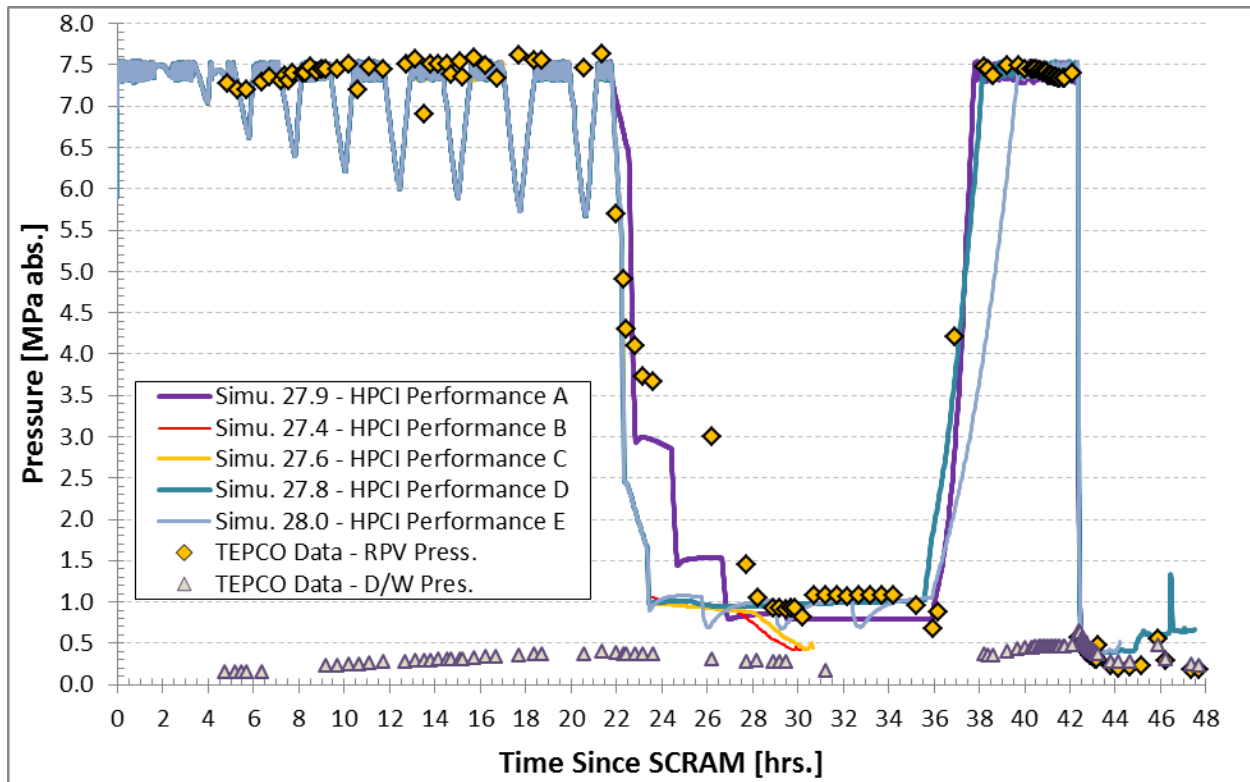
Figure 86. HPCI Performance on RPV Pressure.

6.3.2 Recirculation Pump Seal Leakage

These simulations were performed under the modeling conditions described in Section 5.2.

Under station blackout conditions, the recirculation pump seals may not be cooled and may fail. Appendix B of NUREG-1401 discusses the seal response to station blackout conditions for a BWR [31]. The maximum leak rate per pump was estimated to be 100 GPM when the reactor is at operating pressure.

Leakage from the seal would increase the D/W pressure due to flashing of the liquid. A leak could also have a substantial impact the water level in the core and therefore fuel damage. The RCIC flow is around 425 GPM and the water injection via the fire engines was mostly below 100 GPM. The leak would also impact the water level in containment impacting melt relocation and MCCI phenomena. A 10 GPM leak is equivalent to about a foot/day of water into the D/W [31].

To investigate the impact of recirculation pump seal leakage, a preliminary simulation was performed assuming a constant 10 GPM leak from the recirculation line into the D/W. This leak was initiated at reactor SCRAM. It is noted this simulation may not be very representative of a pump seal leak as the leak rate would depend upon the primary side pressure and the leak rate was arbitrarily chosen.

141

The leak increased early pressurization by 16% during the first 20 hours (RCIC operation period). Seal leakage combined with core failure produced very high PCV pressures between {36:00} and {42:00}. Pump seal leakage should be considered for further investigation.
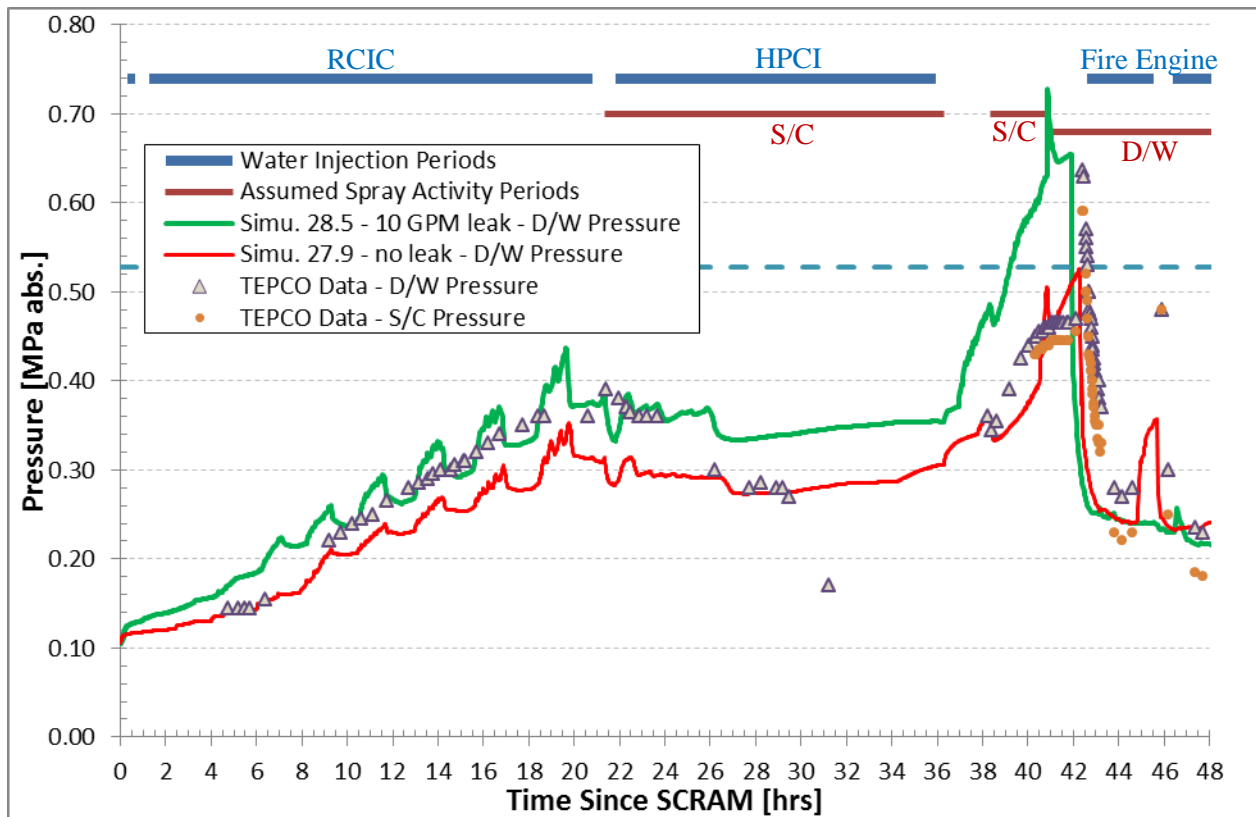
Figure 87. Recirculation Seal Leak impact on D/W Pressure

NOTE: For the following sections (6.3.3-6.3.7) the HPCI performance was assumed to follow that of Figure 66 (performance curve A with system trip at 100 psig). There is no PCV spray activity (except for the two cases in Section 5.2.8 where they were investigated). The RCIC was assumed to operate at 75% steam flow and 50% pumped liquid flow (in contrast to 100% steam flow and 75% liquid flow shown in Figure 65).

6.3.3   S/C Nodalization

The MELCOR simulations under predicted the D/W pressurization rate compared to the Unit 3 plant data. A similar discrepancy also exists in the MAAP and MELCOR simulations for Unit 3 contained in the first IAEA report [15, Attachment IV-1 and IV-2]. To understand this discrepancy, the torus nodalization was investigated.

D. H. Cook previously investigated mixing and thermal stratification phenomena in the Mk-I torus [5]. Localized heat up and thermal stratification of the S/C can occur if steam vented from the RPV into the S/C non-uniformly, i.e., through only one SRV (with lowest set point) or

through the single HPCI steam vent location. The localized energy deposition results in local saturation of the pool and a sharp decrease in S/C efficiency in condensing the vented steam.

D. H. Cook developed a computer model for the torus consisting of mass, momentum, and energy balances, as well as correlations for two phase hydrodynamics and heat transfer [5]. For verification, the model was compared against SRV actuation tests performed at the Monticello nuclear power plant. Based on the comparison, a discretization of the torus into 16 divisions in the circumferential direction and at least 8 divisions in the vertical direction was recommended.

The Peach Bottom MELCOR model, used as the basis for this modeling study, used one control volume to represent the torus with one vent line connecting the D/W to the S/C. Modeling the S/C in this manner cannot capture localized saturation of the S/C. Three different cases of S/C modeling are presented in Figure 88, Figure 89, and Figure 90. Utilizing only one S/C control volume results in the pool remaining subcooled until the containment is vented (around {42:00}).

Dividing the pool into eight divisions in the circumferential direction allows for the temperature to vary circumferentially and allows for the possibility of local saturation. Indeed, using eight control volumes, the section where most of the steam is vented rapidly becomes saturated (around {00:42}) and the D/W pressurization rate increases. However, the predicted pressurization rate is still much slower than the data suggests.

Further dividing the pool into 16 divisions, eight in the circumferential direction and two in the vertical direction, allows for circulation cells to form in the pool. Using 16 divisions resulted in stratification of the pool and rapid saturation (around {00:31} for bottom and {00:57} for top cell) near the main venting location. The S/C and D/W then begin to pressurize rapidly as the steam vented into the S/C is not efficiently condensed in the pool. However, from around {08:30} to {11:30}, a convection cell forms bringing subcooled water in from neighboring torus control volumes. This results in sub-cooling of the previously saturated control volumes in the S/C and increases the efficiency of the S/C at condensing the vented steam. Note the trend in D/W pressurization is then similar to the one S/C control volume case.

These results demonstrate the impact the S/C nodalization has on D/W pressurization. More specifically, the results demonstrate the impact of the S/C phenomena of circumferential variations of pool temperature (eight control volume case) and the impact of convection cells (16 control volume case). It is possible the D/W pressurization discrepancy may be resolved through refinement of the S/C nodalization.
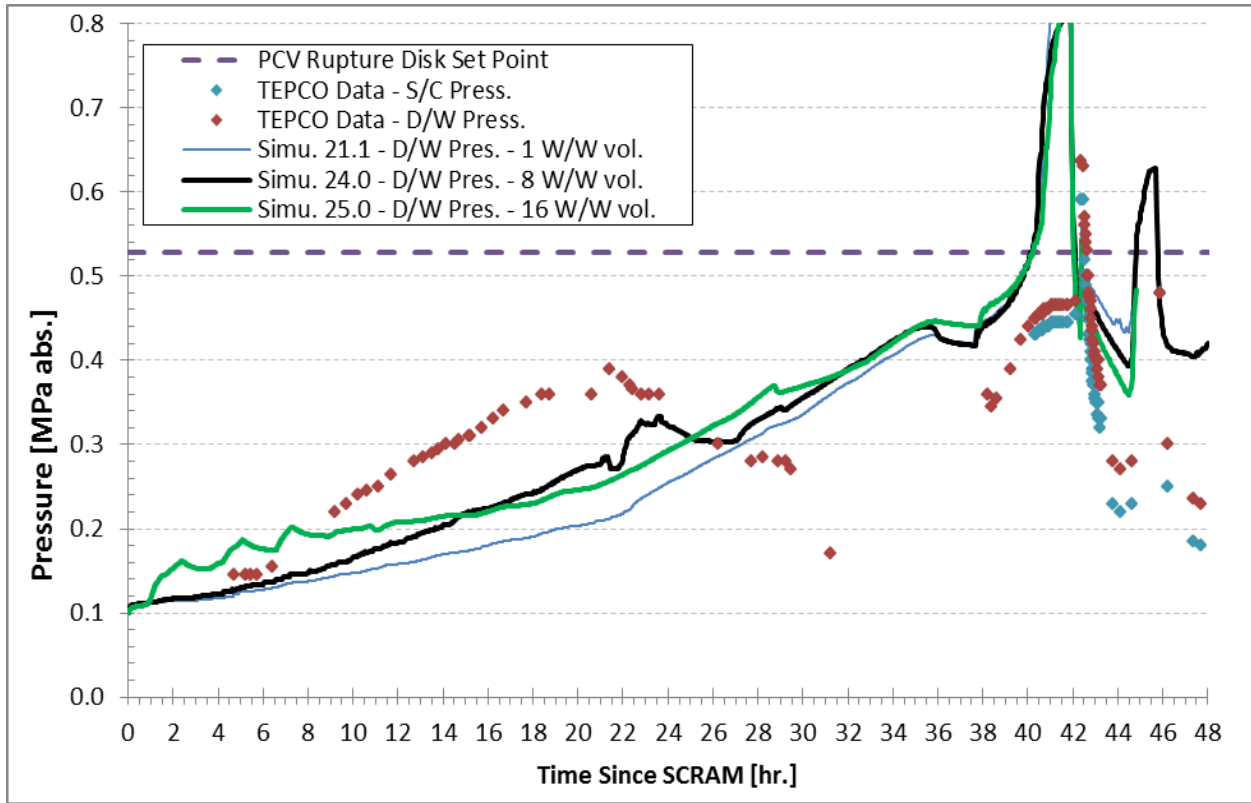
Figure 88. S/C Nodalization Impact on D/W Pressure.
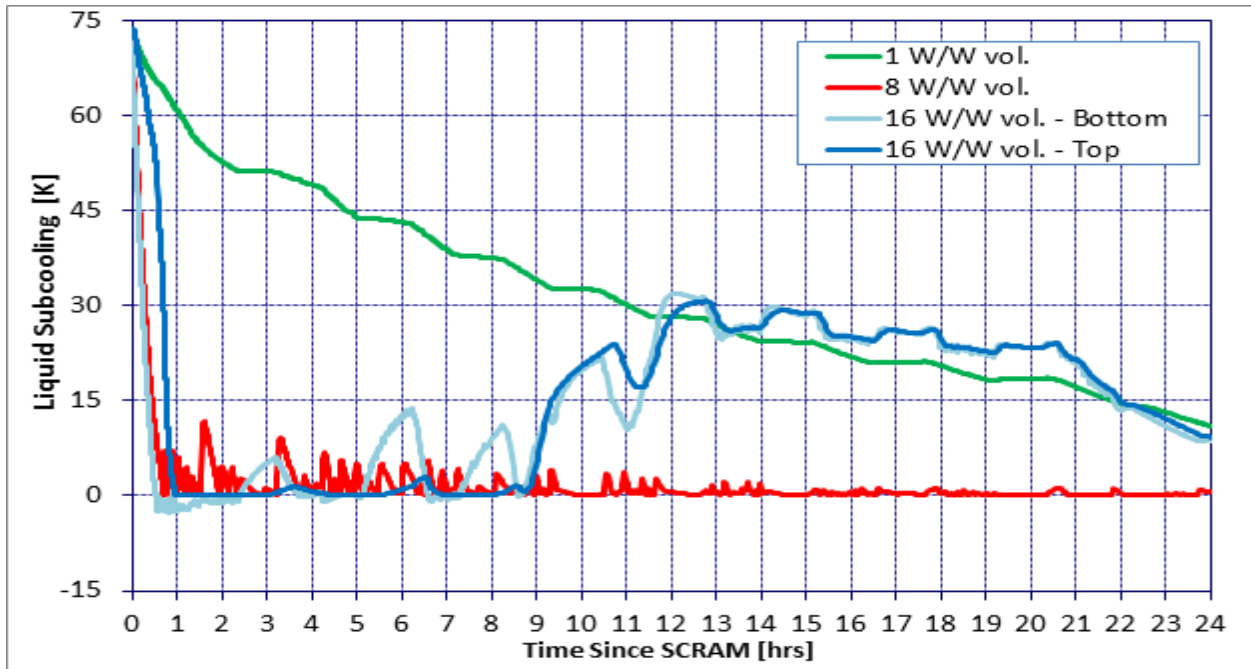
Figure 89. S/C Nodalization Impact on S/C Water Subcooling.

144
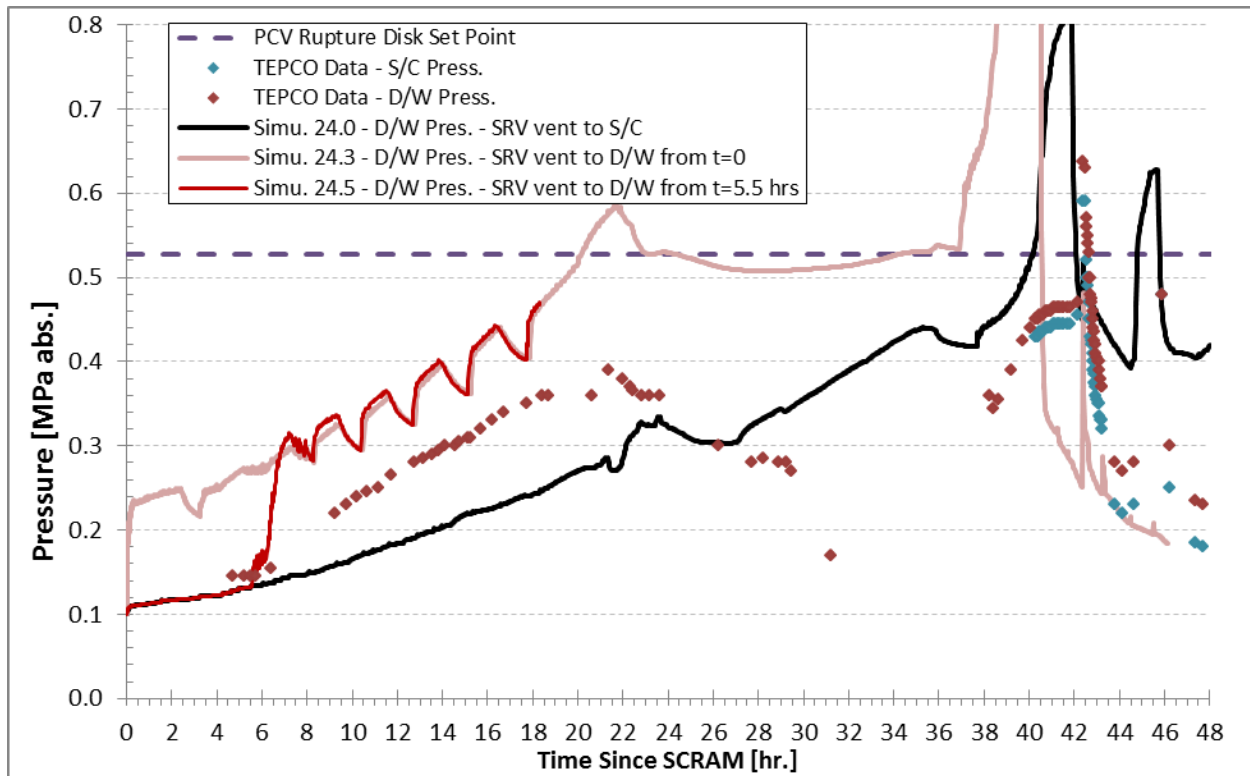
Figure 90. SRV Vent to D/W, Impact on D/W Pressure.

6.3.4 SRV Venting Bypass of S/C

Another possibility for the pressurization discrepancy between the D/W data and the MELCOR simulations during the first 20 hours is if steam was directly vented into the PCV, bypassing the S/C pool. This may occur if part of the SRV or SRV vent piping failed.

Two simulations were run where the SRV vented steam was diverted directly into the D/W (at the SRV elevation). In the first case the steam was diverted at SCRAM initiation, while in the second case the steam was diverted to the D/W at time {05:30}.

The results suggest if the steam was vented directly into the D/W, it would result in a rapid increase in D/W pressure. This scenario is unlikely to have occurred as the plant data does not exhibit such a trend.

6.3.5 Containment Sprays

The two IAEA reports [20, 21] and the INPO report [15] do not indicate containment sprays were used during the period when the HPCI was operating ({21:48} to {35:55}). However, the English translation of the operator log book [36] suggested the diesel driven fire pump was operating during this period and the pump discharge pressure was above the D/W pressure but below the RPV pressure (Figure 68 and Figure 69). In addition, the PCV pressure decreased during this period. These three observations suggest the possibility that the containment sprays, powered by the diesel driven fire pump, were being used during this period.

145

Two simulations were performed to investigate the impact of the containment sprays. One case injected 50 GPM and the other case injected 200 GPM of water through the S/C or D/W sprays during assumed periods (see Figure 91). Activating the sprays did result in a decrease in PCV pressure. The flow rate and precise timing of the spray activity are currently unknown.
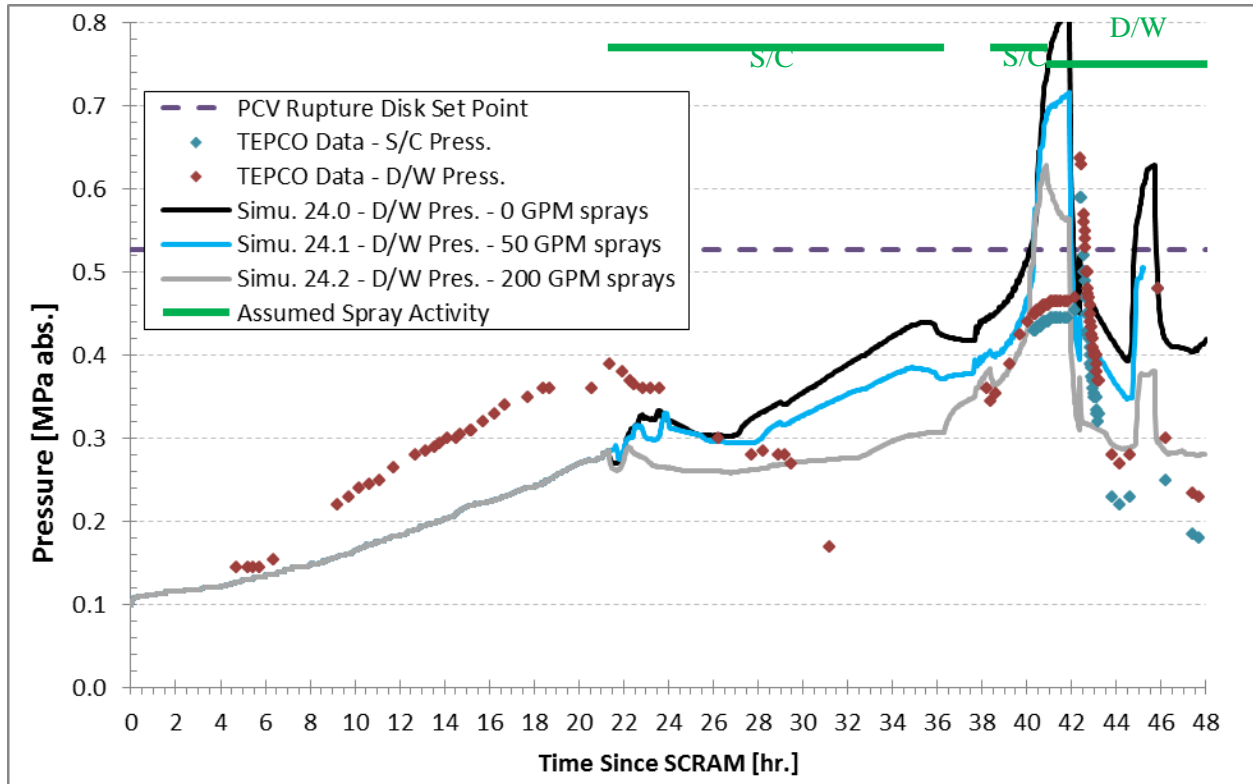
Figure 91. PCV Sprays Impact on D/W Pressure.

The TEPCO representative at the January 25, 2012, technical exchange meeting noted the TEPCO report released on Dec. 22, 2011, which is still in Japanese at this time, contains information indicating the containment sprays were used during the period of HPCI operation and later. The flow rate and precise timing of the spray activity are currently unknown.

6.3.6 Containment Leakage

Another possible cause for the decrease in containment pressure (Section 6.2.2) during the period where the HPCI was operating ({21:48} to {35:55}) is if there were leakage from the PCV. To investigate the impact of D/W leakage into the reactor building, two different leak rates were "hard coded" into the simulation. Leakage rates of 0.35 and 0.75 kg/s were used, which were approximately 35× and 75× higher than the nominal leakage from the PCV (Figure 92).

As expected, the leakage decreases the PCV pressure; however, the pressure continues to rise after approximately {25:00}. The PCV temperature decreases to the point where the water in the

146

PCV becomes saturated and begins to flash. At some point, the steaming rate surpasses the leakage rate and the PCV pressure begins to rise.

Currently, utilization of the containment sprays is thought to be the cause for the decrease in PCV pressure around the period {21:48} to {35:55}. However, a possible alternate scenario, leakage from the PCV, could also cause the decrease in PCV pressure. Flashing of the water in containment works to limit the depressurization.
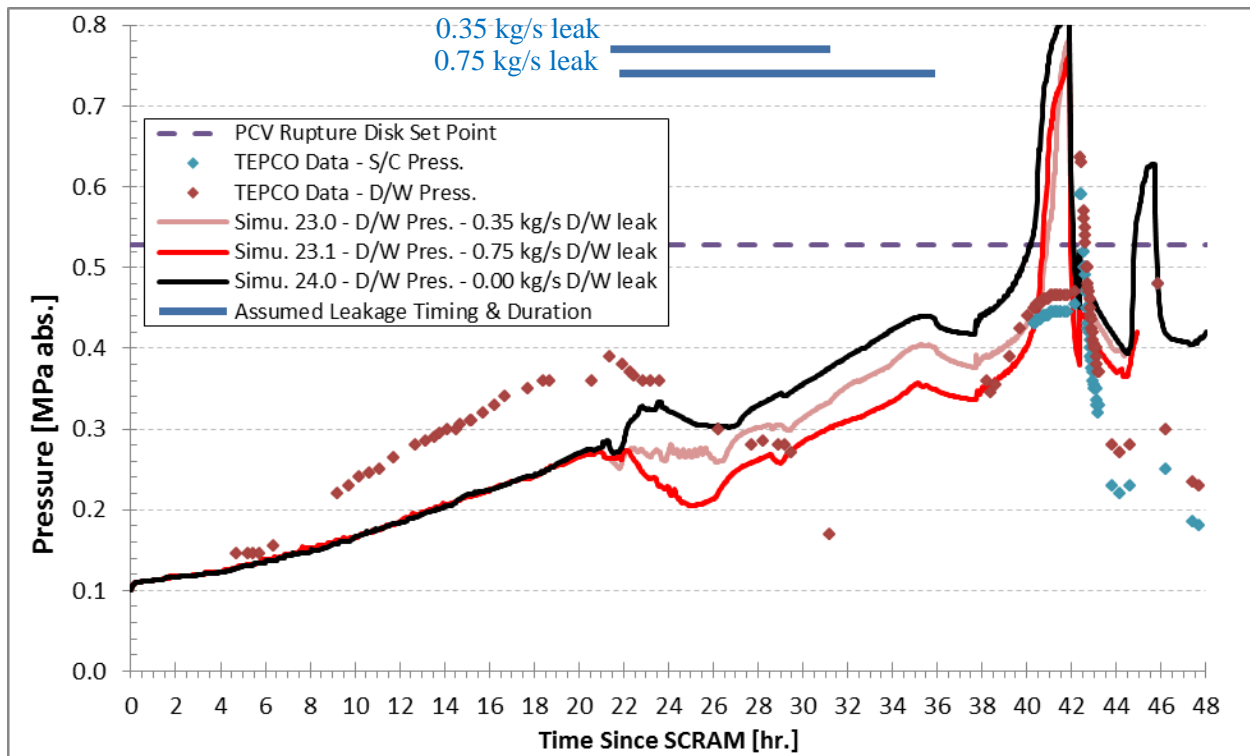
Figure 92. PCV Leakage Impact on D/W Pressure.

6.3.7 Fire Engine Water Injection Rate

The modeled water injection rate and duration from the fire engines into the Unit 3 feed water line are given in Table 13. At those injection rates, the amount of heat the injected water can remove through boiling is greater than the decay heat. Therefore, the core is quenched and the water level is restored in the RPV.

However, possible leakage through connections, piping, or valves as well as possible valve misalignments may have affected the timing, rate, and amount of water that made its way to the core region. Also, the instantaneous flow rates are unknown.

A simulation was performed assuming half of the fire engine water was injected into the feed water line (half the values in Table 13). The half fire engine water addition simulation was extended to {61:30}(Table 16).

147

Table 16. Fire Engine Water Addition Impact on Accident Progression

Time	Simulation Case	Event
{34:00}	Both	Water Reaches TAF
{40:45}	Both	1st Fuel Failure
{42:38}	Both	Fire Engine Water Addition Starts
{45:33}	Both	Fire Engine Water Addition Stops
{45:37}	½ Fire Injection	Lower Core Plate Fails
{46:25}	Both	Fire Engine Water Addition Starts
{47:37}	Full Fire Injection	Lower Core Plate Fails
{48:01}	Full Fire Injection	End Simulation
{52:52}	½ Fire Injection	Lower Head Failure
{52:53}	½ Fire Injection	Begin Melt Relocation to Cavity
{58:23}	½ Fire Injection	Fire Engine Water Addition Stops
{58:23}	½ Fire Injection	Lower Head Dries Out
{~60:00}	½ Fire Injection	Second Major Period of Melt Relocation to Cavity Begins
{60:33}	½ Fire Injection	Fire Engine Water Addition Starts
{61:30}	½ Fire Injection	End Simulation

The water level in the core region, as well as in the annulus is plotted in Figure 93. Note that both of the simulations are the same until the water injection via the fire engines start. As expected, for the case where only half of the fire engine water is added, the bottom head dries out and fails, causing melt to be relocated into the PCV. Note that for the ½ fire engine water addition case, less zirconium is oxidized and less hydrogen gas is generated (Figure 94). This is due to the water level dropping below the bottom core plate, reducing the steam generation, which drives the hydrogen generation process.
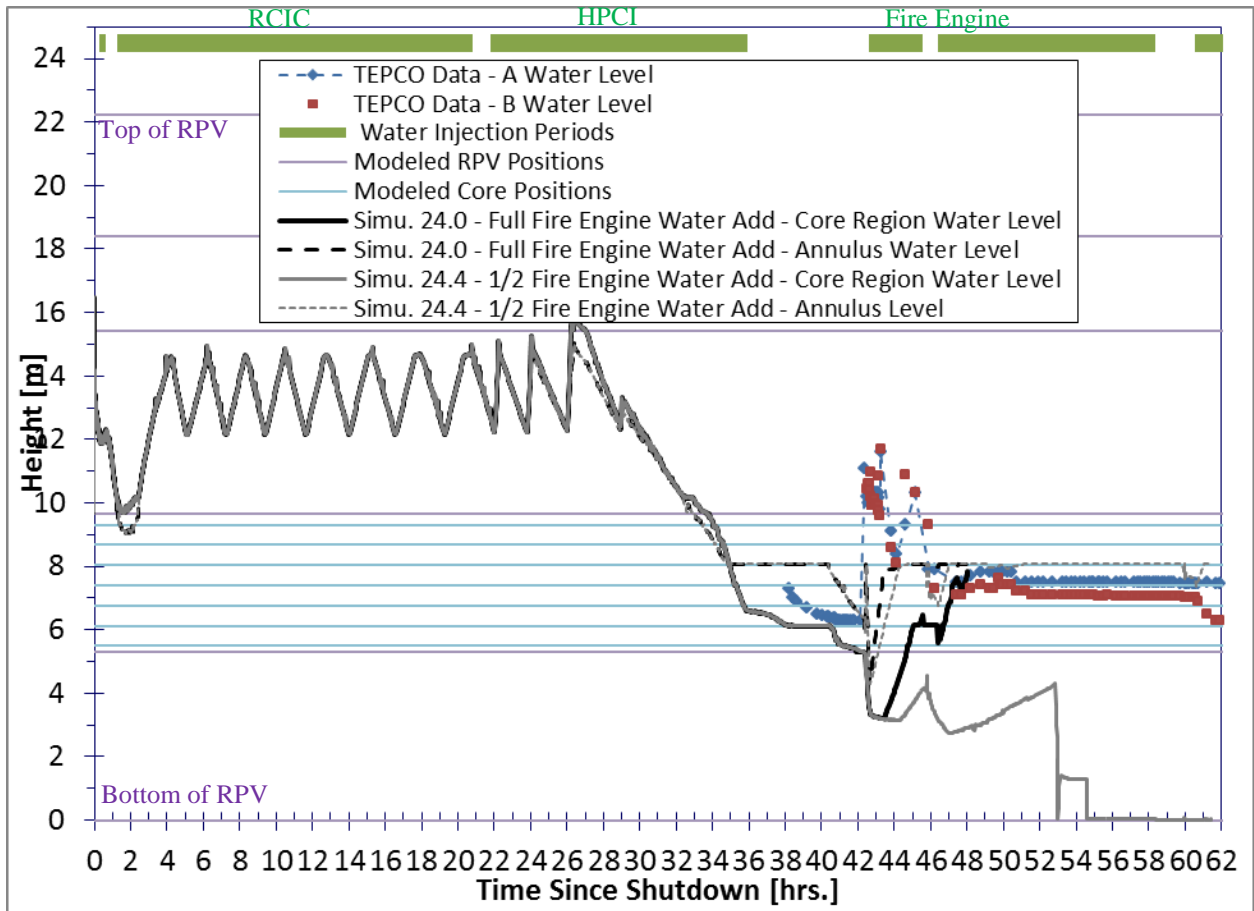
Figure 93. Fire Engine Water Addition Rate Impact on Water Level.

149
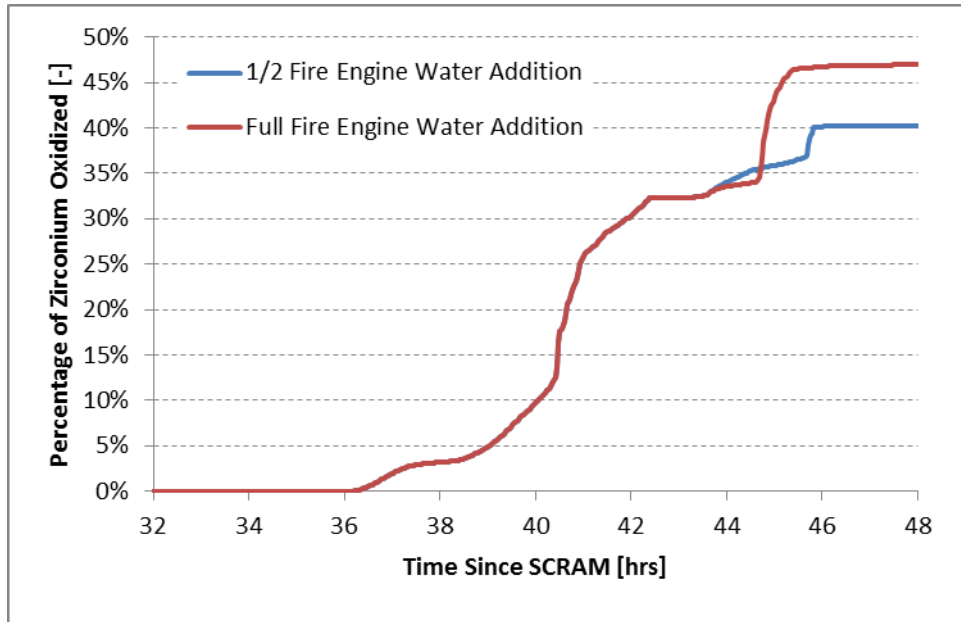
Figure 94. Fire Engine Water Addition Rate Impact on Zirconium Oxidation.

6.3.8 Comparison of SNL and ORNL MELCOR Simulations of Unit 3

Generally, the SNL and ORNL results tend to agree well for the calculations of RPV and containment pressure. Predictions of core damage and hydrogen generation are also comparable. Comparing Figure 60 to Figure 75, it appears the SNL and ORNL predictions of core damage are reasonably similar near 46.5-48 hours. In the SNL calculation, the top core node (top plate) has completely relocated, and the fuel assemblies in the center ring, axial levels 13-16, have collapsed. In the ORNL calculation, the top plate node has also completely relocated, and there is fuel damage in rings 1-4, and spanning one-half the axial length of the active core region. Thus, although it appears the ORNL calculation is predicting slightly more core damage by 48 hours, the calculations are fairly similar given they are from independently developed models. The SNL and ORNL calculations of hydrogen generation from metal oxidation are quite similar as well. By comparing Figure 58 to Figure 76 (ORNL's "Simu. 27.9 – HPCI A"), it appears that SNL and ORNL both predict an integral hydrogen mass in the range of 1200 to 1300 kg. However, in the ORNL calculation, the hydrogen generation begins eight hours before the SNL calculation predicts hydrogen generation.

The subtle differences in core damage and hydrogen generation are a result of the different HPCI modeling in the SNL and ORNL MELCOR models of Unit 3. In the ORNL model, the water injection by the HPCI is assumed to degrade, but the HPCI turbine continues to draw steam until 36 hours (which is the time the HPCI ceased operation in the timeline) (Figure 80). In contrast, the SNL HPCI model continues to inject water into the RPV until 36 hours. Thus, there is a significant difference in RPV water level between the SNL and ORNL simulations. The ORNL simulations uncover the active fuel near 35-39 hours, while the SNL model uncovers the fuel at 42.3 hours. Therefore, the ORNL core is uncovered longer before the injection of freshwater at 42.6 hours, and more fuel and clad material relocates from the central-upper regions of the core.

Such differences in core damage timing may impact predicting a hydrogen explosion in the reactor building at 68.2 hours.

Although the general trends in containment and RPV pressure are comparable, the SNL and ORNL models contain several different inputs to obtain these results. Besides many differences in the nodalization of the core and the RCS, the most significant differences between the SNL and ORNL models are:

1. Decay heat: SNL used the TEPCO-provided decay heat and power distributions. ORNL used the MELCOR option for the ANS standard decay heat curve (ANSI/ANS-5.1-1979) for a BWR reactor with a thermal rating of 2381 MW (Section 5.2.3), which may be overestimate the decay power provided by TEPCO. It should also be noted that the Unit 3 axial power distribution according to TEPCO is much more bottom-peaked than the distributions in the legacy and SOARCA BWR/4 Mk-I models, which would affect the degradation of a partially covered core. The overall decay heat has a major effect on the accident sequence, such the initial pressurization in the containment from 0 to 22 hours.

2. CVH nodalization of the suppression chamber: Both ORNL and SNL have investigated a variety of wetwell nodalizations in order to capture the initial pressurization in the containment from 0 to 22 hours. However, the SNL model presented in this report used only a two-volume (axially stacked) wetwell model. With only one wetwell volume in the circumferential direction, SRV steam discharge is distributed throughout the entire wetwell torus. This nodalization effect cannot capture the local pool saturation that could result when the SRV discharge is directed to a single location in the torus. The current ORNL wetwell CVH mesh is much more detailed than the current mesh in the base case SNL model that is presented in Section 3, and it better simulates the initial 0-22 hour heatup of the wetwell by accounting for the localized point of steam introduction to the torus pool.

3. HPCI/RCIC modeling: The current SNL model presented in Section 3 assumed minimum flow operation of the HPCI temporarily cools the wetwell after 22 hours. In contrast, the ORNL model diverts HPCI injection to the CST when the RPV level gets too high via the test line. There may also be differences in the steam flow pulled by the RCIC and HPCI turbines. The ORNL HPCI model assumes a degraded ability to inject water, while the SNL HPCI model continues injection until 36 hours.

4. Containment sprays: The current SNL model does not use any containment spray model. The ORNL model uses containment sprays in order to explain the drop in containment pressure after 22 hours.

5. Freshwater and seawater injection: The ORNL flow rate for the freshwater injection is greater than the SNL freshwater injection flow rate (7.88 kg/s vs. 2.43 kg/s) (see Figure 13 and Figure 70). The ORNL seawater injection flow rates are less than the SNL seawater injection flow rates (ORNL: 5.41 to 8.94 kg/s; SNL: 9.97 to 16.6 kg/s). Slight differences exist in the start and stop times of the seawater injections.

6. Water injection site: The ORNL model injects into the RPV via the feedwater lines, which means injection water first goes into the downcomer, then the jet jumps, down into the lower plenum, and up into the core. The SNL model injects into the RPV via the core spray lines, which deposits water directly above the core (where it then falls down and

floods the core). Different injection sites could lead to different predictions of coolability of the degraded fuel, especially after lower head failure.

7. Code differences: ORNL used MELCOR 1.8.5, whereas SNL used the current development version, MELCOR 2.1.

8. Treatment of water level data: The SNL analyses tend to discredit the reliability of the TEPCO water level data. Conversely, the ORNL analyses more closely reproduce the TEPCO water level data. Early water level data (0 – 30 hours), which is still present in the TEPCO analyses [19], was removed from the TEPCO website and the INL portal. Later water level data may be unreliable due to the sudden RPV depressurization from HPCI operation and the SRV opening.

9. Simulation truncation time: The Unit 3 SNL simulations end at 96 hours. The ORNL simulations presented in this report run to 48-62 hours.

Most of the differences listed above are due to the nature of the events at Fukushima. The plant data (e.g., decay power) and the assumed operator actions (e.g. sprays vs. HPCI minimum flow) have evolved significantly since the severe accidents occurred. Based on the level of knowledge of the events and plant details at the time of this analysis, there were a variety of possible scenarios and modeling techniques to explain the various stages of the accidents at each reactor. The only way to resolve such uncertainties is through further research and analysis.

7   ORNL MODEL OF THE UNIT 4 SPENT FUEL POOL

The study on characterization of the Fukushima Daiichi unit 4 spent fuel pool (SFP4) will be focused on the analysis of pool boil-off and fuel heat-up following the accident. The study end date for the spent fuel pool 4 (SFP4) is March 22, when TEPCO began using a concrete pumper truck to inject water into the pool.

In addition, a study on SFP-4 beyond March 22 is also presented in this report. The objective of this study is to complement the TRACE analysis, and therefore provide a more realistic and complete picture of the accident progress of SFP4 with available measured data.

7.1   Chronology of Fukushima SFP4

The condition of the SFP4 and the emergency responses taken after the earthquake and tsunami were described in reports prepared by the Japanese government for the International Atomic Energy Agency (IAEA) [20, 21].

At 14:46 on March 11, 2011, SFP4 lost all AC power when one emergency diesel generator (DG) stopped functioning due to flooding of the seawater pumps and electrical gear caused by the tsunami. The cooling and water supply for the spent fuel pool likewise failed. On March 15, the reactor building was damaged by what was assumed to be a hydrogen gas explosion. On March 16, a helicopter flew close to the operating floor of Unit 4, at which time the water surface of the pool could be seen but no exposed fuel was observed.

On March 20, freshwater was sprayed into the pool by a water-spraying truck provided by the Japanese Self-Defense Force (SDF). By March 21, about 250 tons of water had been sprayed into the pool from the ground. On March 22, a concrete pump truck began spraying seawater into the pool, and by June 14 approximately 5,700 tons of water had been added to the pool as a result (freshwater spraying had been continued after March 30).

On June 16, water injection by a temporary SFP injection facility was started, and by July 31 about 280 tons of water had been injected by this facility. On June 19, water injection from the In Core Monitor (ICM) piping to the reactor well and Dryer and Separator (DS) pit was performed to reduce the level of radiation coming from the in-core structure stored inside of the DS pit. On June 31, pool water cooling by the alternative cooling system was started. The water temperature was around 75 °C when the cooling was started and reached a steady condition on August 3, where the water temperature stabilized at 40 °C.

Water was sampled using the concrete pump truck on April 12, April 28, and May 7. Outflow water from the pool to the Skimmer Surge Tank was sampled on August 20, and nuclide analysis of the water was conducted. Analysis results indicated that most of the fuel in the pool was in sound condition.

7.2   SFP4 Design Characteristics

Fukushima Daiichi Unit 4 employs an Mk-I containment, as shown in Figure 95. The elevated spent fuel pool is located in the secondary containment. The Fukushima Daiichi Unit 4 reactor was shut down for core shroud replacement on November 29, 2010. A total of 548 reactor fuel assemblies were removed from the core and stored in the pool after the shutdown. In addition to these recently discharged fuel assemblies, the pool also contains 783 older spent fuel assemblies discharged from previous refuelings, and 204 fresh assemblies. All of the fuel assemblies are stored vertically in the fuel storage racks sitting on the pool floor. The total of 1535 fuel assemblies occupy about 95% of the total storage capacity of the pool.
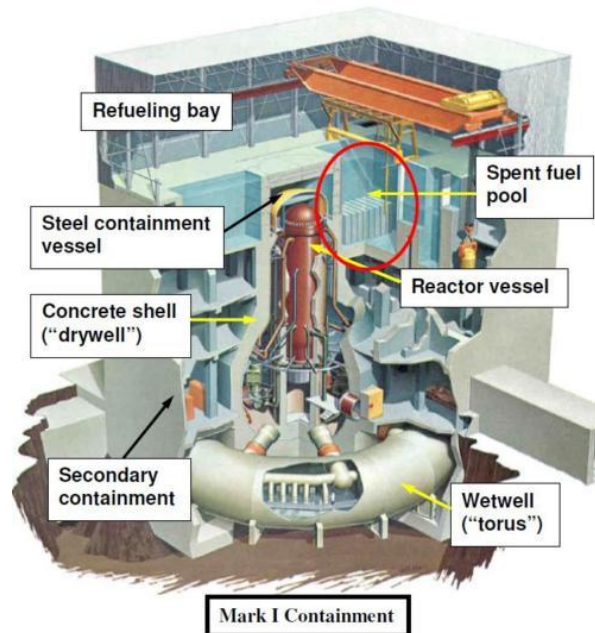
Figure 95. Schematic of a typical Mk-I containment.

7.2.1   Spent Fuel Pool

A typical boiling water reactor (BWR) spent fuel pool is rectangular in cross section and about 40 ft (12 m) deep. Cross-sectional dimensions can be 40 or more ft (12 m). The pool walls are constructed of reinforced concrete, typically having a thickness between 4 and 8 ft (1.2 to 2.4 m). The pools contain a ¼ to ½ in. (6 to 13 mm) thick stainless steel liner, which is attached to the inside walls with studs embedded in the concrete. The inside geometric dimensions of the Fukushima Daiichi SFP4 are 12.2 m (length) × 9.9 m (width) × 11.8 m (depth), as shown in Figure 96.
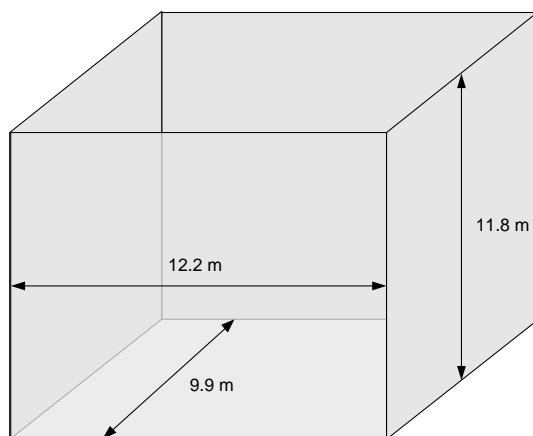
Figure 96. SFP4 Dimensions.

7.2.2 Fuel Assemblies

SFP4 contains 204 fresh STEP-3B fuel assemblies, 548 recently discharged STEP3-B fuel assemblies, 560 older STEP2 fuel assemblies, 30 older 8×8BJ fuel assemblies, 4 older 8×8 fuel assemblies, and 1 older 7×7RD fuel assembly. It is noted that typical GE design parameters (rod diameter, rod pitch, etc.) for these assemblies are used in our analysis because specific design data for each fuel type is not available. Table 17 summarizes the SFP4 fuel inventory and their cooling times.

Table 17. SFP4 Inventory

Fuel Type	Assembly Configuration	Number of FAs	Discharge Data	Cooling Duration as of 3/11/2011 (yrs)
7x7RD	7x7	1	9/26/1980	30.5
8x8	8x8	4	9/2/1986	24.5
8x8BJ	8x8	2	2/26/1995	16
		6	4/21/1996	14.9
		10	3/19/1999	12
		12	5/17/2000	10.8
STEP2	8x8	16	3/19/1999	12
		92	5/17/2000	10.8
		132	10/2/2001	9.4
		88	9/16/2002	8.5
		78	6/25/2005	5.7
		4	10/2/2006	4.4
		101	2/11/2007	4.1
		49	3/28/2008	3
STEP3-B	9x9	1	10/2/2006	4.4
		87	3/28/2008	3
		100	9/29/2009	1.5
		548	11/30/2010	0.3
STEP3-B Fresh Fuel	9x9	204		

7.2.3 Spent Fuel Storage Racks

In SFP4, all the fuel assemblies are stored vertically in 53 fuel storage racks as shown in Figure 97. The fuel storage racks are of a high density design in a 3 × 10 configuration. Each rack has 30 storage cells, each 0.15 m × 0.15 m square. The separation walls between cells are made of stainless steel. The total height of the racks was modeled as 4.44 m. Likewise the baseplate was modeled as 0.14 m in height containing holes on each side to allow pool water circulation. All of the racks sit on the floor pads. In this analysis, the rack floor pad is assumed to be 0.293 m in height.
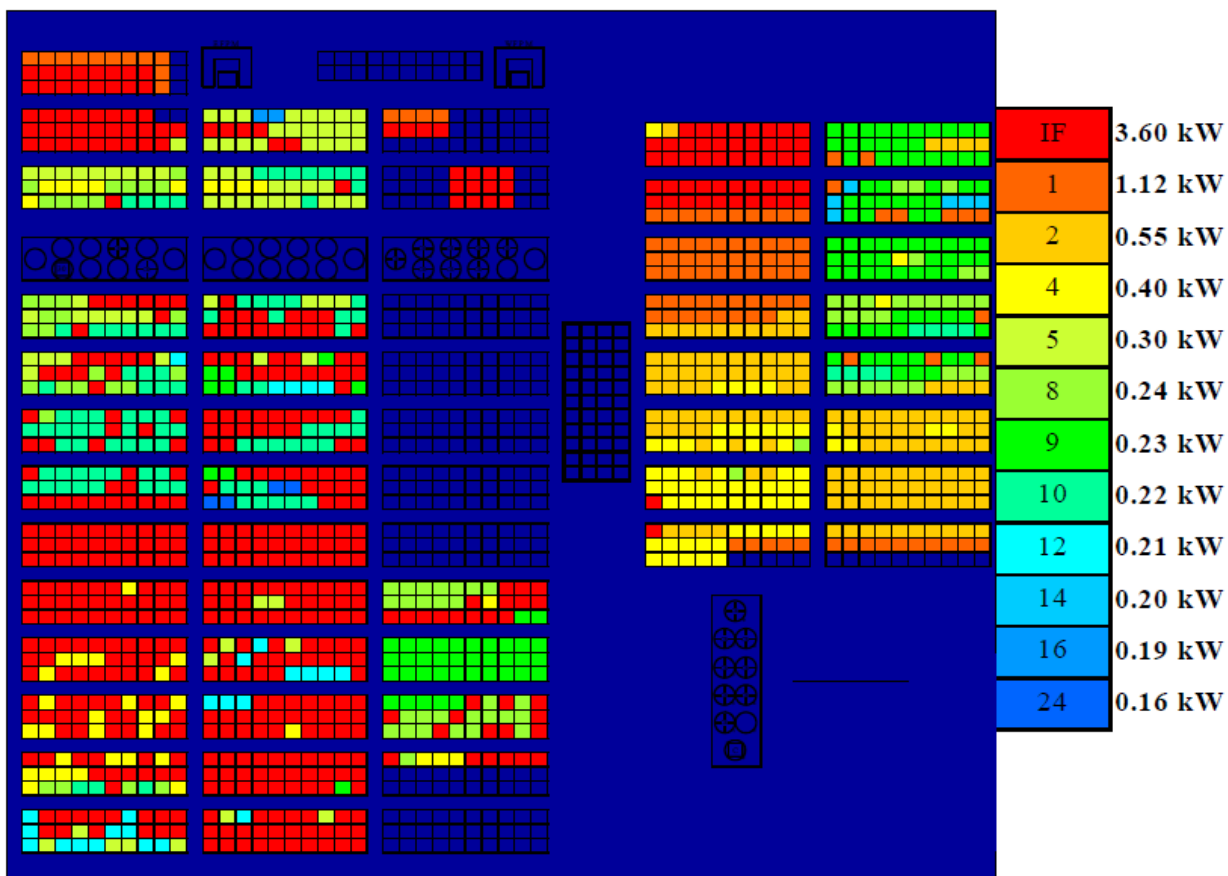
Figure 97. SFP4 Fuel Loading.

7.3 SFP4 Heat Transfer and Evaporation

Parameters or physical processes and phenomena important to pool boil-off and fuel heat-up following the loss of pool cooling can be identified as follows:

Fuel Assemblies:
1) Decay heat
2) Heat conductivity and capacity of the fuel assembly structures (fuel rods and channel, tieplates, grid spacers)
3) Zircaloy oxidation
4) Radiative heat transfer between the upper tieplates and the atmosphere.

Fuel Storage Racks:
1) Convective heat transfer through water within the gap between fuel channel walls and the rack walls
2) Radiative heat transfer between the fuel channel walls and the rack walls
3) Heat conductivity and capacity of the rack structures

Spent Fuel Pool Walls and Pool Surface:
1) Heat conductivity and capacity of the pool wall structures
2) Pool surface heat transfer through air convention
3) Pool surface heat transfer by evaporation
4) Pool surface heat transfer by radiation
5) Pool surface evaporation
6) Air wind velocity
7) Reactor building ventilation

Some important parameters are discussed in detail in the following sections.

7.3.1 Decay Heat

In this study, the decay heat in SFP4 was calculated using ORIGEN. Table 18 summarizes assembly design and the decay heat for each fuel type based on its cooling time. The calculated total decay heat on March 11, 2011, in SFP4 is about 2.28 MW, of which about 82% is produced by the 548 recently discharged fuel assemblies with 101 days of cooling. Figure 98 shows the predicted decay heat as a function of cooling time for all of the fuel of SFP4. The accuracy of the prediction should be within ± 2.4% of actual values [14]. It is noted that the TEPCO-calculated decay heat was 2.26 MW as of March 11 and 1.58 MW as of June 11 [21].

Table 18. SFP4 Decay Heat

Fuel Type	Assembly Configuration	Number of Fuel Assemblies	Discharge Data	Cooling Duration as of 3/11/2011 (yrs)	Decay Heat as of 3/11/2011 (watts/assembly)
7x7RD	7x7	1	9/26/1980	30.5	186.2
8x8	8x8	4	9/2/1986	24.5	209.1
8x8BJ	8x8	2	2/26/1995	16	250.3
		6	4/21/1996	14.9	257.3
		10	3/19/1999	12	278.2
		12	5/17/2000	10.8	288.9
STEP2	8x8	16	3/19/1999	12	278.2
		92	5/17/2000	10.8	288.9
		132	10/2/2001	9.4	304.6
		88	9/16/2002	8.5	318.5
		78	6/25/2005	5.7	393.6
		4	10/2/2006	4.4	472.5
		101	2/11/2007	4.1	506.6
		49	3/28/2008	3	676.9
STEP3-B	9x9	1	10/2/2006	4.4	472.5
		87	3/28/2008	3	676.9
		100	9/29/2009	1.5	1267
		548	11/30/2010	0.3	3416
STEP3-B Fresh Fuel	9x9	204			0
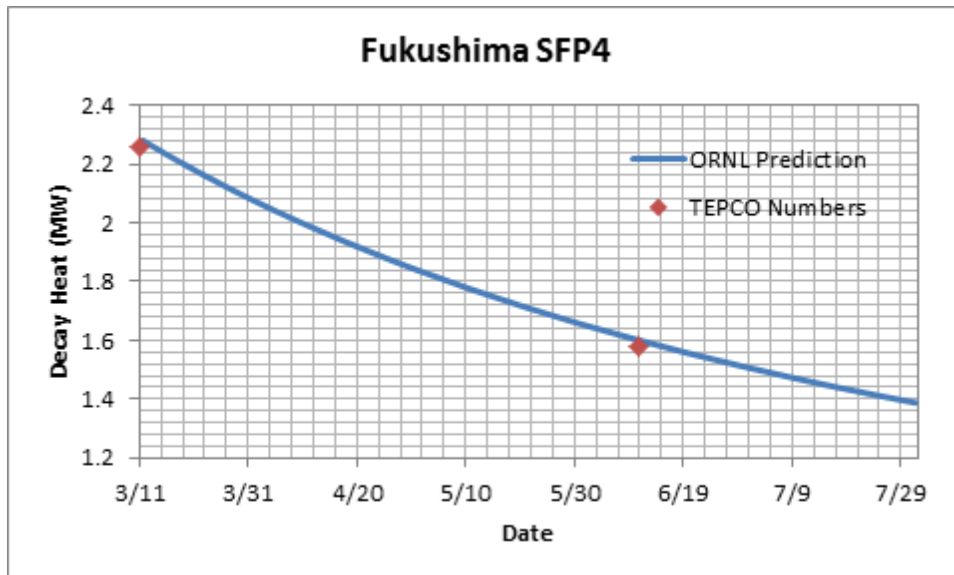
Figure 98. SFP4 Decay Heat Load.

7.3.2 Pool Heat Losses

For the pool boil-off analysis, it is important to know various heat losses in the pool. The heat losses of interest are discussed as follows.

7.3.2.1 Pool Surface Heat Transfer through Air Convection

SFP4 has a surface area of 120.78 m². Heat loss through the air free convection could be significant when the pool temperature becomes high. A simple calculation to estimate this heat loss is given as follows:

Inputs:

SFP surface area:
$$A_s = 12.2 \times 9.9 = 120.78 \ \text{m}^2$$

Ambient air Temperature:
$$T_{air} = 300 \ \text{K}$$

Air properties at 300 K:
$$v = 15.89 \times 10^{-6} \frac{m^2}{s}, \alpha = 22.5 \times 10^{-6} \frac{m^2}{s}, k = 0.0263 \frac{W}{m} \cdot k, \beta = 0.0033 \ K^{-1}$$

Natural Convection Heat Transfer Formula for a horizontal plate surface [16]:

$$\overline{Nu_L} = 0.54 Ra_L^{1/4} \qquad \left(10^4 \leq Ra_L \leq 10^7\right) \tag{7.1}$$

$$\overline{Nu_L} = 0.15 Ra_L^{1/3} \qquad \left(10^7 \leq Ra_L \leq 10^{11}\right) \tag{7.2}$$

Analysis:
$$Ra_L = \frac{g\beta(T_s - T_{air})L^3}{v\alpha} = \frac{9.8 \times 0.0033\,(T_s - T_{air})L^3}{15.89 \times 10^{-6} \times 22.5 \times 10^{-6}} = 9.046 \times 10^7\,(T_s - T_{air})L^3$$

For the pool water surface, $L = \frac{A_s}{P} = \frac{120.78}{2(12.2 + 9.9)} = 2.73 \ m$, hence $Ra_L > 10^7$.

So, we have:
$$\overline{Nu_L} = 0.15 Ra_L^{\frac{1}{3}} = 0.15 \times [9.046 \times 10^7\,(T_s - T_{air})L^3]^{1/3} = 67.33(T_s - T_{air})^{1/3}L$$

$$\overline{h_s} = \frac{k}{L}\overline{Nu_L} = \frac{0.0263}{L} \times 67.33(T_s - T_{air})^{1/3}L = 1.771(T_s - T_{air})^{1/3} \tag{7.3}$$

When the pool reaches the water saturation temperature, we have:

$$\overline{h_s} = 1.771(T_s - T_{air})^{1/3} = 1.771(373.15 - 300)^{1/3} = 7.41 \, W/m^2 \cdot K$$

The rate of heat transfer through the pool surface is:

$$q = \overline{h_s}(T_s - T_{air}) \, A_s = 7.41 \times (373.15 - 300) \times 120.78 = 0.0654 \, MW$$

With an assumed total decay power in SFP4 of about 2.3 MW, the heat loss through the pool surface is only about 2.8% of the total SFP heat load for the pool surface water temperature at 100 °C.

7.3.2.2 Heat Conduction through Pool Side Walls and Floor

Heat transfer through the pool side walls and floor can be estimated based on the total heat transfer area, overall heat transfer coefficients, and temperature differences between the pool and the outside environment. The overall heat transfer coefficients are mainly dependent upon the heat resistance of the concrete walls because of their large thickness and low conductivity. Therefore, we can estimate an upper bound of the heat transfer by simply making the following assumptions.

1) The thickness of the pool concrete walls and floor are assumed to be 1 m. Note that the thickness of the pool walls is between 1.2 m and 2.4 m for a typical BWR spent fuel pool in a Mk-I containment.
2) The inside surface temperature of the walls is assumed to be 100 °C and the outside surface temperature of the walls is assumed to be 20 °C. This assumption is conservative in view of the actual conditions. The outside temperatures of the walls are usually higher than 20 °C.
3) The total heat transfer area is the total wall surface area:
$S = 12.2 \times 9.9 + (12.2 + 9.9) * 11.8 * 2 = 642.34 \, m^2$. This is the maximum heat transfer area. Actually, the effective heat transfer area decreases as the water level in the pool drops during the boil-off.

The maximum heat transfer can be calculated as below.

$$q = k\frac{\Delta T}{\Delta x} \cdot S \qquad\qquad (7.4)$$

Where

q is the total heat transfer rate through the pool walls and floor
k is the wall concrete conductivity. It is assumed to be 0.93 W/mK
ΔT is the temperature drop through the wall
Δx is the wall thickness
S is the total heat transfer area

So, based on the above the assumptions, the total heat transfer rate through the pool walls and floor can be calculated as below.

$$q = k\frac{\Delta T}{\Delta x}\cdot S = 0.93 \times \frac{100-20}{1} \times 642.34 = 47.79\ kW$$

This value is about 2% of the total decay heat load in the Fukushima SFP4. Therefore, the heat loss through the walls and the floor is negligible.

7.3.2.3   Heat Transfer through Surface Evaporation

In a loss of pool cooling event, the decay heat of the spent fuel will heat up the pool. Heat will eventually leave the pool by the conduction through the side walls and the floor, air convection on the surface, and evaporation or boiling. For a typical BWR spent fuel pool, heat loss by the wall conduction or the pool water surface convection is usually less than a few percentage of the total decay load of the pool; for example, they are less than 5% in the Fukushima SFP4, as discussed previously.

When the pool temperature increases above 70°C the evaporation on the pool surface becomes significant in taking away heat and water from the pool. Therefore, an accurate prediction of water evaporation plays a very important role in analyzing heat and mass balance of the pool, in particular, early pool temperature rising, and steady pool temperature. A correlation was derived for calculating the pool evaporation rate based on the analogy between the heat transfer and mass transfer for the free convection phenomena.

For a typical BWR pool, the Raleigh number $Ra_L > 10^7$ for the surface natural convection heat transfer, hence, the heat transfer Nu number for the spent fuel pool surface can be readily calculated by [16]:

$$Nu = 0.15(Ra_L)^{1/3} = 0.15(GrPr)^{1/3}\left(10^7 \le Ra_L \le 10^{11}\right) \tag{7.5}$$

With the analogy between heat transfer and mass transfer, the Sherwood number Sh can be calculated as:

$$Sh = \frac{k_\omega l}{\rho D_{AB}} = 0.15[(Gr + Gr_m)Sc]^{1/3} \tag{7.6}$$

Where

$$Gr = \frac{gl^3 \bar{\beta}(T_1-T_0)}{v^2}, \qquad \bar{\beta} = -\frac{1}{\rho}\left(\frac{\partial \rho}{\partial T}\right)_P$$

$$Gr_m = \frac{gl^3 \bar{\zeta}(\omega_{A1}-\omega_{A0})}{v^2}, \qquad \bar{\zeta} = -\frac{1}{\rho}\left(\frac{\partial \rho}{\partial \omega_A}\right)_{P,T}$$

$$Sc = \frac{v}{D_{AB}}$$

Note that thermal Grashof number in Equation 7.6 is replaced by the sum (Gr + Gr$_{m}$). This simplification is widely used for the air-water system, where the small difference between the Sc and Pr numbers does not have a significant effect [1].

Hence, we have the mass transfer coefficient or the evaporation coefficient as

$$k_\omega = \frac{\rho D_{AB}}{l} Sh = \frac{\rho D_{AB}}{l} \cdot 0.15 \cdot \left[\left(\frac{gl^3 \bar{\beta}(T_1 - T_0)}{v^2} + \frac{gl^3 \bar{\zeta}(\omega_{A1} - \omega_{A0})}{v^2} \right) \cdot \frac{v}{D_{AB}} \right]^{1/3}$$

$$= 0.15 \cdot \rho \cdot \frac{D_{AB}^{\frac{2}{3}}}{v^{\frac{1}{3}}} \cdot g^{\frac{1}{3}} \cdot \left[\bar{\beta}(T_1 - T_0) + \bar{\zeta}(\omega_{A1} - \omega_{A0}) \right]^{\frac{1}{3}}$$

$$\boldsymbol{= 0.321 \cdot \rho \cdot \frac{D_{AB}^{\frac{2}{3}}}{v^{\frac{1}{3}}} \cdot \left[\bar{\beta}(T_1 - T_0) + \bar{\zeta}(\omega_{A1} - \omega_{A0}) \right]^{\frac{1}{3}}} \qquad (7.7)$$

Normally, the diffusional Grashof number Gr$_{m}$ is much less than the thermal Grashof number Gr; therefore the second term in the brackets of Equation 7.6 can be omitted when calculating the evaporation coefficient. It shows that that the evaporation coefficient is dependent on temperature (i.e., it increases as the water surface temperature increases because free convection flow is enhanced by the increased surface temperature).

Finally, the evaporation rate can be calculated with the equation as

$$W_{A0} = k_\omega A \frac{\omega_{A1} - \omega_{A0}}{1 - \omega_{A1}} \qquad (7.8)$$

Where

> W_{A0} is the water evaporation rate (kg/s)
> A is the pool surface area (m^2)
> ω_{A1} is the vapor mass fraction in the saturated air at the same temperature as the pool surface water temperature
> ω_{A0} is the vapor mass fraction in the air at the atmospheric air temperature

For air with temperature 20 °C and 50% relative humidity, the water (vapor) mass ratio in the air is $\omega_{A0} = 0.00721$. Using the above Equation 7.7, the evaporation rates at various pool temperatures for the Fukushima SFP4 with A = 120.78 m^2 are calculated and summarized in Table 19. In addition, the heat supply for maintaining the pool water temperature is calculated

based on the evaporation rate. They are also included in the table. Figure 99 shows the evaporation rate as a function of pool temperature.

However, it should be noted that there are uncertainties in any actual situation and the boundary layer model on which the evaporation model is essentially based. For example, the free convention flow could be disturbed by the air flow across the pool surface. In general, the evaporation increases with the wind speed. It is worth to mention that our evaporation model has very good agreement with an engineering empirical model [7].

It is interesting to make some simple calculations. For example, the pool will daily lose 2 tons of water when the pool temperature is at 40°C. The water loss would increase to 86 tons when the pool temperature reaches 87.5°C, which means that such an evaporation rate would take away all the decay heat of the Fukushima SPF4 without reaching the boiling temperature. It should be pointed out that this analysis is very important to understand the pool temperature data collected in the Fukushima SFP4. The Fukushima SFP4 would reach the equilibrium temperature within 2 days during the loss of pool cooling. We should not expect any observable changes in the pool temperature over a short time (days to months) during a loss-of-cooling event since the decay heat change is small. We will expand upon this later.

In addition, the evaporation rate at the equilibrium temperature can be calculated simply based on the energy balance between the evaporation rate and decay heat, which means all decay heat is used to evaporate water.

$$Evaporation\ Rate\ at\ the\ Equilibrium\ Temperature = \frac{Decay\ Heat}{h_v - h_l} \tag{7.9}$$

Where, $h_v - h_l$ is the water latent heat between the liquid and vapor phase. It has a very weak dependence on temperature.

Table 19. Calculated Evaporation Rates for SFP4

Pool Temperature (^{0}C)	Saturated Vapor Pressure (Pa)	ω_{A1}	ω_{A0}	k_{ω}	Evaporation Rate (kg/s)	Heat Supply to Maintain Temp (MW)
25	3170	0.0197		0.0	~0.0	0.000
30	4247	0.0265		0.003430	0.007	0.017
40	7385	0.0466		0.004947	0.023	0.056
50	12352	0.0794		0.005865	0.054	0.128
60	19946	0.1322		0.006561	0.112	0.264
70	31201	0.2167	0.00721	0.007135	0.228	0.531
80	47414	0.3535		0.007628	0.490	1.130
87	62556	0.5008		0.007939	0.943	2.160
87.5	63776	0.4532		0.007960	0.996	2.279
88	65017	0.5268		0.007982	1.053	2.409
89	67558	0.5543		0.008024	1.184	2.706
90	70182	0.5835		0.008065	1.342	3.063
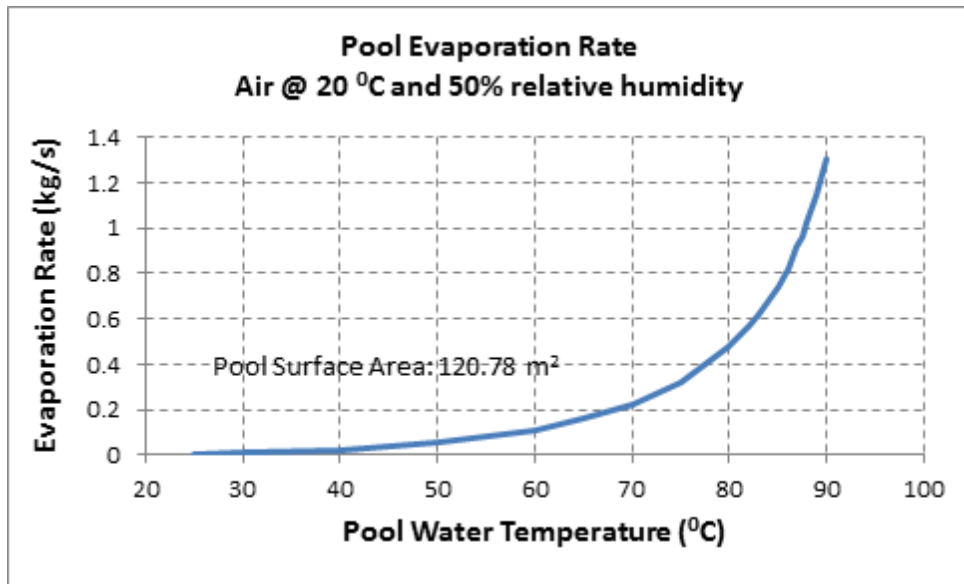
Figure 99. Evaporation Rate in SFP4.

7.4   TRACE Model

The TRACE SFP4 model consists of seven hydraulic components, four heat structures, a power component, and control systems. A SNAP nodalization diagram of the TRACE model is shown in Figure 100. The spent fuel pool is modeled with a TRACE 2-D VESSEL component (VESSEL1). The fuel assemblies are modeled with the four CHAN components (CHANs 101 through 104). A POWER component (POWER 11) is used to model the decay heat of the fuel assemblies. The storage racks are modeled with four HTSTR components (HTSTRs 41 through 44). A BREAK component (BREAK 21) is used to model the pressure boundary condition of the atmosphere. Each component will be discussed in detail in the following subsections.
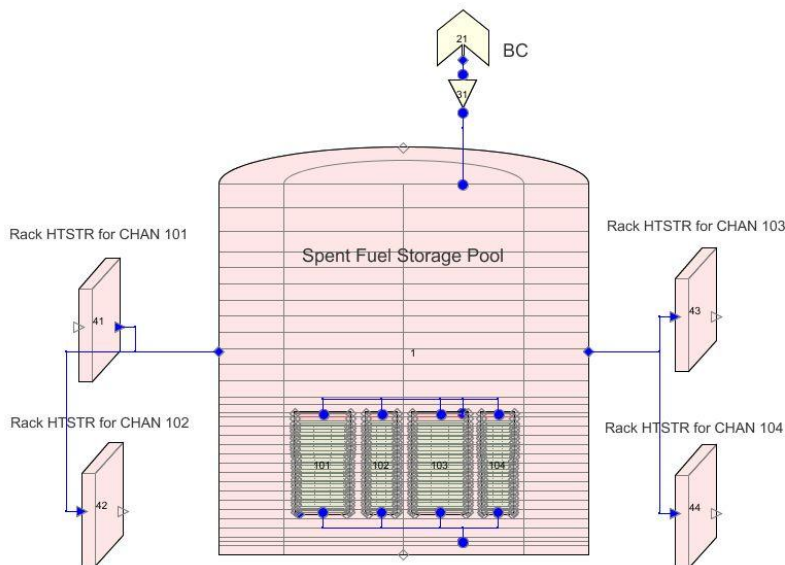
Figure 100.   TRACE Nodding Diagram.

7.4.1   Spent Fuel Pool – VESSEL 1

A schematic of pool natural convection flow during a loss of pool cooling event is shown in Figure 101. The water inside the fuel channels is heated up by the decay heat and flows upwards, and the water descends in the gaps between the racks as well as in the gaps between the racks and pool side walls. Eventually, a natural flow circulation is established. It is also possible that a flow circulation occurs between the fuel assemblies with high decay power and with low decay power. This kind of density-driven natural flow circulation is very efficient to take the decay heat away from the fuel assemblies. When the water level drops below the top of the fuel storage racks, such a flow circulation pattern will be broken. Heat-up may occur when the natural circulation flow stops.

In the TRACE model, the SFP is modeled with a 2D VESSEL component. It has 31 axial levels, two radial rings. The fuel storage racks are located in the radial ring 1, and from axial levels 3 through 17. The outer ring is the for the pool downcomer region (gaps between the fuel storage racks and gaps between the fuel racks and pool walls). All the fuel assemblies are vertically stored in the fuel storage racks. The bottom two levels are the region for the rack bottom pad, which is assumed to be about 0.433 m in height. Heat transfer through the wall and the floor is not considered in this model because the effect on the overall heat transfer is negligible.
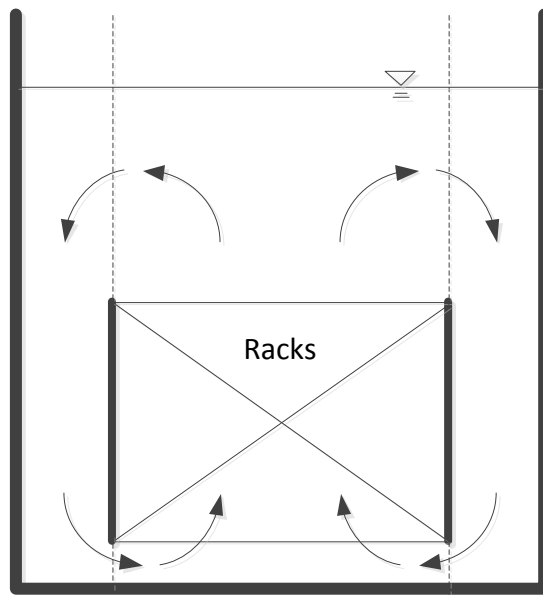
Figure 101. Schematic of Pool Flow.

7.4.2 Fuel Assemblies – CHANs 101 through 104

There are 1,535 fuel assemblies in the pool, which are modeled with four CHAN components as shown in Figure 100. Among of them, 548 STEP3-B fuel assemblies, recently discharged from the core after the shutdown of November 29, 2010, are modeled with CHAN 101. CHAN 102 represents another 188 STEP3-B fuel assemblies, which were discharged from previous refueling cycles. All other 595 older fuel assemblies in the 8×8 array are modeled with CHAN 103, including one 7×7, four 8×8, 30 8×8BJ, and 560 STEP2 fuel assemblies. There are also 204 fresh assemblies in the pool, and they are modeled with CHAN 104. The fresh assemblies provide a heat sink, although they do not have any decay heat.

Because of a lack of information about the design specifications for the fuel assemblies in SFP4, typical GE design parameters for the 8×8 and 9×9 lattice arrays are used for our analysis. The uncertainties in the fuel design would have very minimal effect on the boil-off simulation.

7.4.3 Fuel Storage Racks – HTSTRs 41 through 44

The fuel storage racks of the Fukushima SPF4 are a high-density design. In TRACE, all the rack side walls are lumped into four separate slab heat structures (each is coupled with a CHAN

component), as shown in Figure 100. The rack separation wall is made of stainless steel with a thickness of 0.018 m.

7.4.4 Decay Heat

The decay heat of the fuel assemblies in the pool was calculated using ORIGEN. A TRACE POWER component with a time-dependent table for the decay heat load is employed to model the decay heat. The POWER component is coupled with the four CHAN components. The power level for each CHAN component is defined based on their relative decay heat ratios. The power ratio for CHAN 104 (fresh fuel) is zero.

A typical BWR axial power shape is used for all the powered fuel assemblies in this study. The axial power shape may affect the heat-up when the fuel in the pool is uncovered.
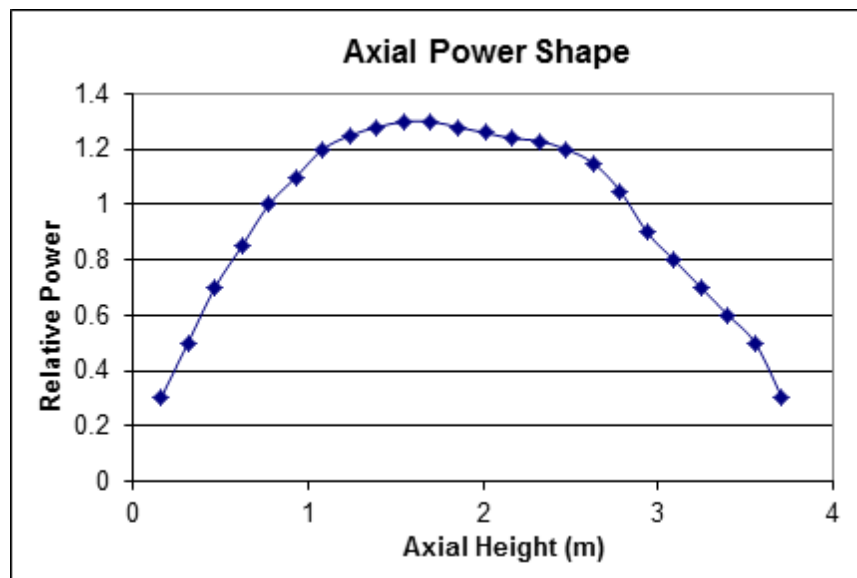
Figure 102. Axial Power Shape.

7.4.5 Signal Variables and Controls

Five signal variables (SVs 2, 3, 61, 62, and 64) are included in the TRACE model to calculate the collapsed water level in the pool and four CHANs, respectively. In addition, two controls (CBs 1 and 2) are used to calculate the average void fraction in CHAN 101 and CHAN 102. Pool temperatures at different locations are also available.

7.4.6 Limitations of TRACE

In terms of SFP modeling, limitations of TRACE are summarized as follows.
  - Surface evaporation model. TRACE does not have an open pool model to calculate surface evaporation, which means that TRACE does not predict water loss by evaporation during the early pool temperature rise. It has shown that evaporation

168

becomes significant only when the pool temperature reaches above 70°C. The code deficiency has no significant impact on our analysis of SFP4 since the pool boil-off process is dominated by the time period in which the pool is saturated.

- Pool temperature. It has been discussed previously that at the pool temperature 87.15°C, evaporation would reach an energy balance with the decay heat load of SFP4. So the pool temperature should be around 90°C. However, TRACE-predicted pool temperature will be around 100°C.

- Surface convection heat transfer. TRACE cannot model heat loss through air convection flow on the pool surface. However, this heat loss is only less than 3% of the total heat load of SFP4. So it is negligible.

- TRACE cannot model radiation heat transfer between the fuel channel walls and the storage racks. TRACE can model radiation between fuel rods, and between the fuel channel wall and fuel rods. TRACE may predict an earlier fuel heat-up with this deficiency.

- TRACE cannot model air inflow from the top of fuel assemblies when fuel exposure occurs during the boil-off. It should be anticipated that some air circulation flow may form in the upper section of the fuel bundles when the pool level is low and steam generation from the bottom covered section of the fuel bundles become insignificant. The air circulation flow may delay fuel heat-up. This effect needs to be investigated further (CFD or experiment).

7.5 TRACE Simulations of SFP4

The main objective of the SFP4 analyses was to determine whether the pool boil-off could have resulted in the Unit 4 building explosion. Due to a lack of accurate information about initial conditions, assumptions have to be made for the TRACE simulations. They are:

1) Initial pool water level. It was indicated in the Japanese report (June 2011) that "the fuel pool was fully filled with water as the cutting work of the shroud had been carried out at the reactor side." However, it is not clear whether the earthquake sloshed out some water. In our analysis, TRACE simulations were performed assuming two initial pool water levels. The first one was to assume that the initial pool level was at 11.2 m, and the second was that the initial pool level was at 4.73 m (right above the top of racks). However, in the second report of the government of Japan to IAEA, TEPCO presented an evaluation analysis for SFP4 assuming that a significant amount of water had been sloshed out by the earthquake and rubble dropping [21].

2) Inflow from the reactor well side. We did not consider any inflow to the pool from the reactor well in our analysis. In the second report of the government of Japan to IAEA [21], TEPCO assumed that there was water inflow from the reactor well through the pool gate.

3) Pool leakage. No pool leakage was considered in our TRACE analysis. It was confirmed by TEPCO that there should be no significant leakage in the pool.

TRACE results for the two cases are shown in Figure 103 through Figure 105.

Figure 103 shows the predicted collapsed water level and the peak cladding temperature (PCT) for the first case with the initial pool level 11.22 m. Figure 104 shows the integrated water boil-off mass. The TRACE simulation shows that the pool level increased in the first two days as the water temperature was rising. When the pool water temperature reached to the saturation point, the pool started to boil off water at a rate of about 0.99 kg/s and consequently the pool level started to decrease. It would take about 11 days for the water level to drop down to the top of fuel racks (7.43 m) from the initial level. Therefore, if the pool was at this initial level at the time of the accident, the fuel would not have been uncovered by the time of the explosion in the Unit 4 building. If the pool level had fallen below the top of fuel racks, natural circulation flow would have stopped. Shortly after the fuel became uncovered the fuel cladding temperature would have started to increase as shown in Figure 103. If the cladding temperature had reached above 1000 °C, the chemical reaction between the zircaloy clad and vapor would have taken place, resulting in hydrogen generation. The reaction would have generated significant heat and therefore accelerated fuel heat-up. Eventually the cladding temperature would have reached its melting point. However, fuel heat-up would have been a slow process and would have taken about two and a half days.

Figure 105 shows TRACE results for the second case with the initial water level 4.73 m. Fuel heat-up took place sooner than the first case because it started at a very low pool level. However, even if the water level somehow dropped to right above the racks, the time for the fuel to heat up to above 1000°C so that hydrogen generation could begin still does not align with an explosion on the morning of March 15.
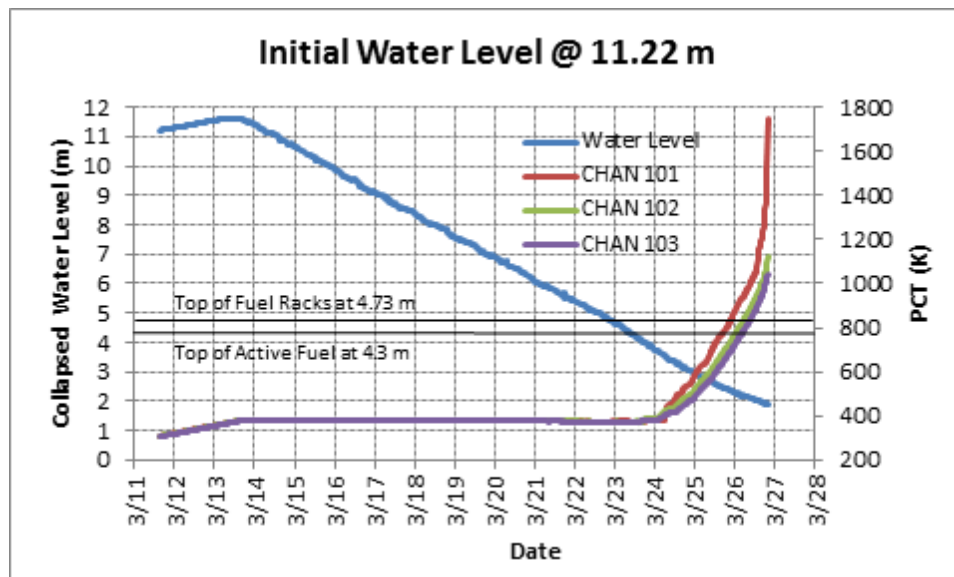
Figure 103. Calculated Pool Level and PCT for Initial Pool Level 11.22 m.
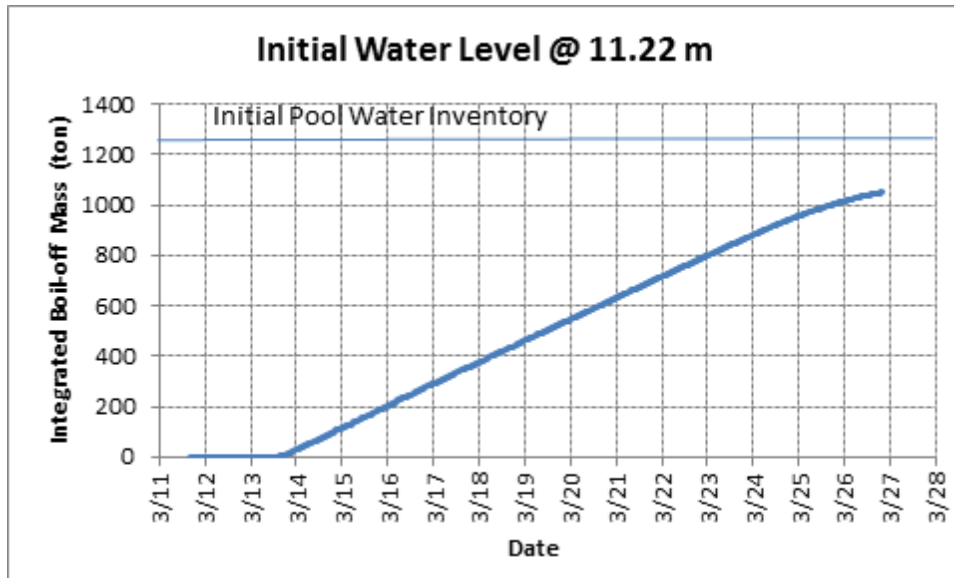
Figure 104. Integrated Boil-off Mass.
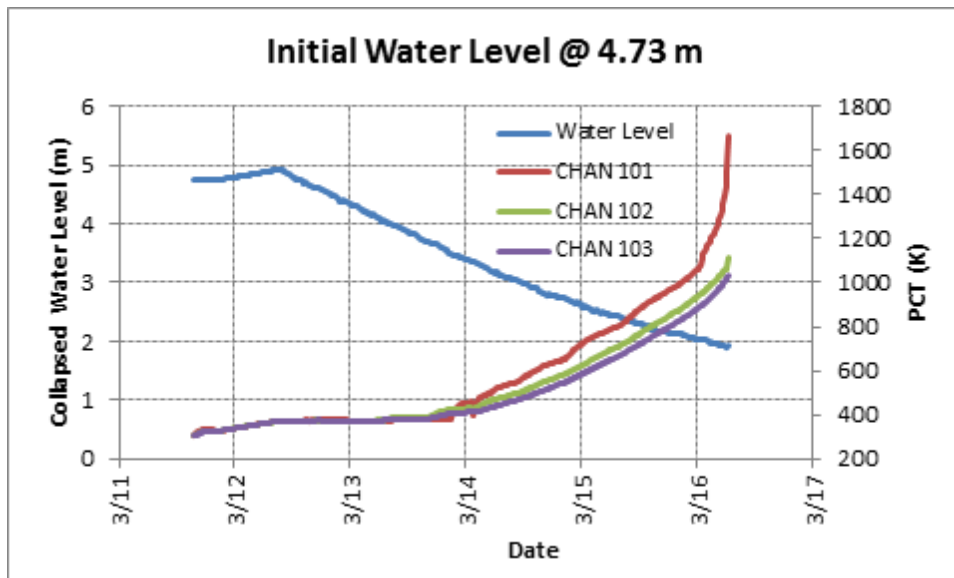
Figure 105. Calculated Pool Level and PCT for Initial Pool Level 4.73 m.

7.6 Study on Fukushima SFP4 beyond March 22

As discussed previously, there are many unknowns about the conditions of SFP4 and what actually happened in the pool due to the lack of measurements and observations in the first few days of the accident. Therefore, it is worthwhile to extend our analysis beyond March 22 since there is more information regarding the pool situations, in particular, pool level and temperature measurements since April 22. We hope that the analysis can shed some light on the early situation of the pool by comparing the analysis with the measurements conducted since April 22.

Recently, the government of Japan released the second IAEA report on the Fukushima accident [21]. The report presents results of evaluation of Fukushima NPS pools conducted by TEPCO. The results of SFP4 are shown in Figure 106. The major assumptions in TEPCO analysis are as follows:

- The water level is presumed to have been reduced by 1.5 m (~181 tons of water) as a result of sloshing by the earthquake and the explosion.
- Inflow from the reactor well occurred before April 22 (see discussions that follows). The water level was calculated by considering the water in the pool and the water in the reactor well and DS pit collectively. After April 22, the pool gate gap was closed, and no inflow from the reactor well was considered.
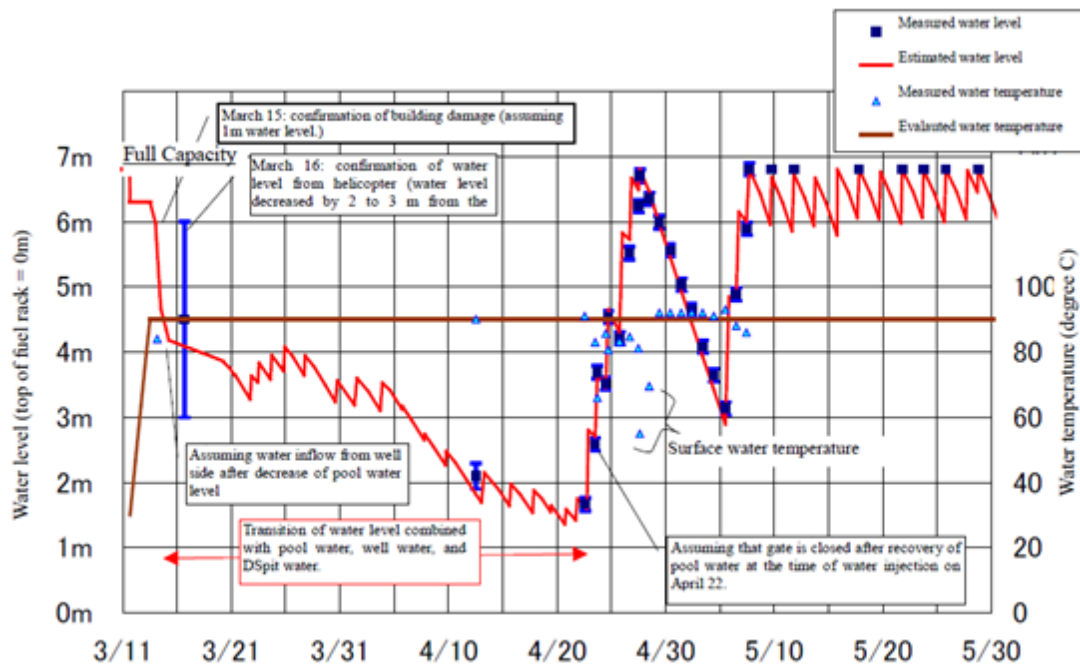
Figure 106. TEPCO Evaluation Results of SFP4.

172

We did a similar calculation of SFP4 based on the fundamental conservation laws of energy and mass. Assumptions used in our analysis are

- The pool initial water level was at 11.58 m. It is indicated in the report of Japanese Government (June 2011) that "the fuel pool was fully filled with water at the cutting work of the shroud had been carried out at the reactor side."
- The pool initial water temperature was at 27°C.
- There was no pool leakage.
- Only 50% of SDF spray in the first 2 days went into the pool. Thereafter all concrete pump spray went into the pool.
- The sprayed water temperature was at 25°C.
- Heat conduction loss through the pool walls and floor, and radiation through the pool surface, and heat convection loss through the pool surface, were not considered. The effect is actually negligible compared to the total decay heat load in the pool.

The results of our analysis are presented in Figure 107. For comparison TEPCO results are included. Our analysis matches the measured data very well (except for April 12). The key differences between the TEPCO assumptions and ours are the initial water level and the inflow from the reactor well.

As discussed in the Japan September report, the reactor well and dryer and separator pit (DS pit) were full of water before the earthquake since the reactor was under regular maintenance. The water-tightness of the pool gate was lost because the gate received water pressure from the reactor well side when the pool level became low. Then the water flowed into the pool through a small pool-gate gap.

Figure 108 shows accumulated water amounts of spray and evaporation since March 11, respectively. This figure plays a key role in understanding the pool level change. It is interesting to see that the total amount of evaporated water and the total amount of sprayed water approached a balance on April 27. It implies that the total inflow from the reactor well side should be about the same as the total sloshed water caused by the earthquake and explosion. So we can estimate the diminished water level at the beginning of the accident based on the total amount of inflow. On April 27, the measurement of water level on the reactor well side was conducted and the level was TAF + 1.8 m. If we assume the initial water level in the reactor well and DS pit is TAF + 7.2 m, there would be 150 - 300 ton of water which had entered the pool from the reactor well side. In other words, the diminished water level by the earthquake and explosion would be 1.2 – 2.4 m.
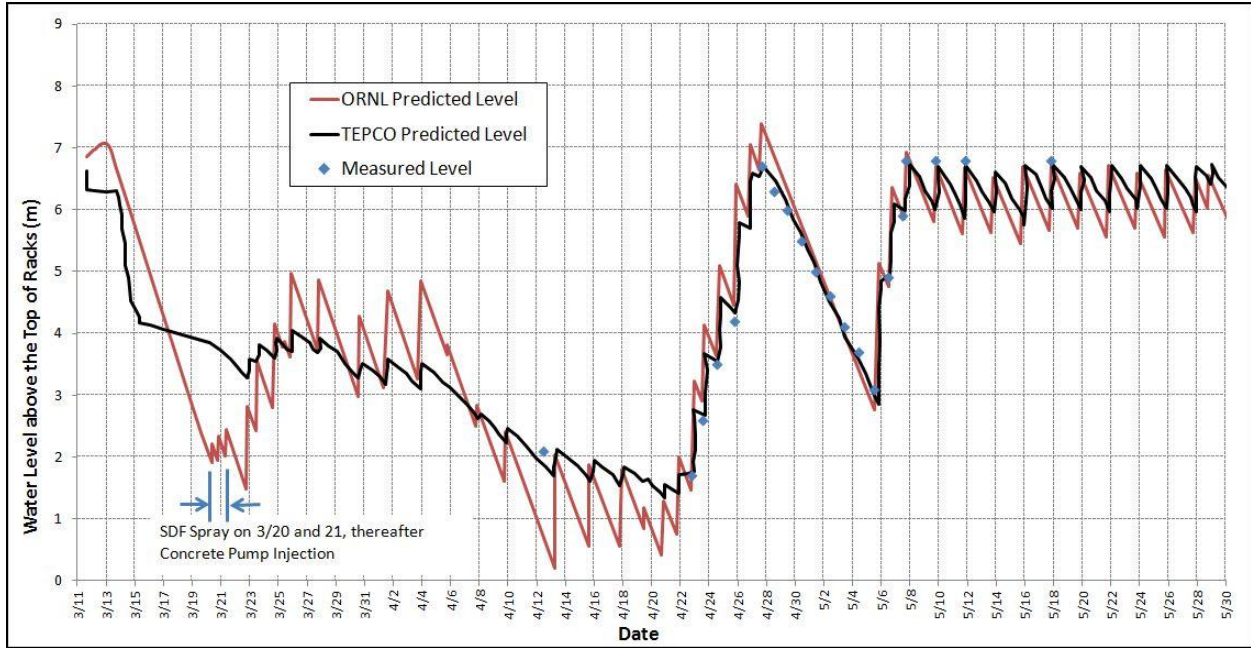
Figure 107. ORNL Level Results for SFP4.
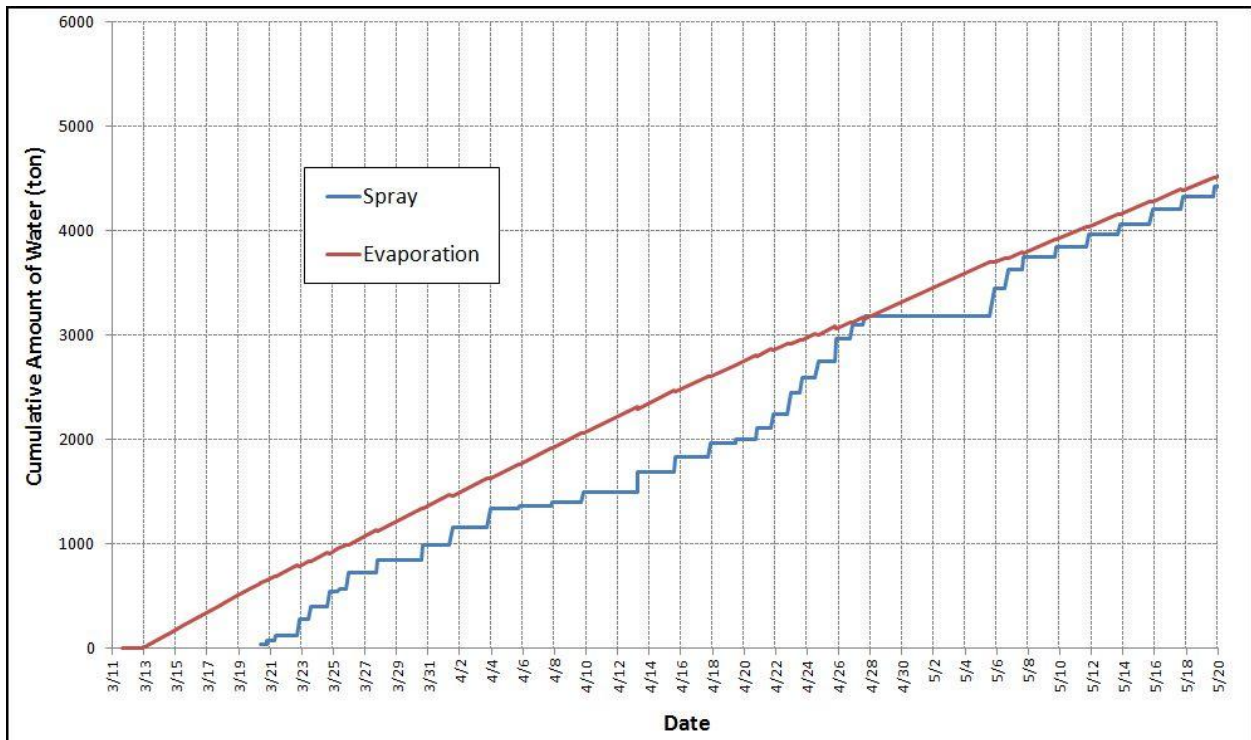
Figure 108. ORNL Spray and Evaporation Results for SFP4.

174

It can be concluded from the analysis and measurements that there should be no big leakage in the pool. The predicted pool level has a good agreement with the measurements since April 22. It means that the pool level change was solely determined by the mass balance between the spray and evaporation and no leakage should be involved. In addition, the diminished water by the earthquake and explosion can be estimated based on the inflow from the reactor well side.

8   SNL MODEL OF THE UNIT 4 SPENT FUEL POOL

The Fukushima plant is typical of many boiling water reactors (BWR) with fuel in the spent fuel pool (SFP) from several older cycles to the most recent offload. The plant removes an equivalent amount of various aged fuel between outages for storage in a common pool and reprocessing, thereby maintaining a relatively constant number of assemblies in the SFP. Hence, the SFP is maintained with generally recently offloaded fuel. In addition, the SFP racks have enough empty cell locations to permit a complete emergency reactor offload.

The MELCOR 2.1 severe accident computer code [29] Version RL_NL, Revision 3843, was used to simulate the SFP accident response. MELCOR includes radiation, convection, and conduction heat transfer models, fuel degradation models for pressurized water reactor (PWR) and BWR fuel, air and steam oxidation models, hydrogen burn models, two-phase thermal-hydraulic models, and fission product release and transport models. Therefore, it contains the basic models to address questions and phenomena expected during a SFP accident.

MELCOR 2.1 contains models applicable to BWR SFP models including: (1) a rack component, which permits modeling of the SFP racks, and (2) an oxidation kinetics model. The BWR SFP rack component permits proper radiative modeling of the SFP rack between groups of different assemblies. The oxidation kinetics model predicts the transition to breakaway oxidation in air environments on a node-by-node basis.

8.1   Model Description and Inputs

A description of the MELCOR SFP model is provided below. Details of the Fukushima SFP that were not available during the creation of the MELCOR model were completed using information from a reference BWR. The reference plant for the Fukushima SFP analysis is a large BWR. Like most other nuclear plants, the reference plant has installed high-density racks to maximize the storage of fuel in the SFP.

The spent fuel pool, 9.9 m wide by 12.2 m long by 11.8 m deep, is located on the refueling floor of the reactor building. The pool is constructed of reinforced concrete with a wall and floor lining of 0.635 cm thick stainless steel. The walls and the floor of the spent fuel pool are approximately 2 m thick. One corner of the SFP is devoted to a cask loading area. The general attributes of the spent fuel pool, the fuel assemblies, the spent fuel pool racks, and the assembly and rack flow areas are described in Table 20, Table 21, Table 22, and Table 23, respectively. Although there are multiple assembly types in the SFP, the most common type was chosen to model the whole pool.

Table 20. Spent Fuel Pool Data

SFP Characteristics	Description or Dimensions
Dimensions	9.9 m x 12.2 m, 11.8 m high walls (water filled to 11.5 m)
Concrete Thickness	~2 m
SFP Volume	1389 m^3 (367,000 gal)
Number of Storage Locations	1590

Table 21. Fuel Assembly Data

Assembly Characteristics	Description or Dimensions
Fuel Type	GE 9x9
Number of Fuel Rods	74
Fuel Pitch	1.438 cm
Fuel Rod Dimensions	1.118 cm OD 7.112 mm Clad thickness 3.7084 m Active Length
Maximum Initial Enrichment	4% U-235 by weight
Number of Water Rods	2
Water Rod Dimensions	2.489 cm OD Zircaloy

Table 22. Spent Fuel Pool Rack Data

SFP Rack Characteristic	Description or Dimensions
Rack Height above the Base Plate	4.293 m
Baseplate Thickness	1.27 cm
Support Leg Height	0.1842 m
Poison Material	Boraflex
Cell Pitch	0.1595 m
Cell Construction	1.905 cm (Gage 14) 304 stainless steel walls with Bisco Boraflex B$_4$C particles clad in a non-metallic binder (2.057 cm) with 5.08 mm stainless wrapper[22]

---

[22] The construction of the racks was not known at the time the MELCOR model was developed. It was later discovered that the racks are made completely of stainless steel; however, it is anticipated that this change in the MELCOR model would not significantly affect the results.

Table 23. Fuel Assembly and Rack Flow Area Data

Region	Area [m^2]
Upper bundle above partial rods	1.06×10^{-2}
Lower bundle	9.79×10^{-3}
Interstitial space between the rack and the bundle	5.11×10^{-3}
Rack cell (empty)	2.40×10^{-2}

The high density SFP racks provide spent fuel storage at the bottom of the SFP. The pool is normally filled with about 11.5 m of water, providing about 7 m of water for radiation shielding. The SFP racks are freestanding, full length, top entry and are designed to maintain the spent fuel in a spaced geometry, which precludes the possibility of criticality conditions.

The high-density SFP racks are of the "poison" type, utilizing a neutron absorbing material to maintain a subcritical fuel array. The racks are rectilinear in shape and are of nine different sizes. The racks are constructed of stainless steel materials and each rack module is composed of cell assemblies, a base plate, and base support assemblies. Each cell is composed of (1) a full-length enclosure constructed of 0.2 cm thick stainless steel, (2) sections of Bisco Boraflex,[23] which is a neutron absorbing material, and (3) wrapper plates constructed of 0.051 cm thick stainless steel. The inside square dimension of a cell enclosure is 0.1542 m. The cell pitch is 0.1595 m.

The base plate is 1.27 cm thick stainless steel with 9.652 cm chamfered through holes centered at each storage location, which provides a seating surface for the fuel assemblies. These holes also provide passage for coolant flow.

Each rack module has base support assemblies located at the center of the corner cells within the module and at interior locations to distribute the pool floor loading, as seen in Figure 109. Each base assembly is composed of a level block assembly, a leveling screw, and a support pad. The top of the leveling block assembly is welded to the bottom of the base plate. SFP fuel cells are located above each rack foot. Four 2.54 cm holes are drilled into the side of the support pad. The interior of the support pad is hollow and permits flow to the opening in the base plate.

---

[23] The construction of the racks was not known at the time the MELCOR model was developed. It was later discovered that the racks are made completely of stainless steel, however, it is anticipated that this change in the MELCOR model would not significantly affect the results.
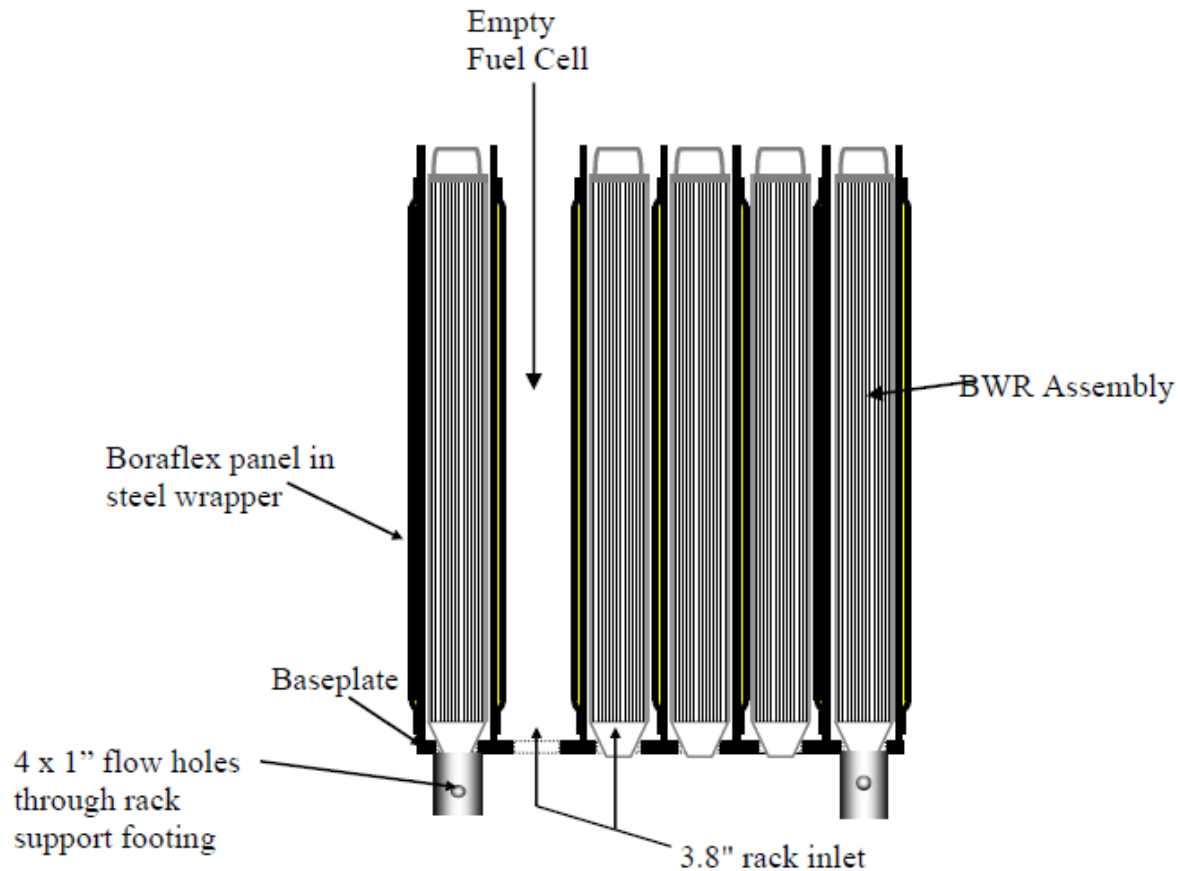
Figure 109. Typical Spent Fuel Pool Rack Cut-Away Cross-Section Showing the Fuel Assembly.

The SFP assemblies are divided into three radial rings and are modeled using the MELCOR "SFP-BWR" designation. Ring 1 contains the most recently offloaded assemblies, Ring 2 contains the previous offloads, and Ring 3 contains the empty rack cells. Each ring has 1 axial control volume, which represent the fluid volume within the fuel assembly.

The interstitial area between the canister wall and the rack wall is modeled as the BWR bypass region. The bypass uses the same control volume axial nodalization as the channel region. A radial cross-flow path is located between the bypass and channel region. The cross-flow paths are controlled by the COR package and open if the canister wall should fail. A single control volume represents the region below the assemblies.

The hydraulic resistance was specified using the results from the SNL experimental test program [9]. The flow resistance under the racks was represented using typical contraction inertial loss coefficients and viscous losses consistent with a flow length to the center of the SFP.

The BWR assembly canister is modeled with the MELCOR canister component. The rack walls are modeled with the rack component and are made of stainless steel and Boraflex.[24] MELCOR does not include an option to model the two large water rods in the assembly. Consequently, the water rod mass and surface area was included in the canister wall.

The axial and canister wall blockage models were active and controlled the resistance in the respective flow paths. The blockage model monitors the porosity of the materials in the various core regions. If a debris bed forms, the flow resistance is adjusted via an Ergun flow resistance model [29]. The canister wall radial blockage model controls flow paths between the bypass region and the assembly. Initially, the canister wall precludes flow. However, if the canister fails, a radial flow path is activated that permits flow between the two regions. Similar to the axial blockage model, the flow resistance is adjusted based on the local debris porosity.

The BWR fuel assembly is represented by 14 axial levels in the COR Package:

> Level 1 is the region below the core,
> Level 2 is the base plate
> Level 3 is the inlet region between the inlet nozzle and the lower tieplate
> Level 4 is the start of the active fuel region
> Level 8 is the top of the partial rod active fuel region
> Level 9 represents the region of the plenum of partial rods
> Level 12 is the top of the full length rod active fuel region
> Level 13 represents the plenum region of the full-length rods
> Level 14 represents the region between the upper tieplate and the top of the racks

The upper and lower tieplates are modeled as supporting plate structures, made of stainless steel. The 1.27 cm rack support plate in Level 2 is also modeled as a stainless-steel supporting structure. The assembly ring-to-ring radiation is modeled between the outer surfaces of the Ring 1 rack wall to the outer surface of the canister in the adjacent ring. Radiative coupling was enabled for all calculations.

If the fuel rods heat up to the point of degradation, the debris is expected to relocate to the bottom of the SFP cell. The thermal load on the rack base plate will eventually fail the rack and allow debris to relocate onto the steel liner of the SFP. The steel liner is modeled in the COR package as the lower head. The lower head is represented with a 0.635 cm steel liner and a 1.83 m thick concrete slab. If the steel liner should fail, the debris is "transferred" to a special model for core concrete interaction, which models the ablation of the concrete.

The assembly decay heat is specified separately for each core ring. The decay heat load is primarily deposited in the fuel. However, as calculated by the gamma heating model, a small fraction of the decay heat is deposited directly in the cladding, canister, and surrounding structures (i.e., the rack wall). The outer boundary heat structures (i.e., ordinarily modeling the core barrel) outside Ring 3 simulate the SFP concrete walls.

---

[24] The construction of the racks was not known at the time the MELCOR model was developed. It was later discovered that the racks are made completely of stainless steel, however, it is anticipated that this change in the MELCOR model would not significantly affect the results.

The whole pool model includes the entire spent fuel pool including all the assemblies and the reactor building refueling bay. The fuel assemblies and empty rack cells are represented by 3 three rings in the MELCOR model. Figure 110 shows the CVH nodalization of the SFP region of the whole pool model. The lower SFP was divided into four regions. CV-299 represents all the open regions in the SFP around the racks, including the cask loading area. The racks are divided into three regions. Due to the random nature in which assemblies were offloaded and shuffled (see Figure 111), the first ring of the model contains all the recently offloaded fuel. Results for this model are therefore going to be somewhat conservative since it assumes the highest heat load is located in the central ring, accounting for 79% of the total power. Ring 2 contains all remaining assemblies in the SFP. Ring 3 of the model represents empty rack cells. The region above the racks is divided into two control volumes.
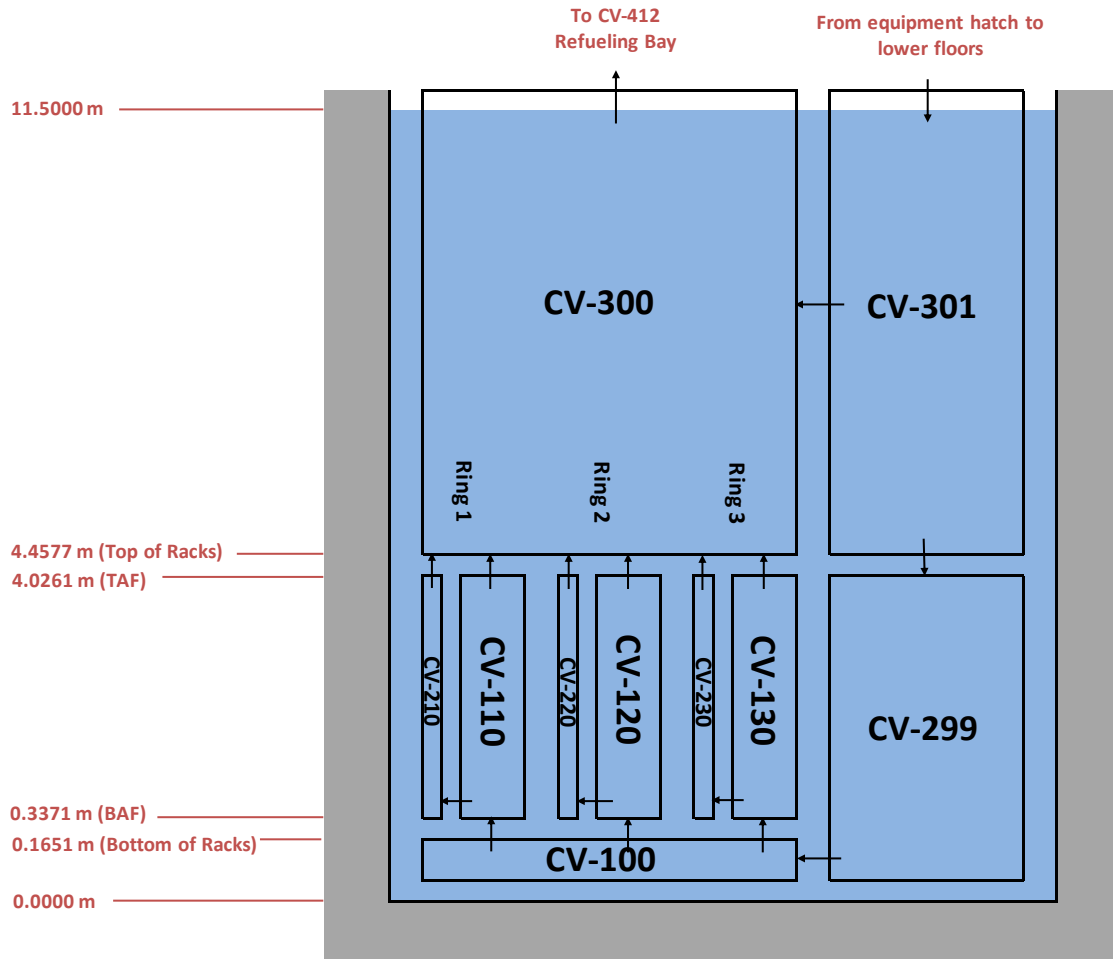
Figure 110. Schematic of the Whole Pool Model Configuration.
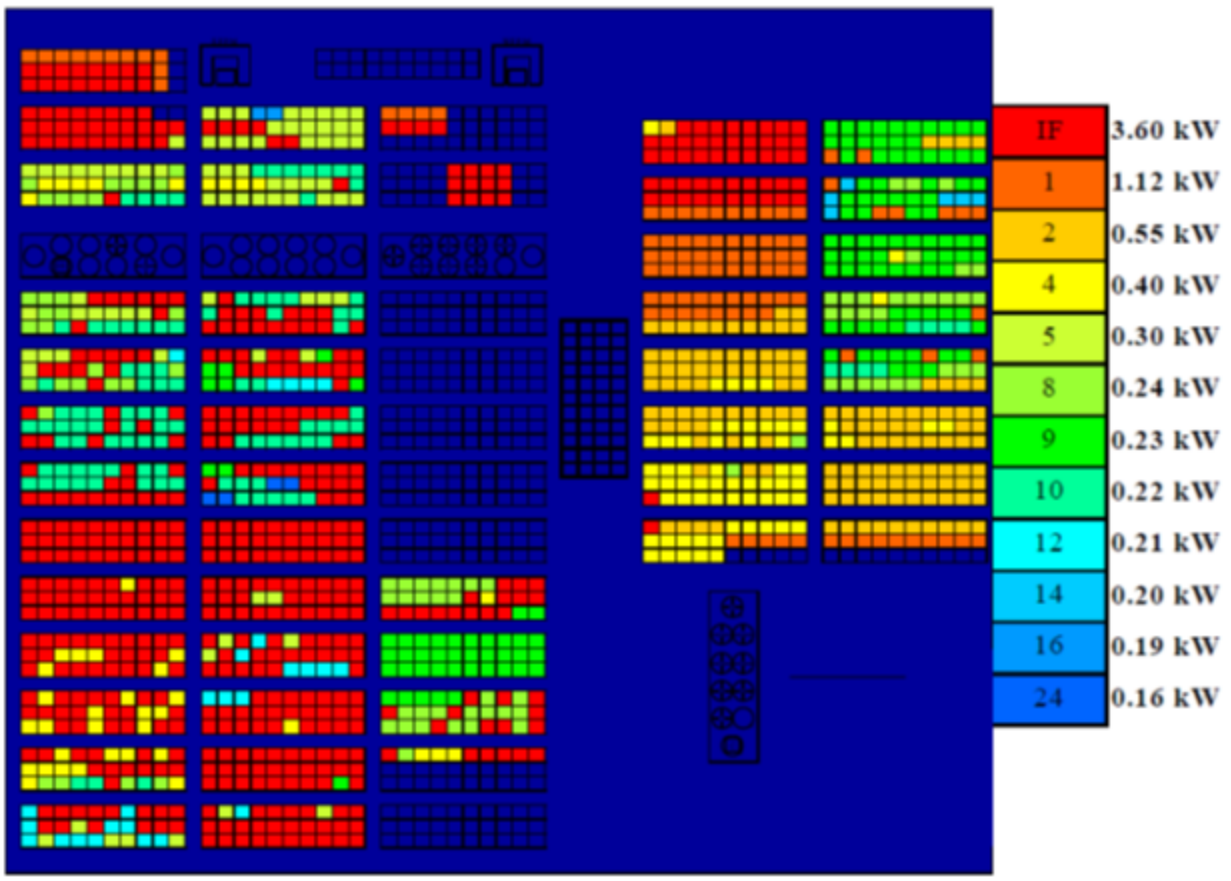
Figure 111. Fukushima Unit 4 Spent Fuel Pool Offload Configuration.

8.2   Spent Fuel Pool Accident Scenarios

Three accident scenarios were analyzed for this work. The models assumed there was no spray or refill capability available during the course of the accident. The first scenario assumed that there was no loss of water due to sloshing caused by the earthquake and therefore had a pool water level of 11.5 m. The second scenario was similar to the first, with the exception that the reactor building and its corresponding heat structures were removed from the model. The third scenario assumed there was a major loss of water by sloshing, a leak in the pool, or both. This scenario assumed a standing water level of 4.96 m, or 0.5 m above the racks, as the initial condition. All scenarios assumed an initial water temperature of 301 Kelvin (82 °F).

The different water levels were chosen to explore the conditions required to reach the events that happened at the Unit 4 reactor building. The scenario with the full pool was chosen as a baseline condition to determine the length of time required to uncover and dry-out the pool had no water been lost during the earthquake or due to a liner tear. The scenario with the initial water level starting 0.5 m above the racks was chosen as an extreme case. The water level was arbitrarily chosen, however, the results give the reader an idea of how severe the damage would have had to

be if the explosion in the Unit 4 reactor building was caused by hydrogen produced from oxidation reactions of the zircaloy cladding.

From a natural circulation flow perspective, the SFP accidents can be described in two stages. The first stage has water above the base plate of the racks. In this stage, the water at the bottom of the pool acts as a "plug," which prevents cooling of the assemblies by natural air circulation. The second stage occurs when the water boils down far enough (below the base plate of the racks) to allow cooling of assemblies by natural circulation.

In the first stage, where water is above the base plate of the racks, the gases above the top of the pool level are relatively stagnant, with the exception of steam flow from boiling. In this condition, steam cooling and/or a level swell from boiling will keep the fuel rods cool unless the pool level drops too far. However, once the level drops below roughly one-half of the fuel height, the top of the fuel rods will heat-up and degrade.

Oxidation rate of Zircaloy during this stage will be different than if the assemblies were being cooled by the natural circulation stage. The fluid next to the assemblies in this stage is steam rather than air. Steam also reacts exothermically with Zircaloy but at a slower rate than with air. In addition, hydrogen is a byproduct when oxidation occurs by steam. Eventually the hydrogen produced will replace the steam and retard or stop the Zircaloy/steam reaction. Consequently, the reaction could become "steam starved" and controlled by the rate of steam production by boiling below the pool level. If there is adequate steam when the Zircaloy reaches high temperatures (i.e., greater than 1500 K), the power from metal water reactions can be much larger than decay heat.

As hydrogen is produced during cladding oxidation, the hydrogen may collect and mix with oxygen in the air above the pool. Given the appropriate conditions, the hydrogen could ignite and possibly cause structural damage to the reactor building. Any damage or enhanced leakage caused by the pressure wave caused by the hydrogen burn could increase the release of fission products.

When the water level falls below the rack base plates, complex flow patterns develop around the SFP racks. Heat up of the assemblies causes the surrounding air to heat up and create a natural circulation pattern. Assemblies are air cooled in this case. If inadequate cooling is provided, then the cladding will heat up and will rapidly oxidize (i.e., burn) and to a lesser extent, nitride (i.e., combine with nitrogen if no oxygen or steam are available). Since the oxidation and nitride processes are exothermic, the fuel rods could heat to melting conditions and structurally degrade. The steel racks supporting the fuel assemblies will also heat due to the convection and radiation from the assemblies. Timing of the degradation of the specific fuel assemblies and racks are affected by the decay heat power, assembly inlet temperature, convective and conductive heat removal rates, and the heat transfer rate from/to adjacent assemblies.

An accurate analysis of the SFP response requires consideration of the aforementioned phenomena. As evidenced by the accident description, there is a large range of geometric length scales and modeling requirements. The length scales depend on details of the individual assembly heat generation and flow patterns, intra-assembly heat transfer, large-scale flow

patterns above, below, and through the racks, and the building response (e.g., ventilation, heat loss, structural integrity, etc.). The relevant physics and phenomena include heat transfer, fluid flow (small scale to large scale), chemical reactions (oxidation), severe accident fuel degradation behavior, and fission product release and transport.

8.3 Analysis Methodology

8.3.1 MELCOR Breakaway Oxidation Model

Argonne National Laboratory (ANL) has performed oxidation kinetics testing on Zr-based alloys including Zircaloy-4, which is similar to the Zircaloy-2 alloy used in the reference BWR plant assemblies. The testing showed that air oxidation can be observed at temperatures as low as 600 Kelvin. In the tests, a specimen was held at constant temperature and the weight gain due to oxidation as a function of time was measured. The reaction rates for air oxidation are described by parabolic kinetics similar to the ones used to describe steam oxidation. The general form of the equation is,

$$\frac{dw^2}{dt} = K(T) \tag{8.1}$$

where w is oxide scale thickness, or in the MELCOR convention, reacted metal mass.

The rate of oxidation was initially steady versus the square root of time at a particular temperature. However, the rate of oxidation increased after some time and persisted for the remainder of the test.

A new oxidation model was implemented in MELCOR by adding a breakaway lifetime calculation. The model calculates an oxidation "lifetime" value for Zircaloy components in each cell using the local Zircaloy cladding temperature for both air and steam oxidation conditions. Figure 112 presents the breakaway timing data from the ANL tests and shows the 95% confidence interval for seven degrees of freedom. The uncertainty in Figure 112 for breakaway timing is insignificant on the scale of the accident timeline. The uncertainty represents about a 2.5 hour window in which breakaway could occur. As the specimen temperature increased, the amount of time until breakaway became shorter.

For implementation into MELCOR, the ANL data was curve fit as follows,

$$LF = \int_0^t dt' \frac{t'}{\tau(T)} \tag{8.2}$$

where

$$\tau(T) = 10^{P_{LOX}} \tag{8.3}$$

and

$$P_{LOX} = -12.528 \cdot \log_{10} T + 42.038 \qquad\qquad \textbf{(8.4)}$$

A comparison of the data with Equation 8.4 is shown in Figure 112 Specific values of the breakaway timing are provided in Table 24.

The new MELCOR breakaway oxidation model calculates the lifetime function at every node in the MELCOR model with Zircaloy cladding. The oxidation kinetics linearly transitions from the pre-breakaway correlation at *LF = 1* to post-breakaway kinetics at *LF = 1.25*. Hence, only nodes that have exceeded the lifetime function will have the higher post-breakaway oxidation kinetics.
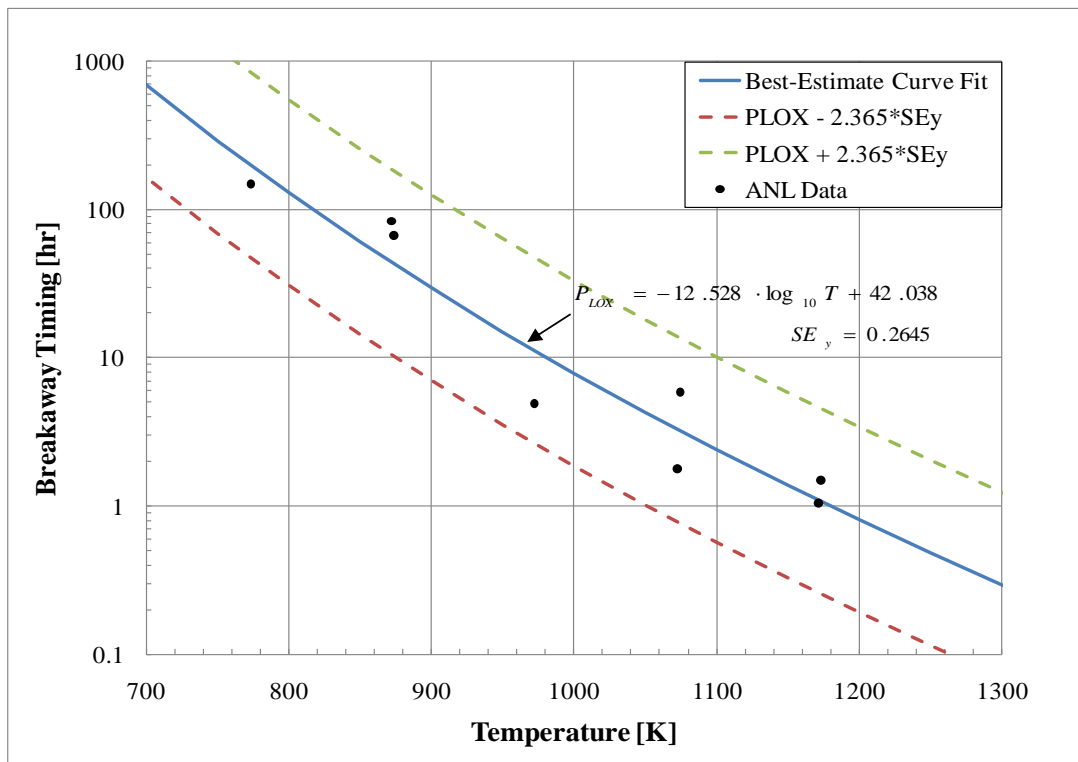

Figure 112. Comparison of the MELCOR Breakaway Timing Fit to the Zirlo and Zr-4 Data from ANL Air Oxidation Tests.

Table 24. MELCOR Fit of the Timing for Transition from Pre-Breakaway to Post-Breakaway Oxidation Reaction Kinetics for Zirlo and Zircaloy-4 in the ANL Experiments [18]

Specimen Temperature	Breakaway Timing [hr] (Eqn 4)	ANL Data Used in Curve Fit [hr]
400°C (673 K)	1125 (Extrapolated)	-
450°C (723 K)	458 (Extrapolated)	-
500°C (773 K)	198	144
550°C (823 K)	90	-
600°C (873 K)	43	64 and 81
650°C (923 K)	22	-
700°C (973 K)	11	4.8
750°C (1023 K)	5.9	-
800°C (1073 K)	3.3	1.7 and 5.8
850°C (1123 K)	1.8	-
900°C (1173 K)	1.1	1 and 1.4

8.3.2 Hydraulic Resistance Model

Recently, hydraulic resistance measurements were performed on a Global Nuclear Fuel (GNF) 9×9 BWR assembly at Sandia National Laboratories [7]. Commercial components were purchased to create the assembly including the top and bottom tie plates, spacers, water rods, channel box, and all related assembly hardware. Stainless steel conduit was substituted for the fuel pins for hydraulic testing. The stainless steel mock fuel pins were fabricated based on drawings and physical examples provided by GNF.

From a series of experimental runs, local and total pressure drops and flow rates for a range of Reynolds Numbers were measured. The data from the runs was processed in terms of inputs for the MELCOR code (i.e., see below, S_{LAM} and k). An error analysis of the measurements revealed an uncertainty of hydraulic resistance values for input into MELCOR to be very small (i.e., S_{LAM} equal to ±4 and k equal to ±1).

MELCOR, like other control volume codes, includes constitutive relationships to specify form losses (i.e., minor losses) and wall friction losses (i.e., major or viscous losses) along a flow path as a hydraulic flow loss term to the momentum equation. The format of the user-specified input for MELCOR is defined from the sum of the local viscous and major pressure drops,

$$\Delta P = \frac{1}{2}\rho v^2 \left(f\, L/D + k \right) \tag{8.5}$$

The laminar friction factor, f, for laminar flow is written explicitly as,

$$f = S_{LAM}/\mathrm{Re} \tag{8.6}$$

where,

$S_{LAM} = 64$ for pipe flow (and $S_{LAM} = 100$ for bundle flow in the BWR SFP model in [42] and [43])

Re =   Reynolds Number

r =   local density

v =   local velocity

The BWR fuel assembly contains seven grid spacers, upper and lower tie-plates, full and partial rod regions, two water rods, and an inlet nozzle. However, it is not practical to include a detailed representation of all the geometry changes in the MELCOR model. In addition, the MELCOR code includes some hard-wired geometry models that further limit the modeling of the two large water rods inside the assembly and their associated flow. Consequently, modeling choices are required to represent the geometry of the BWR assembly.

8.4   Analysis Results

As described earlier, three accident scenarios were considered. The first scenario assumed that there was no loss of water due to sloshing caused by the earthquake and therefore had an initial pool water level of 11.5 m. The second scenario was similar to the first, except the reactor building was removed from the model. The third scenario assumed there was a major loss of water either by sloshing, a leak in the pool, or both. This scenario assumed an initial water level of 4.96 m, or 0.5 m above the racks and an intact reactor building.

The different water levels were chosen to explore the conditions required to reach the events that happened at the Unit 4 reactor building. The scenario with the full pool was chosen as a baseline condition to determine the length of time required to uncover and dry-out the pool had no water been lost during the earthquake or due to a liner tear. The scenario with the initial water level starting 0.5 m above the racks was chosen as an extreme case. The water level was arbitrarily chosen; however, the results give the reader an idea of how severe the damage would have been if the explosion in the Unit 4 reactor building were caused by hydrogen produced from oxidation reactions of the zircaloy cladding.

All scenarios assumed an initial water temperature of 301 Kelvin (82 °F) and that no water recovery system was available throughout the duration of the accident (e.g., sprays). A summary of the results is provided in Table 25.

Table 25. Summary of Spent Fuel Pool Analysis Results

Event	Scenario 1 (Full Pool)	Scenario 2 (Full Pool, no Reactor Building)	Scenario 3 (0.5m above top of racks)
Pool level reaches top of rack	24.9 days	12.3 days	3.2 days
Pool level reaches bottom of rack	31.9 days	18.9 days	10.5 days
Pool dryout	37.0 days	21.8 days	16.0 days
Cs release fraction when pool at top of rack	0.0%	0.0%	0.0%
Cs release fraction when pool at bottom of rack	33.7%	23.2%	42.4%
Cs release fraction at pool dryout	87.4%	82.4%	82.9%
Total Hydrogen Production (at 1000 hours from accident initiation)	1732 kg	2525 kg	2098 kg
Percentage of Zr Oxidized (at 1000 hours)	35.8%	52.2%	43.3%

8.4.1 Full Pool Case

The full pool SFP accident scenario occurs over a large timeframe and is dominated by the evaporation of the SFP water inventory. Loss of water inventory via evaporation is important until the water level reaches the top of the racks, at which point the water begins to boil. The evaporation and boil-off rate is dependent upon the whole pool decay heat, which for the accident scenarios was held at a constant value of 2.23 MW, the oxidation power generated after fuel uncovery, and the partial pressure of water vapor above the pool. As can be seen in Figure 113, the evaporation portion for this case takes about 598 hours (24.9 days) to reach the top of the spent fuel pool racks. The increase in water level at the beginning of the accident is due to the change in water density as the water reaches saturation temperature. As the spent fuel uncovers, the rate of boil-off increases due to increased cladding temperatures caused by cladding oxidation, which is an exothermic reaction. At roughly 750 hours (31.25 days) the cladding temperature in the upper levels reaches 2000 K causing failure and relocation of the upper levels of the rack to the lower levels of the pool, resulting in a rapid boil-off of water that is still partially covering the assemblies. The pool completely dries out after 888 hours (37.0 days).

The maximum SFP cladding temperatures can be seen in Figure 114 and Figure 115. Cladding is sufficiently cooled during the evaporation to the top of the racks. As the cladding is uncovered, cladding oxidation reactions begin in the upper portions of the assembly causing an increase in temperature, hydrogen generation, and embrittlement of the cladding. The maximum cladding temperature peaks at 2174 K, at which point it reverses direction and cools before the lower levels of the assembly begin to oxidize. The cool down is caused by the rapid boil down shown in Figure 113, which is caused by the failure and relocation of the upper portions of the rack. The increased steaming rate caused by the rapid boil-off of the remaining pool is enough to

cool the cladding, but not enough to arrest the oxidation reaction. Once the pool level drops below the bottom of the racks, a natural circulation pattern forms. The increased air and steam flow at this point causes cladding oxidation at the lower levels of the assemblies.

As the cladding oxidizes in the steam rich environment, hydrogen is generated as the cladding strips the water of its oxygen. Hydrogen generation is shown in Figure 116. Roughly 1732 kg of hydrogen is produced over the timeframe of the calculation (1000 hours). The cladding also become brittle during the oxidation process and is more likely to fail mechanically. The failure of cladding produces releases to the environment. The fractional release of Cesium to the environment is shown in Figure 117.
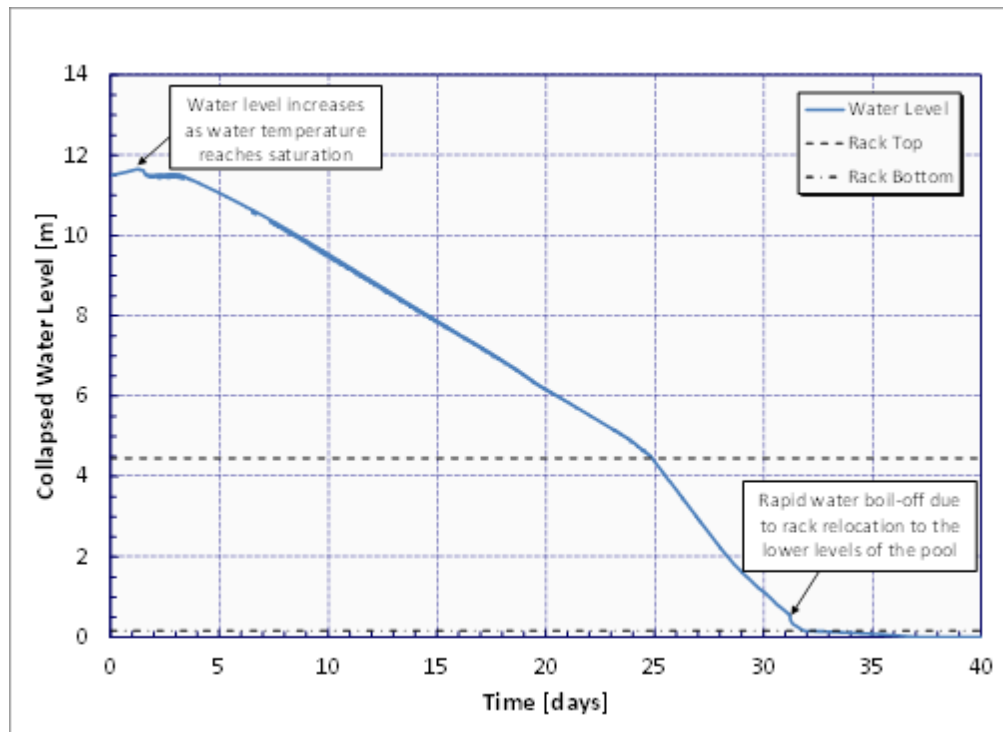
Figure 113. MELCOR Predicted Spent Fuel Pool Collapsed Water Level (Full Pool Case).
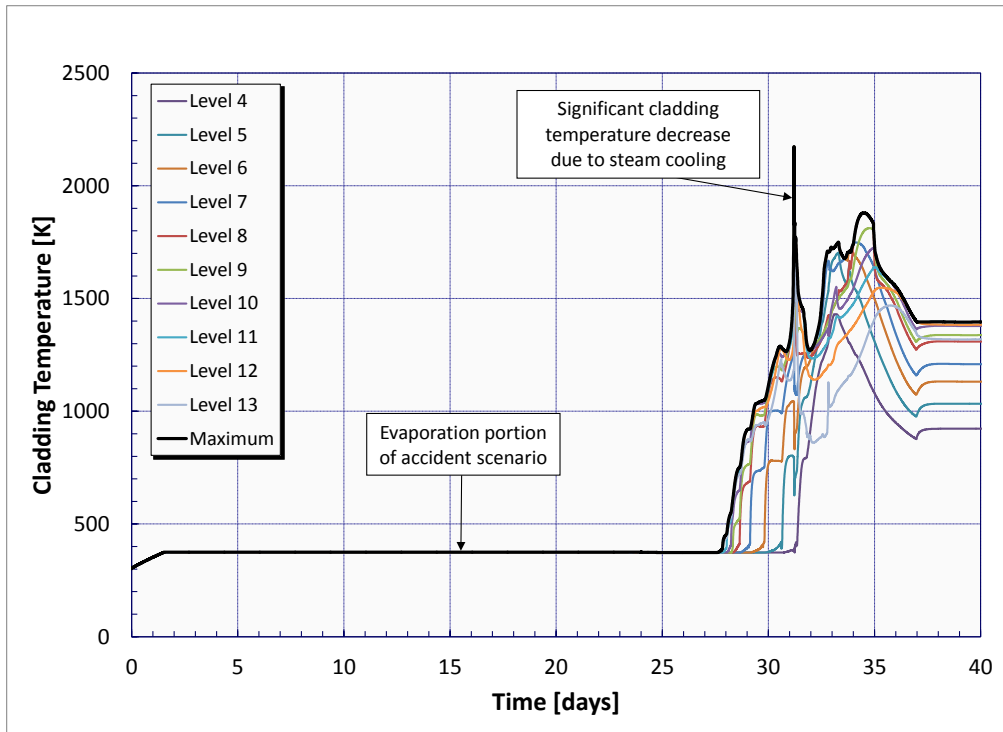
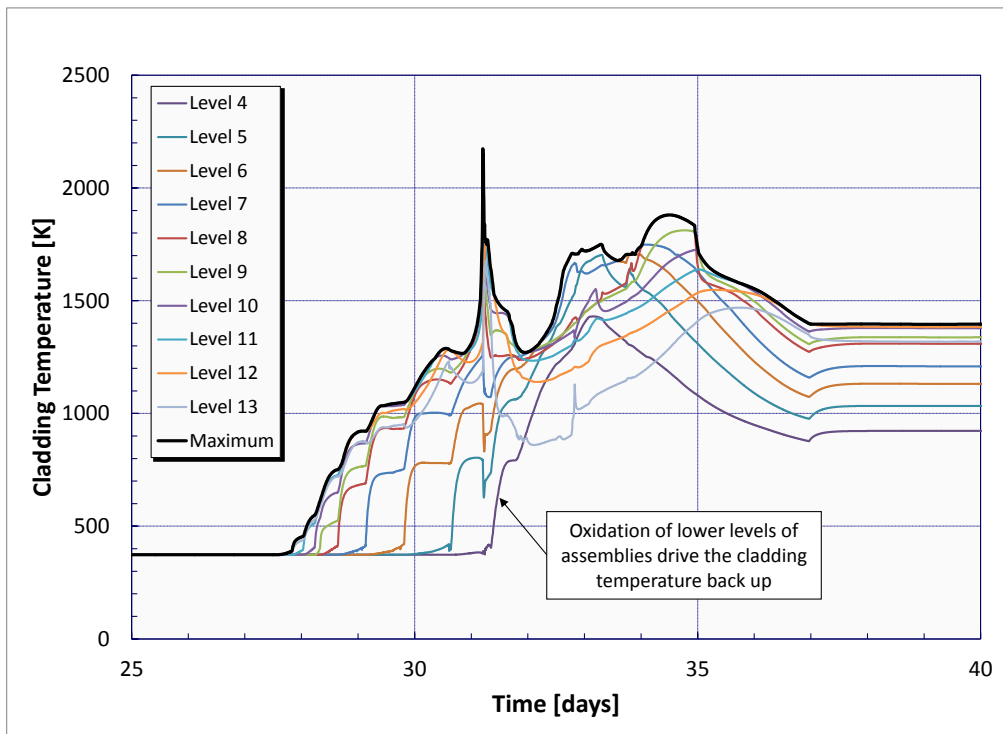**Figure 114. MELCOR Predicted Spent Fuel Pool Maximum Cladding Temperatures (Full Pool Case).**

Figure 115. MELCOR Predicted Spent Fuel Pool Maximum Cladding Temperatures (Full Pool Case, Detailed View).
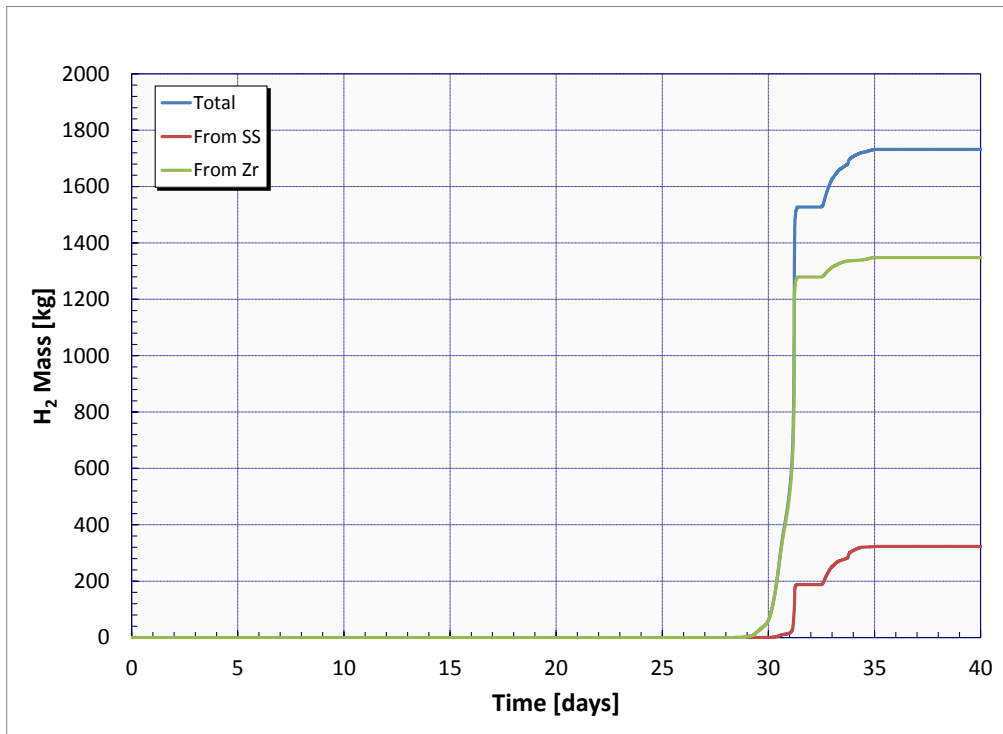
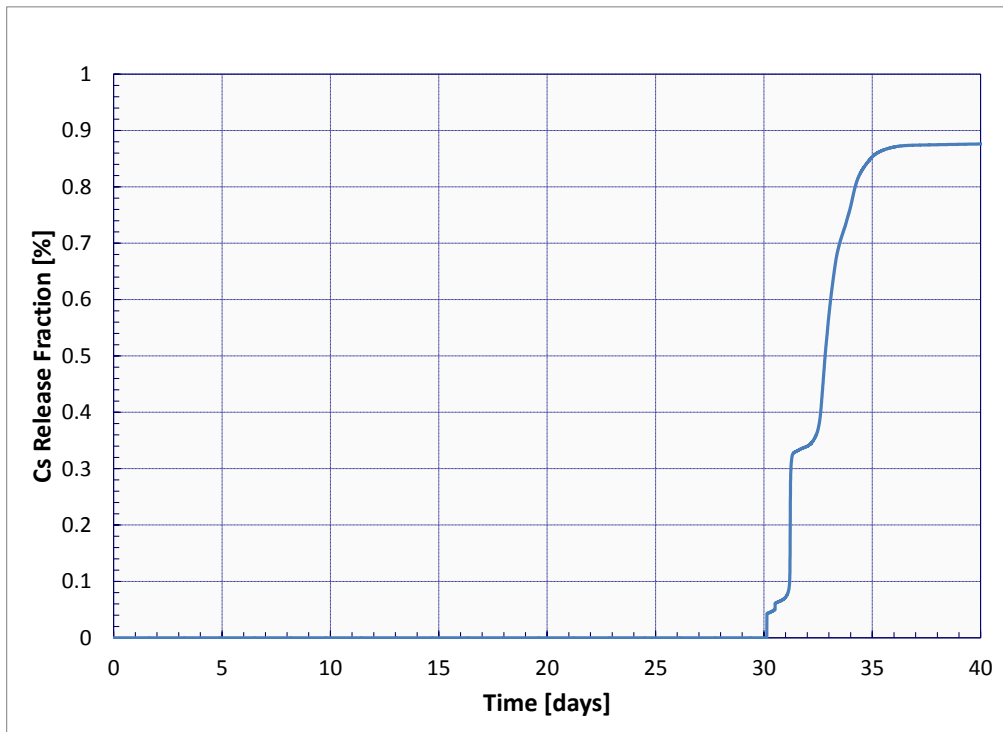**Figure 116. MELCOR Predicted Hydrogen Generation (Full Pool Case).**

Figure 117. MELCOR Predicted Fraction of Initial Cesium Inventory Released (Full Pool Case).

8.4.2 Full Pool, No Reactor Building

The full pool SFP accident scenario without the reactor building modeled occurs over a much shorter timeframe than when the reactor building is modeled. The evaporation and boil-off rate is dependent upon the whole pool decay heat, the oxidation power generated after fuel uncovery, and the partial pressure of water vapor above the pool. When the reactor building was modeled above the pool, the partial pressure of water above the pool was less than unity because the upper structures were condensing the vapor. Also, a portion of the condensate found its way back to the pool. During the length of the postulated event with a reactor building, roughly 1811 m^3 of water condenses on the interior structures of the reactor building with about 57% of that (or 1037 m^3) returning to the pool. This is the dominant process in delaying fuel uncovery between the two cases. In this case, there are no upper structures to condense the vapor. As can be seen in Figure 118, the evaporation portion for this case takes about 295 hours (12.3 days) to reach the top of the spent fuel pool racks. The increase in water level at the beginning of the accident is due to the change in water density as the water reaches saturation temperature. As the spent fuel uncovers, the rate of boil-off increases due to increased cladding temperatures caused by cladding oxidation. At roughly 425 hours (17.7 days) the cladding temperature in the upper levels reaches 2300 K, causing failure of the upper rack and cladding structures and ultimately a rapid boil-off of water that is still partially covering the assemblies. The pool completely dries out after 523 hours (21.8 days).
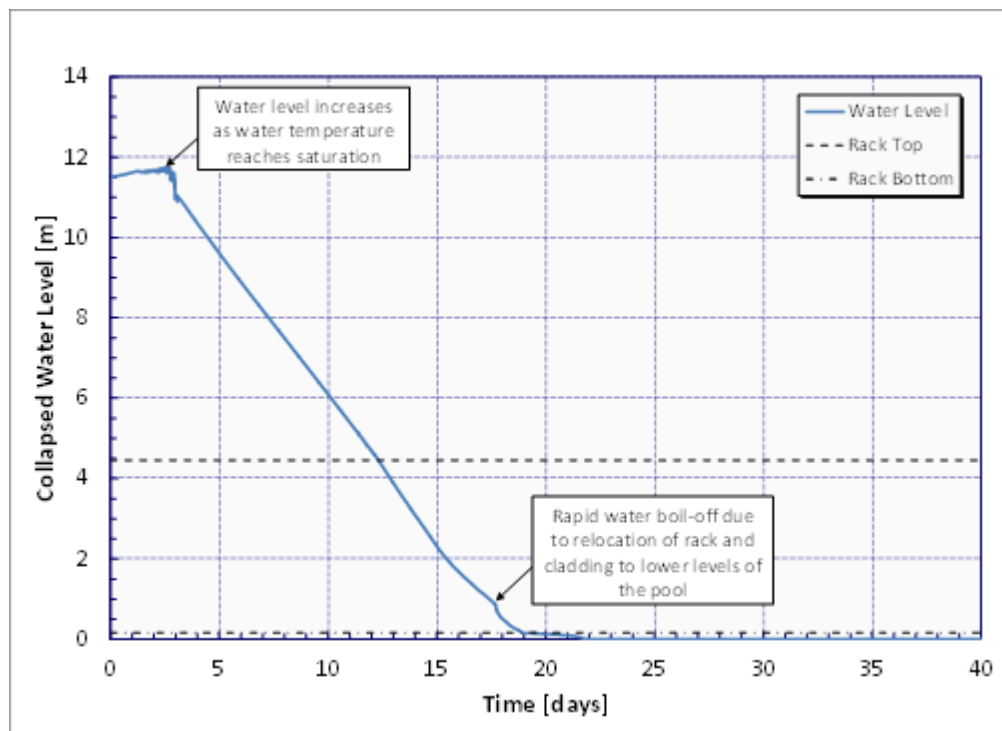
Figure 118. MELCOR Predicted Spent Fuel Pool Collapsed Water Level (Full Pool, No Reactor Building).

The maximum SFP cladding temperatures can be seen in Figure 119. Cladding is sufficiently cooled during the boil-off stage. As the cladding is uncovered, cladding oxidation reactions begin in the upper portions of the assembly causing an increase in temperature, hydrogen generation, and embrittlement of the cladding. The maximum cladding temperature peaks at 2310 K, at which point it reverses direction and cools before the lower levels of the assembly begin to oxidize. The cool down is caused by the rapid boil down shown in Figure 118. The steam generated during this portion of the accident cools the cladding. Once the pool level drops below the bottom of the racks, a natural circulation pattern forms. The increased air and steam flow at this point causes cladding oxidation at the lower levels of the assemblies.
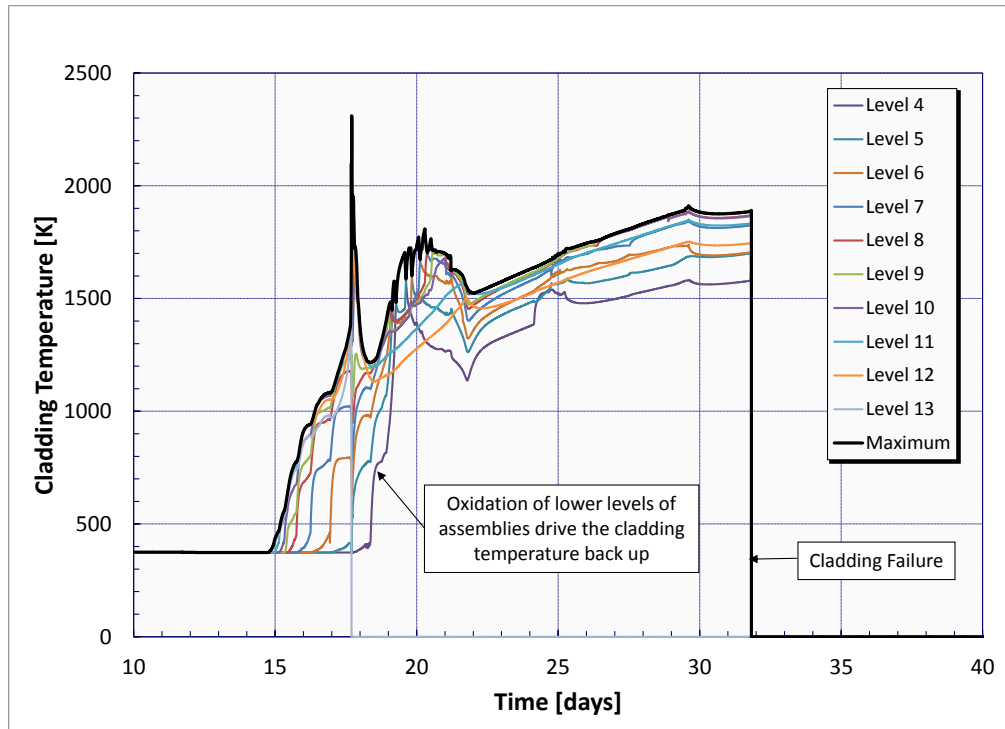
Figure 119. MELCOR Predicted Spent Fuel Pool Maximum Cladding Temperatures (Full Pool, No Reactor Building).

As the cladding oxidizes in the steam rich environment, hydrogen is generated as the cladding strips the water of its oxygen. Hydrogen generation is shown in Figure 120. Roughly 2525 kg of hydrogen is produced over the timeframe of the calculation (1000 hours). The cladding also become brittle during the oxidation process and is more likely to fail mechanically. The failure of cladding produces releases to the environment. The fractional release of Cesium to the environment is shown in Figure 121.
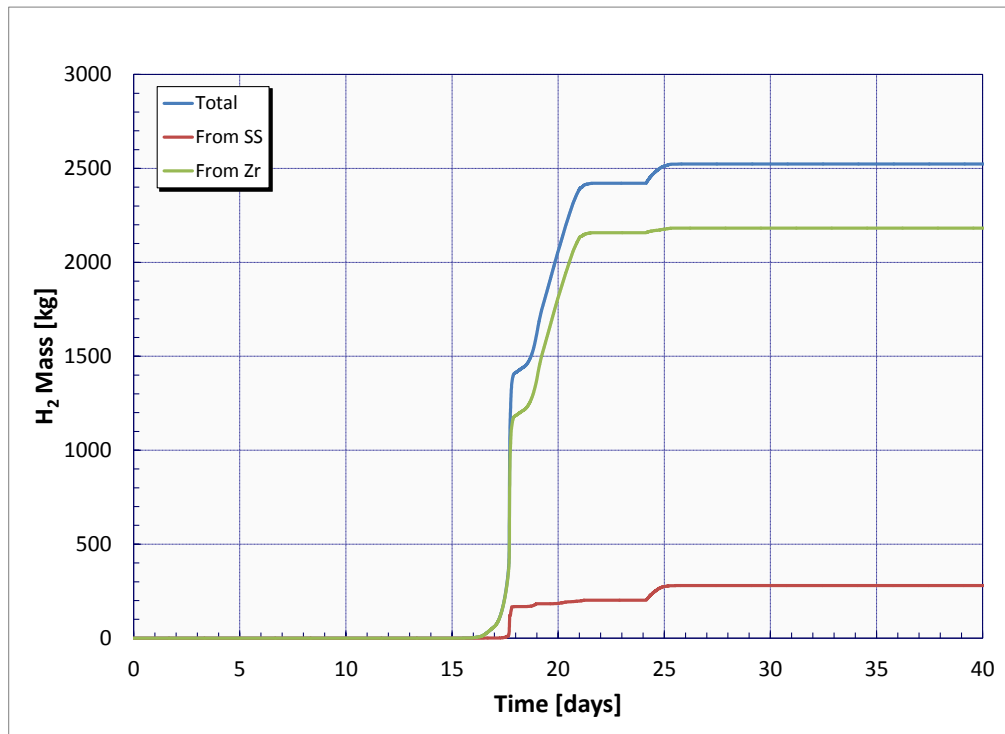
Figure 120. MELCOR Predicted Hydrogen Generation (Full Pool, No Reactor Building).
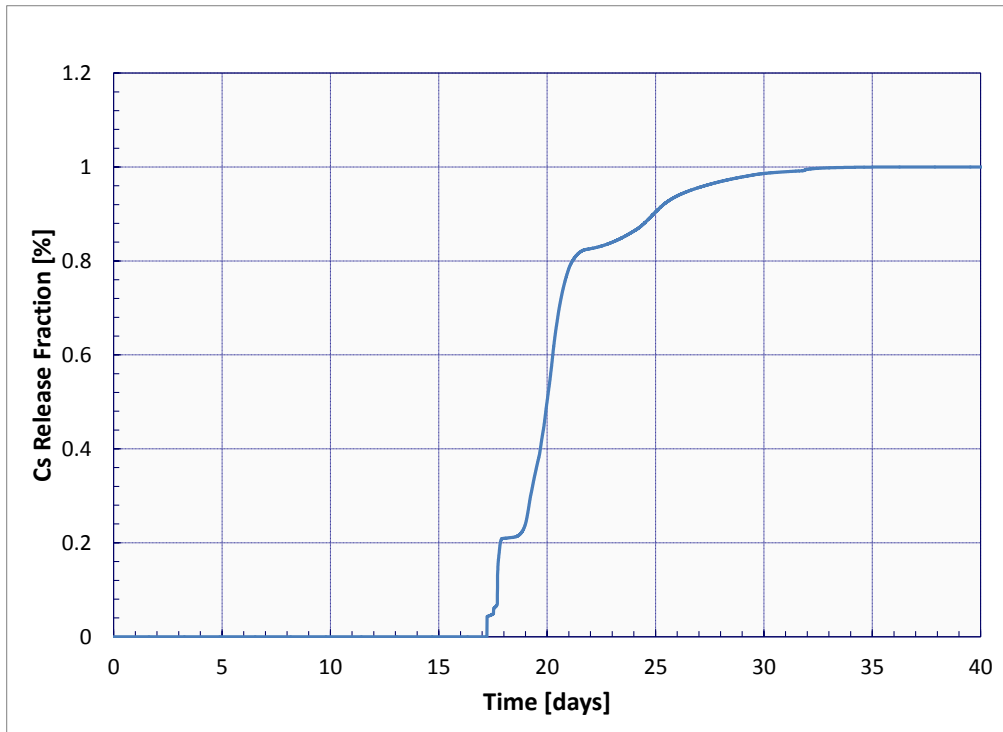
Figure 121. MELCOR Predicted Fraction of Initial Cesium Inventory Released (Full Pool, No Reactor Building).

8.4.3 Pool 0.5 m above Top of Racks

The progression of this case is very similar to the full pool case, except it occurs over a much shorter timeframe because there is less water to boil. As can be seen in Figure 122, the evaporation portion for this case takes about 77 hours (3.2 days) to reach the top of the spent fuel pool racks. The increase in water level at the beginning of the accident is due to the change in water density as the water reaches saturation temperature. As the spent fuel uncovers, the rate of boil-off increases due to increased cladding temperatures caused by cladding oxidation. At roughly 225 hours (9.4 days), the cladding temperature in the upper levels reaches 2000 K causing failure of upper rack and cladding structures and ultimately a rapid boil-off of water that is still partially covering the assemblies. The pool completely dries out after 384 hours (16.0 days).
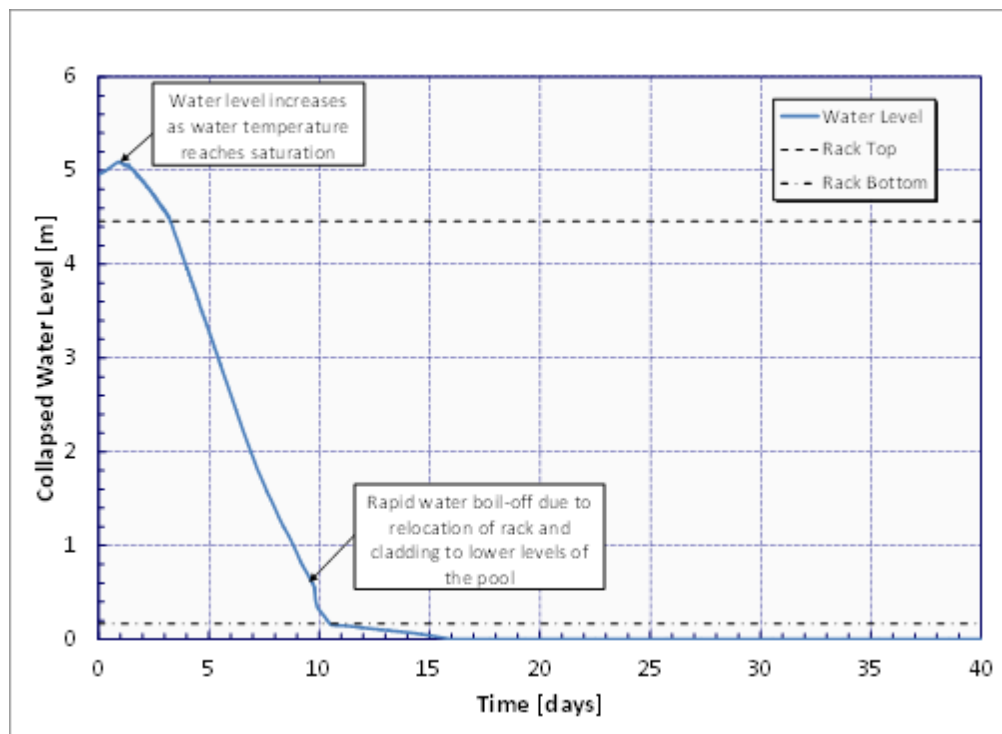
Figure 122. MELCOR Predicted Spent Fuel Pool Collapsed Water Level (0.5 m above Top of Racks Case).

The maximum SFP cladding temperatures can be seen in Figure 123 and Figure 124. Cladding is sufficiently cooled during the evaporation stage. As the cladding is uncovered, cladding oxidation reactions begin in the upper portions of the assembly causing an increase in temperature, hydrogen generation, and embrittlement of the cladding. The maximum cladding temperature peaks at 2361 K, at which point it reverses direction and cools before the lower levels of the assembly begin to oxidize. The cool down is caused by the rapid boil down shown in Figure 122. The steam generated during this portion of the accident cools the cladding. Once the pool level drops below the bottom of the racks, a natural circulation pattern forms. The increased air and steam flow at this point causes cladding oxidation at the lower levels of the assemblies.
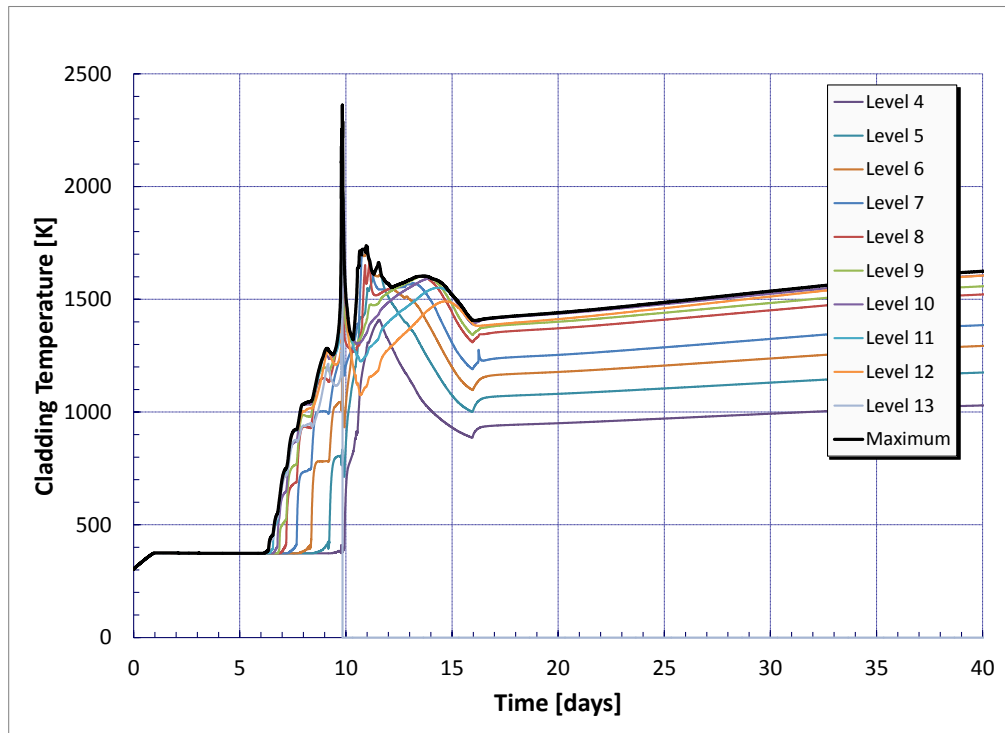
Figure 123. MELCOR Predicted Spent Fuel Pool Maximum Cladding Temperatures (0.5 m above Top of Racks Case).
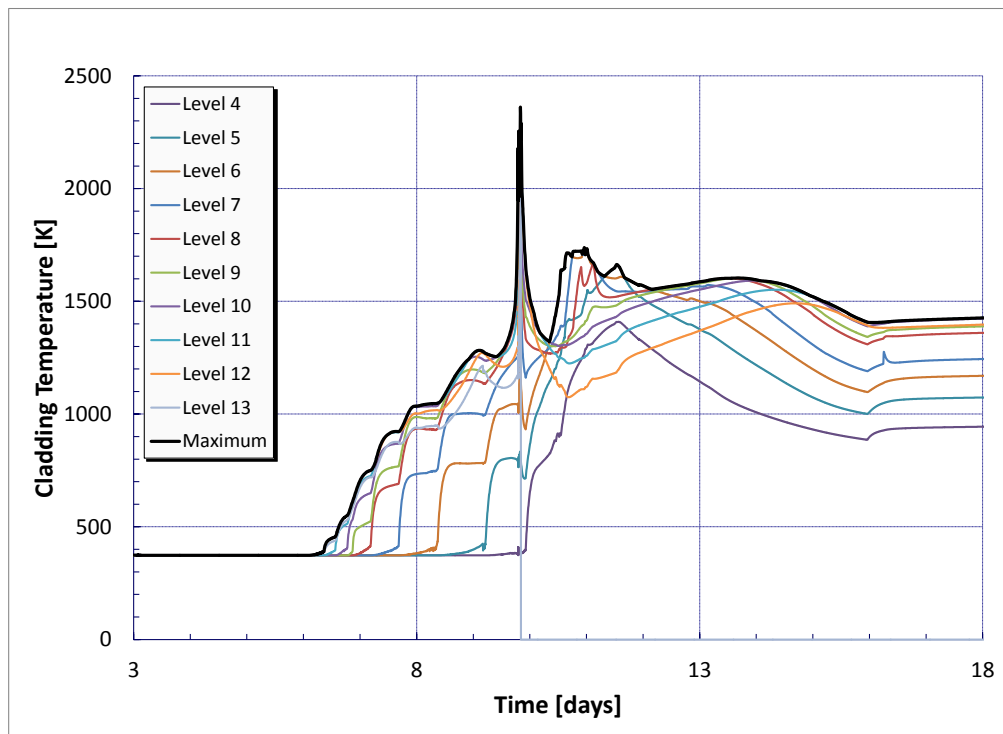
Figure 124. MELCOR Predicted Spent Fuel Pool Maximum Cladding Temperatures (0.5 m above Top of Racks Case, Detailed View).

As the cladding oxidizes in the steam rich environment, hydrogen is generated as the cladding strips the water of its oxygen. Hydrogen generation is shown in Figure 125. A total of roughly 2098 kg of hydrogen is produced over the timeframe of the calculation (1000 hours). The cladding also become brittle during the oxidation process and is more likely to fail mechanically. The failure of cladding produces releases to the environment. The fractional release of Cesium to the environment is shown in Figure 126.
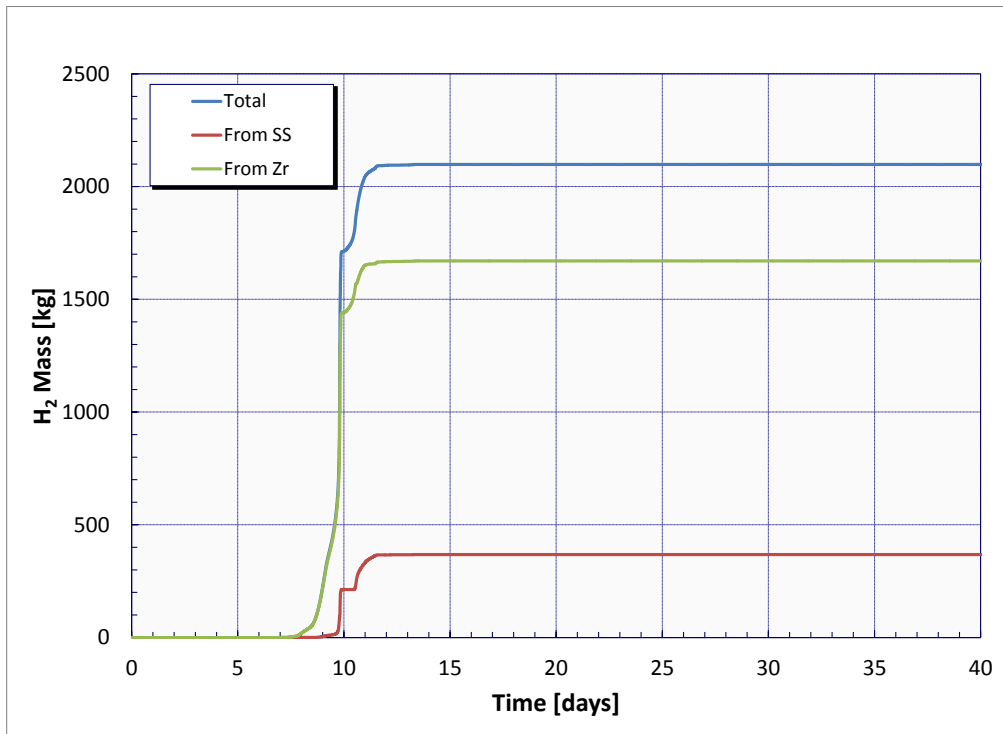
Figure 125. MELCOR Predicted Hydrogen Generation (0.5 m above Top of Racks Case).
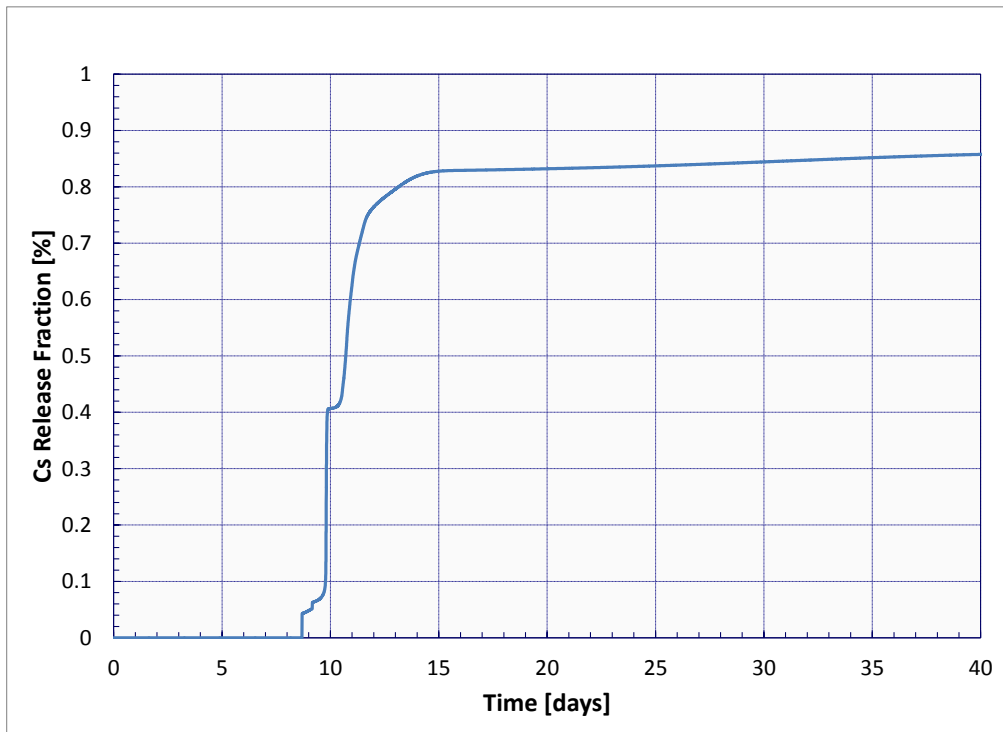
Figure 126. MELCOR Predicted Fraction of Initial Cesium Inventory Released (0.5 m above Top of Racks Case).

9   CONCLUSIONS

9.1   Status of MELCOR Validation

The MELCOR code is a repository of cumulative understanding and learning concerning reactor accident progression. MELCOR was motivated by the TMI-2 accident and the realization that severe accidents are characterized by a complex interplay of coupled phenomena. Examples of the subtle interplay that were realized early on were the importance of material interactions that impact the loss of core geometry as the core overheats. Core structures do not liquefy according to the pure material melting points of their components. Rather, they are strongly affected by key material interactions such as eutectic formation.

The validation of MELCOR is an ongoing and cumulative process where each new piece of experimental information becomes incorporated into the body of knowledge that resides in MELCOR. Fundamental in the validation of MELCOR are the many separate-effects experiments covering a wide range of phenomena, such as fuel/cladding liquefaction, Zr-steam oxidation, Steel-Zr eutectic liquefactions, and separation of metallic and ceramic phases, as the core gradually loses rod geometry and assumes debris or melted pool geometry. Other experiments characterize the thermal release of volatile fission products from the overheating fuel, and still other experiments characterize the aerosol formation of the condensing fission product vapors. The integral computer code, MELCOR, assembles each of these phenomena in their individual domains of relevance into composite prediction of the complex system response.

The correct interplay of these individual physical processes are verified by means of larger, more integral experiments, such as the Phebus in-pile tests [30], or other predecessor testing programs such as the ACRR DF-4 [12] and PBF SFD 1-4 tests [24]. These larger experiments include a wider range of phenomena wherein the interaction and coupling of effects can be observed.

Finally, the few real-world full-scale accidents, most notably the TMI-2 accident and now the Fukushima Daiichi accidents, provide the most complete verification of our understanding and modeling of severe accidents. The TMI-2 accident was a very problematic accident in terms of code analysis, as this was actually very early on in the code development timeline; and code modeling improvements, such as the importance of treating multi-dimensional flow effects, had to be appreciated and accommodated before the accident could be understood with confidence. In contrast to the many years following the TMI-2 accident before reasonable code analyses were able to characterize the events at TMI, we are developing good insights into the accident progression in the Fukushima reactors during the first year after these accidents. This is due largely to the significant gains in severe accident modeling in the interim period between the accident at TMI-2 and the accidents at Fukushima Daiichi

The analyses presented in this report were based on the best information available at the time concerning reactor-specific information, accident timeline, and other boundary condition details such as actual reactor decay power and reactor water injection flows. At the onset of this work, it was realized that there was large uncertainty in the coolant injection data. The Unit 1 analysis is perhaps the most well characterized of the accident sequences since essentially none of the emergency cooling systems were functional and emergency water injection was not

accomplished until very late in the core damage evolution. The analysis of Units 2 and 3 are less well characterized in terms of boundary conditions due to large uncertainty in the actual water injection attained following emergency reactor vessel depressurization. This work was largely premised on crediting the stated coolant injection flows for Units 2 and 3 in the analyses, knowing that they were upper bound estimates and would likely not produce the most favorable results.

At this point in the study of these accidents, the principal means for evaluating the goodness of the analyses are comparisons of predicted versus observed RPV, drywell, and wetwell pressures. Water level measurements during the accident are not always reliable owing to instrument accuracy issues under accident conditions. Quantitative comparison can also be made between radiation detector readings and accident progression events (see Section 4.4). Beyond this, presently there are virtually no other measured quantities against which to evaluate the analyses. That said, the pressure measurements provide valuable insights into the adequacy of the analyses and the likely damage state of the reactors. In the years to come, as the reactors at the Daiichi site are decommissioned and disassembled, more material evidence will become available, which can be used to further evaluate and improve code models for core melt progression. The following sections provide a summary of analysis results obtained thus far.

9.2 Validation Objective

One of the objectives of this study was to use the results from the MELCOR models to further the validation of the MELCOR code. Comparison of the MELCOR model results with the available data is a measure success in this regard.

In the Unit 1 model, the following trends are seen in both the TEPCO pressure data and the MELCOR model results:

- RPV depressurization (< 12 hr)
- pressurization of the drywell and wetwell to a steady-state value (~111 psia (0.765 MPa); between 15 and 24 hr) that is consistent with MELCOR's model for the drywell head lifting and attendant venting of the drywell into the reactor building refueling bay
- depressurization of the drywell and wetwell at the time of wetwell venting (~24 hr)
- changes in drywell and wetwell pressures at the start and end times of water injection

In addition, the model predicts the accumulation of combustible gases (e.g., H_2, CO) in the reactor building refueling bay, which is consistent with the observed explosion in the reactor building.

In the Unit 2 model, the following trends are seen in both the TEPCO pressure data and the MELCOR model results:

- initial RPV depressurization (5 to 15 hr)
- RPV pressurization (~67 hr)
- RPV pressure during SRV cycling (70 to 74 hr)
- RPV depressurization (~74 hr)

- drywell pressurization (10 to ~36 hr)
- wetwell depressurization (80 to 88 hr)

In the Unit 3 model, the following trends are seen in both the TEPCO pressure data and the MELCOR model results:

- RPV pressure during RCIC operation (0 to 24 hr)
- RPV depressurization at RCIC shut-down/HPCI start-up (24 hr)
- RPV pressure during HPCI operation (24 to 35 hr)
- RPV pressurization at HPCI shut-down (35 to 39 hr)
- RPV pressure during SRV cycling (39 to 42 hr)
- RPV depressurization (42 hr)
- RPV pressure for the balance of the accident (42 to 96 hr)
- drywell pressurization during RCIC operation (0 to 24 hr)
- drywell depressurization during HPCI operation until CST depletion (24 to 31 hr)
- drywell pressurization during HPCI operation after CST depletion (31 to 35 hr)
- drywell pressurization during SRV cycling (39 to 42 hr)
- drywell and wetwell pressures in response to venting and water injection (42 to 60 hr)

From a qualitative standpoint, all three SNL analyses of the accidents in Units 1 through 3 using MELCOR 2.1 produced accident sequence results that followed the general trends in the TEPCO data and observed events. Moreover, good quantitative comparisons to the TEPCO data are found in portions of all three model results. The results from the ORNL Unit 3 model (created from an older version BWR Mk-I conceptual model and run with an older version of MELCOR) also follow the general trends of the Unit 3 accident sequence.

The good comparison between Unit 4 spent fuel pool results from the MELCOR model (with no reactor building refueling bay) and the TRACE model also provides code-to-code benchmarking for the validation of MELCOR.

Overall, these results increase confidence in the MELCOR code; establish confidence in the Fukushima reactor models and spent fuel pool model; and demonstrate that the code and models are valid for their intended use. They also add more evidence to the existing body of results that, when taken has a whole, build confidence in the validity of the MELCOR code.

9.3   Unit 1 Analysis Summary

The Unit 1 analysis was performed using an input model derived from earlier NRC studies of nuclear power plant vulnerability to aircraft impacts (post 2011) and more recently the NRC State of Art Reactor Consequence Analysis (SOARCA, 2011). Fukushima-specific modifications were made to the original Peach Bottom model in terms of reactor size and power. As discussed earlier, the model embodies numerous predictive component failure treatments for the drywell head flange, SRV seizure under high temperature and potential rupture of the main steam line. These treatments have been evolved over the past ten years based on collective knowledge and insights into severe accidents gained in ongoing research in the area since the accident at Three

Mile Island. The base-case Unit 1 analysis consistently predicts main steam line failure as the mode of vessel depressurization. MELCOR-predicted results compare favorably against the limited data available for the RPV, drywell, and wetwell pressures. An alternative scenario was examined early on in this study prior to receiving plant-specific information concerning decay power where the SRV was assumed to stick open prior to rupture of the main steam line. This analysis produced a similar containment pressure response but resulted in slightly lower drywell/wetwell pressure following RPV blowdown since the blowdown via the stuck-open SRV case directs the steam into the suppression pool instead of to the drywell atmosphere in the MSL rupture case. The SRV seizure case was not included in this report, as it has not been re-run using the more accurate decay power data provided by TEPCO; however, we expect similar outcomes would be produced. While the bases-case analysis predicts MSL rupture as the mechanism for RPV depressurization, it is acknowledged that SRV seizure, or other yet unrecognized means of RPV depressurization, are possible.

In the various cases examined in this study (but not reported on), MSL failure timing varies by about an hour with subsequent lower head failure timing varying between about 10 and 13.5 hours, where between 2.5 and 3 "rings" of the core ultimately relocating to the cavity.

Once core materials fall into the cavity, an MCCI reaction is predicted to initiate, producing non-condensable gas (CO_2, CO, and H_2) as well as some steam generation from water present in the cavity, which raises the drywell/wetwell to about 110 psia (0.765 MPa). MELCOR predicts elastic straining of the drywell head bolts, which limits further elevation of the drywell pressure in a self-regulating manner. This pressure trend is consistent with the observed pressure in the accident. It should be noted that MELCOR's model for drywell head bolt strain was adjusted slightly to open a leak area at a higher pressure than assumed in the original Peach Bottom model in order to better match observed trends in Unit 1. The leak at the drywell head flange effectively prevents further pressurization of the drywell. The leakage of drywell gases at the drywell head flange allows steam and flammable gas to enter the refueling bay region of the reactor building, where steam-inert conditions are sustained for the duration of the drywell head flange leak.

At ~23 hours, operators manually vent the containment, reducing the drywell/wetwell pressure; MELCOR predicts head flange leakage will terminate owing to elastic contraction of the head bolts. Conditions in the refueling bay after this time become increasingly conducive to deflagration of the flammable gases as steam condenses out of the mixture and air is drawn into the building. The gas mixture in the refueling bay is potentially flammable, or even explosive, as a result of the leakage at the drywell head flange; however, it is also possible that malfunctioning of the containment venting system could have allowed additional hydrogen to enter the refueling bay by means of passive failure in the standby gas treatment system (SGTS) or by a break in the venting duct itself.

The sequence of events predicted by MELCOR is consistent with the available pressure response data for the drywell, wetwell, and RPV and, in fact, would appear to agree quite well. That said, alternative scenarios to the one "preferred" by this MELCOR modeling effort have not been explored at this time.

9.3.1 Uncertainties

There are known areas of important phenomenological uncertainty in the analyses (melt progression and core relocation details) and observed areas of sequence sensitivity to uncertain input conditions (water inventory and decay heat). These uncertainties can produce differences in timing of the major events such as water boildown to top of core, onset of rapid zircaloy oxidation, MSL failure, SRV seizure, and lower head failure of 1 to 3 hours. Also, the predicted flammable gas concentrations in the reactor building are impacted by the effect of variations in environment conditions (e.g., air temperature and relative humidity, wind speed and direction) on air exchange between the reactor building and the environment, as well as the by the current treatment of modeling the reactor building refueling bay as a single large (well-mixed) control volume.

9.3.2 Release of Fission Products

Release of fission products to the environment is predicted to be a relatively small fraction of the core inventory, on the order of 1%, by direct transfer to the environment where significant retention in the RPV, drywell, and wetwell are predicted. About 5% of the Cs inventory was predicted to deposit in the reactor building, mainly the refueling bay, and some fraction of that would be expected to be dispersed when the hydrogen explosion occurred. The "source terms" predicted by MELCOR can subsequently be used together with weather data from the Fukushima region to predict the dispersal of fission products, in particular the deposition of Cs, in the region surrounding Fukushima, using atmospheric dispersion codes such as MACCS.

9.3.3 Comparisons to Other Codes

Comparisons between Unit 1 and TEPCO MAAP analyses that SNL staff are aware of would indicate general consistency of timing of first core damage, peak core temperatures, and magnitude of hydrogen generation (neighborhood of 1000 kg). Recent analyses by TEPCO have produced a very similar result to the present MELCOR MSL rupture analyses, except that the TEPCO analysis assumed a number of progressively increasing leaks in the primary pressure boundary, with the largest of those leaks being the blowout of a gasket associated with a SRV. The gasket blowout assumption is effectively equivalent in results with a rupture of the steam line. This indicates that alternative primary system blowdown mechanisms can produce similar accident response signatures.

9.3.4 Status of MELCOR Validation

The present MELCOR Unit 1 analyses are in reasonable agreement with the limited data available on RPV, drywell, and wetwell pressures, and the timing of onset of core damage are consistent with observed increases in radiation levels at the plant. Cross-code comparison with anticipated EPRI MAAP analyses could identify areas of modeling uncertainty or variance in code treatment of important phenomena. Code analyses can be adjusted as new information emerges concerning the precise damage state of the cores, RPV, and cavity, and this potentially offers the greatest opportunity for improving our confidence in code predictions and improving their utility in future safety-enhancing applications such as evaluation of accident

management/severe accident management guidelines success likelihood or alternative mitigation strategies.

9.3.5 Potential Future Activities

Alternate scenarios should be explored to evaluate different accident progression sequences that may nevertheless still be consistent with the presently available information. These alternate scenarios could provide guidance on future forensics activities in the decommissioning stages in that they will suggest key damage state differences that may be discovered in the post-mortem activities. This activity will ensure that the most useful information is gained in the decommissioning activities. It may be essential to identify these plant damage states in advance of decommissioning activities if they are to be resolved at all. Some potential alternative sequence analyses are listed in the Table 26.

In addition, a more detailed treatment of the environment boundary conditions (e.g., air temperature and relative humidity, wind speed and direction) would refine the calculation of reactor building-environment air exchange and combustible gas concentrations.

An examination of the fresh water and seawater injection rates should be performed, including the implementation of a pump head curve model to account for reduction in flow rate due to high containment pressure. This would require additional information concerning the performance characteristics of the pumps used in the accident response.

In addition to alternative scenarios, significant opportunity exists to gain validation for the MACCS code by performing analyses of source term atmospheric dispersion using the source terms predicted by MELCOR. This activity will likely be pursued in the EPRI work and can also be leveraged against work ongoing at NARAC. Good information concerning ground contamination by Cs-134/137 is available from the flyover dose rate measurements made by the U.S. and Japanese governments. This information, used in combination with MELCOR-predicted releases and atmospheric transport analyses, could provide further validation of severe accident models.

Table 26. Unit 1 Summary

Case No.	Case Description	Purpose	Evaluation
1	MSL Failure, No SRV Sticking	Base Case from SOARCA models – RPV depressurization is by MSL rupture: Steam blowdown into drywell and venting into suppression pool	Compare Drywell/Wetwell predictions to data
2	No MSL Failure, SRV sticks open	Alternative RPV depressurization from SRV sticking open: Steam blowdown into subcooled suppression pool	Determine if drywell/wetwell pressure comparison to data looks better or worse
3	No MSL failure, No SRV sticking open	Delay RPV depressurization until vessel head failure – before 15 hours	Compare pressure signatures – need to consider possible pressurized melt ejection and DCH potential
4	No MSL failure, SRV sticks open, Delay LH failure beyond 15 hrs	Allow RPV depressurization but prevent lower head failure to allow water injection reflood vessel	Examine pressure responses in drywell and wetwell
5	MSL Failure, Delay LH failure beyond 15 hrs	Allow RPV depressurization but prevent lower head failure to allow water injection reflood vessel	See if drywell pressure signature is different significantly from case 4
6	Same as Case 1, but Prevent Drywell Head Flange bolt stretching	Prevent containment venting at head flange	Evaluate containment pressurization in presence of MCCI after LH failure and water injection
7	Same as Case 5, but Prevent Drywell Head Flange bolt stretching	Prevent containment venting at head flange, prevent LH failure	Evaluate containment pressurization with water flooding into vessel, but no additional pressurization from MCCI

9.4   Unit 2 Analysis Summary

Similar to Unit 1, the Unit 2 analysis is based on SOARCA BWR/4 Mk-I model. Early analyses of Unit 2 have demonstrated incompatibility between the calculated containment pressure response and the available data of the containment pressure response, with predicted pressures far exceeding the measured values for the containment. To compensate for the conflicting trends between the analysis and available containment pressure data during RCIC operation, leak was postulated from the suppression chamber to the reactor building. The postulated leak provides improved pressure trends following saturation of the suppression pool at about 10 hours when containment pressures are seen to be rising. Since this analysis was performed, alternative theories for the slow containment pressurization rate have emerged that warrant further study. These include possible RCIC turbine system leaks and flooding of the torus room by seawater. Flooding of the Unit 4 torus room was observed to have occurred, and if the same flooding took place in the Unit 2 reactor building, the additional heat sink of the seawater could delay saturation of the torus and slow containment pressurization.

All observed system responses for Unit 2 during the first 70 hr of the accident sequence are strongly affected by the RCIC turbine/pump operational state. The available data suggested that the RCIC system maintained water coverage of the core and the combined operation of the RCIC turbine draw and the SRVs maintained the system pressure. Shortly after 5 hrs, RPV pressure fell below the SRV set point, while the core level readings remained relatively unchanged until RCIC was believed to have failed.

Due to the uncertainty associated with the RCIC operation, improving the agreement with the containment and RPV states was made a priority to permit a meaningful analysis of the core damage state and progression. It was assumed in the analysis that the operational state of RCIC was such that it maintained the core level at the data values indicated and the deviation between the SRV set point and the decreasing pressure was due to an SRV reseat failure leakage. The pump injection rate was controlled to reproduce the RPV level data and a suitable SRV reseat failure leak open area of 3% was assumed in the analysis to achieve reasonable agreement between RPV and containment pressure prior to RCIC failing.

When the RCIC failed, which was indicated by a decrease in the level data and re-pressurization of the RPV, the water inventory in the RPV began to boil away. The reason for the RCIC failing is unknown at this time, but it is likely that suppression pool saturation conditions would challenge pump operation because of steam flashing and pump cavitation effects. Following RCIC pump failure and the loss of water injection to the vessel, water level loss by venting of steam through the SRVs eventually threatens to uncover the reactor fuel. With no high-pressure source of water injection, emergency operating procedures call for depressurizing the RPV in order to allow for low-pressure water injection. This procedure was modeled in the Unit 2 analysis; however, full RPV depressurization relative to the external environment where the low-pressure pumps were located was countered by the relatively high containment pressure. The indicated pressure of the suppression chamber, which is assumed correct at this time, was below the vent line rupture disc set point, preventing containment venting. The model applied an estimated seawater injection of 10 kg/s; however, the RPV data suggest seawater injection would not have ensued during the pressurization events after the RPV was depressurization. When the RPV pressure was low enough to permit injection, the fire engine pump may have operated sporadically prior to RPV pressure falling well below 115 psia (0.793 MPa).

After the seawater injection was aligned, the analysis reproduced the first re-pressurization event. In the analysis, the re-pressurization was induced by the sudden unperturbed seawater injection, which produced an increase in the rate of steam generation. Based on the data, the calculated RPV pressure at the onset of the re-pressurization event should have precluded seawater injection from producing the observed re-pressurization. It seems probable that the original SRV utilized to depressurize the RPV may have failed closed, producing the observed pressure excursion. Operators opened a second SRV to reestablish low RPV pressure near the seawater spray injection limit.

A second re-pressurization event corresponds with the reported closure of the second SRV (opened, 80.22 hr). Due to the excessive RPV flooding and the SRV employed to depressurize the RPV remaining open, the third event is not reproduced by the MELCOR Unit 2 analysis.

The Unit 2 analysis predicts core integrity was largely maintained. However, due to the extensive high temperatures experienced, significant fission products were released. This coupled with the estimated containment breach produced a relatively significant release of radioactive Cs and I.

It is believed that the assumed water injection flow rate in this analysis exceeds what was actually accomplished in the accident owing to pump head limitations, and that proper accounting of this effect would result in lower water injection and greater core damage. This may be investigated at a later time.

9.4.1   Uncertainties

Prior to failure of the RCIC system, the largest uncertainty is associated with the operation of the RCIC system. Typically in the U.S., a loss of DC power will result in the turbine controller repositioning the governor valve of the turbine to the fully open position. With high RPV pressure, the turbine would experience a mechanical over-speed trip, causing RCIC to cease operating. Due to the level and pressure readings, it is apparent RCIC was operating and maintained fuel coverage. The RPV level data was determined from the differential pressure between the reference leg and variable leg. The reference leg readings will be erroneous should the fluid within the leg flash or RPV level rise above the reference leg tap sight. If the reference leg was flooded by RPV water directly, the high RPV level would influence the differential pressure through the alteration of the anticipated reference leg water column implemented during calibration. The nearly constant water level data could indicate that this has occurred, especially should water be flowing into the main steam lines, possibly diminishing RCIC operation. The actual operational state is uncertain at this time.

The reason for the deviation between initial calculation results and observed containment pressure trend is uncertain. In the analysis presented in this report, an assumed containment leak was implemented wherein the area was selected to produce reasonable agreement with the observed data. Other contributors such as wetwell cooling due to flood water in the torus room, or RCIC steam leakage, may be relevant with regard to observed containment pressure.

After RCIC terminates, failure to adequately calculate the seawater injection prevents predicting a meaningful core damage state, given the dependency of core cooling with the core water level. The current model employs a constant estimate for the seawater injection without consideration for the effects of pump performance versus exit pressure. If made available, the actual fire engine pump curve could be incorporated into the model. In addition to the pump curve, the RPV pressure after depressurization is a function of the installed SRV as well as the containment pressure. Should the SRVs be identified as two-stage Target Rock valves, relief mode operation of the SRV could only decrease RPV pressure to within 20 psi (0.138 MPa) of the containment

pressure. This limitation in depressurization would often exceed the reported fire engine injection pump shutoff head, resulting in no seawater injection.

9.4.2   Release of Fission Products

Unlike Unit 1, the final predicted fuel state in this analysis for Unit 2 is largely intact. Releases from the fuel are below 100% for the noble gases, and releases from fuel for Cs and I are on the order of ~60% of the total radioactive inventory. The estimated environmental release of the available inventory of Cs and I were around 9% and 7%, respectively, and are larger than the Unit 1 analysis because of the assumed leak in the suppression pool containment boundary in spite of the lower degree of core damage predicted in Unit 2. The majority of the released Cs and I is predicted to be sequestered within the suppression pool.

9.4.3   Comparisons to other Codes

Comparisons between Unit 2 MELCOR analysis and TEPCO MAAP analyses vary early in time with regard to SRV and RCIC operational state assumptions. Early TEPCO analyses did not achieve good agreement with RPV pressure assuming core level data was correct and nominal RCIC operation. Recent TEPCO analysis predict good agreement between calculated and observed RPV pressure by assuming the RPV level data is incorrect due to reference leg flooding and to RCIC functionality being diminished by two-phase flow through the RCIC turbine. Assumptions regarding the two-phase flow reduction to total injection rate, as well as the enhance mass and energy removal rate from the RPV, have improved pressure comparisons in recent TEPCO analyses.

9.4.4   Status of MELCOR Validation

The present MELCOR Unit 2 analyses are in reasonable agreement with the data available on RPV and containment pressure data. Due to the uncertainty associate with RCIC operation and seawater injection, the boil off rate, core damage progression, limited seawater spray rates, and post depressurization effects have yet to agree well with the Unit 2 data.

9.4.5   Potential Future Activities

Primary areas for future analysis efforts (see Table 27) should be focused on implementing a pump-head injection curve model to attempt to estimate the actual water injections as a function of the back-pressure in the reactor system. The other main area for additional alternative scenario investigation is associated with alternative hypotheses regarding the low observed containment pressure that has been up to now, rationalized as a likely leak pathway in the containment.

Table 27. Unit 2 Summary

Case No.	Case Description	Purpose	Evaluation
1	No Firewater Injection	Determine new core damage state	Compare new core damage progression with the observed containment pressure data for correlation
2	Reference Leg Flooding	Allow RPV to flood to the MSL	Evaluate the impact on boil-off timing and core damage state
3	Torus Room Flooding Rates	Flooding the torus room permits energy removal from the suppression pool	Evaluate the potential pressure suppression due to energy transfer from the suppression pool
4	RCIC Leaking	Leakage from the RCIC system will reduce steam transport to the suppression pool	Evaluate the potential reduction in containment pressurization
5	Same as Case 1, Delay LH Failure	Increase residual melt temperature and materials	Evaluate liner melt through failure as cause of containment depressurization
6	Same as Case 3, With Early Containment Failure	If comparison between Case 3 and the available data compares poorly, investigate multiple means of pressure suppression	Evaluate significance of various coupled depressurization methods

9.5   Unit 3 Analysis Summary – SNL and ORNL

In general, MELCOR appears well-suited for reproducing the thermal-hydraulic response of the severe accident at Unit 3. Using the current SNL MELCOR 2.1 model of Unit 3, the code calculates pressures in the RPV and the containment that agree reasonably well with the TEPCO data. The Unit 3 model uses a minimal number of assumptions in order to capture the TEPCO data, the most significant assumptions being the operation of the HPCI (minimum flow cooling the wetwell) and the timing of the containment vents (chosen to match the data). However, new information released after the completion of the SNL analyses suggests that HPCI injection was throttled using the test line instead of the minimum flow line. Also, containment sprays are said to have depressurized the containment from 22 to 30 hours instead of wetwell cooling by the HPCI minimum flow line. These recent model modifications are demonstrated in the ORNL model results.

The largest discrepancy between the SNL results and the pressure data during the first 40 hours is the containment pressurization rate due to RCIC operation and SRV cycling. A higher fidelity containment model, as demonstrated by the ORNL model, is one possible explanation for this discrepancy. A circumferentially segmented wetwell in MELCOR simulates the asymmetric heating due to SRV1 cycling from 0 to 22 hours. The steam discharged from SRV-1, the lowest pressure set point SRV, effectively saturates a subsection of the torus, before it saturates the

entire wetwell pool, allowing steam to flow into the drywell via the WW-vent vacuum breakers. With only one control volume, MELCOR disperses the SRV steam homogenously over the entire wetwell. Besides a refined wetwell model, leakage from the seals on the recirculation pumps might also explain the higher containment pressures shown by the TEPCO data (pressurized RCS coolant would flash into steam in the containment).

9.5.1 Uncertainties

Since one of the ultimate goals of a MELCOR simulation is to calculate the degree of core damage and the associated radionuclide release, some of the most important input parameters affecting these calculations in a SBO scenario are the decay power, primary side water volume, emergency cooling methods/timing, and radionuclide transport paths.

The RCIC system appears to have successfully managed decay heat by supplying water to the RPV until shutting off at 20.8 hours. The SNL simulations predict the HPCI system was then similarly able to successfully manage decay heat until 36 hours. However, the ORNL simulations assume the ability for the HPCI to inject water was degraded and was unsuccessful in maintaining adequate water level in the core to manage the decay heat. Uncertainties related to HPCI modeling affects the degree and timing of core damage calculated by MELCOR. This effect ranges from rather early core damage predictions (i.e., shortly after HPCI shutdown) in the ORNL simulations, to delayed core damage (i.e., occurring during fire engine water injection) in the SNL simulations. Due to a lack of sufficient information, the modeling of the RCIC and HPCI systems and their operation may not be entirely correct, and the implementation of accurate plant information and higher-fidelity models would facilitate matching the TEPCO data. Reducing the uncertainty in the behavior of the RCIC and HPCI systems with respect to level control and water injection would allow future studies to focus on the uncertainties in the freshwater/seawater injections, as well as the more fundamental phenomenological uncertainties in the MELCOR code.

Uncertainties in the decay power have a direct impact on core degradation predictions. SNL used best-estimate decay heat information provided by TEPCO (lower uncertainty) in contrast to ORNL, which used the more conservative 1979 ANS standard decay heat curve (intentionally biased high to account for uncertainties). In addition, according to TEPCO,[25] the Unit 3 axial power distribution is more bottom-peaked than the axial power distributions from older Peach Bottom models. The axial power profile can impact core damage progression as the core uncovers. The SNL Unit 3 model uses the TEPCO power distributions (lower uncertainty), while the ORNL Unit 3 model uses the Peach Bottom power distributions (higher uncertainty).

During periods of no water injection, the possibility for and associated timing of core uncovery is primarily determined by the decay heat as well as the volume of water in the RCS (system pressure has a secondary effect). After core uncovery, the axial power shape in the core region impacts the rate of core heat up, hydrogen generation (Zr mass), and the total possible melt mass. While the current models are representative of Unit 3, further model refinement using more detailed core information could further reduce model uncertainties.

---

[25] The axial and radial power distributions for the SNL Unit 3 MELCOR model were calculated from 3-D power distribution data provided by TEPCO.

The largest uncertainties that influence the predictions of core failure and vessel breach are the details of the freshwater and seawater injections. There are many other uncertainties in the MELCOR model input, including radionuclide inventory and thermal-hydraulic input; however, the flow rate for emergency water injection appears the be the most significant model uncertainty, and it is the most likely input to cause order-of-magnitude changes in the calculated results for a relatively small change in flow rate (i.e., ranging from minor core damage to total core relocation and vessel failure). Due to the ad-hoc nature of the emergency water injection at Fukushima, it is very unclear how much water actually made it to the core region. Pump-head issues and possible leaks in the injections lines, RCS, and the vessel can vary (by a very wide range) the effective mass of cooling water delivered to the core. Hence, the selection of the injection flow rates can result in MELCOR predictions of plant damage ranging from nearly zero core damage at 96 hours to complete lower head failure before 50 hours. For a more mechanistic simulation, specific information for the pumps and flow paths used to deliver the injection water is necessary.

As currently modeled by SNL, most of the core oxidation is occurring around 44-50 hours, and all of the hydrogen is being vented (via an assumed failure of the wetwell vent line (see Section 3.6.1.4) to the reactor building from the S/C, where it promptly leaks out (Figure 59). Because of this, hydrogen is not predicted to be present in sufficient quantities at the time of the observed hydrogen explosion. Further modifications to the freshwater and seawater injection models could allow some core oxidation to occur after the first few wetwell vents (after 58 hours). Hydrogen generated after 58 hours would be stored in the wetwell, where it could then move to the lower reactor building by the fourth modeled wetwell vent at 67.6 hours. If multiple or extended periods of in-vessel oxidation was the source of the flammable gases for the explosion, there would have to be less early core damage in order to preserve sufficient metal mass for further oxidation reactions closer to the time of the explosion.

It is uncertain how the flammable gases responsible for the Unit 3 explosion were generated (in-vessel and/or ex-vessel), as well as the exact timing of the gas generation. For example, if hydrogen generation near 40 hours caused the Unit 3 explosion, it is uncertain how hydrogen gas could linger for ~24 hours. Similarly, if gas generation near 60 hours in Unit 3 somehow transported to Unit 4, it is uncertain how this flammable gas remained in the Unit 4 building for ~20 hours (the Unit 3 explosion severed the piping that connected Unit 3 and Unit 4).

Alternative scenarios to explain the Unit 3 explosion include: ex-vessel core-concrete interactions generating flammable hydrogen and carbon-monoxide gases (which would also pressurize the containment around 60 hours and provide heavier carbon-monoxide gas for the Unit 4 explosion), hydrogen generated around 40 hours being trapped in piping for ~24 hours and eventually leaking into the reactor building at 68 hours, and flammable gases leaking from containment penetrations into the reactor building around 60 hours. Heavier carbon-monoxide gas, generated in Unit 3 by MCCI around 60 hours, may be more likely to have been transported to the Unit 4 reactor building, where it could accumulate and remain for approximately 20 hours to cause the Unit 4 explosion (87.2 hours after Unit 3 scram).

Uncertainties that impact the transport of radionuclides include details concerning the containment failure (mode, location, timing, etc.) and the reactor building (compartments, flow paths, etc.). Further refinement of these modeling features would reduce uncertainty in the radionuclide dispersal, hydrogen transport, and the predicted timing of the hydrogen explosion.

9.5.2   SNL Release of Fission Products

The MELCOR 2.1 simulation of the Unit 3 reactor predicts low overall fission product release to the environment (see Figure 61 from Section 4.3). The only substantial radionuclide release is the noble gas group. Approximately 86% of the noble gas group is released to the environment. The initial inventory of the noble gas group is 360 kg, which includes the radioactive elements xenon, krypton, and radon. Less than 1.0% of the other radionuclide classes are released to the environment. Currently, the calculated radionuclide releases do not take into account the reactor building explosion at 68 hours.

9.5.3   Comparisons to other Codes

The basic trends in RPV and containment pressures calculated using MELCOR are similar to MAAP calculations performed by TEPCO [19]. Differences between thermal-hydraulic calculations using MAAP and MELCOR (temperatures, pressures, water levels, etc.) are most likely attributable to assumptions in the modeling of RCIC/HPCI, containment sprays, and seawater injection. Furthermore, gross predictions of core degradation appear quite similar. Both MELCOR and MAAP predict a partially degraded core configuration for Unit 3, with roughly 50% of the fuel having been damaged and relocated, but most of the fuel still remaining in the original active region of the core (see Figure 60) [19, 38]. Table 28 provides a comparison of core damage predictions from early MELCOR simulations by JNES [20], early [20] and recent [19] MAAP simulations by TEPCO, and the MELCOR results from the current study. In general, the predicted timings are quite similar; however, ORNL predicts earlier core uncovery and damage as a result of the assumption of degraded HPCI performance.

Table 28. A comparison of MAAP and MELCOR Results for Unit 3 Core Damage

Code	Core Uncovering (Hours after Scram)	Start of Core Damage (Hours after Scram)
MAAP-TEPCO [20]	40	42
MELCOR-JNES [20]	41	44
MAAP-TEPCO [19]	40.0 – 41.0	42.0 – 44.0
MELCOR-SNL	42.33	43.76
MELCOR-ORNL	35 - 39	37-41.5

Table 29 compares TEPCO MAAP and SNL MELCOR calculations of the radionuclide release to the environment for Unit 3. The environmental releases calculated by MAAP and MELCOR, normalized to the initial core inventories, are reasonably similar for the noble gases, alkali metals (Cs), cesium-iodide, and Chalcogens (Te) radionuclide classes.

Table 29. MAAP and MELCOR Predictions of Radionuclide Release for Unit 3

213

Code	Noble gases (Xe)	Cesium-iodide (CsI)	Alkali metals (Cs)	Chalcogens (Te)	Alkaline earths (Ba)	Platinoids (Ru)	Tetravalent (La)
MAAP(1)*	6.5E-01	8.2E-03	5.9E-03	2.7E-03	6.1E-04	2.9E-10	2.7E-08
MAAP(2)*	9.9E-01	3.0E-03	2.7E-03	2.4E-03	4.3E-04	8.6E-10	1.3E-07
MELCOR	8.6E-01	3.2E-03	1.9E-03	2.0E-03	1.7E-05	1.8E-05	1.5E-09

* From Table 4 in the NISA report "Regarding the Evaluation of the Conditions on Reactor Cores of Unit 1, 2 and 3 related to the Accident at Fukushima Daiichi Nuclear Power Station, Tokyo Electric Power Co. Inc." [19]

9.5.4 Status of MELCOR Validation

The SNL and ORNL MELCOR simulations of Unit 3 have been compared to TEPCO data, TEPCO MAAP analyses, and JNES MELCOR analyses. Generally, the various severe accident analyses have yielded similar predictions of thermal-hydraulic conditions in the plant, and similar predictions of the degree of core damage in Unit 3. That said, various sensitivity analyses performed by TEPCO and JNES have also produced results where partial release of core materials via penetration failures illustrate the sensitivity of outcomes on the assumed injection rates. Compared to the TEPCO pressure data for the RPV and containment, MELCOR calculates pressures in close agreement during most of the initial transient. Deviations from the data, such as the initial 0-20 hour pressurization of the containment, have already been discussed. The overall effects of the differences in code results and their deviations from the plant data needs to be evaluated in detail by further research.

9.5.5 Potential Future Activities

There are several areas for further research of the severe accident at the Unit 3 reactor. The following list describes a few areas of potential work that would further the understanding of the severe accident at Unit 3, validate the current tools used for severe accident simulations, and provide new tools for predicting the long-term maintainability of reactor cores in degraded conditions.

1. The degree of core damage is very sensitive to:
    a. HPCI performance
    b. HPCI stop time and subsequent RPV re-pressurization
    c. Time difference between RPV de-pressurization and water injection
    d. Assumed water injection flow rates or pump model (already discussed)
    e. Core decay heat generation rate

SNL MELCOR simulations of Unit 3 have resulted in core damage ranging from zero fuel melt (only some Zircaloy/steel oxidation) up to nearly 100% fuel relocation, depending on the exact combination of the parameters listed above in a-d. The base cases SNL and ORNL for Unit 3 presented in this report do not exhibit lower head failure, but this could easily change with different seawater injection models (see Section 6.3.7). Parameter and sensitivity studies can be performed in order to quantitatively assess the various degrees of core damage that MELCOR can predict for Unit 3.

2. There is room for general model and code improvement:
   a. Higher fidelity vessel and containment models for truly "best-estimate" calculations (e.g. a multivolume suppression chamber)
   b. A new MELCOR model for non-reactor grade water
      This is required in order to simulate the effects of seawater corrosion (enhanced lower head failure), salt and organic material accumulation (reduction in flow), and the associated effects on the long-term coolability of reactor cores in degraded geometries.
   c. Longer transient simulations that take into account the long-term effects of that corrosion have on structural degradation of reactor cores in degraded conditions

3. There is a potential for sensitivity studies:
   a. The event timing of nearly everything from the timeline
   b. Freshwater and seawater injection
   c. Core and thermal-hydraulic nodalization, plant nodalization
   d. MELCOR sensitivity coefficients[26]

9.6 Spent Fuel Pool Conclusions

Analyses for the Unit 4 spent fuel pool were performed by SNL with MELCOR and by ORNL with TRACE. The ORNL TRACE results predict that it would take about 11 days for the pool water level to drop from the initial level to below the top of the fuel racks. The SNL MELCOR results show that it takes approximately 25 days for the same level drop to occur.

This difference in boildown time was found to be due to the inclusion of reactor building refueling bay in the MELCOR model, which traps water vapor over the spent fuel pool and hence reduces the rate of evaporation from the pool. When the reactor building refueling bay is removed from the MELCOR model, its level reduction results are consistent with those from the TRACE analysis. The integral assessment of this problem highlights the importance of building air exchange with the outside environment in terms of determining the relative humidity in the building, especially the region directly above the pool surface, and its effect on mass transport (evaporation) from the pool.

ORNL additionally performed assessments of water-added versus evaporation and determined that there was a relatively good mass balance and that no leakage of water from the pool was indicated.

---

[26] MELCOR sensitivity coefficients are user accessible parameters that allow changes to be made to the models used in the MELCOR code.

9.7　Status of Codes and Implications on Their Use

The analyses performed in this study have provided good examples of their application to real-world applications. In this context, MELCOR has been applied in a best estimate manner, without any of the conservatisms that are commonly used in such codes for regulatory applications. The analysis of the Unit 1 sequence is believed to be the most realistic and accurate of the three reactor analyses, mainly because the boundary and initial conditions are the most well characterized. Because this is a forensics exercise for the most part where only limited information on the accident progression is known, namely pressure response of the RPV and containment, it is natural that there may be many possible sequence interpretations that produce the same observed pressure signatures. This has been observed from the various interpretations that have been generated by different organizations analyzing these accidents. In modeling space, there are sometimes multiple solutions to the problem exhibiting the observed pressure history. For example, a recent MAAP analysis rendered by TEPCO suggested RPV depressurization by gasket degradation in the region around the SRV produces RPV and containment pressure responses that are essentially equivalent to the Unit 1 analysis offered in this report where main steam line rupture is predicted.

The analyses for Unit 2 and 3, while encouraging in terms of replicating observed RPV and containment response prior to core damage, are clearly less accurate that the Unit 1 analysis. The analyses performed by both MAAP and MELCOR reveal that there is something yet unidentified that affects the pressure response of the Unit 2 containment. The codes have supported the formulation of various theories concerning the pressure response, including the formation of a hole in the containment or alternatively the effect of possible flooding of the Unit 2 torus room. The codes provide us with a means to understand and diagnose what must have occurred in this respect. In analyzing the Unit 3 accident progression, the codes have successfully replicated the specific operation strategy of the HPCI system that was used by the operators to keep HPCI running continuously instead of cycling on and off as would occur with simple level control. This illustrates the code's ability to mimic real-world strategies for predicting plant response and their potential utility in designing or optimizing accident management procedures.

Uncertainty in the actual water injection flow following RPV depressurization dominates predicted core damage state in the analysis of Unit 2 and 3. It is believed that the analyses presented in this report underestimate, perhaps considerably, the true damage state of the Unit 2 and Unit 3 accidents. It is apparent from the measured data on pressures in the containment buildings, that low-pressure injection pumps situated outside of containment should have been challenged in pumping against such back-pressure, and it is likely that the actual injection flows were less than have been assumed in these analyses. Improvement in the analyses could be rendered by considering the actual pump-head characteristics of the pumps used to pump against the observed containment pressures.

Severe accident codes such as MELCOR and MAAP provide a valuable means of characterizing accidents such as the ones studied in this effort, revealing issues such as the Unit 2 containment pressure response, which might otherwise never be understood. Uncertainty and variability ensure that such analyses will render possibly wide variations in predicted sequence progression, and this is a reflection of true variability in the potential responses of complex systems.

10   REFERENCES

1. Bird, R.B., et al., Transport Phenomena, Second Edition, Wiley, 2007.

2. BWR Owners Group. "BWR Owners' Group: Emergency Procedure and Severe Accident Guidelines." BWR Owners' Group Emergency Procedures Committee, Rev. 2, General Electric Company: March 2001.

3. Carbajo, J.J. "Severe Accident Source Term Characteristics for Selected Peach Bottom Sequences Predicted by the MELCOR Code." NUREG/CR-5942, Oak Ridge National Laboratory: Oak Ridge, TN. July 1993

4. Chu, T.Y., et al. "Lower Head Failure Experiments and Analyses," NUREG/CR-5582, SAND98-2047, Sandia National Laboratories: Albuquerque, NM. October 1998.

5. Cook, D.H., "Pressure Suppression Pool Thermal Mixing," NUREG/CR-3471, ORNL/TM-8906, Oct. 1984.

6. Dresden Power Station Updated Final Safety Analysis Report, Rev. 9, June 2011, NRC docket STN 50-237 (Unit 2) and 50-249 (Unit 3).

7. http://www.engineeringtoolbox.com/evaporation-water-surface-d_690.html

8. Edwin I. Hatch Nuclear Power Plant Final Safety Analysis Report, Unit 2, Chapter 7, Rev 20, July 2002Durbin reference.

9. Durbin, S., "Hydraulic Analysis of the Spent Fuel Pool Experiment", Revision 4, Sandia National Laboratories Internal Memo dated 11/21/05.

10. Electric Power Research Institute. EPRI Software Product 1021648 Modular Accident Analysis Program (MAAP5) Version 5.0.1 for Windows – NQA, December 2011

11. Francis, M. W., Long-Term Station Blackout Sequence and Mitigation MELCOR Model. A Thesis Presented for the Master of Science Degree, the University of Tennessee, Knoxville TN. May 2006.

12. Gauntt, R.O., et al. "The DF-4 Fuel Damage Experiment in ACRR with a BWR Control Blade and Channel Box", NUREG/CR-4671, SAND86-1443 (1989).

13. Gauntt, R.O., et al, "MELCOR Best Practices. to be published as a NUREG Report, Nuclear Regulatory Commission: Washington DC. 2012.

14. Ilas, G. and Gauld, I.C.,, "Analysis of Decay Heat Measurements for BWR Fuel Assemblies," Trans. Am. Nuc. Soc. 94, 2006.

15. Institute of Nuclear Power Operators (INPO), "Special Report on the Nuclear Accident at the Fukushima Daiichi Nuclear Power Station," Revision 0, INPO 11-005, November 2011.
    http://www.nei.org/filefolder/11_005_Special_Report_on_Fukushima_Daiichi_MASTER_11_08_11_1.pdf

16. Incropera, F.P., et al., Fundamentals of Heat and Mass Transfer, Sixth Edition, Wiley, 2007.

17. Leonard, M.T., Nause, R.C., and Gauntt, R.O. "A General Purpose MELCOR Model of a BWR/4 Mark I Nuclear Power Plant," DRAFT, Sandia National Laboratories, Albuquerque, NM. 2008.

18. Natesan, K., and Scoppet, W.K., "Air Oxidation Kinetics for Zr-Based Alloys", NUREG/CR-6846, Argonne National Laboratories, June 2004.

19. NISA News Release, "Regarding the Evaluation of the Conditions on Reactor Cores of Unit 1, 2 and 3 related to the Accident at Fukushima Daiichi Nuclear Power Station, Tokyo Electric Power Co. Inc," June 6, 2011.

20. Nuclear Emergency Response Headquarters, Government of Japan, "Report of Japanese Government to the IAEA Ministerial Conference on Nuclear Safety - The Accident at TEPCO's Fukushima Nuclear Power Stations", June 2011. http://www.kantei.go.jp/foreign/kan/topics/201106/iaea_houkokusho_e.html

21. Nuclear Emergency Response Headquarters, Government of Japan, "Additional Report of Japanese Government to the IAEA - The Accident at TEPCO's Fukushima Nuclear Power Stations (Second Report)", Sept. 2011. http://www.meti.go.jp/english/earthquake/nuclear/iaea/iaea_110911.html

22. Oak Ridge National Laboratory, "SCALE: A Modular Code System for Performing Standardized Computer Analyses for Licensing Evaluations," ORNL/TM-2005/39, Version 5.1, Vols. I-III, Oak Ridge National Laboratory: Oak Ridge, TN. November 2006.

23. "Peach Bottom Atomic Power Station Final Safety Analysis Report," Rev. 14, Exelon Nuclear, May 1997.

24. Petti, D.A., et al., "Power Burst Facility (PBF) Severe Fuel Damage Test 1-4 Test Results", NUREG/CR-5163 (1989).

25. Philadelphia Electric Company, "Individual Plant Examination, Peach Bottom Atomic Power Station, Units 2 and 3," August 1992.

26. Powers, D.A, et al. "Accident Source Terms for Light-Water Nuclear Power Plants Using High-Burnup or MOX Fuel," SAND2011-0128, Sandia National Laboratories: Albuquerque, NM. January 2011.

27. Rempe, J.L., et al. "Light Water Reactor Lower Head Failure Analysis," NUREG/CR-5642, EGG-2618, Idaho National Engineering Laboratory: Idaho Falls, ID. September 1993

28. Sanders, R.L., "Analysis of a MELCOR Input Deck for the Peach Bottom Atomic Power Station." Oak Ridge National Laboratory, ORNL/NRC/LTR-03/03, 2003.

29. Sandia National Laboratories, "MELCOR Computer Code Manuals," Version 2.1, DRAFT.

30. Schwarz, M., et al. "Applicability of Phebus FP Results to Severe Accident Safety Evaluations and Accident Management"' Nuc. Eng. Design 209, 173-181 (2001).

31.   Shaukat, S.K., Jackson, J.E., Thatcher, D.F., "Regulatory Analysis for Generic Issue 23: Reactor Coolant Pump Seal Failure", U.S. Nuclear Regulator Commission, NUREG-1401, draft report, April 1991.

32.   Soffer, L, et al. "Accident Source Terms for Light-Water Nuclear Power Plants," NUREG-1465, U.S. Nuclear Regulatory Commission: Washington, DC. February, 1995.

33.   Theofanous, T.G., et al. "The Probability of Liner Failure in a Mark I Containment," NUREG/CR-5423, U.S. Nuclear Regulatory Commission: Washington DC. 1989.

34.   Tokyo Electric Power Company (TEPCO), "Fukushima Daiichi Nuclear Power Station Unit3 Parameters of Water level and Pressure", accessed Dec. 1, 2011. http://www.tepco.co.jp/en/nu/fukushima-np/f1/images/csv_level_pr_data_3u-e.csv.

35.   Tokyo Electric Power Company (TEPCO), "Fukushima Daiichi Nuclear Power Station Unit3 Parameters of Temperature", accessed Dec. 1, 2011. http://www.tepco.co.jp/en/nu/fukushima-np/f1/images/csv_temp_data_3u-e.csv.

36.   Tokyo Electric Power Company (TEPCO), "Unit 3, 4 Shift Supervisor Task Handover", English translation, accessed Dec. 1, 2011. http://www.tepco.co.jp/en/nu/fukushima-np/plant-data/f1_4_Nisshi3_4.pdf.

37.   Tokyo Electric Power Company (TEPCO), "Volume of water injected into the reactor of Unit 1 to Unit 3 of Fukushima Nuclear Power Station," May 31, 2011. http://www.tepco.co.jp/en/nu/fukushima-np/f1/images/110613sanko_table_tyusui-e.pdf.

38.   Tokyo Electric Power Company, "Reactor core conditions of unit 1-3 of Fukushima Daiichi Nuclear Power Station," November 30, 2011.

39.   Tokyo Electric Power Company, "Fukushima Nuclear Accident Aanlysis Report (Interim Report)", December 2, 2011.

40.   US. NRC. "MELCOR Computer Code Manuals, Volume 3: Demonstration Problems, Version 1.8.5, May 2001s," NUREG/CR-6119, Volume 3, Rev. 0, U.S. Nuclear Regulatory Commission: Washington DC. 2001.

41.   US. NRC. "State-of-the-Art Reactor Consequence Analysis Project, Volume 1: Peach Bottom Integrated Analysis," NUREG/CR-7110, Volume 1, U.S. Nuclear Regulatory Commission: Washington DC. 2012.

42.   Ross, K.W., Wagner, K.C., and Gauntt, R.O., "Analysis of Spent Fuel Pool Flow Patterns Using Computational Fluid Dynamics: Part 2 – Partial Water Cases", Sandia National Laboratories, Informal Report, April 2003.

43.   Wagner, K.C., and Gauntt, R.O., "Evaluation of a BWR Spent Fuel Pool Accident Response to Loss-of-Coolant Inventory Scenarios Using MELCOR 1.8.5", Sandia National Laboratories, Draft Informal Report, Revision 2, December 2004.

44.   Private Communication from K. Tateiwa to D. Peko, February 15, 2012.

45.   Private Communication from M.T. Leonard to Don Kalinich, June 2012.

46.   Private Communication from TEPCO to Randy Gauntt, April 2012.

47.   Yamanaka, Y., "Research plan regarding improvement of simulation code for understanding the status of fuel debris in the reactor," Int. Symposium on the

Decommissioning of TEPCO's Fukushima Daiichi Nuclear Power Plant Unit 1-4, Mar. 14, 2012.

APPENDIX A FUKUSHIMA DAIICHI ACCIDENT STUDY INFORMATION PORTAL

Fukushima Daiichi Accident Study Information Portal

Table of Contents

Fukushima Daiichi Accident Study
Information Portal

Fukushima Daiichi Accident Study
Information Portal

Introduction

The accident at the Fukushima Daiichi nuclear power station in Japan is one of the most serious in commercial nuclear power plant operating history. As its story unfolds, much will be learned that may be applicable to the U.S. reactor fleet, nuclear fuel cycle facilities and supporting systems, and the international reactor fleet. For example, lessons from Fukushima may be applied to emergency response planning, reactor operator training, accident scenario modeling, human factors engineering, radiation protection, and accident mitigation; as well as influence U.S. policies towards the nuclear fuel cycle including power generation, and spent fuel storage, reprocessing, and disposal.

The NRC and DOE NE have agreed to jointly sponsor an accident reconstruction study. The study team will include subject matter experts from Idaho National Laboratory (INL), Oak Ridge National Laboratory (ORNL), and Sandia National Laboratories (SNL).

The intent of this portal is to provide an approach to collecting, storing, retrieving, and validating information and data for use in reconstructing the Fukushima accidents and to assist the other team members by providing support for the technical basis behind the event reconstruction.

Unit 1 Timeline

Friday, March 11, 2011

Time	Event
12:00:00 PM	Isolation Condenser - Actuation Train - IC A - Standby
12:00:00 PM	High Pressure Coolant Injection - Turbine driven pump - HPCI - Standby
12:00:00 PM	Service Water System - Motor driven pump - CCSW - Operating
12:00:00 PM	DC Power - Battery - 125 V Battery - Operating
12:00:00 PM	Power Conversion - Main steam isolation valve - MSIVs - Normally Open; Not failed
12:00:00 PM	Offsite Electrical Power - System level event - Offsite Power Sources - Operating
12:00:00 PM	Reactor Protection - Actuation Train - Reactor - Operating
12:00:00 PM	AC Power System - Emergency diesel generator - EDG 2 - Standby
12:00:00 PM	AC Power System - Emergency diesel generator - EDG 1 - Standby
2:46:00 PM	Earthquake (Tohoku)
2:46:00 PM	Unit 1 Shut Down
2:46:01 PM	Reactor Protection - Actuation Train - Reactor - Reactor Scram
2:47:00 PM	Offsite Electrical Power - System level event - Offsite Power Sources - No power-loss of power
2:47:00 PM	Power Conversion - Main steam isolation valve - MSIVs - Normally open; fail in closed position
2:47:00 PM	AC Power System - Emergency diesel generator - EDG 2 - Automatically Started
2:47:00 PM	AC Power System - Emergency diesel generator - EDG 1 - Automatically Started
2:47:00 PM	Loss of Offsite Power
2:52:00 PM	Isolation Condenser - Actuation Train - IC B - Automatically Started
2:52:00 PM	Isolation Condenser - Actuation Train - IC A - Automatically Started
3:02:00 PM	Unit 1 subcriticality confirmed
3:03:00 PM	Isolation Condenser - Actuation Train - IC B - Manually Shutdown
3:03:00 PM	Isolation Condenser - Actuation Train - IC A - Manually Shutdown
3:27:00 PM	1st Tsunami wave hits unit 1
3:35:00 PM	2nd Tsunami wave hits unit 1
3:37:00 PM	High Pressure Coolant Injection - Turbine driven pump - HPCI - Fail to start
3:37:00 PM	Service Water System - Motor driven pump - CCSW - Fail to continue running
3:37:00 PM	DC Power - Battery - 125 V Battery - Fail to operate
3:37:00 PM	AC Power System - Emergency diesel generator - EDG 2 - Fail to continue running
3:37:00 PM	AC Power System - Emergency diesel generator - EDG 1 - Fail to continue running
3:37:00 PM	Station Blackout, Unit 1
5:30:00 PM	Firewater Injection - Engine driven pump - Diesel driven fire pump - Manually Started
6:18:00 PM	Isolation Condenser - Actuation Train - IC A - Manually Started
6:25:00 PM	Isolation Condenser - Actuation Train - IC A - Manually Shutdown
8:07:00 PM	Reactor pressure checked locally in reactor building, 1015 psia

8:49:00 PM MCR lit by temporary lighting

9:30:00 PM Isolation Condenser - Actuation Train - IC A - Manually Started

11:50:00 PM Restoration team provides temp power to MCR. D/W pressure 87 psia (600 kPaa)

Saturday, March 12, 2011

1:48:00 AM Firewater Injection - Engine driven pump - Diesel driven fire pump - Fail to continue running

2:30:00 AM Drywell pressure had increased to 122 psia (.84 MPaa).

2:45:00 AM Reactor pressure checked, 131 psia (901 kPaa)

4:19:00 AM Drywell pressure lowered and stabilized without venting to 113 psia(.78 MPaa)

5:46:00 AM Firewater Injection - Engine driven pump - Fire Engine - Manually Started

11:00:00 AM Isolation Condenser - Actuation Train - IC A - Fail to continue running

2:30:00 PM Containment Vent - Air operated valve - S/C Large vent valve - Manually Opened

2:30:00 PM   Venting Suppression Chamber began

2:50:00 PM Drywell pressure decreases, indicating venting successful.

2:53:00 PM Firewater Injection - Engine driven pump - Fire Engine - Loss of function

3:36:00 PM Hydrogen Explosion

7:04:00 PM Firewater Injection - Engine driven pump - Fire Engine - Manually Started

8:45:00 PM Boric acid added to seawater

Fukushima Daiichi Accident Study
Information Portal

Unit 2 Timeline

Friday, March 11, 2011

12:00:00 PM	High Pressure Coolant Injection - Turbine driven pump - HPCI - Standby
12:00:00 PM	Residual Heat Removal Service Water - Motor driven pump - RHRS - Standby
12:00:00 PM	Service Water System - Motor driven pump - CCSW - Operating
12:00:00 PM	DC Power - Battery - 125 V Battery - Operating
12:00:00 PM	Reactor Core Isolation Cooling - Turbine driven pump - RCIC system - Standby
12:00:00 PM	Offsite Electrical Power - System level event - Offsite Power Sources - Operating
12:00:00 PM	Power Conversion - Main steam isolation valve - MSIVs - Normally Open; Not failed
12:00:00 PM	Reactor Protection - Actuation Train - Reactor - Operating
12:00:00 PM	AC Power System - Emergency diesel generator - EDG 2 - Standby
12:00:00 PM	AC Power System - Emergency diesel generator - EDG 1 - Standby
2:46:00 PM	Earthquake (Tohoku)
2:47:00 PM	Offsite Electrical Power - System level event - Offsite Power Sources - No power-loss of power
2:47:00 PM	Power Conversion - Main steam isolation valve - MSIVs - Normally open; fail in closed position
2:47:00 PM	Reactor Protection - Actuation Train - Reactor - Reactor Scram
2:47:00 PM	AC Power System - Emergency diesel generator - EDG 2 - Automatically Started
2:47:00 PM	AC Power System - Emergency diesel generator - EDG 1 - Automatically Started
2:47:00 PM	Loss of Offsite Power
2:47:00 PM	Unit 2 Shutdown
2:50:00 PM	Reactor Core Isolation Cooling - Turbine driven pump - RCIC system - Manually Started
2:51:00 PM	Reactor Core Isolation Cooling - Turbine driven pump - RCIC system - Automatically Shutdown
3:00:00 PM	Residual Heat Removal Service Water - Motor driven pump - RHRS - Manually Started
3:01:00 PM	Unit 2 subcriticality confirmed
3:02:00 PM	Reactor Core Isolation Cooling - Turbine driven pump - RCIC system - Manually Started
3:07:00 PM	Torus cooling placed in service
3:25:00 PM	Torus spray placed in service
3:27:00 PM	1st Tsunami wave hits unit 2
3:28:00 PM	Reactor Core Isolation Cooling - Turbine driven pump - RCIC system - Automatically Shutdown
3:35:00 PM	2nd Tsunami wave hits unit 2
3:39:00 PM	Reactor Core Isolation Cooling - Turbine driven pump - RCIC system - Manually

Started
3:41:00 PM High Pressure Coolant Injection - Turbine driven pump - HPCI - Fail to start
3:41:00 PM Residual Heat Removal Service Water - Motor driven pump - RHRS - Fail to continue
running
3:41:00 PM Service Water System - Motor driven pump - CCSW - Fail to continue running
3:41:00 PM DC Power - Battery - 125 V Battery - Fail to operate
3:41:00 PM AC Power System - Emergency diesel generator - EDG 2 - Fail to continue running
3:41:00 PM AC Power System - Emergency diesel generator - EDG 1 - Fail to continue running
3:41:00 PM Station Blackout, Unit 2
8:49:00 PM MCR lit by temporary lighting
9:50:00 PM Reactor water level 3,400 mm > TAF
11:25:00 PM Drywell pressure indication restored. DW pressure 20 psia (.141 MPaa)
Saturday, March 12, 2011
2:00:00 AM RCIC verified to be operating
4:20:00 AM RCIC suction swapped (CST to torus)
Monday, March 14, 2011
1:18:00 PM Reactor water level 2400 mm > TAF
1:25:11 PM Reactor Core Isolation Cooling - Turbine driven pump - RCIC system - Fail to continue
running
4:43:00 PM Below Top of Active Fuel (TAF)
5:12:00 PM Reactor Pressure 1088 psia, too high for seawater injection
5:17:00 PM Reactor water level decreased to TAF
6:03:00 PM Reactor depressurization begins
6:06:00 PM Main Steam - Safety relief valve - SRV - Manually Opened
6:30:00 PM Firewater Injection - Engine driven pump - Fire Engine - Manually Started
7:03:00 PM Reactor pressure stabilizes following depressurization
7:20:00 PM Firewater Injection - Engine driven pump - Fire Engine - Fail to continue running
7:54:00 PM Firewater Injection - Engine driven pump - Fire Engine - Manually Started
9:03:00 PM Reactor pressure increasing
9:20:00 PM Main Steam - Safety relief valve - SRV - Manually Opened
10:50:00 PM Drywell pressure exceeds design pressure
Tuesday, March 15, 2011
12:45:00 AM Injection not likely at this pressure
6:00:00 AM Loud Noise Reported
11:25:00 AM Drywell pressure decreased, likely related to loud noise heard at 0600

Fukushima Daiichi Accident Study
Information Portal

Unit 3 Timeline

Friday, March 11, 2011

12:00:00 PM	DC Power - Battery - 125 V Battery - Operating
12:00:00 PM	High Pressure Coolant Injection - Turbine driven pump - HPCI - Standby
12:00:00 PM	Residual Heat Removal Service Water - Motor driven pump - RHRS - Standby
12:00:00 PM	Service Water System - Motor driven pump - CCSW - Operating
12:00:00 PM	Reactor Core Isolation Cooling - Turbine driven pump - RCIC system - Standby
12:00:00 PM	Power Conversion - Main steam isolation valve - MSIVs - Normally Open; Not failed
12:00:00 PM	Offsite Electrical Power - System level event - Offsite Power Sources - Operating
12:00:00 PM	Reactor Protection - Actuation Train - Reactor - Operating
12:00:00 PM	AC Power System - Emergency diesel generator - EDG 2 - Standby
12:00:00 PM	AC Power System - Emergency diesel generator - EDG 1 - Standby
2:46:00 PM	Earthquake (Tohoku)
2:47:00 PM	Offsite Electrical Power - System level event - Offsite Power Sources - No power-loss of power
2:47:00 PM	Reactor Protection - Actuation Train - Reactor - Reactor Scram
2:47:00 PM	AC Power System - Emergency diesel generator - EDG 2 - Automatically Started
2:47:00 PM	AC Power System - Emergency diesel generator - EDG 1 - Automatically Started
2:47:00 PM	Loss of Offsite Power
2:47:00 PM	Unit 3 Shutdown
2:48:00 PM	Power Conversion - Main steam isolation valve - MSIVs - Normally open; fail in closed position
2:54:00 PM	Unit 3 subcriticallity confirmed
3:05:00 PM	Reactor Core Isolation Cooling - Turbine driven pump - RCIC system - Manually Started
3:25:00 PM	Reactor Core Isolation Cooling - Turbine driven pump - RCIC system - Automatically Shutdown
3:27:00 PM	1st Tsunami Wave hits Unit 3
3:35:00 PM	2nd Tsunami Wave hits unit 3
3:38:00 PM	Station Blackout, Unit 3
3:41:00 PM	Residual Heat Removal Service Water - Motor driven pump - RHRS - Fail to start
3:41:00 PM	Service Water System - Motor driven pump - CCSW - Fail to continue running
3:41:00 PM	AC Power System - Emergency diesel generator - EDG 2 - Fail to continue running
3:41:00 PM	AC Power System - Emergency diesel generator - EDG 1 - Fail to continue running
4:03:00 PM	Reactor Core Isolation Cooling - Turbine driven pump - RCIC system - Manually Started
9:58:00 PM	Temporary lighting for unit 3 MCR

Saturday, March 12, 2011

11:36:00 AM Reactor Core Isolation Cooling - Turbine driven pump - RCIC system - Fail to continue running

12:10:00 PM Primary pressure had slowly increased to 57 psia (0.39 MPaa)

12:35:00 PM High Pressure Coolant Injection - Turbine driven pump - HPCI - Automatically Started

9:30:00 PM DC Power - Battery - 125 V Battery - Fail to operate

Sunday, March 13, 2011

2:42:00 AM High Pressure Coolant Injection - Turbine driven pump - HPCI - Fail to continue running

5:00:00 AM Reactor Pressure had increased to 1,085 psia (7.48 MPa abs).

7:45:00 AM Drywell pressure had increased to 67 psia (.46 Mpaa)

9:08:00 AM Main Steam - Safety relief valve - SRV - Manually Opened

9:20:00 AM Containment Vent - Air operated valve - S/C Large vent valve - Manually Opened

9:20:00 AM Venting determined to have started.

9:24:00 AM Drywell Pressure lowering, venting successful.

9:25:00 AM Firewater Injection - Engine driven pump - Fire Engine - Manually Started

11:17:00 AM Containment Vent - Air operated valve - S/C Large vent valve - Normally closed; fail in the closed position

12:20:00 PM Firewater Injection - Engine driven pump - Fire Engine - Fail to continue running

12:30:00 PM Containment Vent - Air operated valve - S/C Large vent valve - Manually Opened

1:12:00 PM Firewater Injection - Engine driven pump - Fire Engine - Manually Started

3:00:00 PM Containment Vent - Air operated valve - S/C Large vent valve - Normally closed; fail in the closed position

8:10:00 PM Containment Vent - Air operated valve - S/C Large vent valve - Manually Opened

Monday, March 14, 2011

1:00:00 AM Containment Vent - Air operated valve - S/C Large vent valve - Normally closed; fail in the closed position

1:10:00 AM Firewater Injection - Engine driven pump - Fire Engine - Fail to continue running

3:20:00 AM Firewater Injection - Engine driven pump - Fire Engine - Manually Started

6:10:00 AM S/C small vent valve opened

11:01:00 AM Firewater Injection - Engine driven pump - Fire Engine - Fail to continue running

11:01:00 AM Hydrogen Explosion

4:30:00 PM Firewater Injection - Engine driven pump - Fire Engine - Manually Started

Tuesday, March 15, 2011

4:05:00 PM Containment Vent - Air operated valve - S/C Large vent valve - Manually Opened

Unit 4 Timeline

Friday, March 11, 2011
    12:00:00 PM Unit 4 Initial Condition
    2:46:00 PM Earthquake (Tohoku)
    2:47:00 PM Loss of Offsite Power
    3:38:00 PM Station Blackout, Unit 4
Tuesday, March 15, 2011
    6:00:00 AM Explosion in Unit 4 reactor building
    6:00:00 AM Loud Noise Reported

Unit 5 Timeline

Friday, March 11, 2011
    12:00:00 PM Initial Conditions of Unit 5
    2:46:00 PM Earthquake (Tohoku)
    2:47:00 PM Loss of Offsite Power
    3:40:00 PM Station blackout, Unit 5
Sunday, March 20, 2011
    2:30:00 PM Unit 5 Achieves Cold Shutdown

Fukushima Daiichi Accident Study
Information Portal

Unit 6 Timeline

Friday, March 11, 2011
    12:00:00 PM Initial Conditions of Unit 6
    2:46:00 PM Earthquake (Tohoku)
    2:47:00 PM Loss of Offsite Power
    3:40:00 PM EDG status after Tsunami
Sunday, March 20, 2011
    7:27:00 PM Unit 6 achieves cold shutdown

Event Details

3/11/2011 12:00:00 PM Initial Conditions of Unit 5
Description: Unit 5 was in an outage with fuel assemblies in the core and RPV intact.
Applicable Locations: Unit5
Applicable Artifacts:
- Report of the Japanese Government to the IAEA Ministerial Conference on Nuclear Safety. Chapter iv.

3/11/2011 12:00:00 PM Initial Conditions of Unit 6
Description: Unit 6 was in an outage with all fuel assemblies loaded in the core and in cold shutdown mode.
Applicable Locations: Unit6
Applicable Artifacts:
- Report of the Japanese Government to the IAEA Ministerial Conference on Nuclear Safety. Chapter iv.

3/11/2011 12:00:00 PM Unit 4 Initial Condition
Description: Unit 4 was in an outage with the core offloaded to the spent fuel pool.
Applicable Locations: Unit4
Applicable Artifacts:
- Report of the Japanese Government to the IAEA Ministerial Conference on Nuclear Safety. Chapter iv.

3/11/2011 2:46:00 PM Earthquake (Tohoku)
Description: A major earthquake occurred located off the coast of the Miyagi Prefecture.
Cause: Earthquake
Applicable Locations: Unit1, Unit2, Unit3, Unit4, Unit5, Unit6, On-Site, Off-Site
Applicable Artifacts:
- Additional Report of the Japanese Government to the IAEA - The accident at TEPCO's Fukushima Nuclear Power Stations - (Second Report)

3/11/2011 2:46:00 PM Unit 1 Shut Down
Description: Reactor Scram, Turbine Trip, all control rods fully inserted.
Cause: Automated Action
Applicable Locations: Unit1
Applicable Artifacts:
- Chronology of Main Events at Fukushima Daiichi Nuclear Power Station

[Unit 1 from Impact of Earthquake through Saturday, March 12]

3/11/2011 2:47:00 PM Loss of Offsite Power
    Description: Loss of all offsite power sources.
    Cause: Loss of Power
    Applicable Locations: Unit1, Unit2, Unit3, Unit4, Unit5, Unit6, On-Site, Off-Site
    Applicable Artifacts:
- [Report of the Japanese Government to the IAEA Ministerial Conference on Nuclear Safety. Chapter iv.]

3/11/2011 2:47:00 PM Unit 2 Shutdown
    Description: Reactor Scram, Turbine Trip, all control rods fully inserted.
    Cause: Automated Action
    Applicable Locations: Unit2
    Applicable Artifacts:
- [Report of the Japanese Government to the IAEA Ministerial Conference on Nuclear Safety. Chapter iv.]

3/11/2011 2:47:00 PM Unit 3 Shutdown
    Description: Reactor scram, turbine trip, all control rods fully inserted.
    Cause: Automated Action
    Applicable Locations: Unit3
    Applicable Artifacts:
- [Report of the Japanese Government to the IAEA Ministerial Conference on Nuclear Safety. Chapter iv.]

3/11/2011 2:54:00 PM Unit 3 subcriticallity confirmed
    Description: Unit 3 reactor verified subcritical
    Cause: Operator Action
    Applicable Locations: Unit3
    Applicable Artifacts:
- [Chronology of Main Events at Fukushima Daiichi Nuclear Power Station Unit 3 from Impact of Earthquake through Tuesday, March 15]

3/11/2011 3:01:00 PM Unit 2 subcriticality confirmed
    Description: Unit 2 reactor confirmed to be subcritical.
    Cause: Operator Action
    Applicable Locations: Unit2
    Applicable Artifacts:

- Chronology of Main Events at Fukushima Daiichi Nuclear Power Station Unit 2 from Impact of Earthquake through Tuesday, March 15

3/11/2011 3:02:00 PM Unit 1 subcriticality confirmed
Description: Reactor subcriticality confirmed.
Cause: Operator Action
Applicable Locations: Unit1
Applicable Artifacts:
- Chronology of Main Events at Fukushima Daiichi Nuclear Power Station Unit 1 from Impact of Earthquake through Saturday, March 12

3/11/2011 3:07:00 PM Torus cooling placed in service
Description: Torus cooling manually started.
Cause: Operator Action
Applicable Locations: Unit2
Applicable Artifacts:
- Special Report on the Nuclear Accident at the Fukushima Daiichi Nuclear Power Station.

3/11/2011 3:25:00 PM Torus spray placed in service
Description: Torus spray manually started.
Cause: Operator Action
Applicable Locations: Unit2
Applicable Artifacts:
- Special Report on the Nuclear Accident at the Fukushima Daiichi Nuclear Power Station.

3/11/2011 3:27:00 PM 1st Tsunami wave hits unit 1
Description: Tsunami Wave generated by the earthquake strikes the plant
Cause: Earthquake
Applicable Locations: Unit1
Applicable Artifacts:
- Report of the Japanese Government to the IAEA Ministerial Conference on Nuclear Safety. Chapter iv.

3/11/2011 3:27:00 PM 1st Tsunami wave hits unit 2
Description: Tsunami Wave generated by the earthquake strikes the plant
Cause: Earthquake
Applicable Locations: Unit2
Applicable Artifacts:
- Report of the Japanese Government to the IAEA Ministerial Conference on Nuclear Safety.

Fukushima Daiichi Accident Study
Information Portal

3/11/2011 3:27:00 PM 1st Tsunami Wave hits Unit 3
    Description: Tsunami Wave generated by the earthquake strikes the plant
    Cause: Earthquake
    Applicable Locations: Unit3
    Applicable Artifacts:
- Additional Report of the Japanese Government to the IAEA - The accident at TEPCO's Fukushima Nuclear Power Stations - (Second Report)

3/11/2011 3:35:00 PM 2nd Tsunami wave hits unit 1
    Description: Tsunami Wave generated by the earthquake strikes the plant
    Cause: Earthquake
    Applicable Locations: Unit1
    Applicable Artifacts:
- Report of the Japanese Government to the IAEA Ministerial Conference on Nuclear Safety. Chapter iv.

3/11/2011 3:35:00 PM 2nd Tsunami wave hits unit 2
    Description: Tsunami Wave generated by the earthquake strikes the plant
    Cause: Earthquake
    Applicable Locations: Unit2
    Applicable Artifacts:
- Report of the Japanese Government to the IAEA Ministerial Conference on Nuclear Safety. Chapter iv.

3/11/2011 3:35:00 PM 2nd Tsunami Wave hits unit 3
    Description: Tsunami Wave strikes plant
    Cause: Earthquake
    Applicable Locations: Unit3
    Applicable Artifacts:
- Additional Report of the Japanese Government to the IAEA - The accident at TEPCO's Fukushima Nuclear Power Stations - (Second Report)

3/11/2011 3:37:00 PM Station Blackout, Unit 1
    Description: Loss of off site and on site AC power sources
    Cause: Tsunami Flooding
    Applicable Locations: Unit1
    Applicable Artifacts:

- [Report of the Japanese Government to the IAEA Ministerial Conference on Nuclear Safety. Chapter iv.](#)

3/11/2011 3:38:00 PM Station Blackout, Unit 3
Description: Loss of both offsite and onsite AC power sources.
Cause: Tsunami Flooding
Applicable Locations: Unit3
Applicable Artifacts:
- [Fukushima Accident: An overview.](#)

3/11/2011 3:38:00 PM Station Blackout, Unit 4
Description: Loss of all onsite and offsite AC power.
Cause: Tsunami Flooding
Applicable Locations: Unit4
Applicable Artifacts:
- [Report of the Japanese Government to the IAEA Ministerial Conference on Nuclear Safety. Chapter iv.](#)

3/11/2011 3:40:00 PM EDG status after Tsunami
Description: After the Tsunami flooding, EDGs 6A and 6H failed. EDG 6B continued to run and provided AC power.
Cause: Tsunami Flooding
Applicable Locations: Unit6
Applicable Artifacts:
- [Report of the Japanese Government to the IAEA Ministerial Conference on Nuclear Safety. Chapter iv.](#)

3/11/2011 3:40:00 PM Station blackout, Unit 5
Description: Loss of all onsite and offsite AC power sources.
Cause: Tsunami Flooding
Applicable Locations: Unit5
Applicable Artifacts:
- [Report of the Japanese Government to the IAEA Ministerial Conference on Nuclear Safety. Chapter iv.](#)

3/11/2011 3:41:00 PM Station Blackout, Unit 2
Description: Loss of off site and on site AC power.
Cause: Tsunami Flooding
Applicable Locations: Unit2

Fukushima Daiichi Accident Study
Information Portal

Applicable Artifacts:
- [Report of the Japanese Government to the IAEA Ministerial Conference on Nuclear Safety. Chapter iv.](#)

3/11/2011 8:49:00 PM MCR lit by temporary lighting
Description: Main Control Room lit by temporary lighting.
Cause: Operator Action
Applicable Locations: Unit1
Applicable Artifacts:
- [Chronology of Main Events at Fukushima Daiichi Nuclear Power Station Unit 1 from Impact of Earthquake through Saturday, March 12](#)

3/11/2011 8:49:00 PM MCR lit by temporary lighting
Description: Main control room lit by temporary lighting
Cause: Operator Action
Applicable Locations: Unit2
Applicable Artifacts:
- [Chronology of Main Events at Fukushima Daiichi Nuclear Power Station Unit 2 from Impact of Earthquake through Tuesday, March 15](#)

3/11/2011 9:50:00 PM Reactor water level 3,400 mm > TAF
Description: Reactor water level indication restored in control room. Vessel level indicated 3,400 mm above TAF.
Cause: Operator Action
Applicable Locations: Unit2
Applicable Artifacts:
- [Special Report on the Nuclear Accident at the Fukushima Daiichi Nuclear Power Station.](#)

3/11/2011 9:58:00 PM Temporary lighting for unit 3 MCR
Description: Temporary lighting established for unit 3 main control room using portable generator.
Cause: Operator Action
Applicable Locations: Unit3

3/12/2011 2:00:00 AM RCIC verified to be operating
Description: Workers verified RCIC pump discharge pressure in the field.
Cause: Operator Action
Applicable Locations: Unit2
Applicable Artifacts:
- [Special Report on the Nuclear Accident at the Fukushima Daiichi Nuclear Power Station.](#)

3/12/2011 4:20:00 AM RCIC suction swapped (CST to torus)
    Description: RCIC suction was swapped from the CST to the torus.
    Cause: Operator Action
    Applicable Locations: Unit2
    Applicable Artifacts:
- Report of the Japanese Government to the IAEA Ministerial Conference on Nuclear Safety. Chapter iv.

3/12/2011 2:30:00 PM   Venting Suppression Chamber began
    Description: Opened large suppression chamber vent valve with temporary air compressor. Release of radioactive material and decrease in containment pressure confirmed.
    Cause: Operator Action
    Applicable Locations: Unit1
    Applicable Artifacts:
- Fukushima Daiichi Nuclear Power Station Unit 1 Circumstances of Venting of Containment Vessel

3/12/2011 3:36:00 PM Hydrogen Explosion
    Description: Hydrogen Explosion in the Unit 1 Reactor Building
    Cause: Explosion
    Applicable Locations: Unit1
    Applicable Artifacts:
- Report of the Japanese Government to the IAEA Ministerial Conference on Nuclear Safety. Chapter iv.
- Damage to unit 1 after hydrogen explosion

3/12/2011 8:45:00 PM Boric acid added to seawater
    Description: Commenced adding boric acid to seawater injection
    Cause: Operator Action
    Applicable Locations: Unit1
    Applicable Artifacts:
- Chronology of Main Events at Fukushima Daiichi Nuclear Power Station Unit 1 from Impact of Earthquake through Saturday, March 12

3/13/2011 9:20:00 AM Venting determined to have started.
    Description: Venting determined to have successfully started due to decreasing containment pressure.
    Cause: Operator Action
    Applicable Locations: Unit3

Applicable Artifacts:
- Fukushima Daiichi Power Station Unit 3 Circumstances of Venting of Containment Vessel

3/14/2011 6:10:00 AM S/C small vent valve opened
Description: S/C small vent valve confirmed to have been opened, however containment pressure readings indicate little if any venting resulted.
Cause: Operator Action
Applicable Locations: Unit3

3/14/2011 11:01:00 AM Hydrogen Explosion
Description: Hydrogen Explosion in the Unit 3 Reactor Building
Cause: Explosion
Applicable Locations: Unit3
Applicable Artifacts:
- Report of the Japanese Government to the IAEA Ministerial Conference on Nuclear Safety. Chapter iv.
- Satellite image on March 14, 2011, at 11:04 am, three minutes after an explosion at Unit 3 (by Digital Globe).
Applicable Reviews:
- Review by: Shawn St. Germain Confidence Level: High
  Confidence high due to video taken at the time of the explosion.

3/14/2011 1:18:00 PM Reactor water level 2400 mm > TAF
Description: Reactor water level was 2400 mm above TAF and trending downward.
Cause: Operator Action
Applicable Locations: Unit2
Applicable Artifacts:
- Special Report on the Nuclear Accident at the Fukushima Daiichi Nuclear Power Station.

3/14/2011 5:17:00 PM Reactor water level decreased to TAF
Description: Indicated reactor water level decreased to TAF.
Cause: Loss of Power
Applicable Locations: Unit2

3/15/2011 6:00:00 AM Explosion in Unit 4 reactor building
Description: An explosion occured in the unit 4 reactor building. It is assumed to be caused by Hydrogen from venting unit 3.
Cause: Explosion
Applicable Locations: Unit4

Applicable Artifacts:
- Report of the Japanese Government to the IAEA Ministerial Conference on Nuclear Safety. Chapter iv.
- Additional Report of the Japanese Government to the IAEA - The accident at TEPCO's Fukushima Nuclear Power Stations - (Second Report)

3/15/2011 6:00:00 AM Loud Noise Reported
Description: A loud noise was heard. Possibly in the area of the torus (Unit 2) or from the explosions in Unit 4.
Cause: Unknown
Applicable Locations: Unit2, Unit4
Applicable Artifacts:
- Report of the Japanese Government to the IAEA Ministerial Conference on Nuclear Safety. Chapter iv.

3/20/2011 2:30:00 PM Unit 5 Achieves Cold Shutdown
Description: Unit 5 reaches cold shutdown conditions
Cause: Operator Action
Applicable Locations: Unit5
Applicable Artifacts:
- Report of the Japanese Government to the IAEA Ministerial Conference on Nuclear Safety. Chapter iv.

3/20/2011 7:27:00 PM Unit 6 achieves cold shutdown
Description: Unit 6 reaches cold shutdown conditions
Cause: Operator Action
Applicable Locations: Unit6
Applicable Artifacts:
- Report of the Japanese Government to the IAEA Ministerial Conference on Nuclear Safety. Chapter iv.

Fukushima Daiichi Accident Study
Information Portal

Artifact Details

Media File Artifacts

Description: Nuclear and Industrial Safety Agency (NISA) News Release
Source: NISA news release
File Name: en20110312-1.pdf

Description: The 2011 off the Pacific coast of Tohoku Pacific Earthquake and 4th April, 2011 the seismic damage to the NPPs.
Source: Japan Nuclear Energy Safety Organization (JNES)
File Name: 20110404 JNES Presentation.pdf

Description: Report of the Japanese Government to the IAEA Ministerial Conference on Nuclear Safety. Chapter iv.

Source: Nuclear Emergency Response Headquarters, Government of Japan, (June 2011)

File Name: chapter_iv_all.pdf

Description: Damage to unit 1 after hydrogen explosion
Source: ISIS
File Name: Damage to unit 1 after hydrogen explosion.jpg

Description: The Great East Japan Earthquake Expert Mission.
Source: IAEA
File Name: cn200_Final-Fukushima-Mission_Report.pdf

Description: Fukushima Accident: An overview.
Source: Akira Omoto, presentation.
File Name: ANS Omoto.pptx

Description: Additional Report of the Japanese Government to the IAEA - The accident at TEPCO's Fukushima Nuclear Power Stations - (Second Report)
Source: Second report from the Government of Japan to the IAEA (September 2011)
URL: http://www.meti.go.jp/english/earthquake/nuclear/iaea/iaea_110911.html

Description: INL Timeline data with injection rates
Source: Collection of timeline data from other sources
File Name: Fukushima Timeline Data with Injection Rates.pdf

Description: Chronology of Main Events at Fukushima Daiichi Nuclear Power Station
Unit 1 from Impact of Earthquake through Saturday, March 12
Source: Tepco Report
File Name: 08102011 1F Timeline-unit1.pdf

Description: Fukushima Daiichi Nuclear Power Station Unit 1
State of Alternate Coolant Injection
Source: TEPCO Report
File Name: 08102011 1F Timeline-unit1 injection.pdf

Description: Fukushima Daiichi Nuclear Power Station Unit 1
Circumstances of Venting of Containment Vessel
Source: TEPCO Report
File Name: 08102011 1F Timeline-unit1 vent.pdf

Description: Chronology of Main Events at Fukushima Daiichi Nuclear Power Station
Unit 2 from Impact of Earthquake through Tuesday, March 15
Source: TEPCO Report
File Name: 08102011 1F Timeline-unit2.pdf

Description: Fukushima Nuclear Power Station Unit 2 State of Alternate Coolant Injection
Source: TEPCO Report
File Name: 08102011 1F Timeline-unit2 injection.pdf

Description: Fukushima Daiichi Nuclear Power Station Unit 2 Circumstances of Venting of
Containment Vessel
Source: TEPCO Report
File Name: 08102011 1F Timeline-unit2 vent.pdf

Description: Chronology of Main Events at Fukushima Daiichi Nuclear Power Station Unit 3 from
Impact of Earthquake through Tuesday, March 15
Source: TEPCO Report

File Name: 08102011 1F Timeline-unit3.pdf

Description: Fukushima Daiichi Nuclear Power Station Unit 3 State of Alternate Coolant Injection
Source: TEPCO Report
File Name: 08102011 1F Timeline-unit3 injection.pdf

Description: Fukushima Daiichi Power Station Unit 3 Circumstances of Venting of Containment Vessel
Source: TEPCO Report
File Name: 08102011 1F Timeline-unit3 vent.pdf

Description: State of Immediate Response after Disaster Struck at Fukushima Daiichi Power Station
Source: TEPCO Report
File Name: 08102011 1F Timeline-general.pdf

Description: Radiation monitoring data for 3/14/11
Source: TEPCO
File Name: f1-mc-2011031424-e.xlsx

Description: Survey map of Fukushima Daiichi Nuclear Power Station on March 23, 2011
Source: TEPCO
File Name: f1-sv-20110323-e.pdf

Description: US DOE/NNSA Response to 2011 Fukushima Incident: Field Team Radiological Measurements
Source: US DOE
File Name: FieldMeasurements_DOE_1.xlsx

Description: Survey map of Fukushima Daiichi Nuclear Power Station on 3/31/11
Source: TEPCO
File Name: f1-sv-20110331-e.pdf

Description: Results of Airborne Monitoring by the Ministry of Education, Culture, Sports, Science and Technology and the U.S. Department of Energy (As of 4/29/11)
Source: MEXT and US DOE
File Name: 1304797_0506.pdf

Description: Review of Accident at Tokyo Electric Power Company Incorporated's Fukushima Daiichi Nuclear Power Station and Proposed Countermeasures (DRAFT)
Source: Japan Nuclear Technology Institute
File Name: Japan Nuclear Technology Institute Timeline.pdf

Description: Special Report on the Nuclear Accident at the Fukushima Daiichi Nuclear Power Station.
Source: INPO
File Name: 11_005_Special_Report_on_Fukushima_Daiichi_MASTER_11_08_11.pdf

Description: Satellite image on March 18, 2011, by Digital Globe.
Source: Digital Globe
Usage Information: www.digitalglobe.com/policies/usage
File Name: Fukushima_Daiichi_March_18_2011_digital_globe.jpg
   URL:
http://www.digitalglobe.com/downloads/featured_images/09_japan_earthquaketsu_fukushima_daiichi_march18_2011_dg.jpg

Description: Satellite image on March 14, 2011, at 11:04 am, three minutes after an explosion at Unit 3 (by Digital Globe).
Source: Digital Globe
Usage Information: www.digitalglobe.com/policies/usage
File Name: Unit 1 and 3 after explosions - Digital Globe.jpg

Description: Fukushima Nuclear Accident Analysis Report (Interim Report)
Source: TEPCO report dated 12/2/11
File Name: Fukushima Nuclear Accidents Investigation Report (Interim) Main body.pdf

Description: Fukushima Nuclear Accident Analysis Report (Interim Report) Summary
Source: TEPCO Report dated 12/2/11
File Name: Fukushima Nuclear Accidents Investigation Report (Interim) Main body (Summary).pdf

Description: Fukushima Nuclear Accident Investigation Report (Interim Report - Supplementary Volume)
Source: TEPCO report dated 12/2/11

File Name: Fukushima Nuclear Accidents Investigation Report (Interim) Schedule (Individual Items).pdf

Description: The Nuclear Safety and Quality Assurance Meeting's Accident Investigation Verification Committee
Source: TEPCO report dated November 2011
File Name: Opinions from Nuclear Safety and Quality Assurance Meeting Accident Investigation Verification Committee.pdf

Description: Examination of Accident at Tokyo Electric Power Co., Inc.'s Fukushima Daiichi Nuclear Power Station and Proposal of Countermeasures
Source: Japan Nuclear Technology Institute (JANTI)
File Name: JANTI Fukushima Report - October 2011.pdf
   URL: http://www.gengikyo.jp/english/shokai/Tohoku_Jishin/report.pdf

Description: Fukushima Daiichi –A One Year Review from TEPCO
Source: TEPCO web site March 14, 2012

File Name: Fukushima Daiichi - A One Year Review.pdf
   URL: http://www.tepco.co.jp/en/nu/fukushima-np/review/index-e.html

Description: Volume of water injected into reactors (estimation)
Source: TEPCO data
File Name: 110613sanko_table_tyusui-e.pdf

Component State Artifacts

Unit1 Component States

DC Power (DCP), Battery (BAT), 125 V Battery
  3/11/2011 12:00:00 PM to 3/11/2011 3:37:00 PM Operating
  3/11/2011 3:37:00 PM to 8/1/2011 11:59:00 PM Fail to operate

Service Water System (SWS), Motor driven pump (MDP), CCSW
  3/11/2011 12:00:00 PM to 3/11/2011 3:37:00 PM Operating
  3/11/2011 3:37:00 PM to 8/1/2011 11:59:00 PM Fail to continue running

Firewater Injection (FW1), Engine driven pump (EDP), Diesel driven fire pump
  3/11/2011 5:30:00 PM to 3/12/2011 1:48:00 AM Manually Started
  3/12/2011 1:48:00 AM to 6/1/2011 12:00:00 AM Fail to continue running

AC Power System (ACP), Emergency diesel generator (DGN), EDG 1
  3/11/2011 12:00:00 PM to 3/11/2011 2:46:00 PM Standby
  3/11/2011 2:47:00 PM to 3/11/2011 3:37:00 PM Automatically Started
  3/11/2011 3:37:00 PM to 8/1/2011 11:59:00 PM Fail to continue running

AC Power System (ACP), Emergency diesel generator (DGN), EDG 2
  3/11/2011 12:00:00 PM to 3/11/2011 2:46:00 PM Standby
  3/11/2011 2:47:00 PM to 3/11/2011 3:37:00 PM Automatically Started
  3/11/2011 3:37:00 PM to 8/1/2011 11:59:00 PM Fail to continue running

Firewater Injection (FW1), Engine driven pump (EDP), Fire Engine
  3/12/2011 5:46:00 AM to 3/12/2011 2:53:00 PM Manually Started
  3/12/2011 2:53:00 PM to 3/12/2011 7:04:00 PM Loss of function
  3/12/2011 7:04:00 PM to 8/1/2011 12:00:00 AM Manually Started

High Pressure Coolant Injection (HCI), Turbine driven pump (TDP), HPCI
  3/11/2011 12:00:00 PM to 3/11/2011 3:37:00 PM Standby
  3/11/2011 3:37:00 PM to 8/1/2011 11:59:00 PM Fail to start

Isolation Condenser (ICS), Actuation Train (ACT), IC A
  3/11/2011 12:00:00 PM to 3/11/2011 2:52:00 PM Standby
  3/11/2011 2:52:00 PM to 3/11/2011 3:03:00 PM Automatically Started
  3/11/2011 3:03:00 PM to 3/11/2011 6:18:00 PM Manually Shutdown
  3/11/2011 6:18:00 PM to 3/11/2011 6:25:00 PM Manually Started

3/11/2011 6:25:00 PM to 3/11/2011 9:30:00 PM Manually Shutdown

3/11/2011 9:30:00 PM to 3/12/2011 11:00:00 AM Manually Started

3/12/2011 11:00:00 AM to 8/1/2011 11:59:00 PM Fail to continue running

Isolation Condenser (ICS), Actuation Train (ACT), IC B

3/11/2011 2:52:00 PM to 3/11/2011 3:03:00 PM Automatically Started

3/11/2011 3:03:00 PM to 8/30/2011 12:00:00 AM Manually Shutdown

Power Conversion (PCS), Main steam isolation valve (MSV), MSIVs

3/11/2011 12:00:00 PM to 3/11/2011 2:47:00 PM Normally Open; Not failed

3/11/2011 2:47:00 PM to 8/1/2011 3:41:00 PM Normally open; fail in closed position

Offsite Electrical Power (OEP), System level event (SYS), Offsite Power Sources

3/11/2011 12:00:00 PM to 3/11/2011 2:47:00 PM Operating

3/11/2011 2:47:00 PM to 8/1/2011 11:59:00 PM No power-loss of power

Reactor Protection (RPS), Actuation Train (ACT), Reactor

3/11/2011 12:00:00 PM to 3/11/2011 2:46:00 PM Operating

3/11/2011 2:46:01 PM to 8/1/2011 11:59:00 PM Reactor Scram

Containment Vent (CVS), Air operated valve (AOV), S/C Large vent valve

3/12/2011 2:30:00 PM to 3/31/2011 12:00:00 PM Manually Opened

Unit1 Component States First Week

Unit1 Component States Second Week

Unit2 Component States

DC Power (DCP), Battery (BAT), 125 V Battery
   3/11/2011 12:00:00 PM to 3/11/2011 3:41:00 PM Operating
   3/11/2011 3:41:00 PM to 8/1/2011 11:59:00 PM Fail to operate

Service Water System (SWS), Motor driven pump (MDP), CCSW
   3/11/2011 12:00:00 PM to 3/11/2011 3:41:00 PM Operating
   3/11/2011 3:41:00 PM to 8/1/2011 11:59:00 PM Fail to continue running

AC Power System (ACP), Emergency diesel generator (DGN), EDG 1
   3/11/2011 12:00:00 PM to 3/11/2011 2:47:00 PM Standby
   3/11/2011 2:47:00 PM to 3/11/2011 3:37:00 PM Automatically Started
   3/11/2011 3:41:00 PM to 8/1/2011 11:59:00 PM Fail to continue running

AC Power System (ACP), Emergency diesel generator (DGN), EDG 2
   3/11/2011 12:00:00 PM to 3/11/2011 2:47:00 PM Standby
   3/11/2011 2:47:00 PM to 3/11/2011 3:37:00 PM Automatically Started
   3/11/2011 3:41:00 PM to 8/1/2011 11:59:00 PM Fail to continue running

Firewater Injection (FW1), Engine driven pump (EDP), Fire Engine
   3/14/2011 6:30:00 PM to 3/14/2011 7:20:00 PM Manually Started
   3/14/2011 7:20:00 PM to 3/14/2011 7:54:00 PM Fail to continue running
   3/14/2011 7:54:00 PM to 8/1/2011 12:00:00 PM Manually Started

High Pressure Coolant Injection (HCI), Turbine driven pump (TDP), HPCI
   3/11/2011 12:00:00 PM to 3/11/2011 3:41:00 PM Standby
   3/11/2011 3:41:00 PM to 8/1/2011 11:59:00 PM Fail to start

Power Conversion (PCS), Main steam isolation valve (MSV), MSIVs
   3/11/2011 12:00:00 PM to 3/11/2011 2:47:00 PM Normally Open; Not failed
   3/11/2011 2:47:00 PM to 8/1/2011 3:41:00 PM Normally open; fail in closed position

Offsite Electrical Power (OEP), System level event (SYS), Offsite Power Sources
   3/11/2011 12:00:00 PM to 3/11/2011 2:47:00 PM Operating
   3/11/2011 2:47:00 PM to 8/1/2011 11:59:00 PM No power-loss of power

Reactor Core Isolation Cooling (RCI), Turbine driven pump (TDP), RCIC system
   3/11/2011 12:00:00 PM to 3/11/2011 2:50:00 PM Standby

3/11/2011 2:50:00 PM to 3/11/2011 2:51:00 PM Manually Started
3/11/2011 2:51:00 PM to 3/11/2011 3:02:00 PM Automatically Shutdown
3/11/2011 3:02:00 PM to 3/11/2011 3:28:00 PM Manually Started
3/11/2011 3:28:00 PM to 3/11/2011 3:39:00 PM Automatically Shutdown
3/11/2011 3:39:00 PM to 3/14/2011 1:25:11 PM Manually Started
3/14/2011 1:25:11 PM to 8/1/2011 11:59:00 PM Fail to continue running

Reactor Protection (RPS), Actuation Train (ACT), Reactor
3/11/2011 12:00:00 PM to 3/11/2011 2:47:00 PM Operating
3/11/2011 2:47:00 PM to 8/1/2011 11:59:00 PM Reactor Scram

Residual Heat Removal Service Water (RSW), Motor driven pump (MDP), RHRS
3/11/2011 12:00:00 PM to 3/11/2011 3:00:00 PM Standby
3/11/2011 3:00:00 PM to 3/11/2011 3:41:00 PM Manually Started
3/11/2011 3:41:00 PM to 8/1/2011 11:59:00 PM Fail to continue running

Main Steam (MSS), Safety relief valve (SRV), SRV
3/14/2011 6:06:00 PM to 8/1/2011 12:00:00 AM Manually Opened
3/14/2011 9:20:00 PM to 8/1/2011 12:00:00 AM Manually Opened

Unit2 Component States First Week

Unit2 Component States Second Week

Fukushima Daiichi Accident Study
Information Portal
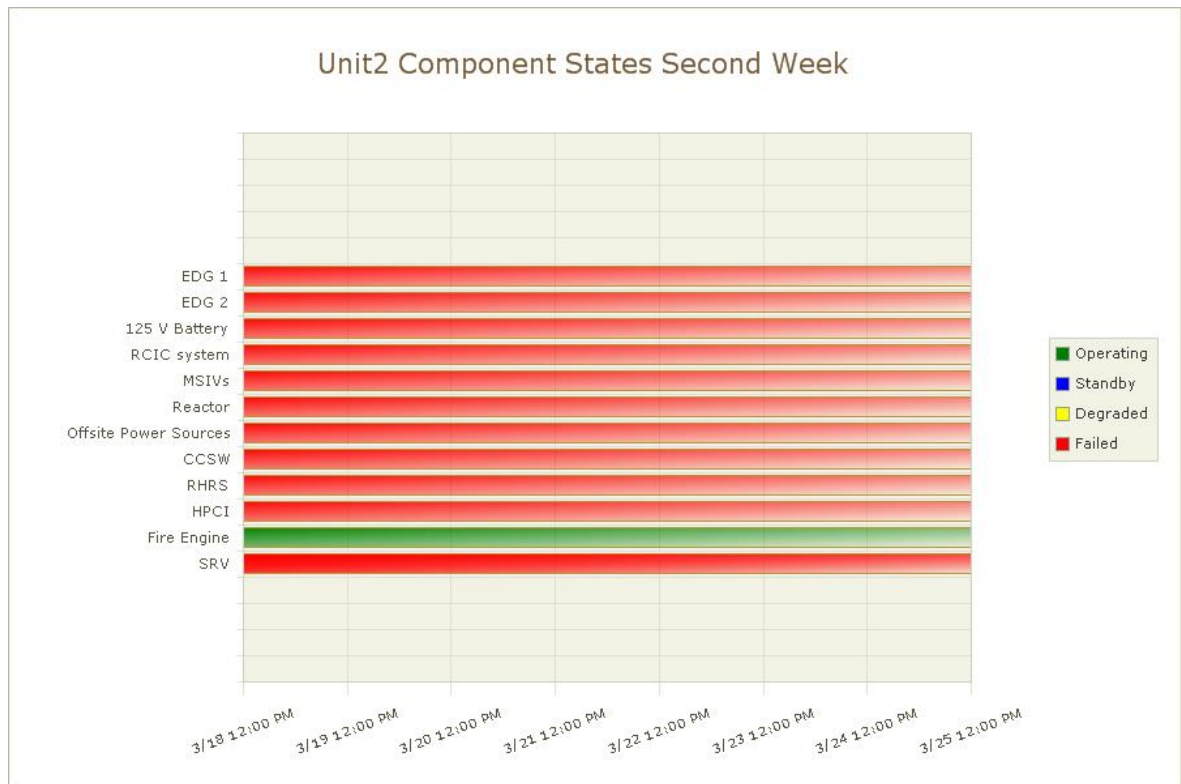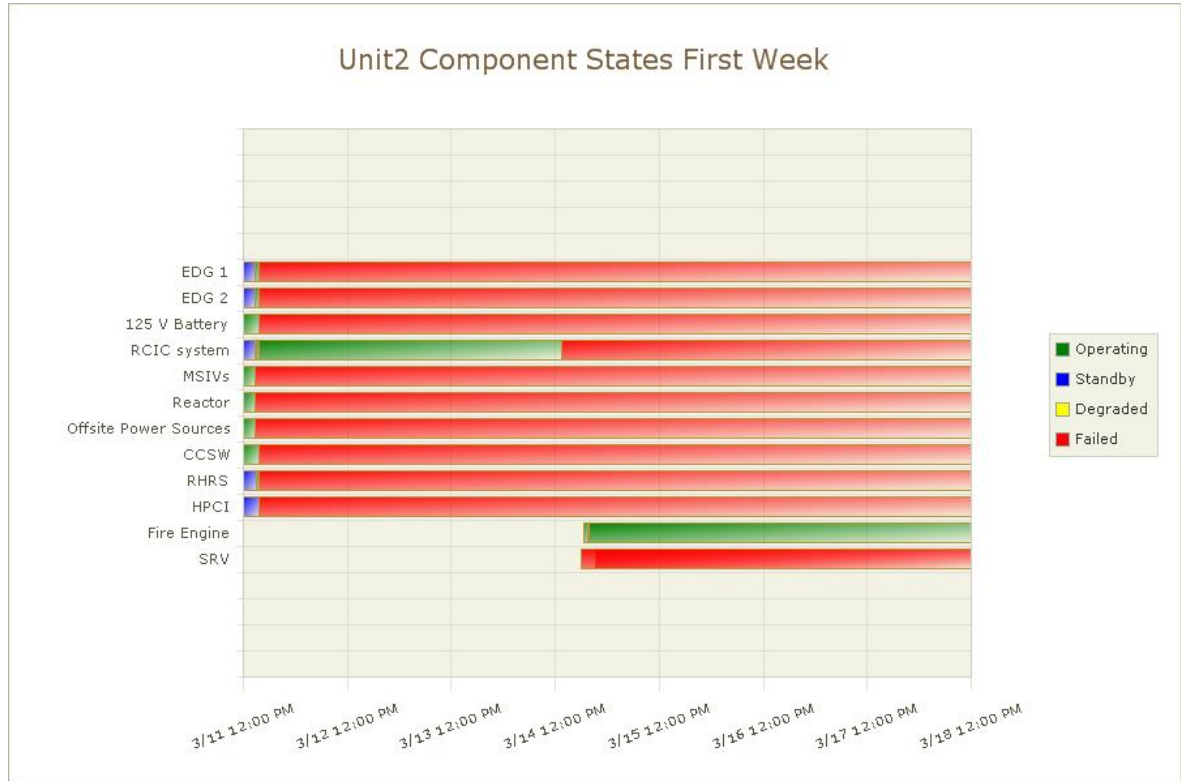
Unit3 Component States

DC Power (DCP), Battery (BAT), 125 V Battery
   3/11/2011 12:00:00 PM to 3/12/2011 9:30:00 PM Operating
   3/12/2011 9:30:00 PM to 8/1/2011 11:59:00 PM Fail to operate

Service Water System (SWS), Motor driven pump (MDP), CCSW
   3/11/2011 12:00:00 PM to 3/11/2011 3:41:00 PM Operating
   3/11/2011 3:41:00 PM to 8/1/2011 11:59:00 PM Fail to continue running

AC Power System (ACP), Emergency diesel generator (DGN), EDG 1
   3/11/2011 12:00:00 PM to 3/11/2011 2:47:00 PM Standby
   3/11/2011 2:47:00 PM to 3/11/2011 3:37:00 PM Automatically Started
   3/11/2011 3:41:00 PM to 8/1/2011 11:59:00 PM Fail to continue running

AC Power System (ACP), Emergency diesel generator (DGN), EDG 2
   3/11/2011 12:00:00 PM to 3/11/2011 2:47:00 PM Standby
   3/11/2011 2:47:00 PM to 3/11/2011 3:37:00 PM Automatically Started
   3/11/2011 3:41:00 PM to 8/1/2011 11:59:00 PM Fail to continue running

Firewater Injection (FW1), Engine driven pump (EDP), Fire Engine
   3/13/2011 9:25:00 AM to 3/13/2011 12:20:00 PM Manually Started
   3/13/2011 12:20:00 PM to 3/13/2011 1:12:00 PM Fail to continue running
   3/13/2011 1:12:00 PM to 3/14/2011 1:10:00 AM Manually Started
   3/14/2011 1:10:00 AM to 3/14/2011 3:20:00 AM Fail to continue running
   3/14/2011 3:20:00 AM to 3/14/2011 11:01:00 AM Manually Started
   3/14/2011 11:01:00 AM to 3/14/2011 4:30:00 PM Fail to continue running
   3/14/2011 4:30:00 PM to 3/31/2011 12:00:00 PM Manually Started

High Pressure Coolant Injection (HCI), Turbine driven pump (TDP), HPCI
   3/11/2011 12:00:00 PM to 3/12/2011 12:35:00 PM Standby
   3/12/2011 12:35:00 PM to 3/13/2011 2:42:00 AM Automatically Started
   3/13/2011 2:42:00 AM to 8/1/2011 11:59:00 PM Fail to continue running

Power Conversion (PCS), Main steam isolation valve (MSV), MSIVs
   3/11/2011 12:00:00 PM to 3/11/2011 2:48:00 PM Normally Open; Not failed
   3/11/2011 2:48:00 PM to 8/1/2011 3:41:00 PM Normally open; fail in closed position

Offsite Electrical Power (OEP), System level event (SYS), Offsite Power Sources

3/11/2011 12:00:00 PM to 3/11/2011 2:47:00 PM Operating

3/11/2011 2:47:00 PM to 8/1/2011 11:59:00 PM No power-loss of power

Reactor Core Isolation Cooling (RCI), Turbine driven pump (TDP), RCIC system

3/11/2011 12:00:00 PM to 3/11/2011 3:05:00 PM Standby

3/11/2011 3:05:00 PM to 3/11/2011 3:25:00 PM Manually Started

3/11/2011 3:25:00 PM to 3/11/2011 4:03:00 PM Automatically Shutdown

3/11/2011 4:03:00 PM to 3/12/2011 11:36:00 AM Manually Started

3/12/2011 11:36:00 AM to 8/1/2011 12:00:00 AM Fail to continue running

Reactor Protection (RPS), Actuation Train (ACT), Reactor

3/11/2011 12:00:00 PM to 3/11/2011 2:47:00 PM Operating

3/11/2011 2:47:00 PM to 8/1/2011 11:59:00 PM Reactor Scram

Residual Heat Removal Service Water (RSW), Motor driven pump (MDP), RHRS

3/11/2011 12:00:00 PM to 3/11/2011 3:41:00 PM Standby

3/11/2011 3:41:00 PM to 8/1/2011 11:59:00 PM Fail to start

Containment Vent (CVS), Air operated valve (AOV), S/C Large vent valve

3/13/2011 9:20:00 AM to 3/13/2011 11:17:00 AM Manually Opened

3/13/2011 11:17:00 AM to 3/13/2011 12:30:00 PM Normally closed; fail in the closed position

3/13/2011 12:30:00 PM to 3/13/2011 3:00:00 PM Manually Opened

3/13/2011 3:00:00 PM to 3/13/2011 8:10:00 PM Normally closed; fail in the closed position

3/13/2011 8:10:00 PM to 3/14/2011 1:00:00 AM Manually Opened

3/14/2011 1:00:00 AM to 3/15/2011 4:05:00 PM Normally closed; fail in the closed position

3/15/2011 4:05:00 PM to 3/16/2011 6:15:00 AM Manually Opened

Main Steam (MSS), Safety relief valve (SRV), SRV

3/13/2011 9:08:00 AM to 5/1/2011 12:00:00 PM Manually Opened
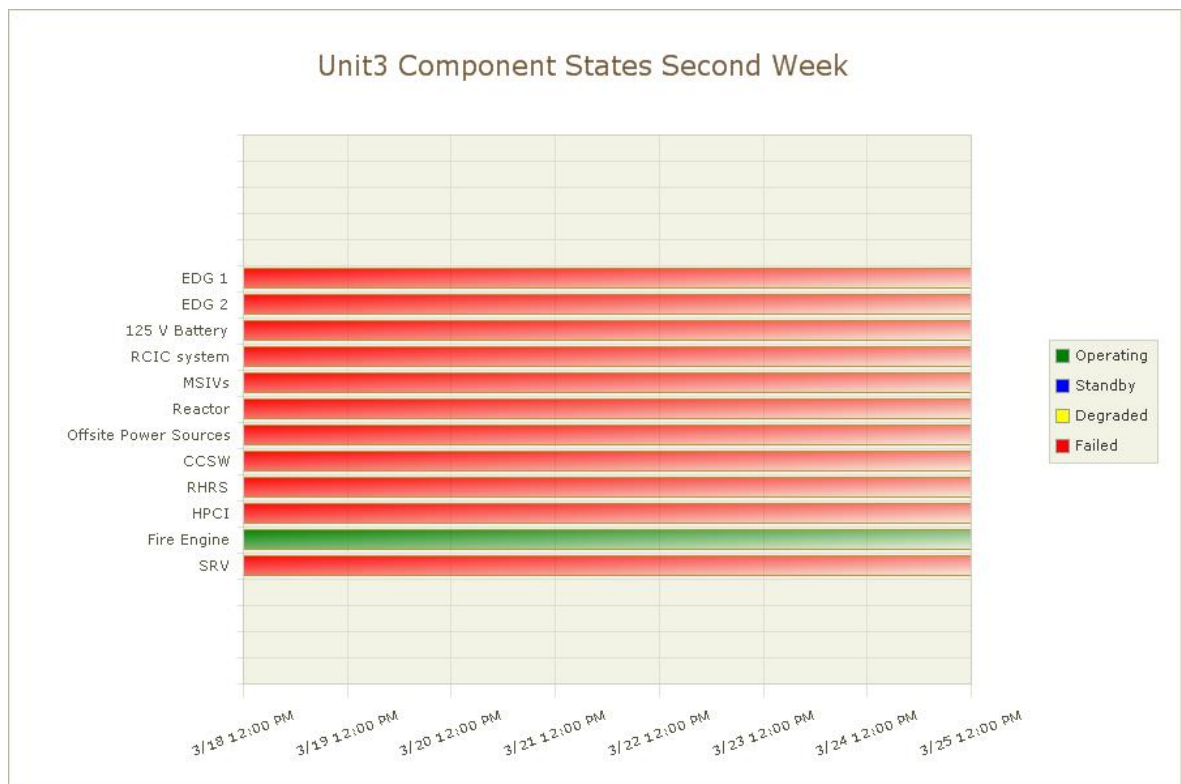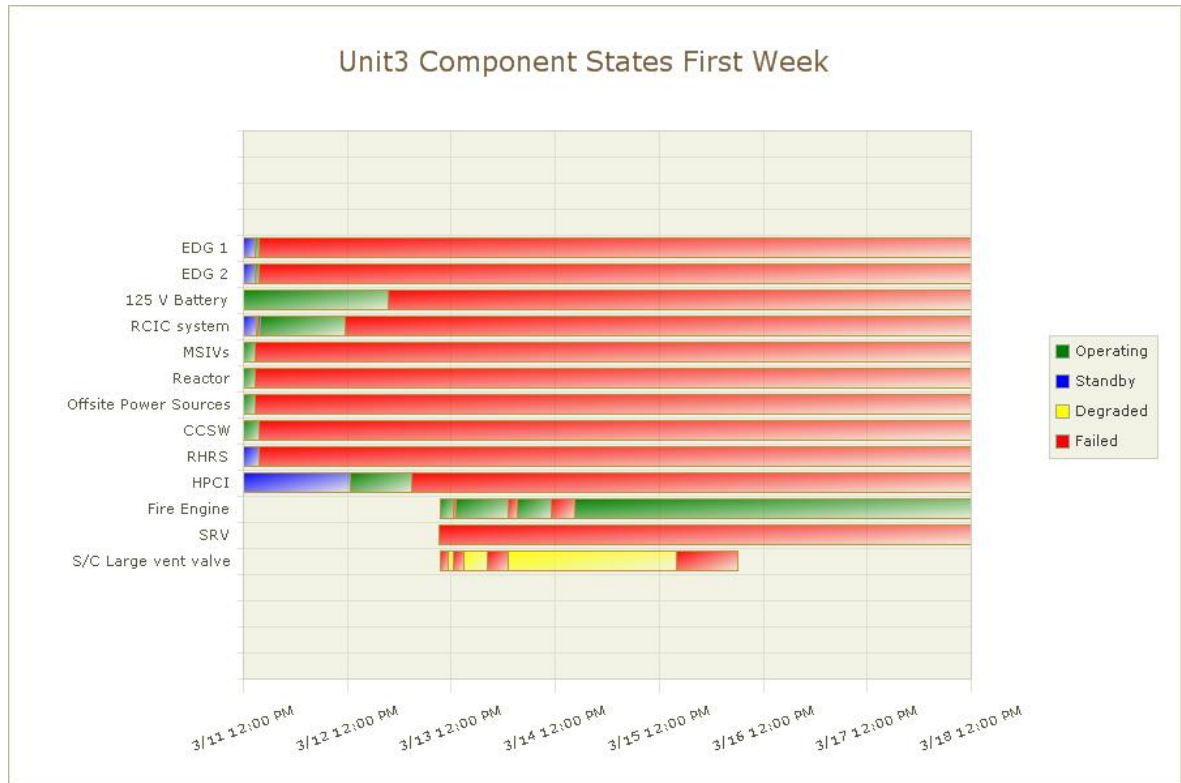
Unit3 Component States First Week

Unit3 Component States Second Week
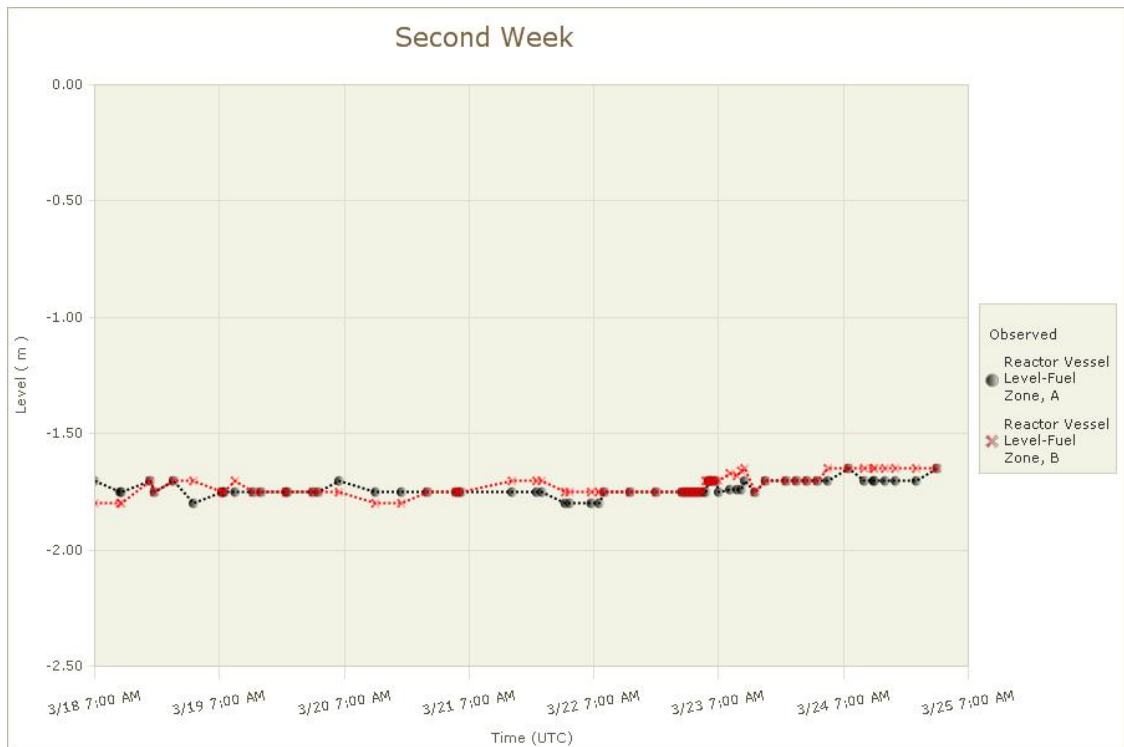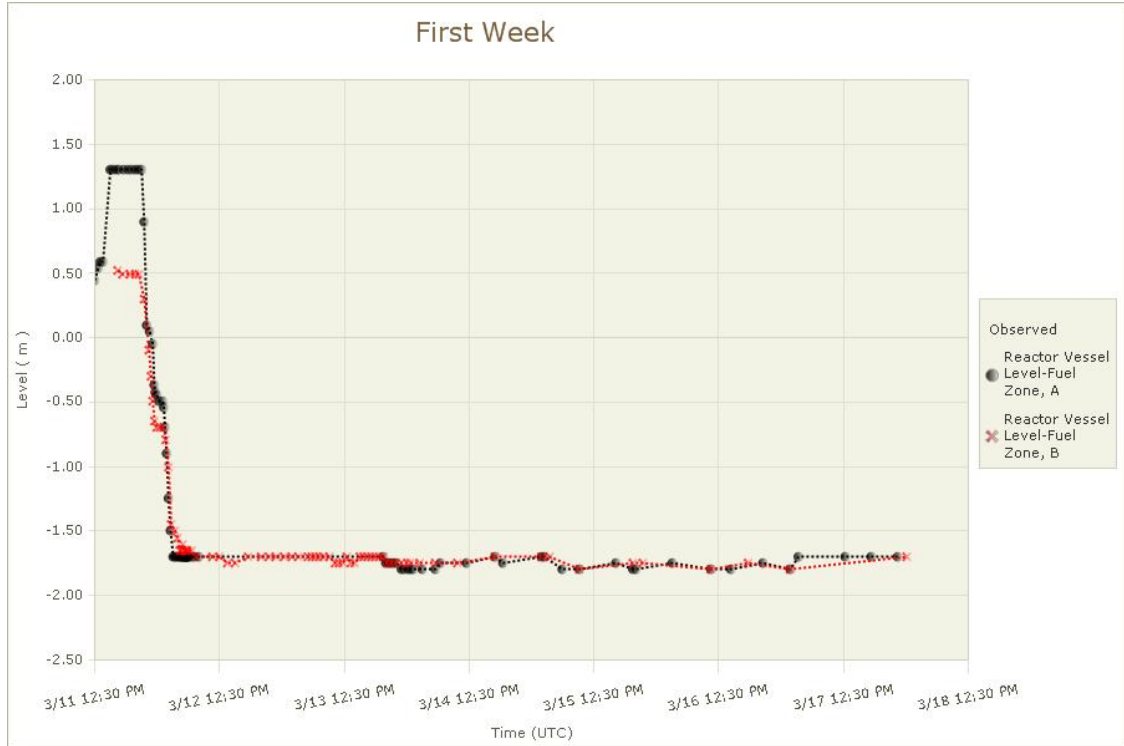
Unit1 Feedwater Nozzle N4B (end) Temperature (Observed)
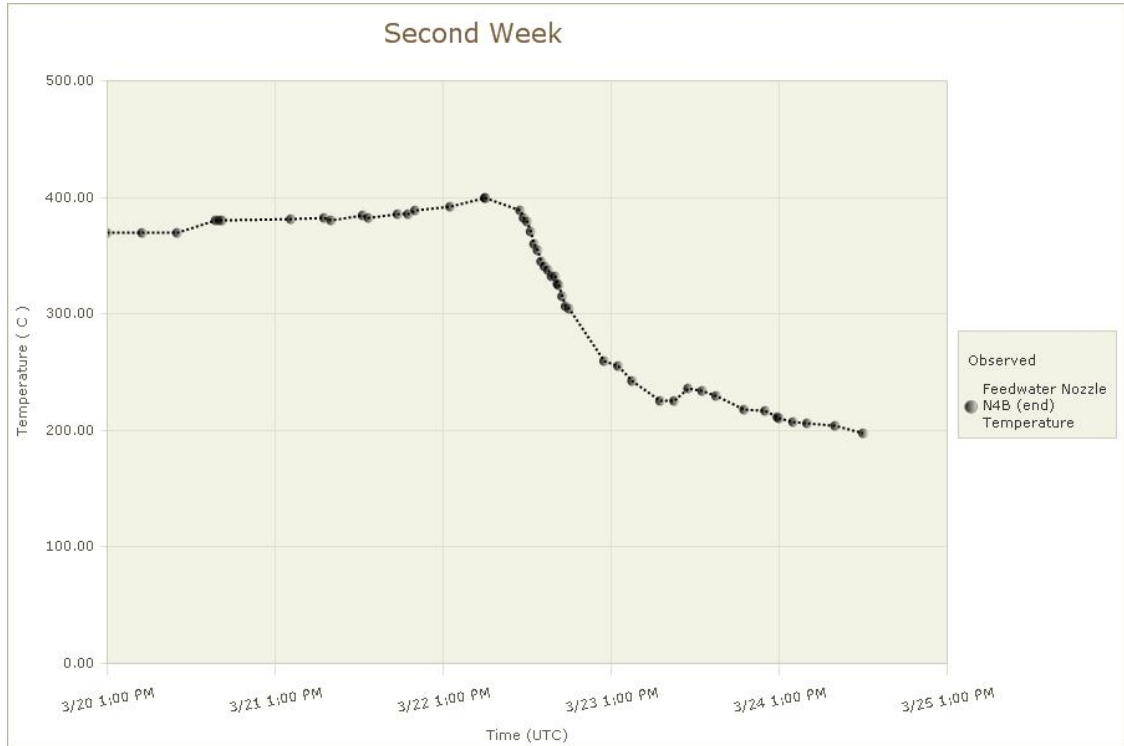
Unit1 Reactor Pressure Vessel Bottom Part Temperature (Observed)
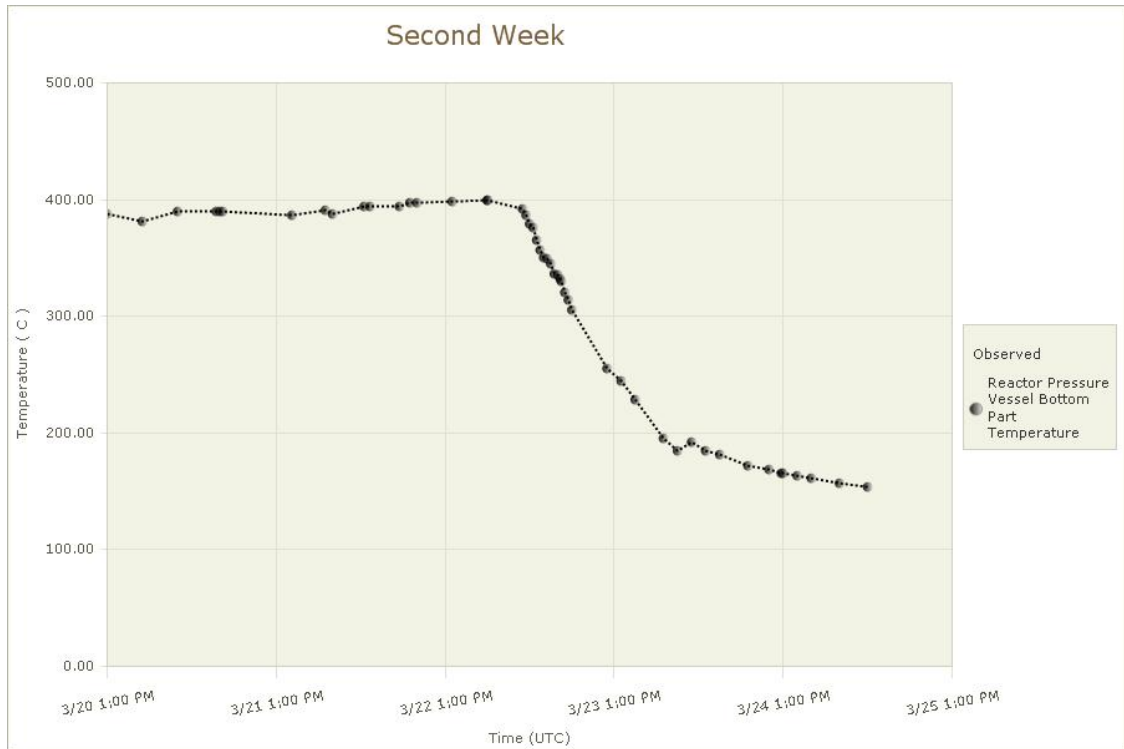
Unit1 Safety Valve (exhaust air)203-4A Temperature (Observed)
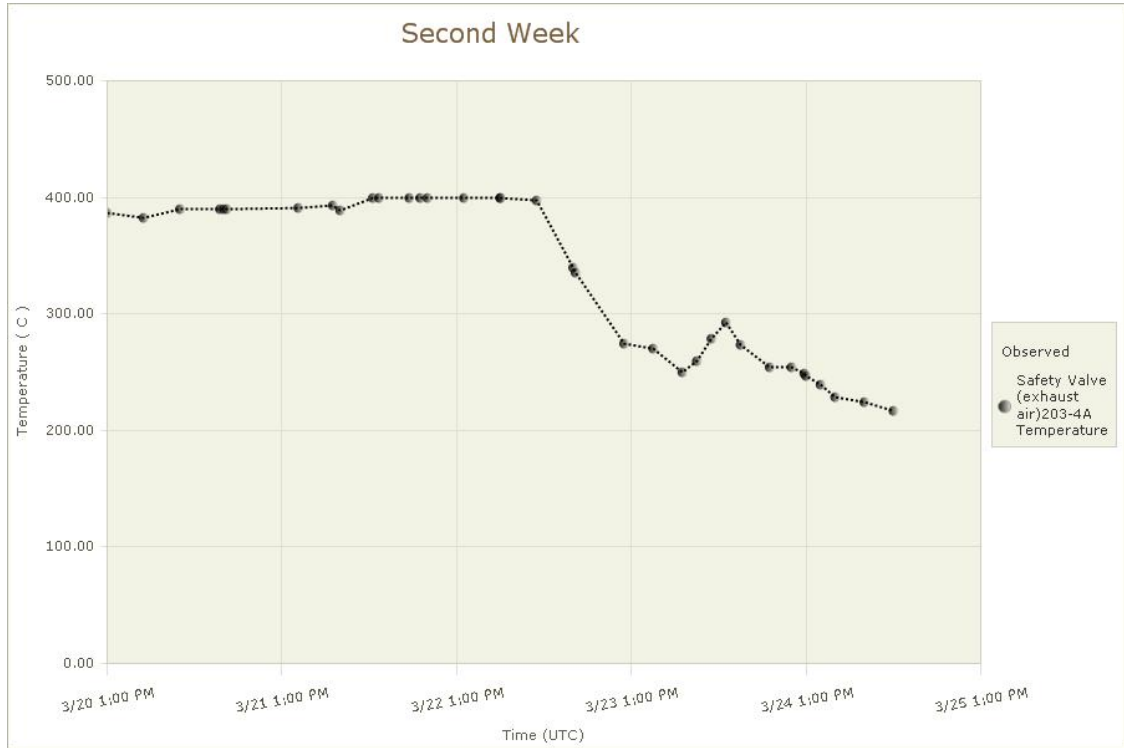
Unit1 D/W HVH Return Air Duct (HVH-12C) Temperature (Observed)
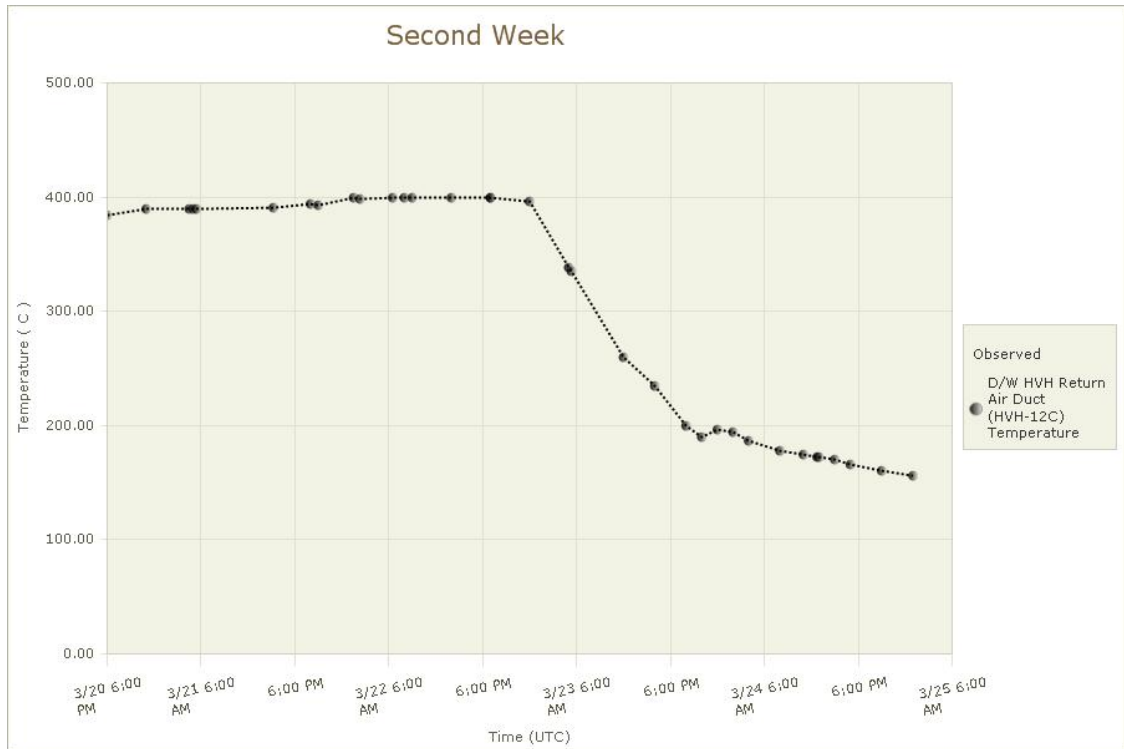
Unit1 Vessel Flange(A) Temperature (Observed)
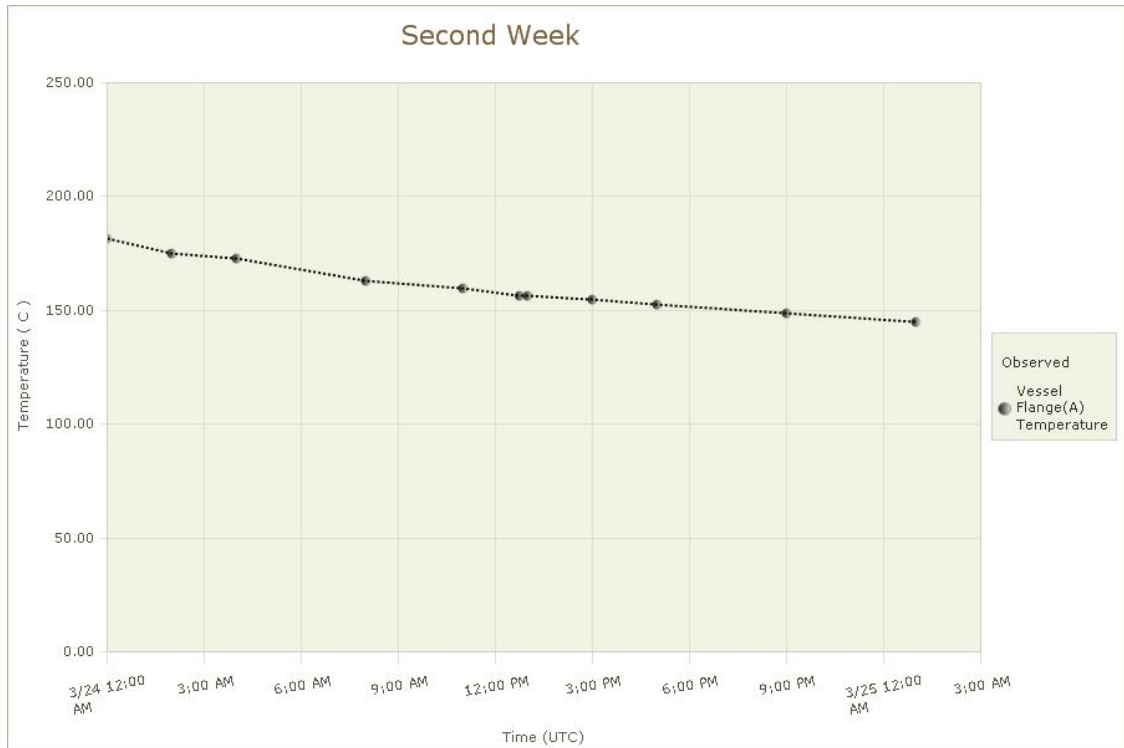
Unit1 Vessel; Core Temperature (Observed)
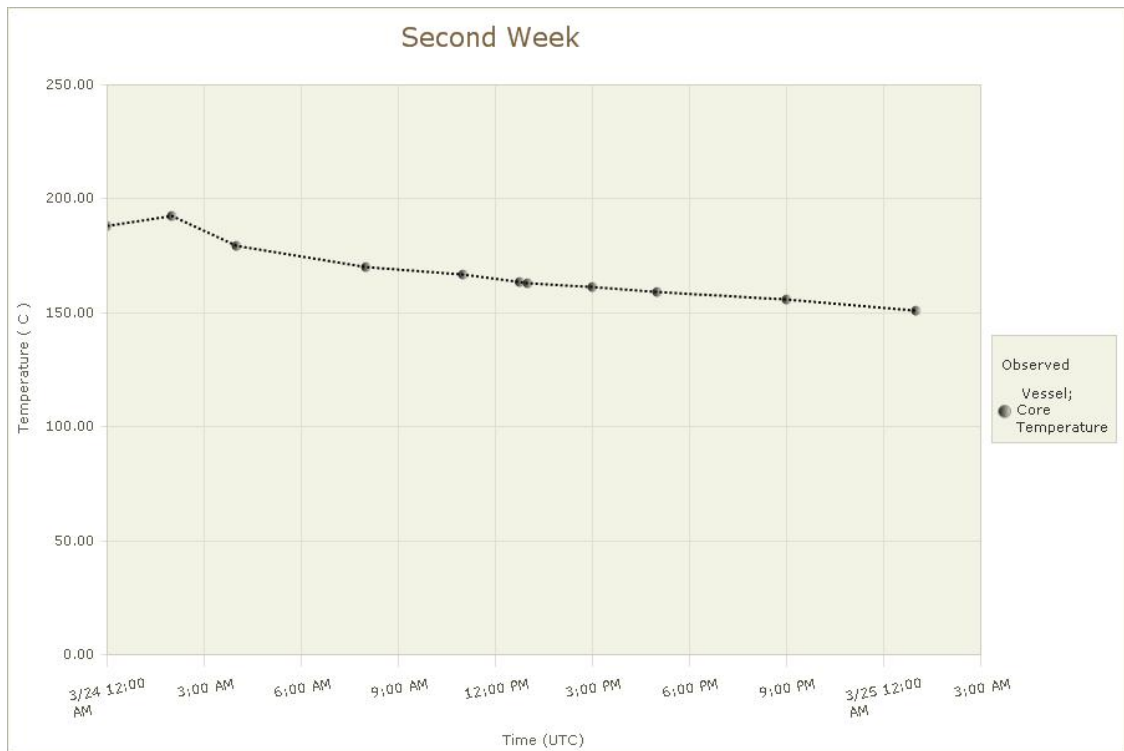
Unit1 RPV Bellows Air (HVH-12A) Temperature (Observed)

Unit1 Reactor Pressure (Observed)

Second Week
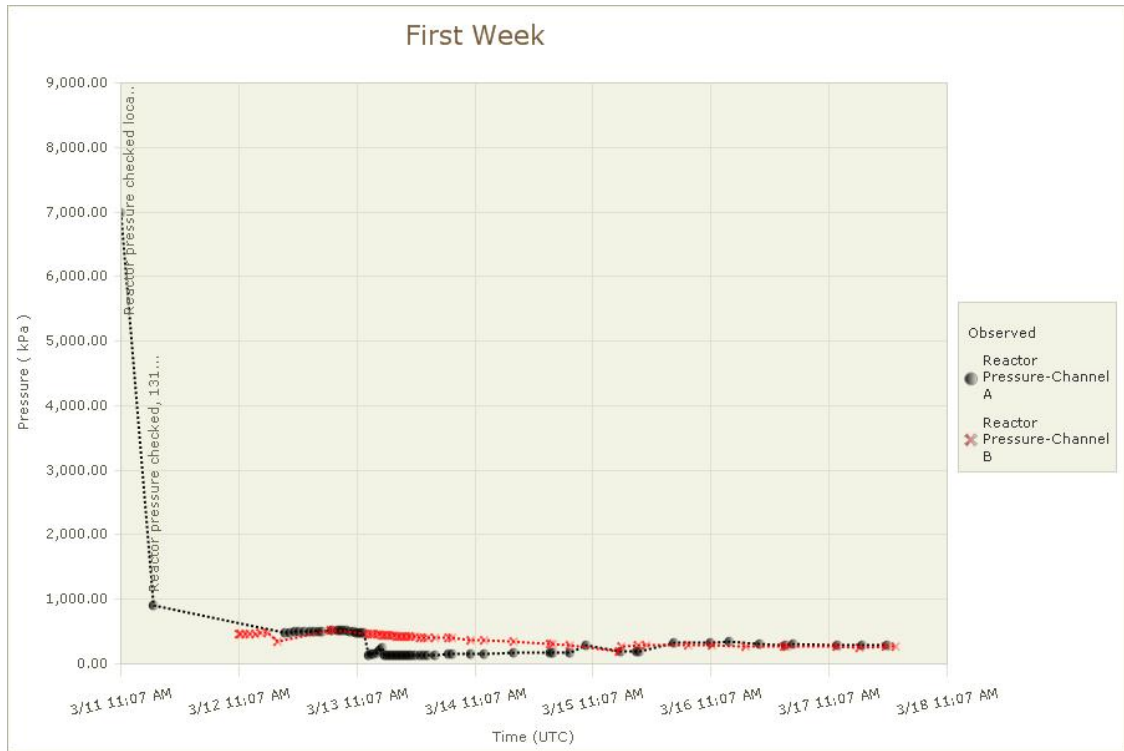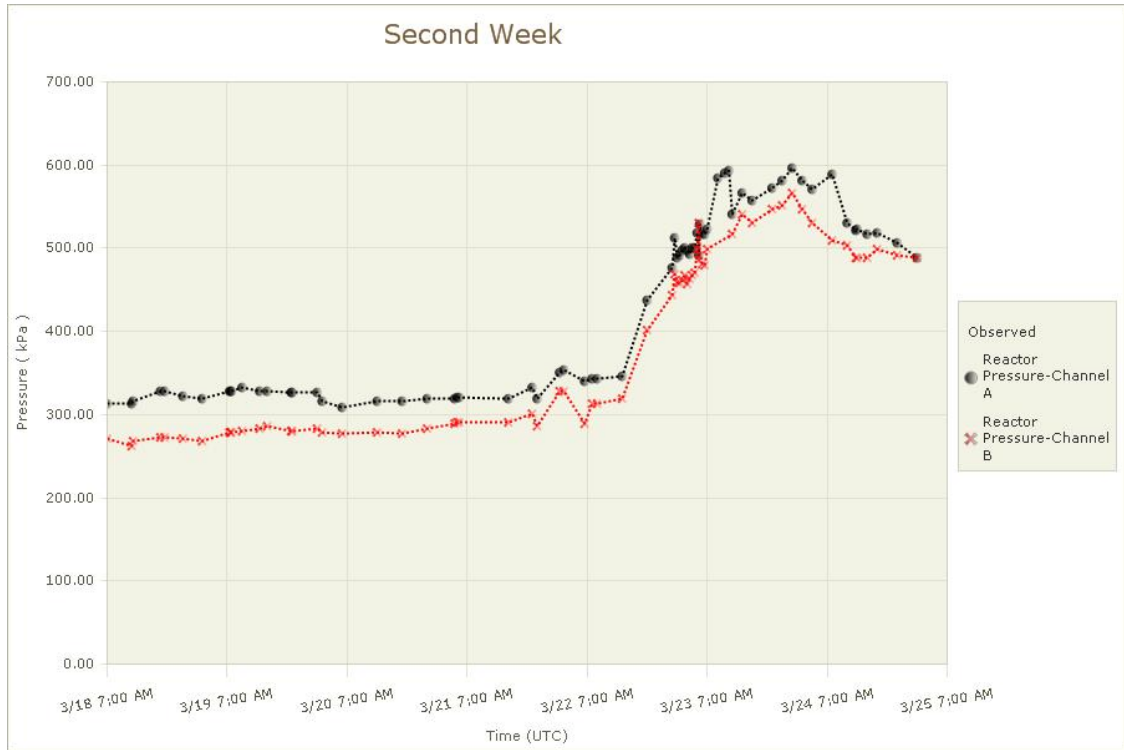
Unit1 D/W Pressure (Observed)
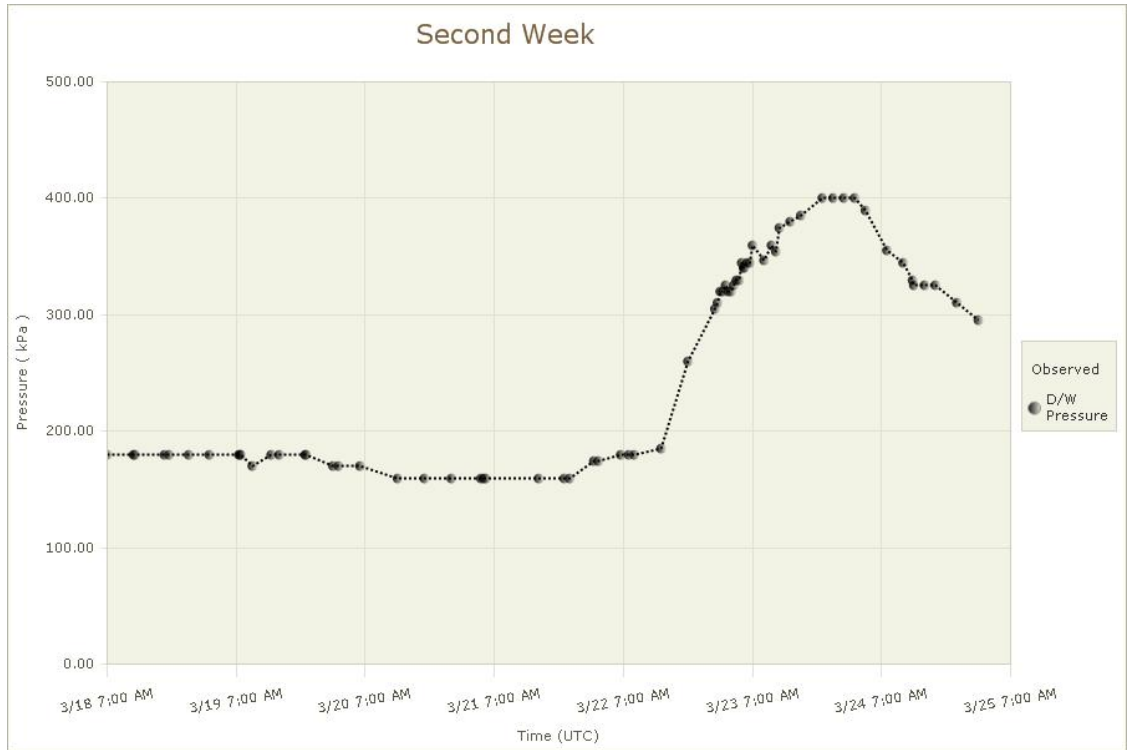
First Week

Fukushima Daiichi Accident Study
Information Portal

Unit1 S/C Pressure (Observed)
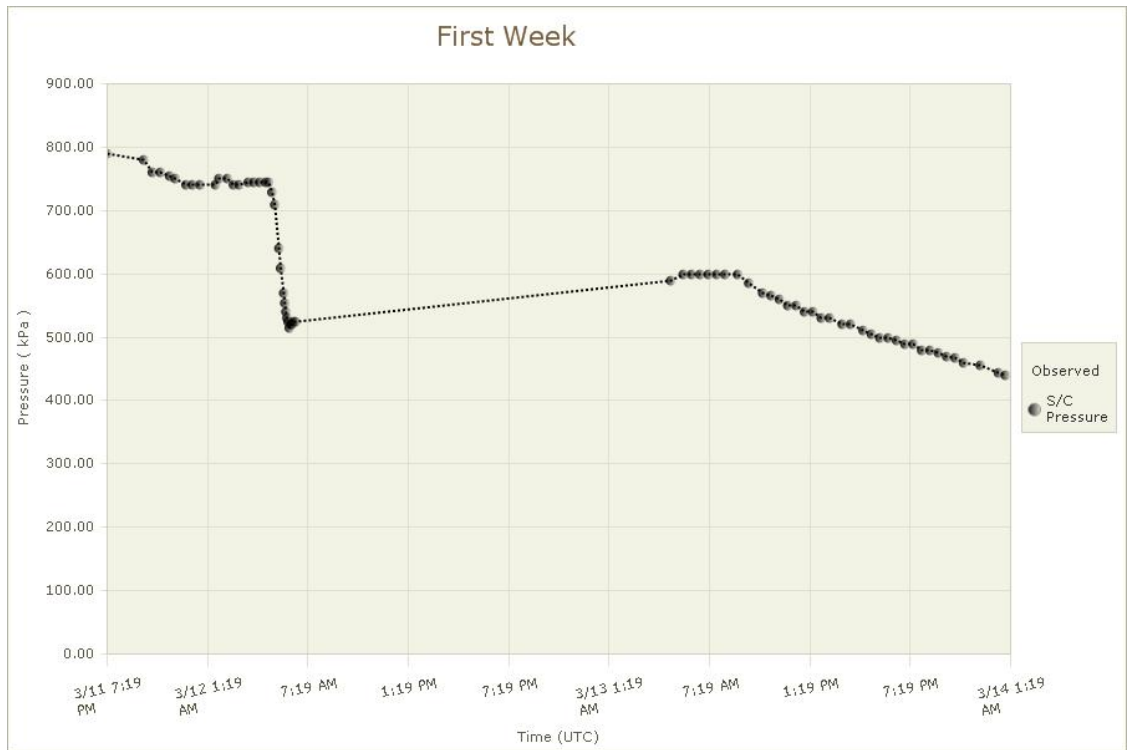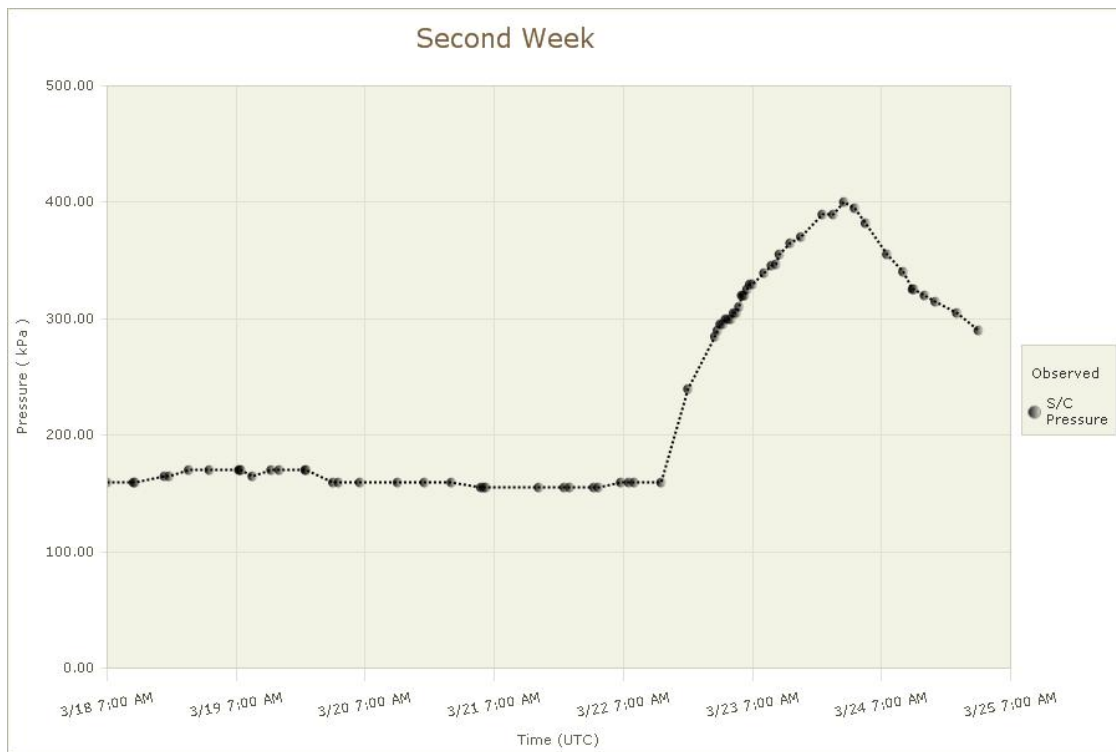
Unit 2 Parameters-Observed

Unit2 Reactor Vessel Level (Observed)
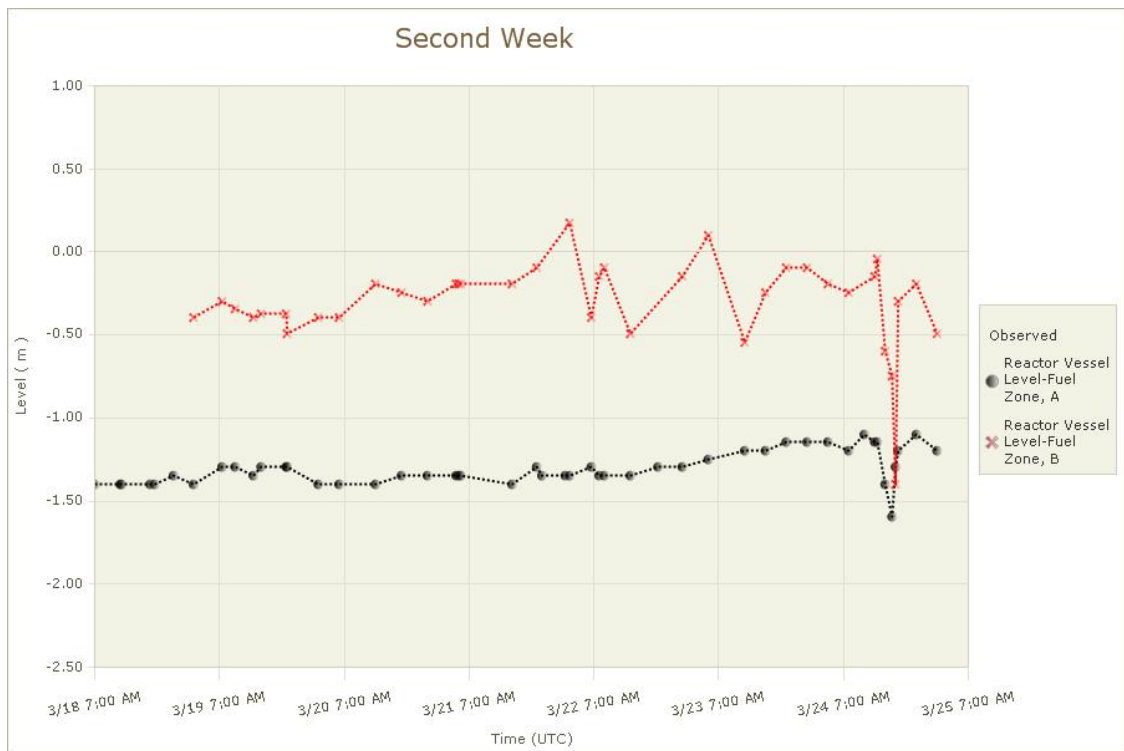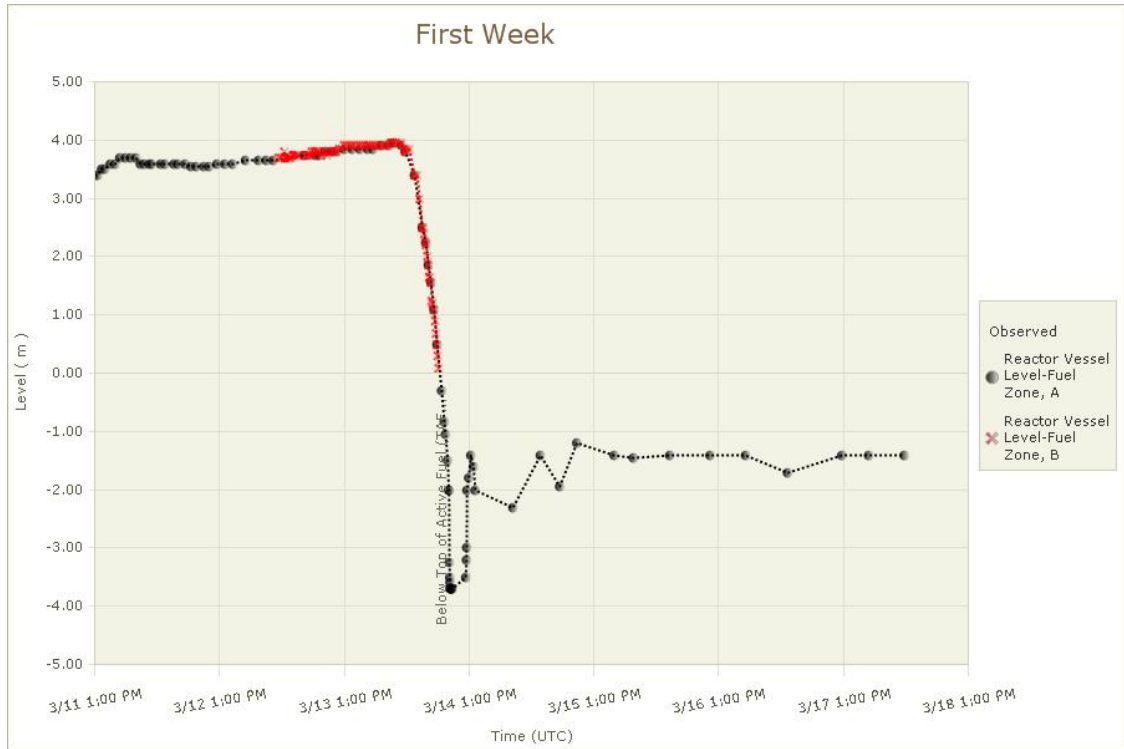
Unit2 Safety Relief Valve RV-2-71A Temperature (Observed)
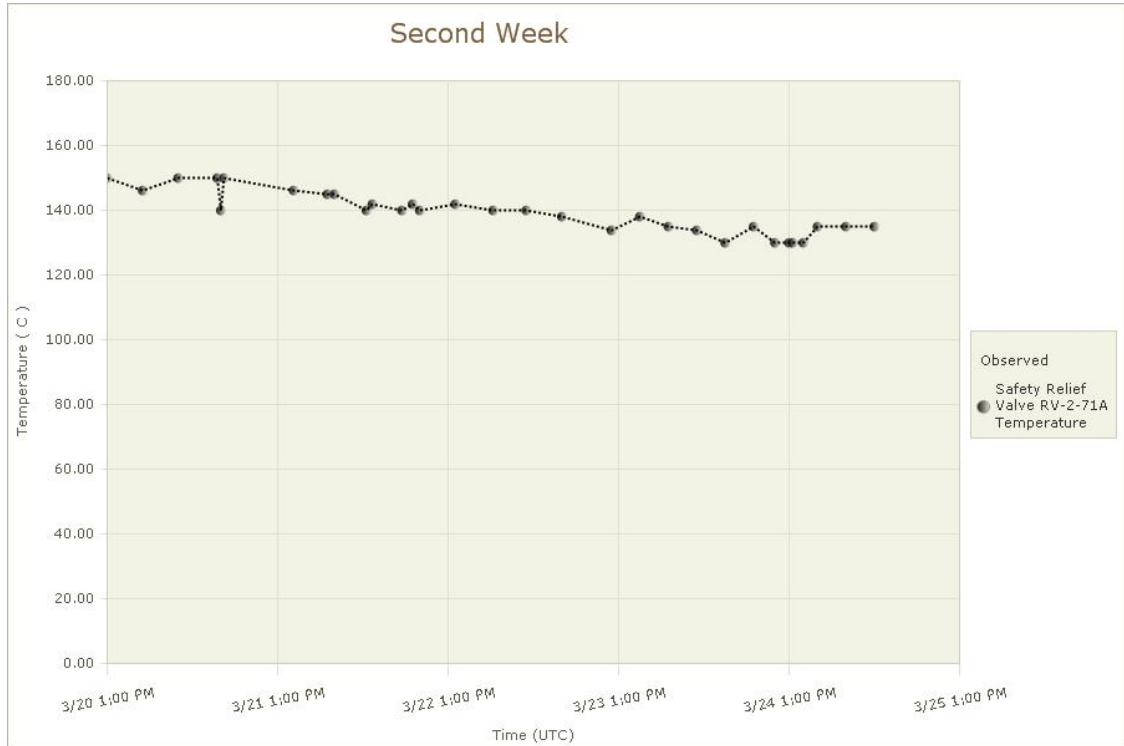
Unit2 Main Steam Isolation Valve 2-86A Temperature (Observed)
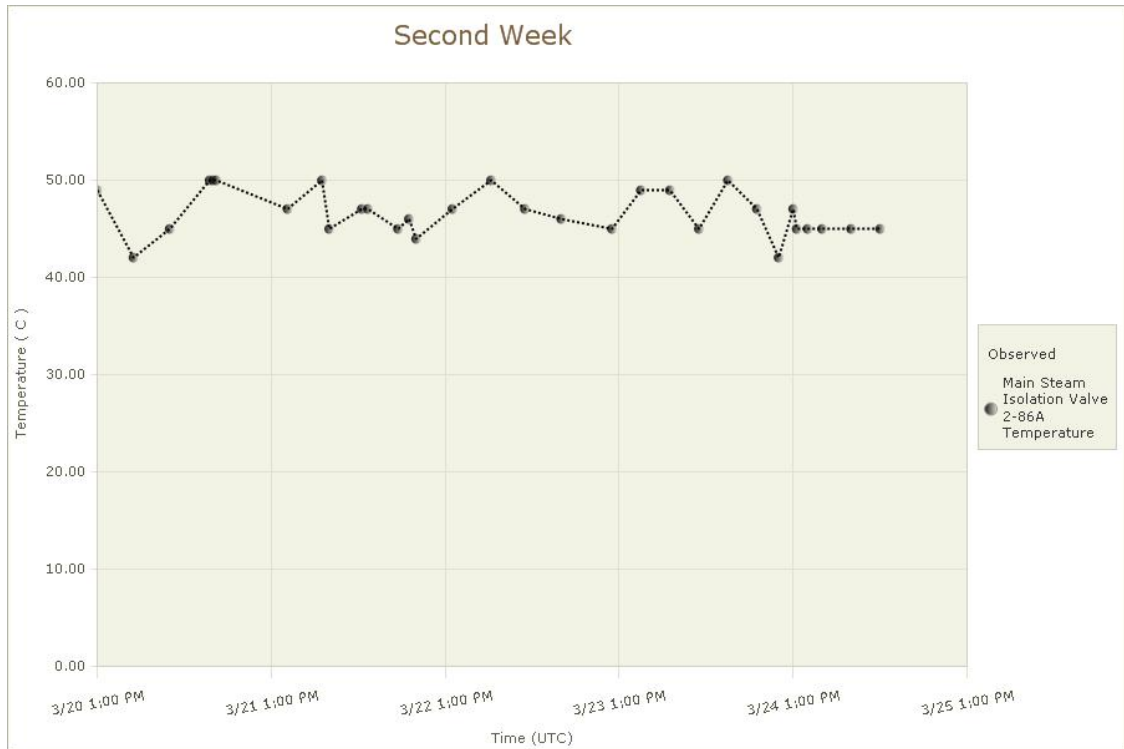
Unit2 Feedwater Nozzle N-4B Temperature (Observed)
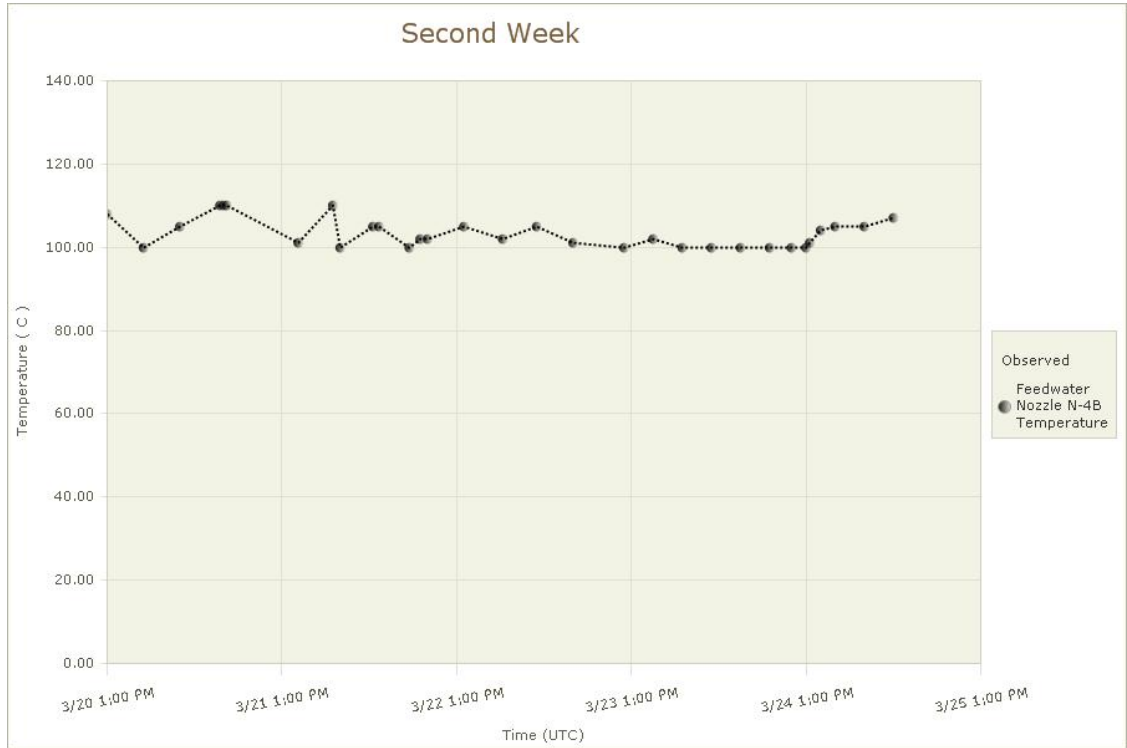
Unit2 Reactor Pressure Vessel Temperature (Observed)
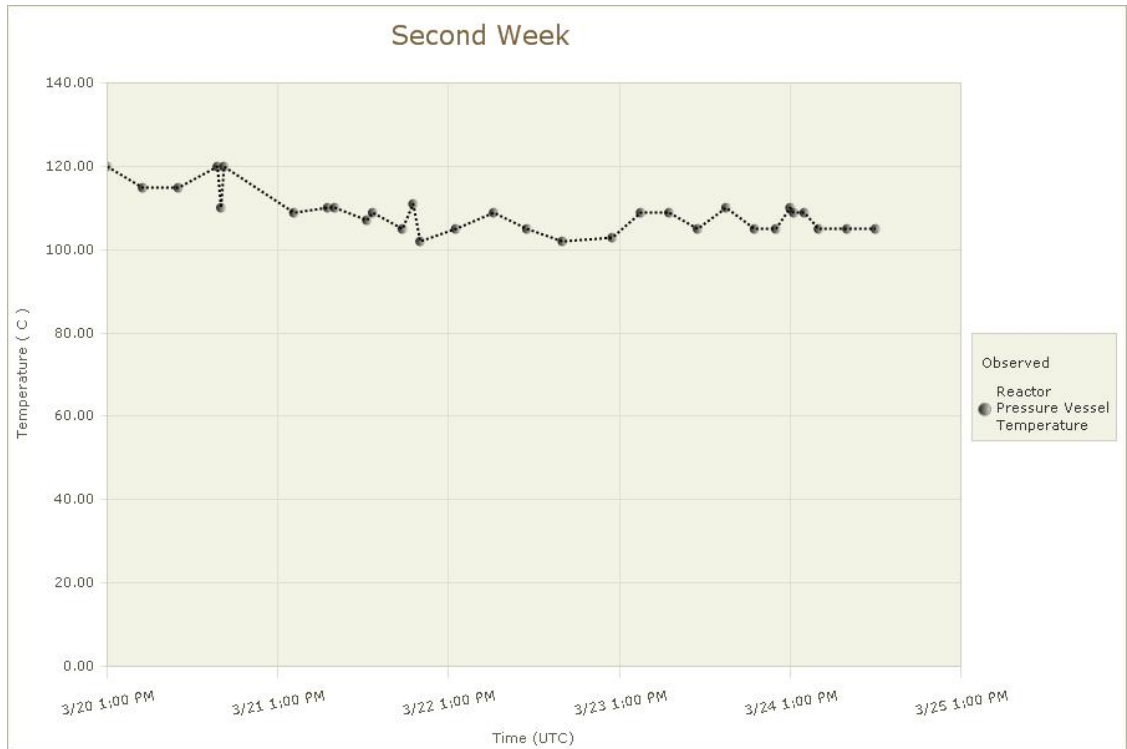
Unit2 D/W HVH Return Air Duct (HVH-16A) Temperature (Observed)
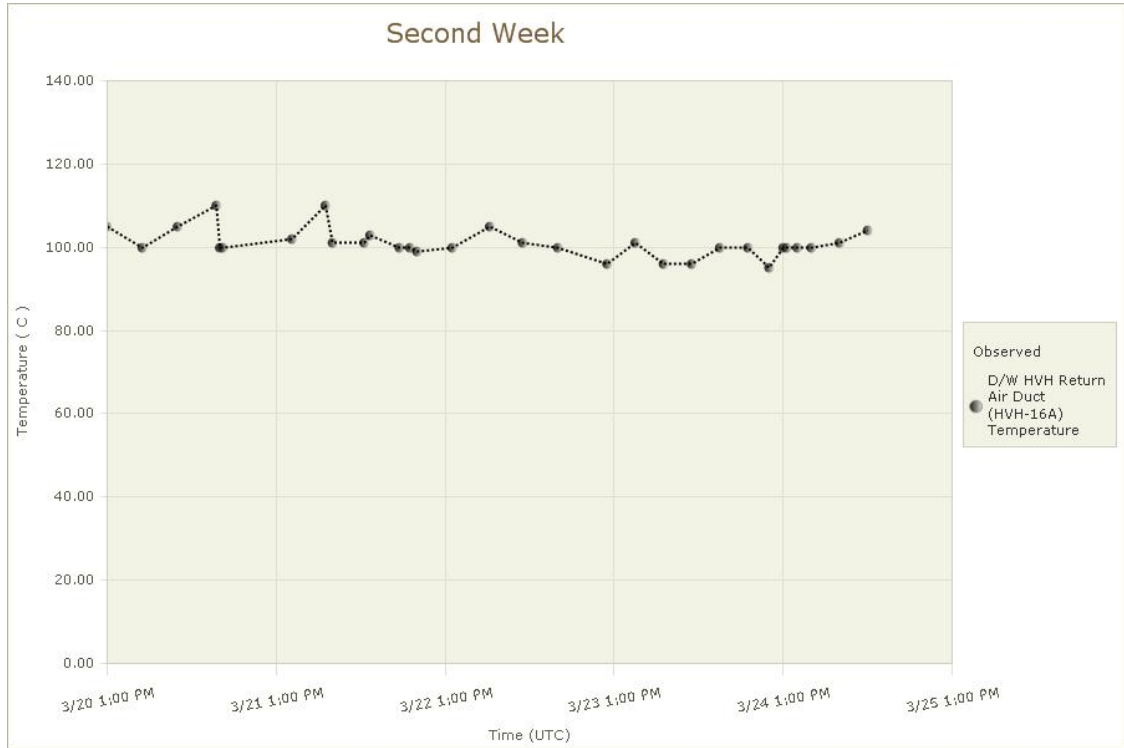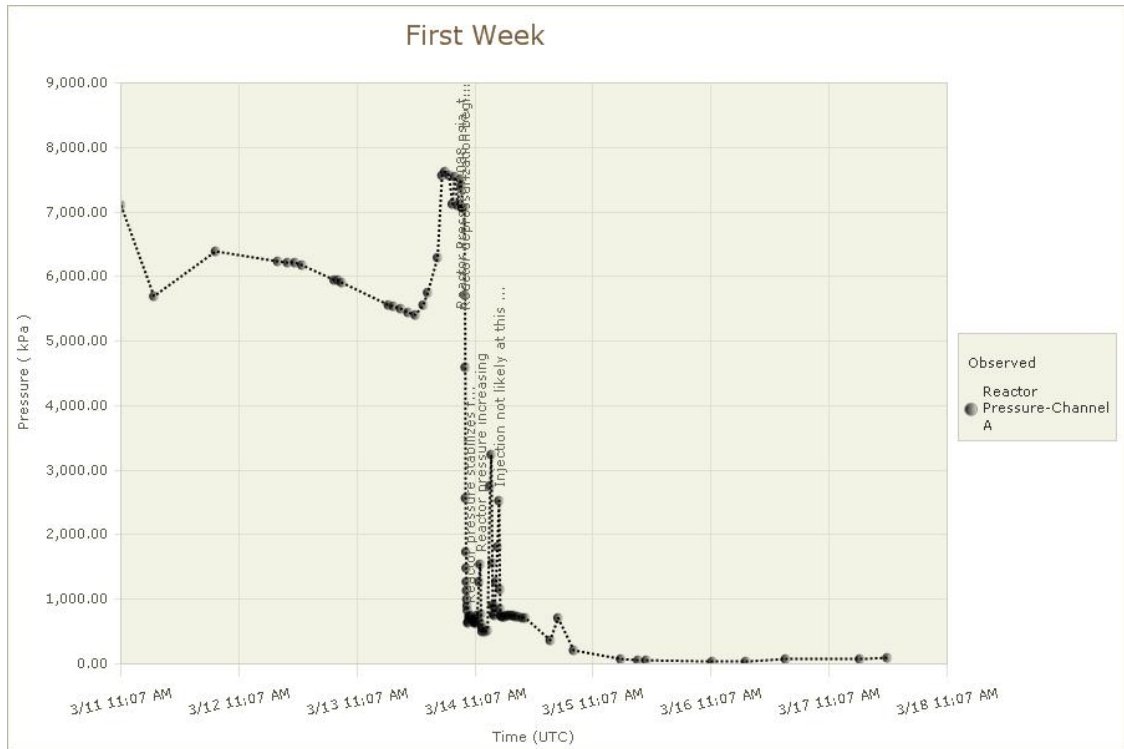
Unit2 Reactor Pressure (Observed)
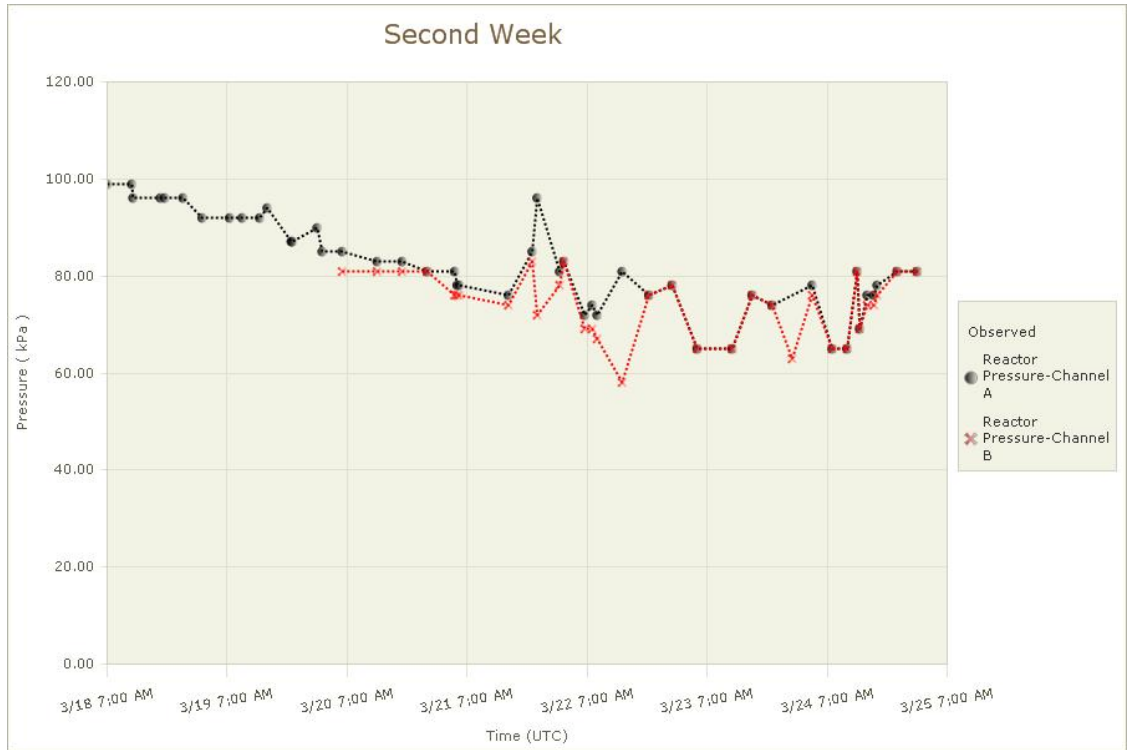
Unit2 D/W Pressure (Observed)

Unit2 S/C Pressure (Observed)

Unit 3 Parameters-Observed
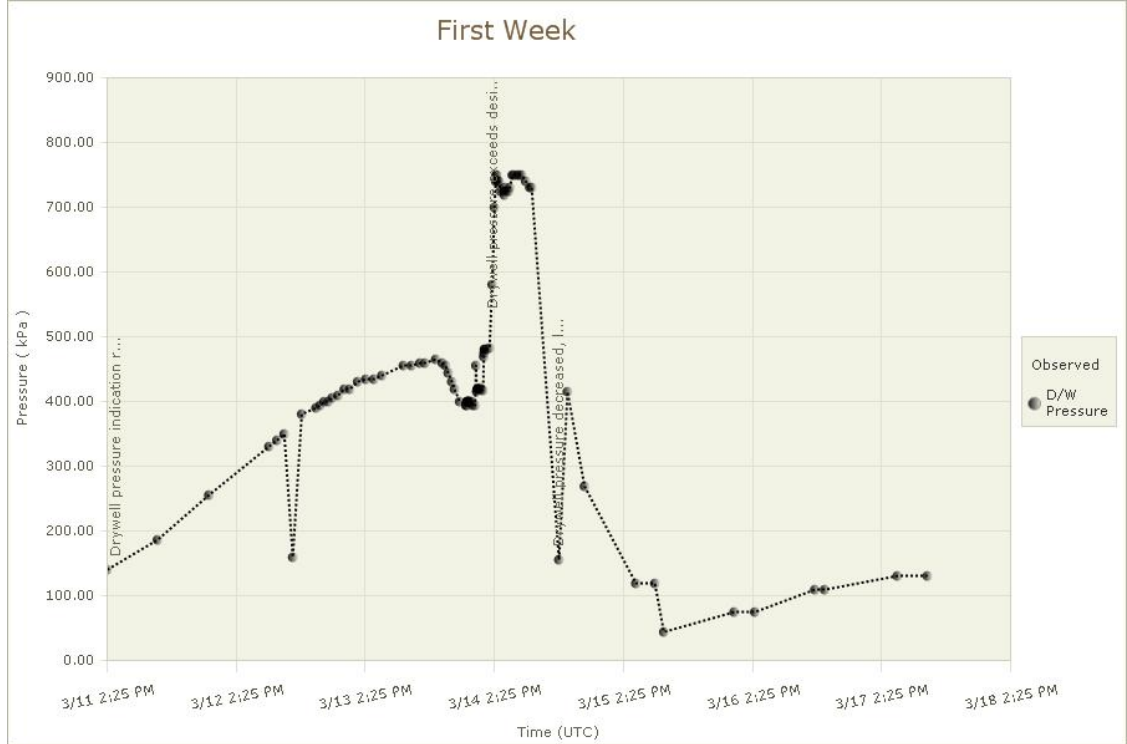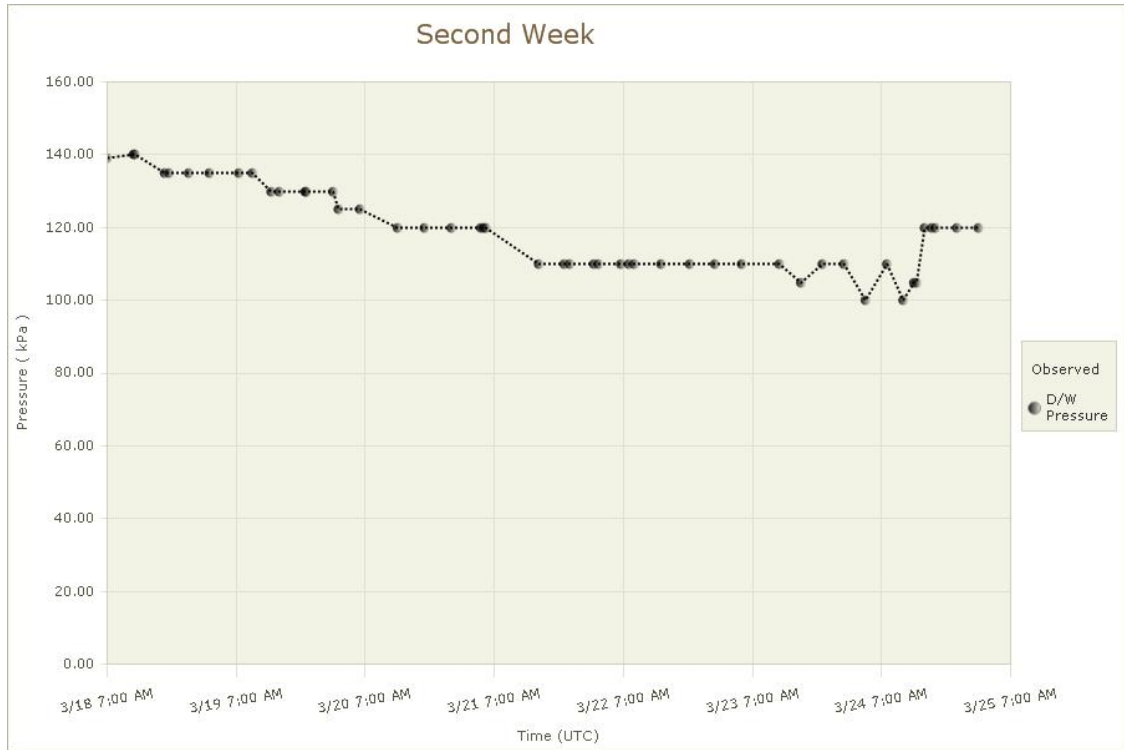
Unit3 Reactor Vessel Level (Observed)
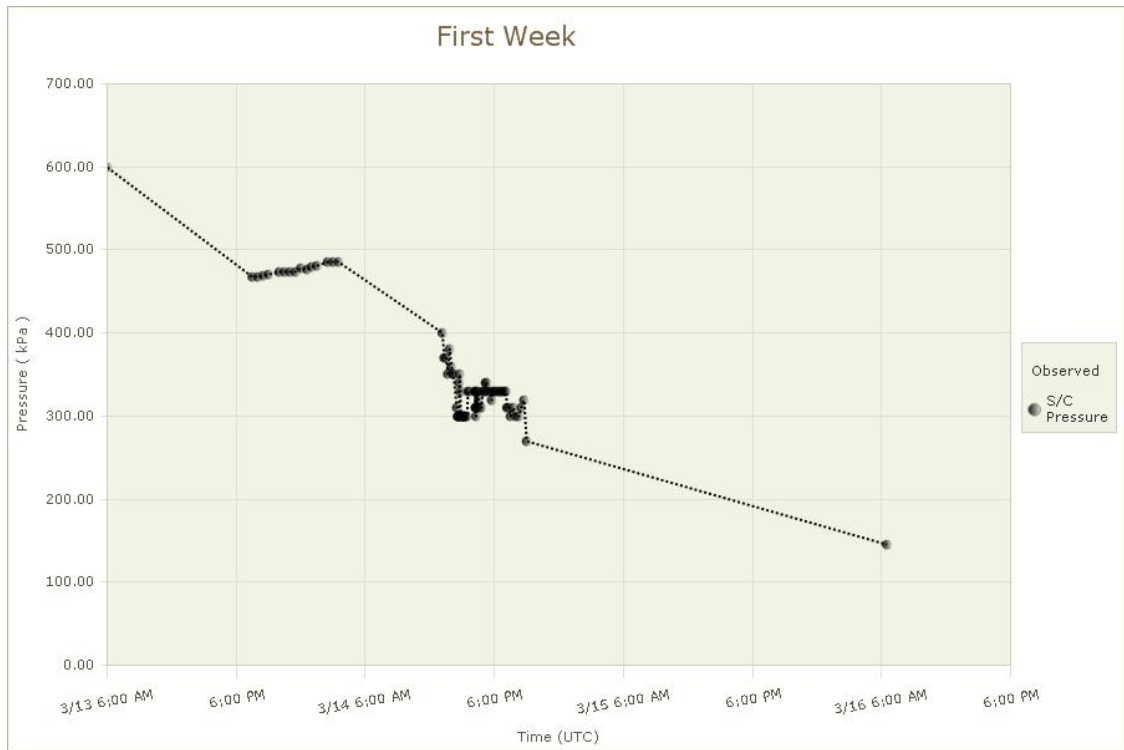
Unit3 Main Steam Isolation Valve 2-86A Temperature (Observed)
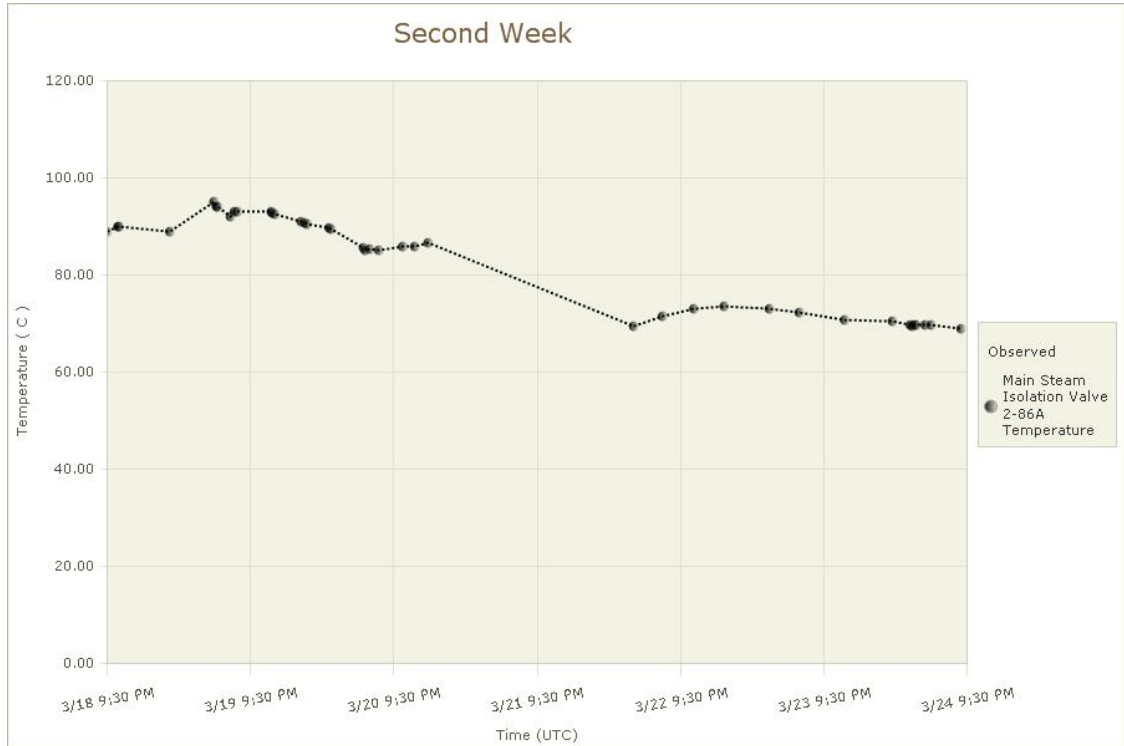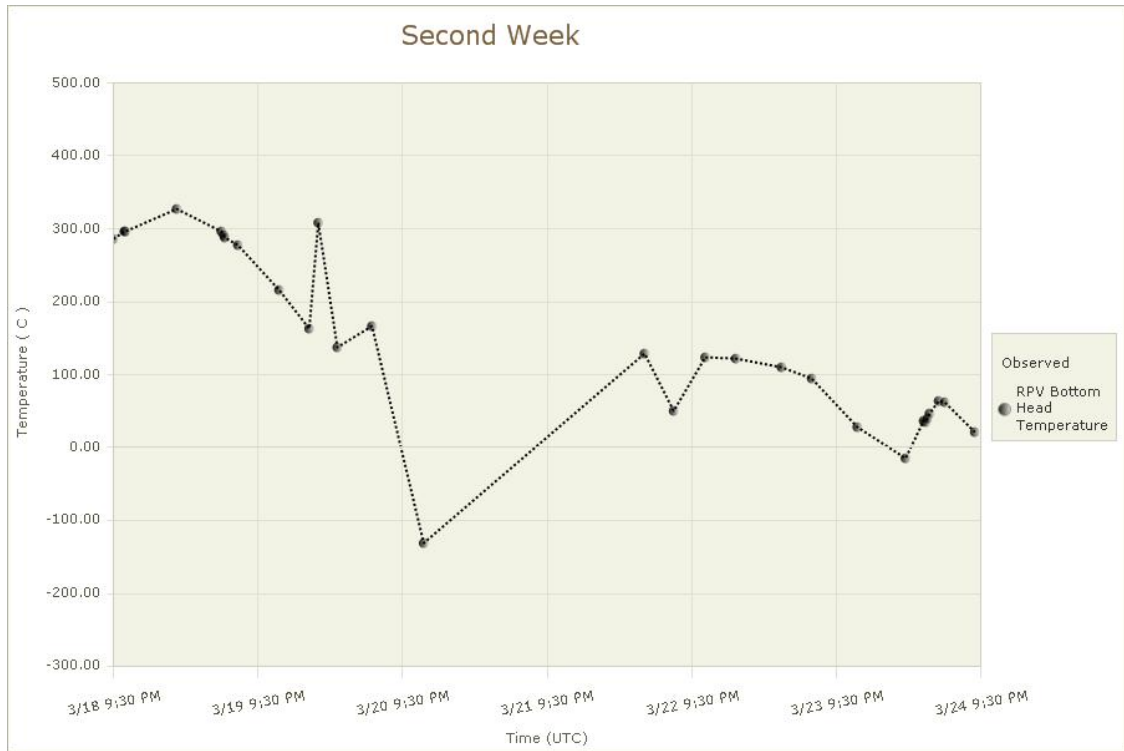

Unit3 RPV Bellows Air Temperature (Observed)
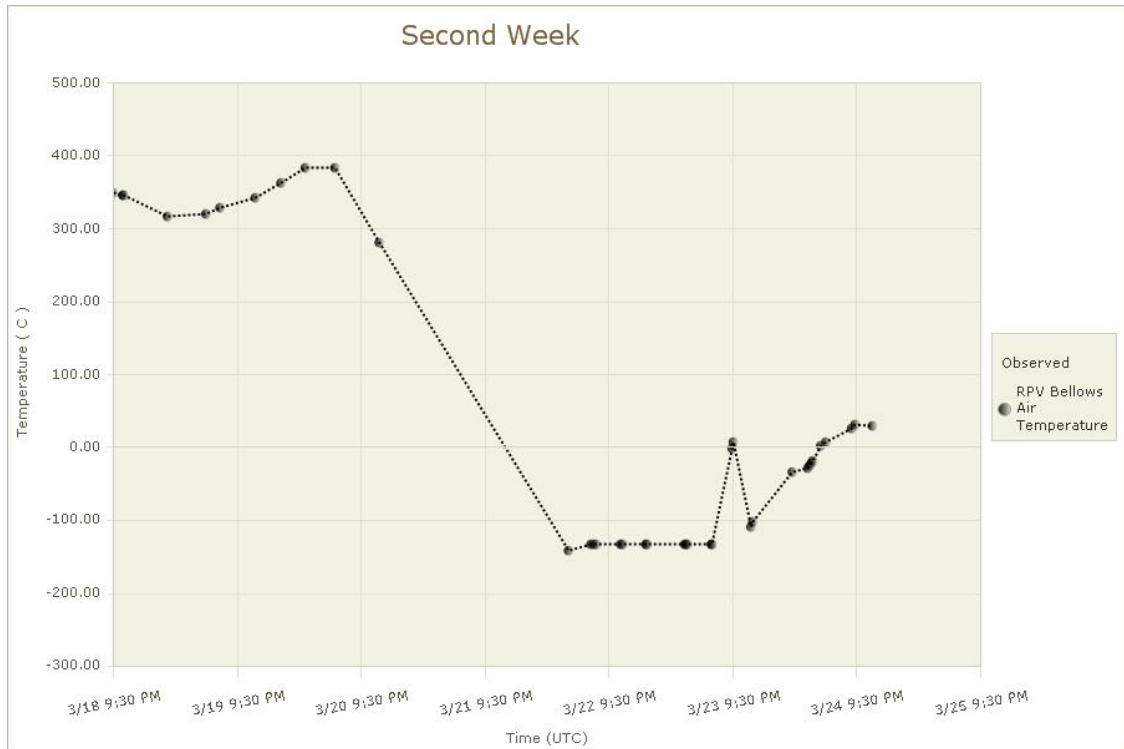
Fukushima Daiichi Accident Study
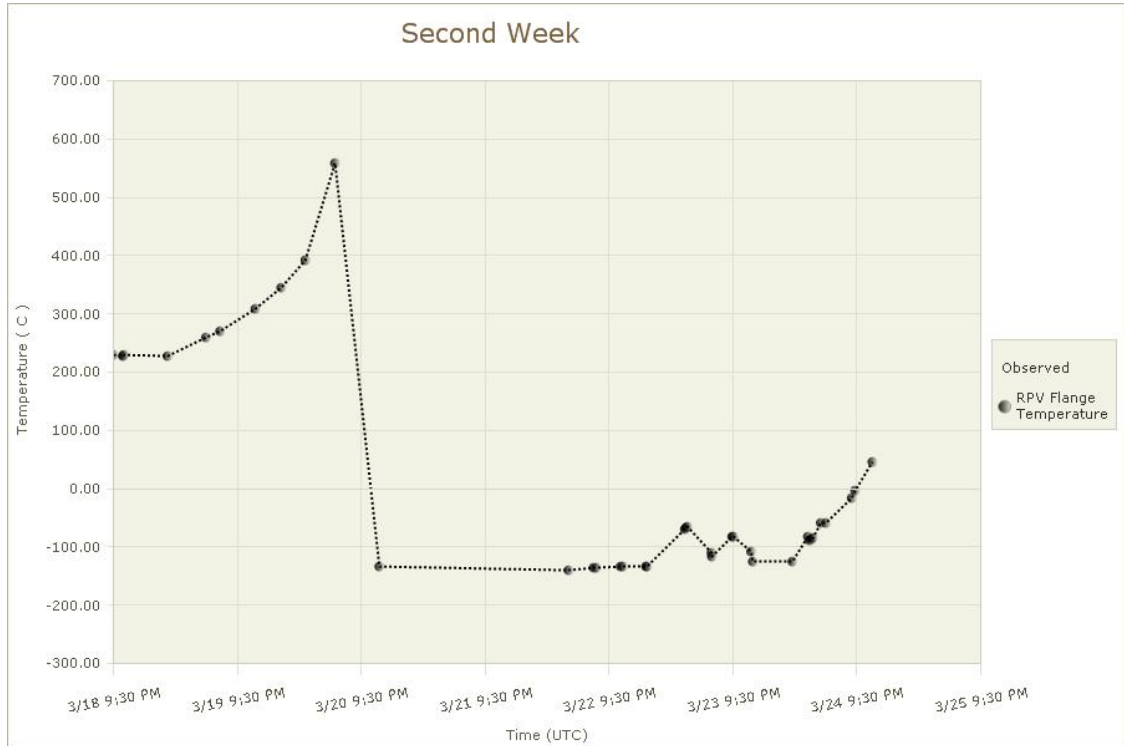# Information Portal

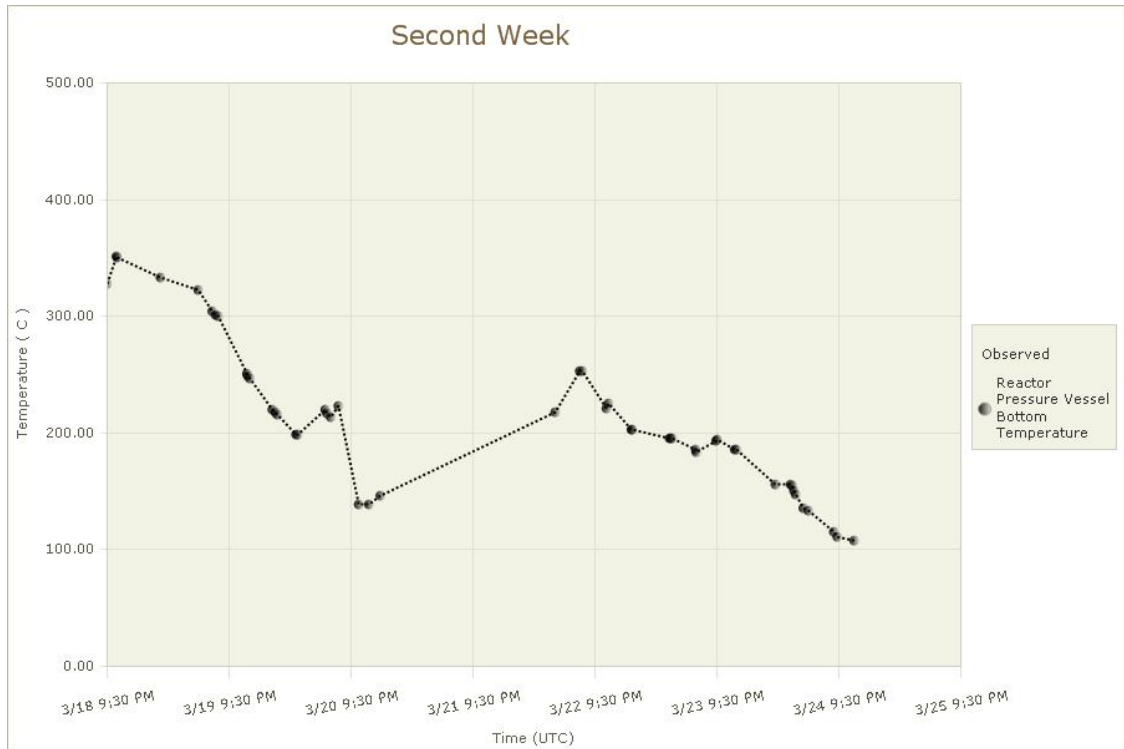Unit3 Feedwater Nozzle N4B Temperature (Observed)
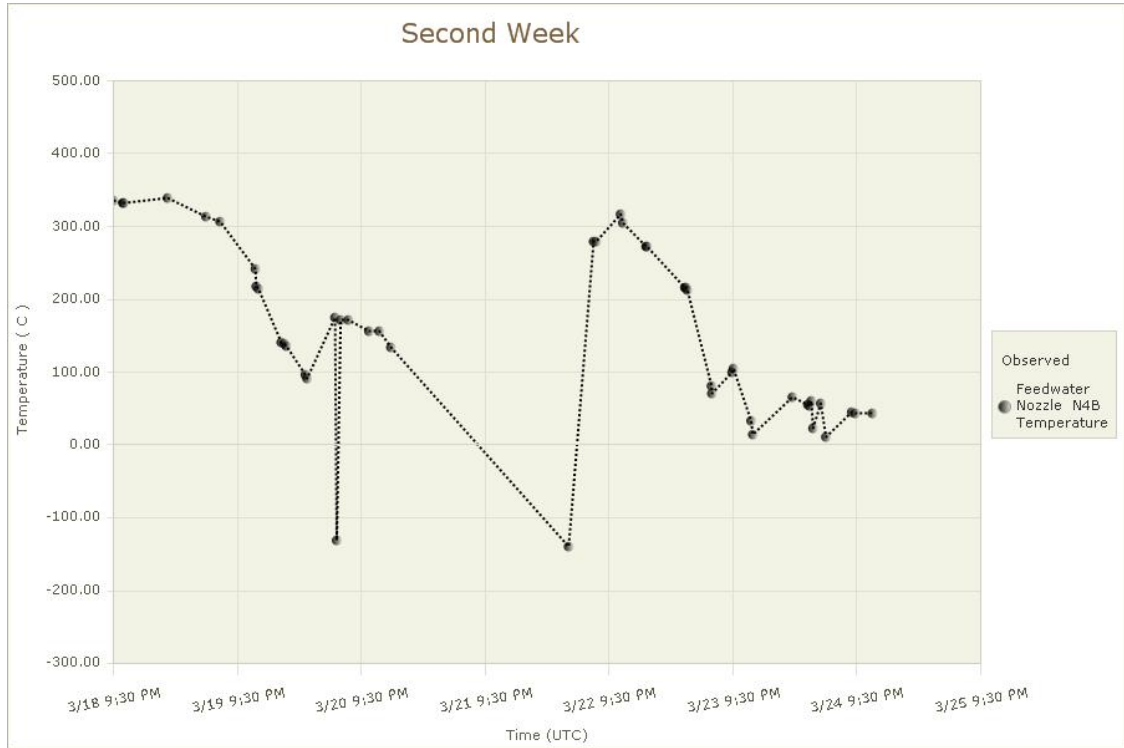
Unit3 RPV Bottom Head Temperature (Observed)

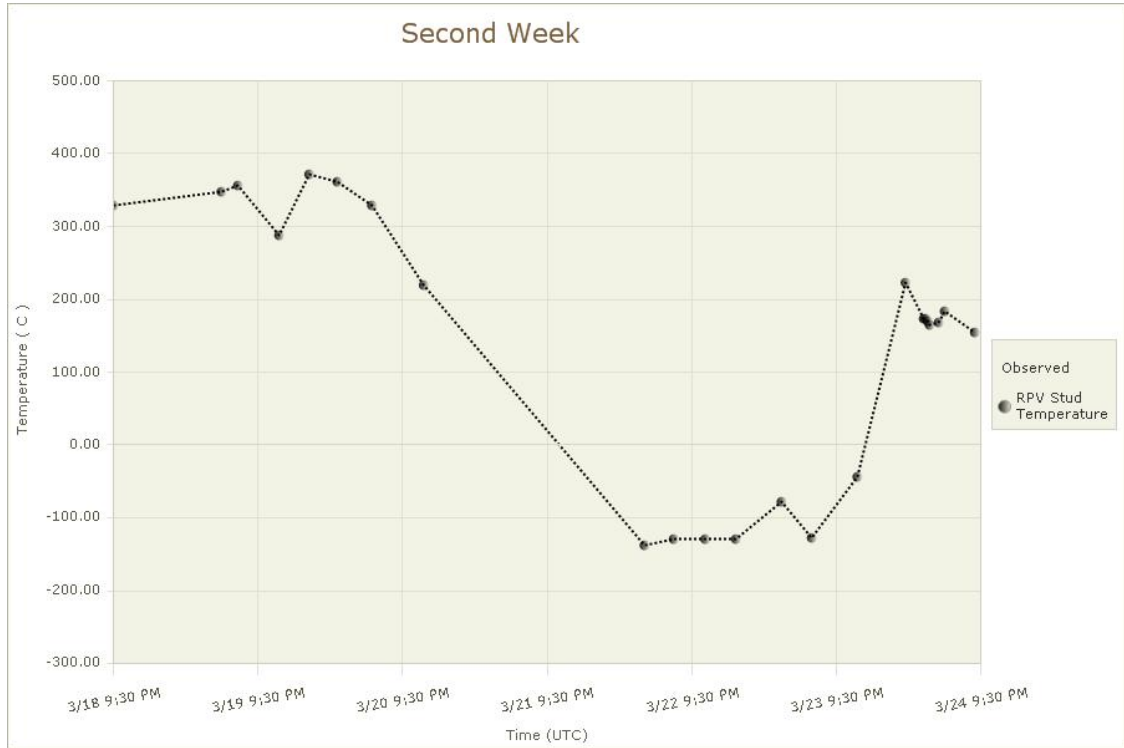Unit3 RPV Flange Temperature (Observed)

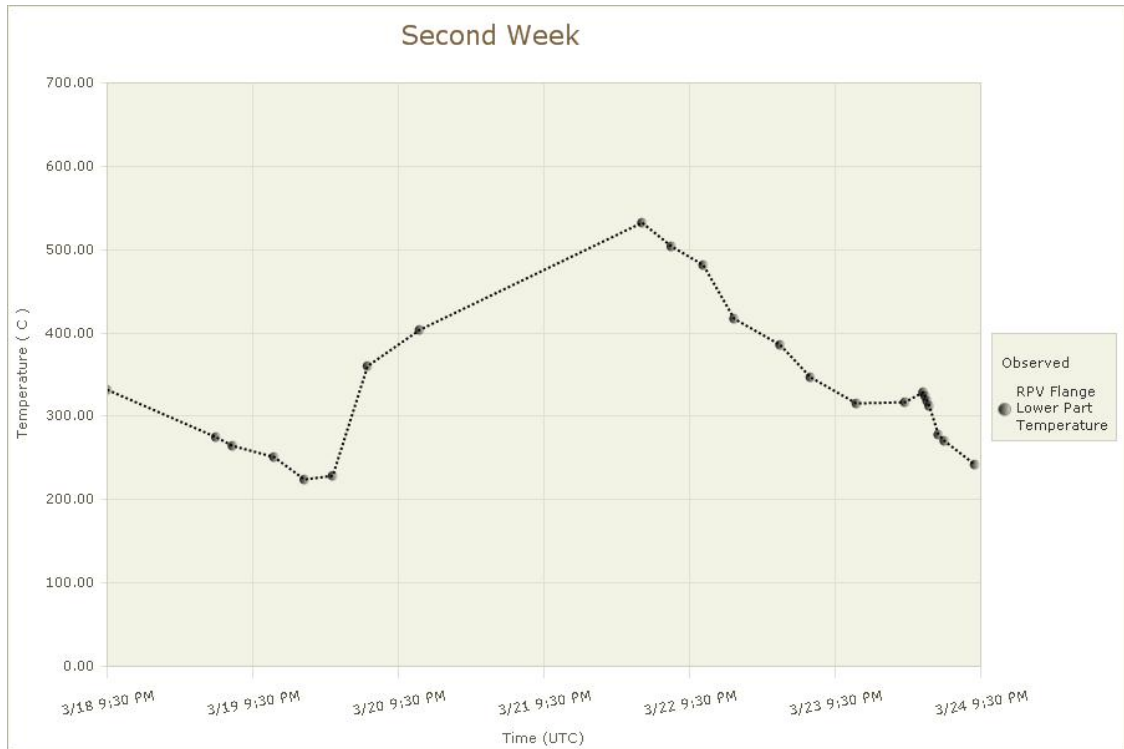Unit3 Reactor Pressure Vessel Bottom Temperature (Observed)

Fukushima Daiichi Accident Study
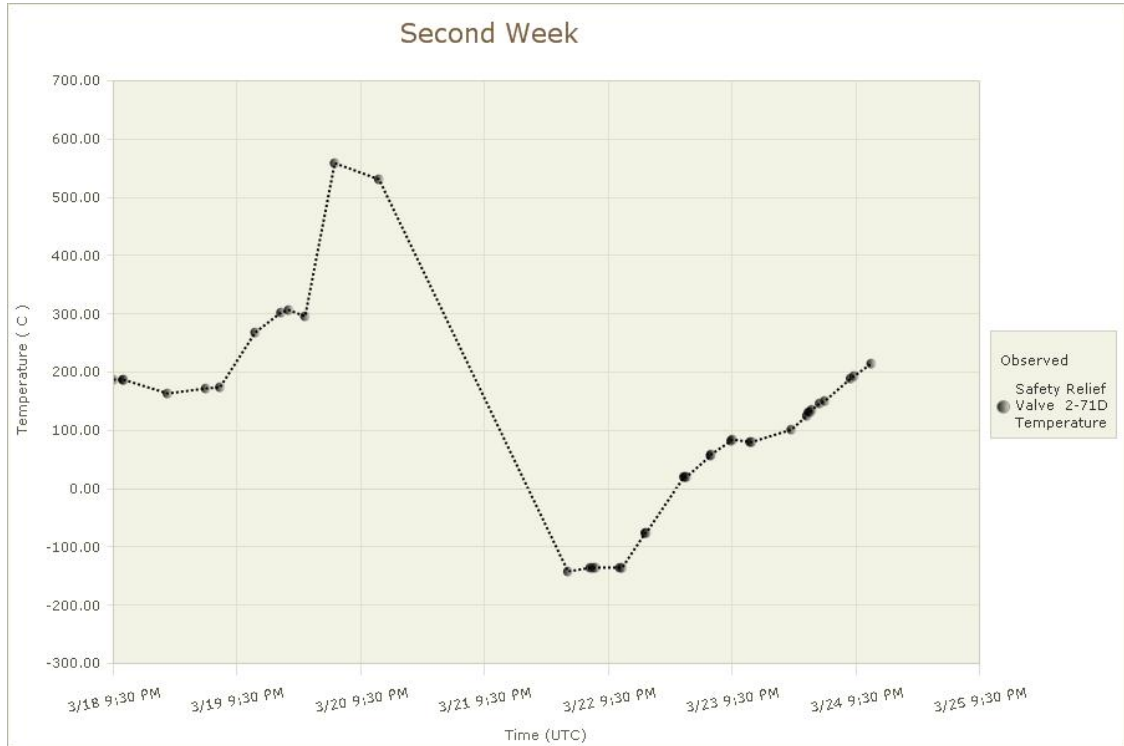# Information Portal

Unit3 RPV Stud Temperature (Observed)
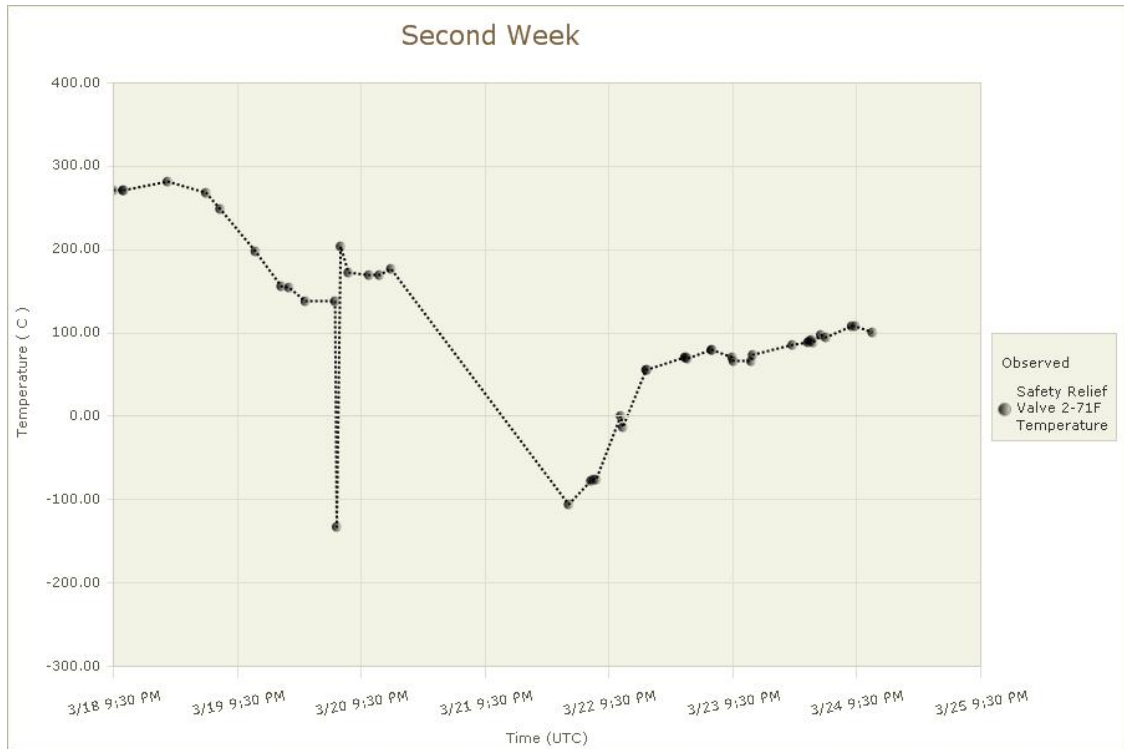

Unit3 RPV Flange Lower Part Temperature (Observed)

Unit3 Safety Relief Valve 2-71D Temperature (Observed)

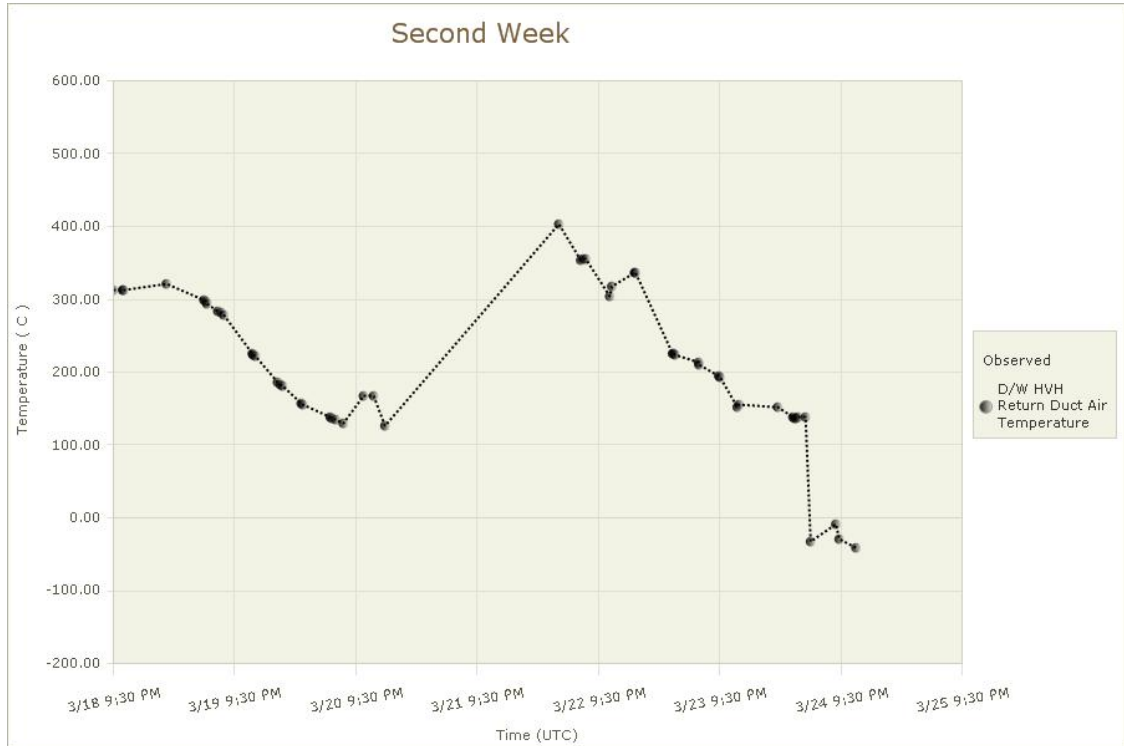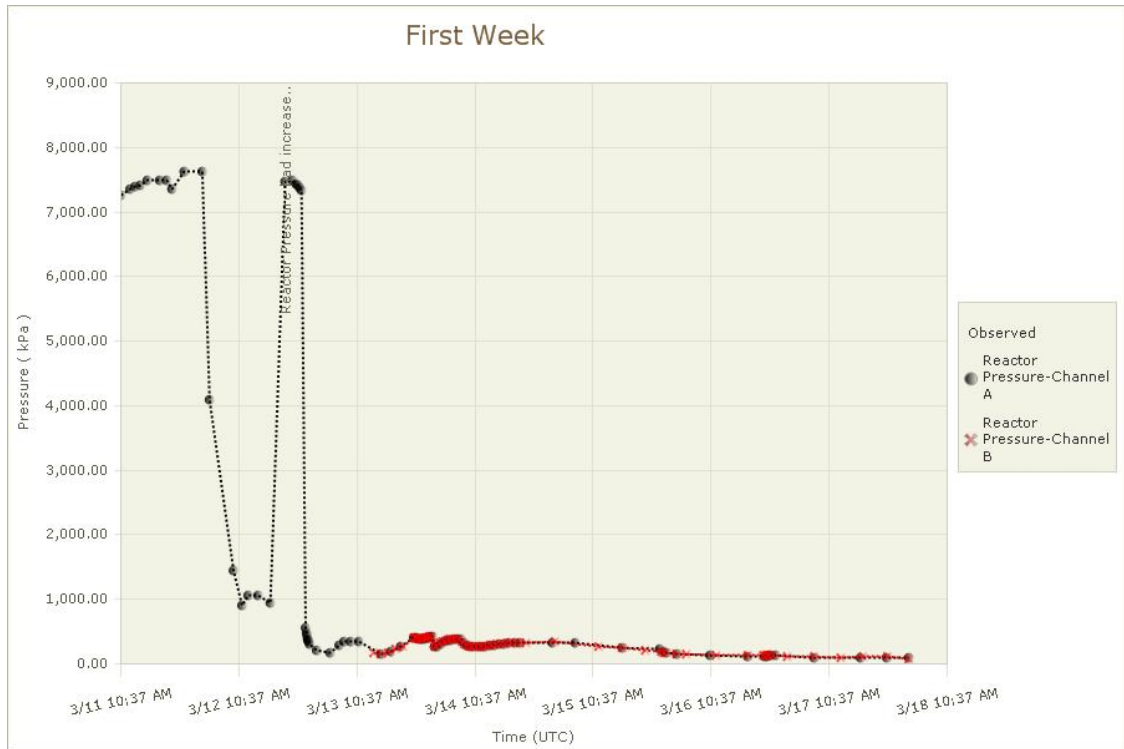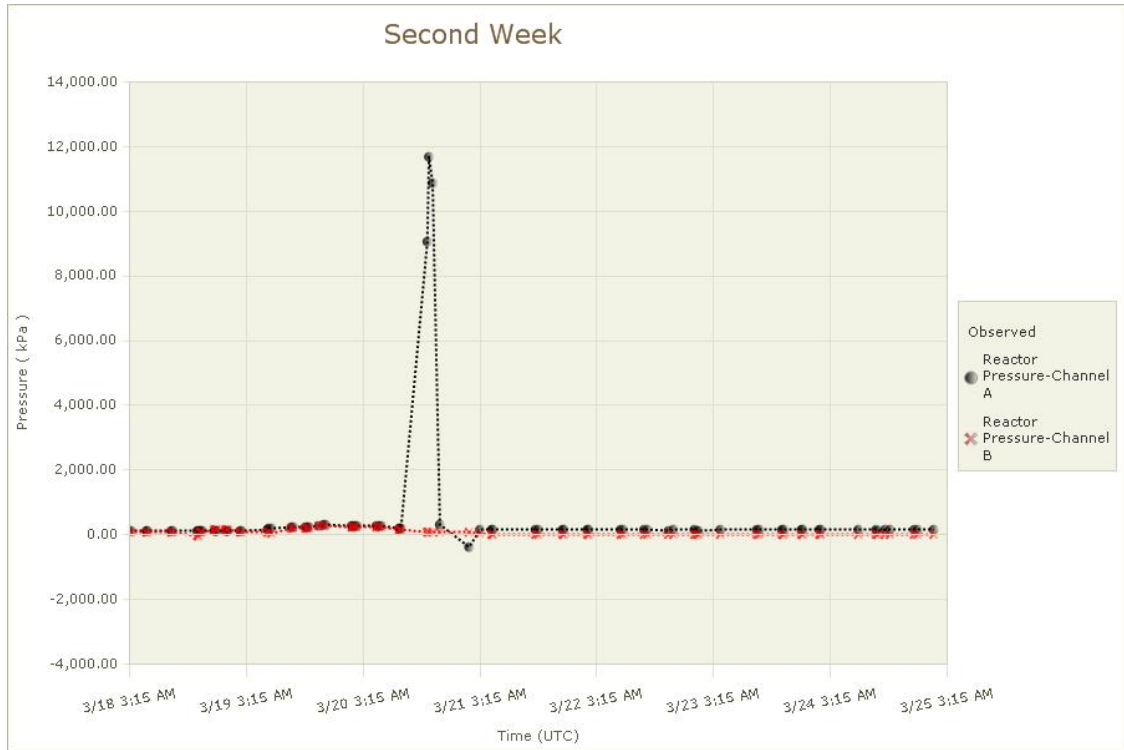Unit3 Safety Relief Valve 2-71F Temperature (Observed)

Unit3 D/W HVH Return Duct Air Temperature (Observed)
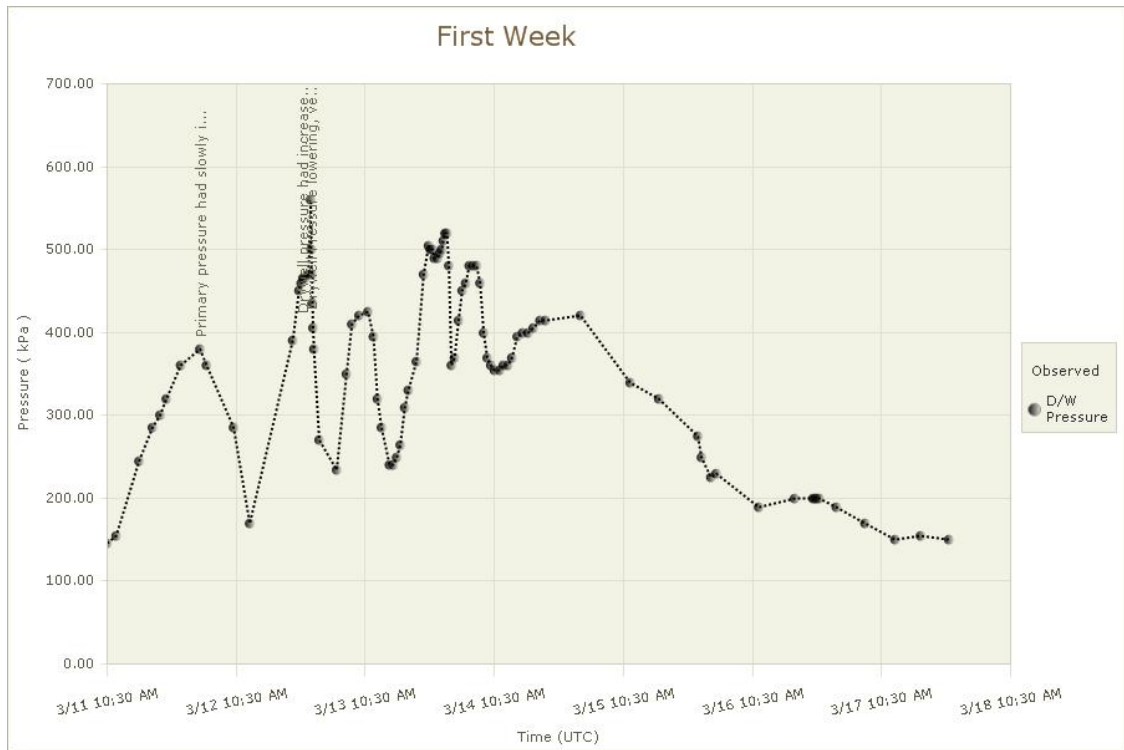

Unit3 Reactor Pressure (Observed)

Unit3 D/W Pressure (Observed)
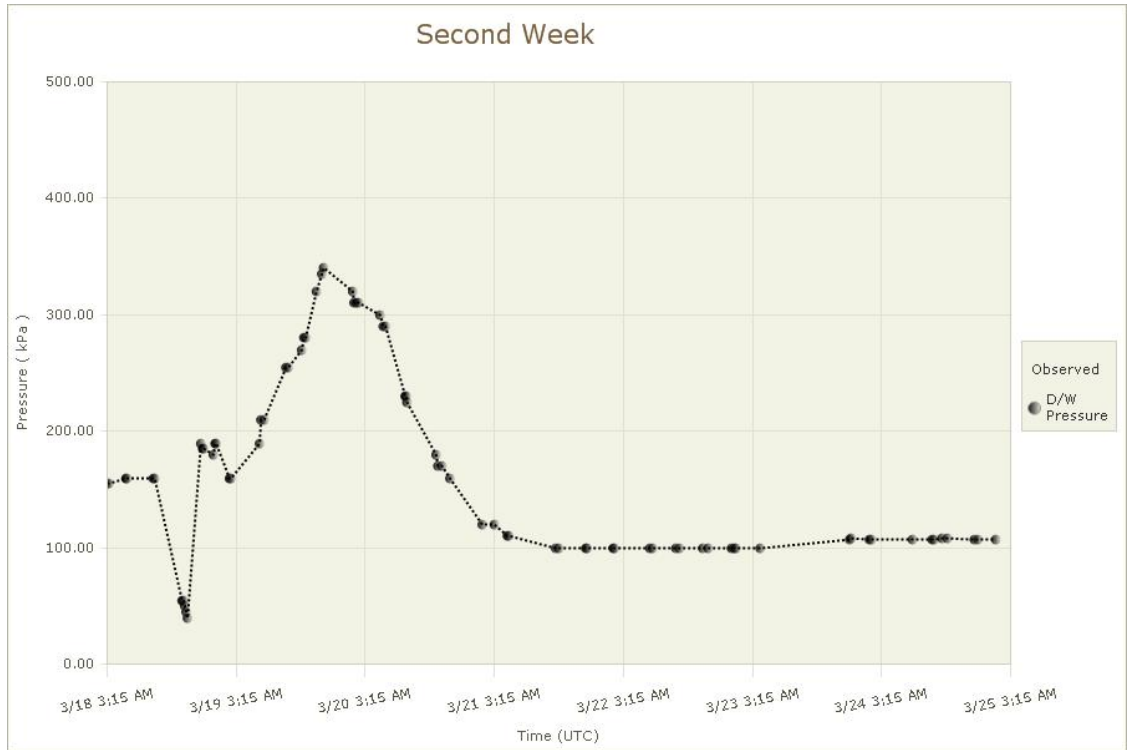
Unit3 S/C Pressure (Observed)
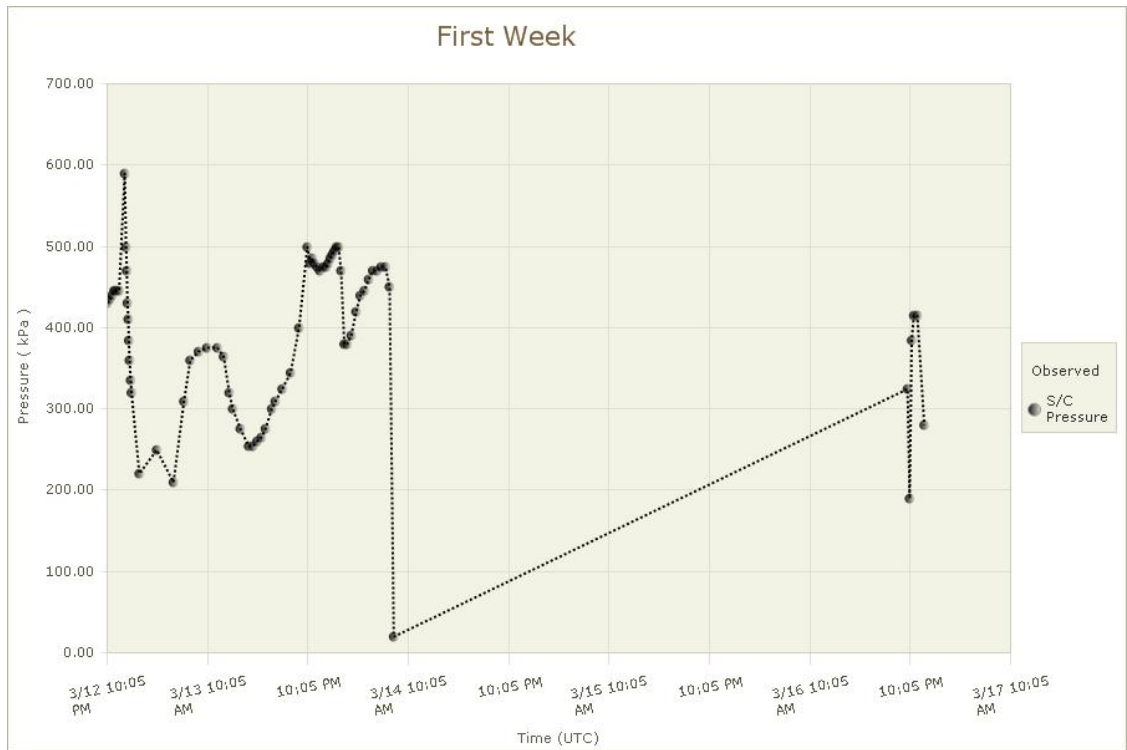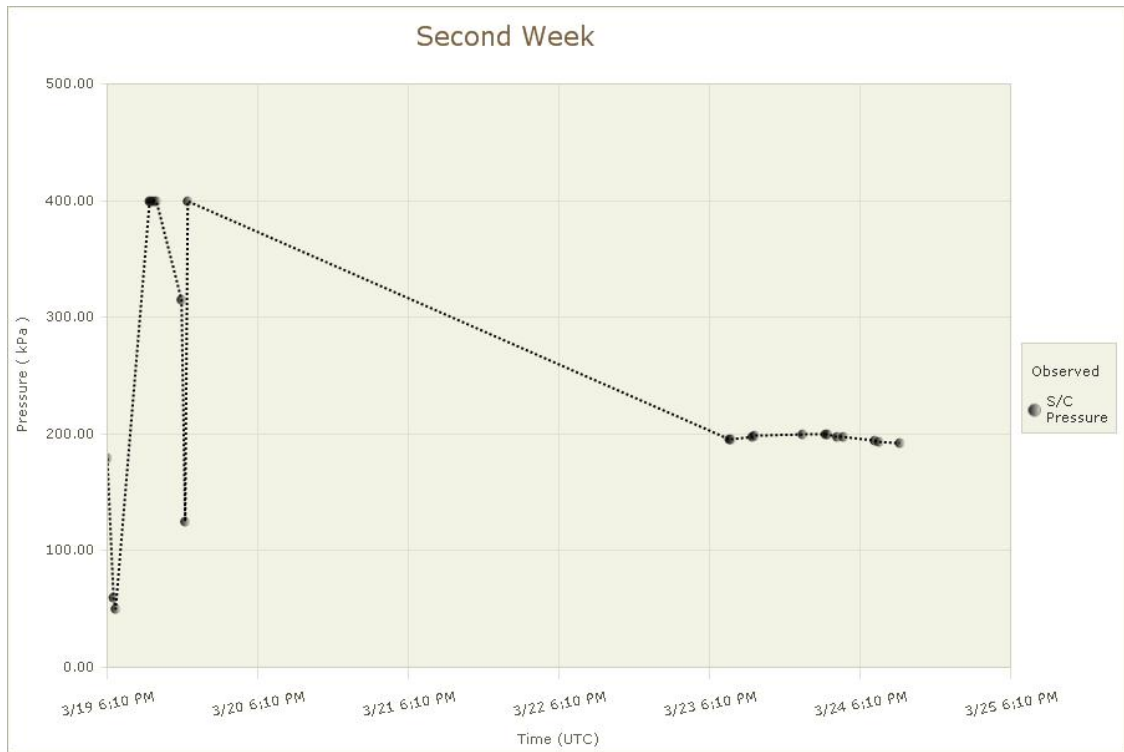
Fukushima Daiichi Accident Study
Information Portal

Appendix A

Unit 1 Detailed Timeline

Friday, March 11, 2011

    12:00:00 PM Isolation Condenser - Actuation Train - IC A
        Standby

    12:00:00 PM High Pressure Coolant Injection - Turbine driven pump - HPCI
        Standby

    12:00:00 PM Service Water System - Motor driven pump - CCSW
        Operating

    12:00:00 PM DC Power - Battery - 125 V Battery
        Operating

    12:00:00 PM Power Conversion - Main steam isolation valve - MSIVs
        Normally Open; Not failed

    12:00:00 PM Offsite Electrical Power - System level event - Offsite Power Sources
        Operating

    12:00:00 PM Reactor Protection - Actuation Train - Reactor
        Operating

    12:00:00 PM AC Power System - Emergency diesel generator - EDG 2
        Standby

    12:00:00 PM AC Power System - Emergency diesel generator - EDG 1
        Standby

    2:46:00 PM Earthquake (Tohoku)
        A major earthquake occurred located off the coast of the Miyagi Prefecture.
        Cause: Earthquake

    2:46:00 PM Unit 1 Shut Down
        Reactor Scram, Turbine Trip, all control rods fully inserted.
        Cause: Automated Action

    2:46:01 PM Reactor Protection - Actuation Train - Reactor
        Reactor Scram

    2:47:00 PM Offsite Electrical Power - System level event - Offsite Power Sources
        No power-loss of power

    2:47:00 PM Power Conversion - Main steam isolation valve - MSIVs
        Normally open; fail in closed position

    2:47:00 PM AC Power System - Emergency diesel generator - EDG 2
        Automatically Started

    2:47:00 PM AC Power System - Emergency diesel generator - EDG 1
        Automatically Started

    2:47:00 PM Loss of Offsite Power

Loss of all offsite power sources.
Cause: Loss of Power

2:52:00 PM Isolation Condenser - Actuation Train - IC B
Automatically Started

2:52:00 PM Isolation Condenser - Actuation Train - IC A
Automatically Started

3:02:00 PM Unit 1 subcriticality confirmed
Reactor subcriticality confirmed.
Cause: Operator Action

3:03:00 PM Isolation Condenser - Actuation Train - IC B
Manually Shutdown

3:03:00 PM Isolation Condenser - Actuation Train - IC A
Manually Shutdown

3:27:00 PM 1st Tsunami wave hits unit 1
Tsunami Wave generated by the earthquake strikes the plant
Cause: Earthquake

3:35:00 PM 2nd Tsunami wave hits unit 1
Tsunami Wave generated by the earthquake strikes the plant
Cause: Earthquake

3:37:00 PM High Pressure Coolant Injection - Turbine driven pump - HPCI
Fail to start

3:37:00 PM Service Water System - Motor driven pump - CCSW
Fail to continue running

3:37:00 PM DC Power - Battery - 125 V Battery
Fail to operate

3:37:00 PM AC Power System - Emergency diesel generator - EDG 2
Fail to continue running

3:37:00 PM AC Power System - Emergency diesel generator - EDG 1
Fail to continue running

3:37:00 PM Station Blackout, Unit 1
Loss of off site and on site AC power sources
Cause: Tsunami Flooding

5:30:00 PM Firewater Injection - Engine driven pump - Diesel driven fire pump
Manually Started

6:18:00 PM Isolation Condenser - Actuation Train - IC A
Manually Started

6:25:00 PM Isolation Condenser - Actuation Train - IC A
Manually Shutdown

8:07:00 PM Reactor pressure checked locally in reactor building, 1015 psia
Data indicated event: Reactor Pressure Channel A (Observed) = 7001 (kPa)

8:49:00 PM MCR lit by temporary lighting
     Main Control Room lit by temporary lighting.
     Cause: Operator Action
9:30:00 PM Isolation Condenser - Actuation Train - IC A
     Manually Started
11:50:00 PM Restoration team provides temp power to MCR. D/W pressure 87 psia (600 kPaa)
     Data indicated event: D/W Pressure (Observed) = 0.6 (kPa)
Saturday, March 12, 2011
   1:48:00 AM Firewater Injection - Engine driven pump - Diesel driven fire pump
     Fail to continue running
   2:30:00 AM Drywell pressure had increased to 122 psia (.84 MPaa).
     Data indicated event: D/W Pressure (Observed) = 0.84 (MPa)
   2:45:00 AM Reactor pressure checked, 131 psia (901 kPaa)
     Data indicated event: Reactor Pressure Channel A (Observed) = 901 (kPa)
   4:19:00 AM Drywell pressure lowered and stabilized without venting to 113 psia(.78 MPaa)
     Data indicated event: D/W Pressure (Observed) = 0.78 (MPa)
   5:46:00 AM Firewater Injection - Engine driven pump - Fire Engine
     Manually Started
   11:00:00 AM Isolation Condenser - Actuation Train - IC A
     Fail to continue running
   2:30:00 PM Containment Vent - Air operated valve - S/C Large vent valve
     Manually Opened
   2:30:00 PM   Venting Suppression Chamber began
     Opened large suppression chamber vent valve with temporary air compressor. Release of
     radioactive material and decrease in containment pressure confirmed.
     Cause: Operator Action
   2:50:00 PM Drywell pressure decreases, indicating venting successful.
     Data indicated event: D/W Pressure (Observed) = 0.58 (MPa)
   2:53:00 PM Firewater Injection - Engine driven pump - Fire Engine
     Loss of function
   3:36:00 PM Hydrogen Explosion
     Hydrogen Explosion in the Unit 1 Reactor Building
     Cause: Explosion
   7:04:00 PM Firewater Injection - Engine driven pump - Fire Engine
     Manually Started
   8:45:00 PM Boric acid added to seawater
     Commenced adding boric acid to seawater injection
     Cause: Operator Action

Unit 2 Detailed Timeline

Friday, March 11, 2011

12:00:00 PM High Pressure Coolant Injection - Turbine driven pump - HPCI
Standby

12:00:00 PM Residual Heat Removal Service Water - Motor driven pump - RHRS
Standby

12:00:00 PM Service Water System - Motor driven pump - CCSW
Operating

12:00:00 PM DC Power - Battery - 125 V Battery
Operating

12:00:00 PM Reactor Core Isolation Cooling - Turbine driven pump - RCIC system
Standby

12:00:00 PM Offsite Electrical Power - System level event - Offsite Power Sources
Operating

12:00:00 PM Power Conversion - Main steam isolation valve - MSIVs
Normally Open; Not failed

12:00:00 PM Reactor Protection - Actuation Train - Reactor
Operating

12:00:00 PM AC Power System - Emergency diesel generator - EDG 2
Standby

12:00:00 PM AC Power System - Emergency diesel generator - EDG 1
Standby

2:46:00 PM Earthquake (Tohoku)
A major earthquake occurred located off the coast of the Miyagi Prefecture.
Cause: Earthquake

2:47:00 PM Offsite Electrical Power - System level event - Offsite Power Sources
No power-loss of power

2:47:00 PM Power Conversion - Main steam isolation valve - MSIVs
Normally open; fail in closed position

2:47:00 PM Reactor Protection - Actuation Train - Reactor
Reactor Scram

2:47:00 PM AC Power System - Emergency diesel generator - EDG 2
Automatically Started

2:47:00 PM AC Power System - Emergency diesel generator - EDG 1
Automatically Started

2:47:00 PM Loss of Offsite Power
Loss of all offsite power sources.
Cause: Loss of Power

2:47:00 PM Unit 2 Shutdown

Reactor Scram, Turbine Trip, all control rods fully inserted.
Cause: Automated Action

2:50:00 PM Reactor Core Isolation Cooling - Turbine driven pump - RCIC system
Manually Started

2:51:00 PM Reactor Core Isolation Cooling - Turbine driven pump - RCIC system
Automatically Shutdown

3:00:00 PM Residual Heat Removal Service Water - Motor driven pump - RHRS
Manually Started

3:01:00 PM Unit 2 subcriticality confirmed
Unit 2 reactor confirmed to be subcritical.
Cause: Operator Action

3:02:00 PM Reactor Core Isolation Cooling - Turbine driven pump - RCIC system
Manually Started

3:07:00 PM Torus cooling placed in service
Torus cooling manually started.
Cause: Operator Action

3:25:00 PM Torus spray placed in service
Torus spray manually started.
Cause: Operator Action

3:27:00 PM 1st Tsunami wave hits unit 2
Tsunami Wave generated by the earthquake strikes the plant
Cause: Earthquake

3:28:00 PM Reactor Core Isolation Cooling - Turbine driven pump - RCIC system
Automatically Shutdown

3:35:00 PM 2nd Tsunami wave hits unit 2
Tsunami Wave generated by the earthquake strikes the plant
Cause: Earthquake

3:39:00 PM Reactor Core Isolation Cooling - Turbine driven pump - RCIC system
Manually Started

3:41:00 PM High Pressure Coolant Injection - Turbine driven pump - HPCI
Fail to start

3:41:00 PM Residual Heat Removal Service Water - Motor driven pump - RHRS
Fail to continue running

3:41:00 PM Service Water System - Motor driven pump - CCSW
Fail to continue running

3:41:00 PM DC Power - Battery - 125 V Battery
Fail to operate

3:41:00 PM AC Power System - Emergency diesel generator - EDG 2
Fail to continue running

3:41:00 PM AC Power System - Emergency diesel generator - EDG 1

Fail to continue running

3:41:00 PM Station Blackout, Unit 2

Loss of off site and on site AC power.

Cause: Tsunami Flooding

8:49:00 PM MCR lit by temporary lighting

Main control room lit by temporary lighting

Cause: Operator Action

9:50:00 PM Reactor water level 3,400 mm > TAF

Reactor water level indication restored in control room. Vessel level indicated 3,400 mm above TAF.

Cause: Operator Action

11:25:00 PM Drywell pressure indication restored. DW pressure 20 psia (.141 MPaa)

Data indicated event: D/W Pressure (Observed) = 0.141 (MPa)

Saturday, March 12, 2011

2:00:00 AM RCIC verified to be operating

Workers verified RCIC pump discharge pressure in the field.

Cause: Operator Action

4:20:00 AM RCIC suction swapped (CST to torus)

RCIC suction was swapped from the CST to the torus.

Cause: Operator Action

Monday, March 14, 2011

1:18:00 PM Reactor water level 2400 mm > TAF

Reactor water level was 2400 mm above TAF and trending downward.

Cause: Operator Action

1:25:11 PM Reactor Core Isolation Cooling - Turbine driven pump - RCIC system

Fail to continue running

4:43:00 PM Below Top of Active Fuel (TAF)

Data indicated event: Reactor Vessel Level Fuel Zone, A (Observed) = -0.3 (m)

5:12:00 PM Reactor Pressure 1088 psia, too high for seawater injection

Data indicated event: Reactor Pressure Channel A (Observed) = 7.504 (MPa)

5:17:00 PM Reactor water level decreased to TAF

Indicated reactor water level decreased to TAF.

Cause: Loss of Power

6:03:00 PM Reactor depressurization begins

Data indicated event: Reactor Pressure Channel A (Observed) = 6.176 (MPa)

6:06:00 PM Main Steam - Safety relief valve - SRV

Manually Opened

6:30:00 PM Firewater Injection - Engine driven pump - Fire Engine

Manually Started

7:03:00 PM Reactor pressure stabilizes following depressurization

Data indicated event: Reactor Pressure Channel A (Observed) = 0.731 (MPa)

7:20:00 PM Firewater Injection - Engine driven pump - Fire Engine
Fail to continue running

7:54:00 PM Firewater Injection - Engine driven pump - Fire Engine
Manually Started

9:03:00 PM Reactor pressure increasing
Data indicated event: Reactor Pressure Channel A (Observed) = 1.519 (MPa)

9:20:00 PM Main Steam - Safety relief valve - SRV
Manually Opened

10:50:00 PM Drywell pressure exceeds design pressure
Data indicated event: D/W Pressure (Observed) = 0.54 (MPa)

Tuesday, March 15, 2011

12:45:00 AM Injection not likely at this pressure
Data indicated event: Reactor Pressure Channel A (Observed) = 1.924 (MPa)

6:00:00 AM Loud Noise Reported
A loud noise was heard. Possibly in the area of the torus (Unit 2) or from the explosions
in Unit 4.
Cause: Unknown

11:25:00 AM Drywell pressure decreased, likely related to loud noise heard at 0600
Data indicated event: D/W Pressure (Observed) = 0.155 (MPa)

Unit 3 Detailed Timeline

Friday, March 11, 2011

12:00:00 PM DC Power - Battery - 125 V Battery
Operating

12:00:00 PM High Pressure Coolant Injection - Turbine driven pump - HPCI
Standby

12:00:00 PM Residual Heat Removal Service Water - Motor driven pump - RHRS
Standby

12:00:00 PM Service Water System - Motor driven pump - CCSW
Operating

12:00:00 PM Reactor Core Isolation Cooling - Turbine driven pump - RCIC system
Standby

12:00:00 PM Power Conversion - Main steam isolation valve - MSIVs
Normally Open; Not failed

12:00:00 PM Offsite Electrical Power - System level event - Offsite Power Sources
Operating

12:00:00 PM Reactor Protection - Actuation Train - Reactor
Operating

12:00:00 PM AC Power System - Emergency diesel generator - EDG 2

Standby
12:00:00 PM AC Power System - Emergency diesel generator - EDG 1
    Standby
2:46:00 PM Earthquake (Tohoku)
    A major earthquake occurred located off the coast of the Miyagi Prefecture.
    Cause: Earthquake
2:47:00 PM Offsite Electrical Power - System level event - Offsite Power Sources
    No power-loss of power
2:47:00 PM Reactor Protection - Actuation Train - Reactor
    Reactor Scram
2:47:00 PM AC Power System - Emergency diesel generator - EDG 2
    Automatically Started
2:47:00 PM AC Power System - Emergency diesel generator - EDG 1
    Automatically Started
2:47:00 PM Loss of Offsite Power
    Loss of all offsite power sources.
    Cause: Loss of Power
2:47:00 PM Unit 3 Shutdown
    Reactor scram, turbine trip, all control rods fully inserted.
    Cause: Automated Action
2:48:00 PM Power Conversion - Main steam isolation valve - MSIVs
    Normally open; fail in closed position
2:54:00 PM Unit 3 subcriticallity confirmed
    Unit 3 reactor verified subcritical
    Cause: Operator Action
3:05:00 PM Reactor Core Isolation Cooling - Turbine driven pump - RCIC system
    Manually Started
3:25:00 PM Reactor Core Isolation Cooling - Turbine driven pump - RCIC system
    Automatically Shutdown
3:27:00 PM 1st Tsunami Wave hits Unit 3
    Tsunami Wave generated by the earthquake strikes the plant
    Cause: Earthquake
3:35:00 PM 2nd Tsunami Wave hits unit 3
    Tsunami Wave strikes plant
    Cause: Earthquake
3:38:00 PM Station Blackout, Unit 3
    Loss of both offsite and onsite AC power sources.
    Cause: Tsunami Flooding
3:41:00 PM Residual Heat Removal Service Water - Motor driven pump - RHRS
    Fail to start

3:41:00 PM Service Water System - Motor driven pump - CCSW
  Fail to continue running

3:41:00 PM AC Power System - Emergency diesel generator - EDG 2
  Fail to continue running

3:41:00 PM AC Power System - Emergency diesel generator - EDG 1
  Fail to continue running

4:03:00 PM Reactor Core Isolation Cooling - Turbine driven pump - RCIC system
  Manually Started

9:58:00 PM Temporary lighting for unit 3 MCR
  Temporary lighting established for unit 3 main control room using portable generator.
  Cause: Operator Action

Saturday, March 12, 2011

11:36:00 AM Reactor Core Isolaiton Cooling - Turbine driven pump - RCIC system
  Fail to continue running

12:10:00 PM Primary pressure had slowly increased to 57 psia (0.39 MPaa)
  Data indicated event: D/W Pressure (Observed) = 0.39 (MPa)

12:35:00 PM High Pressure Coolant Injection - Turbine driven pump - HPCI
  Automatically Started

9:30:00 PM DC Power - Battery - 125 V Battery
  Fail to operate

Sunday, March 13, 2011

2:42:00 AM High Pressure Coolant Injection - Turbine driven pump - HPCI
  Fail to continue running

5:00:00 AM Reactor Pressure had increased to 1,085 psia (7.48 MPa abs).
  Data indicated event: Reactor Pressure Channel A (Observed) = 7.481 (MPa)

7:45:00 AM Drywell pressure had increased to 67 psia (.46 Mpaa)
  Data indicated event: D/W Pressure (Observed) = 0.46 (MPa)

9:08:00 AM Main Steam - Safety relief valve - SRV
  Manually Opened

9:20:00 AM Containment Vent - Air operated valve - S/C Large vent valve
  Manually Opened

9:20:00 AM Venting determined to have started.
  Venting determined to have successfully started due to decreasing containment pressure.
  Cause: Operator Action

9:24:00 AM Drywell Pressure lowering, venting successful.
  Data indicated event: D/W Pressure (Observed) = 0.54 (MPa)

9:25:00 AM Firewater Injection - Engine driven pump - Fire Engine
  Manually Started

11:17:00 AM Containment Vent - Air operated valve - S/C Large vent valve
  Normally closed; fail in the closed position

      12:20:00 PM Firewater Injection - Engine driven pump - Fire Engine
         Fail to continue running

      12:30:00 PM Containment Vent - Air operated valve - S/C Large vent valve
         Manually Opened

      1:12:00 PM Firewater Injection - Engine driven pump - Fire Engine
         Manually Started

      3:00:00 PM Containment Vent - Air operated valve - S/C Large vent valve
         Normally closed; fail in the closed position

      8:10:00 PM Containment Vent - Air operated valve - S/C Large vent valve
         Manually Opened

Monday, March 14, 2011

      1:00:00 AM Containment Vent - Air operated valve - S/C Large vent valve
         Normally closed; fail in the closed position

      1:10:00 AM Firewater Injection - Engine driven pump - Fire Engine
         Fail to continue running

      3:20:00 AM Firewater Injection - Engine driven pump - Fire Engine
         Manually Started

      6:10:00 AM S/C small vent valve opened
         S/C small vent valve confirmed to have been opened, however containment pressure
         readings indicate little if any venting resulted.
         Cause: Operator Action

      11:01:00 AM Firewater Injection - Engine driven pump - Fire Engine
         Fail to continue running

      11:01:00 AM Hydrogen Explosion
         Hydrogen Explosion in the Unit 3 Reactor Building
         Cause: Explosion

      4:30:00 PM Firewater Injection - Engine driven pump - Fire Engine
         Manually Started

Tuesday, March 15, 2011

      4:05:00 PM Containment Vent - Air operated valve - S/C Large vent valve
         Manually Opened

Unit 4 Detailed Timeline

Friday, March 11, 2011

      12:00:00 PM Unit 4 Initial Condition
         Unit 4 was in an outage with the core offloaded to the spent fuel pool.

      2:46:00 PM Earthquake (Tohoku)
         A major earthquake occurred located off the coast of the Miyagi Prefecture.
         Cause: Earthquake

      2:47:00 PM Loss of Offsite Power

> Loss of all offsite power sources.
> Cause: Loss of Power
>
> 3:38:00 PM Station Blackout, Unit 4
> Loss of all onsite and offsite AC power.
> Cause: Tsunami Flooding

Tuesday, March 15, 2011
> 6:00:00 AM Explosion in Unit 4 reactor building
> An explosion occured in the unit 4 reactor building. It is assumed to be caused by Hydrogen from venting unit 3.
> Cause: Explosion
>
> 6:00:00 AM Loud Noise Reported
> A loud noise was heard. Possibly in the area of the torus (Unit 2) or from the explosions in Unit 4.
> Cause: Unknown

Unit 5 Detailed Timeline

Friday, March 11, 2011
> 12:00:00 PM Initial Conditions of Unit 5
> Unit 5 was in an outage with fuel assemblies in the core and RPV intact.
>
> 2:46:00 PM Earthquake (Tohoku)
> A major earthquake occurred located off the coast of the Miyagi Prefecture.
> Cause: Earthquake
>
> 2:47:00 PM Loss of Offsite Power
> Loss of all offsite power sources.
> Cause: Loss of Power
>
> 3:40:00 PM Station blackout, Unit 5
> Loss of all onsite and offsite AC power sources.
> Cause: Tsunami Flooding

Sunday, March 20, 2011
> 2:30:00 PM Unit 5 Achieves Cold Shutdown
> Unit 5 reaches cold shutdown conditions
> Cause: Operator Action

Unit 6 Detailed Timeline

Friday, March 11, 2011
> 12:00:00 PM Initial Conditions of Unit 6
> Unit 6 was in an outage with all fuel assemblies loaded in the core and in cold shutdown mode.
>
> 2:46:00 PM Earthquake (Tohoku)
> A major earthquake occurred located off the coast of the Miyagi Prefecture.
> Cause: Earthquake

2:47:00 PM Loss of Offsite Power
Loss of all offsite power sources.
Cause: Loss of Power

3:40:00 PM EDG status after Tsunami
After the Tsunami flooding, EDGs 6A and 6H failed. EDG 6B continued to run and provided AC power.
Cause: Tsunami Flooding

Sunday, March 20, 2011
7:27:00 PM Unit 6 achieves cold shutdown
Unit 6 reaches cold shutdown conditions
Cause: Operator Action

Distribution

9   US Department of Energy
    Attn: Damian Peko
    NE-72
    1991 Germantown Road
    Germantown, MD 20874

2   US Department of Energy
    Attn: Patrick Schwab
    NE-51
    1991 Germantown Road
    Germantown, MD 20874

6   US Nuclear Regulatory Commission
    Attn: Richard Lee
    MS C3 A7M
    11555 Rockville Pike
    Rockville, MD 20852

6   Oak Ridge National Laboratory
    Attn: Matthew Francis
    One Bethel Valley Road
    Oak Ridge, TN 37831-6172

6   Idaho National Laboratory
    Attn: Curtis Smith
    P.O. Box 1625, MS 3850
    Idaho Falls, ID 83415-3850

2	MS0736	Susan Pickering	6230
3	MS0736	Randall Gauntt	6232
2	MS0736	Donald Kalinich	6232
1	MS0736	Jeff Cardoni	6232
1	MS0736	Jesse Philips	6232
1	MS0736	Andrew Goldmann	6232

| 1 | MS0899 | Technical Library | 9536 (electronic copy) |

Sandia National Laboratories